



**HAL**  
open science

# Copolymer-based PLLA matrix composites produced by TP-RTM

Bernard Miranda Campos

► **To cite this version:**

Bernard Miranda Campos. Copolymer-based PLLA matrix composites produced by TP-RTM. Polymers. Université de Lille, 2023. English. NNT : 2023ULILR042 . tel-04444216

**HAL Id: tel-04444216**

**<https://theses.hal.science/tel-04444216>**

Submitted on 7 Feb 2024

**HAL** is a multi-disciplinary open access archive for the deposit and dissemination of scientific research documents, whether they are published or not. The documents may come from teaching and research institutions in France or abroad, or from public or private research centers.

L'archive ouverte pluridisciplinaire **HAL**, est destinée au dépôt et à la diffusion de documents scientifiques de niveau recherche, publiés ou non, émanant des établissements d'enseignement et de recherche français ou étrangers, des laboratoires publics ou privés.



## Ph.D. thesis

In order to obtain the rank of

**Doctor**

**Delivered by** : Université de Lille, Ecole doctorale Science de la Matière, du Rayonnement et de l'Environnement

**Specialty: Materials Chemistry**

Thesis supervised by

**Dr. Fanny Bonnet, Pr. Gaëlle Fontaine, Dr. Grégory Stoclet**

Ph.D. defense planned at 19/10/2023 by:

**M. Bernard Miranda Campos**

---

## Copolymer-based PLLA matrix composites produced by TP-RTM

---

<b>Chair</b>	Vincent Monteil	Research director	CNRS
<b>Referee</b>	Yves Grohens	Professor	Université Bretagne Sud
<b>Referee</b>	Claire Longuet	Lecturer	IMT Mines Alès
<b>Examiner</b>	Mylène Lagardère	Lecturer	IMT Nord Europe
<b>Director</b>	Fanny Bonnet	Research director	CNRS, Université de Lille
<b>Co-director</b>	Gaëlle Fontaine	Professor	Centrale Lille
<b>Co-supervisor</b>	Grégory Stoclet	Lecturer	Université de Lille
<b>Guest</b>	Serge Bourbigot	Professor	Centrale Lille





## These de doctorat

En vue d'obtenir le grade de

**Docteur**

**Délivrée par** : Université de Lille, Ecole doctorale Science de la Matière, du Rayonnement et de l'Environnement

**Spécialité : Chimie des matériaux**

Thèse dirigée par

**Dr. Fanny Bonnet, Pr. Gaëlle Fontaine, Dr. Grégory Stoclet**

Soutenue le 19/10/2023 par :

**M. Bernard Miranda Campos**

---

## Composites à matrice copolymère à base de PLLA produits par TP-RTM

---

<b>Président du jury</b>	Vincent Monteil	Directeur de recherche	CNRS
<b>Rapporteur</b>	Yves Grohens	Professeur	Université Bretagne Sud
<b>Rapporteuse</b>	Claire Longuet	Maître assistant	IMT Mines Alès
<b>Examinatrice</b>	Mylène Lagardère	Maître de conférence	IMT Nord Europe
<b>Directrice</b>	Fanny Bonnet	Directrice de recherche	CNRS, Université de Lille
<b>Co-directrice</b>	Gaëlle Fontaine	Professeur	Centrale Lille
<b>Co-encadrant</b>	Grégory Stoclet	Maître de conférence	Université de Lille
<b>Invité</b>	Serge Bourbigot	Professeur	Centrale Lille



## **Acknowledgements**

I would like to express my gratitude to my supervisors Dr. Fanny Bonnet, my co-supervisor, Pr. Gaëlle Fontaine and co-supervisor Dr. Grégory Stoclet. Their guidance, support, and mentorship have been invaluable throughout my PhD journey.

I am also thankful to Pr. Serge Bourbigot, leader of “Ingénierie des Systèmes Polymères - ISP” team at UMET, for his scientific contribution and Pr. Patrice Woisel, director of “Unité Matériaux et Transformation – UMET” for allowing me to join the laboratory. I would like to acknowledge the financial support provided by the Région Hauts-de-France and University of Lille, which allowed me to pursue my research with the necessary resources.

I wish to express gratitude to Pr. Yves Grohens and Dr. Claire Longuet, who accepted to review this manuscript and to be part of the jury. I also like to thank Dr. Vincent Monteil, Dr. Mylène Lagardère and Pr. Serge Bourbigot for also accepting to be part of the jury.

I extend my appreciation to my colleagues and fellow researchers for their valuable insights, stimulating discussions, and collaborative efforts that enriched my research. I'd like to mention my appreciation to all Ph.D. students and post-docs, Marie-Odile, Louis, Melvin, Qi, Roxanne, Mingwei, Mathieu, Kimkevin, Xavier, Eric, Manon, Adele, Julie, Olawale, Kossigan. Also, special thanks to my Brazilian friends Ana, Pedro and Renata who chosen the same way as me: the research. A decade past since we met and our passion for research bring us at University of Lille to develop and share our way to do research.

This work could have not been possible without the support of all engineers and technicians. My sincere appreciation to Johan, Pierre, Anaïs, Guillaume, Aurélie, Maxence, Corinne, Isabelle, Severine and Benjamin.

I am grateful to my family for their unwavering support, encouragement and understanding. Their belief in me kept me motivated throughout this challenging journey. Lastly, I am thankful to all my friends in France and in Brazil who stood by me, offering encouragement, reminding me that there is life beyond research.

This thesis would not have been possible without the support and contributions of all these individuals and institutions. Thank you all.



# Summary

<b>CHAPTER I: LITERATURE REVIEW</b> .....	<b>5</b>
<b>1.1 Composite materials</b> .....	<b>7</b>
1.1.1 Polymer composite materials.....	7
1.1.2 Reinforcement fibers.....	9
1.1.2.1 Glass fibers .....	12
1.1.2.2 Carbon fibers.....	14
1.1.2.3 Flax fibers.....	16
<b>1.2 Biopolymers and biocomposites</b> .....	<b>18</b>
1.2.1 Poly(lactic) acid .....	21
1.2.2 PLA synthesis.....	22
1.2.3 PLA/PCL blends .....	27
1.2.4 Poly(L-lactide-co- $\epsilon$ -caprolactone).....	29
1.2.5 PLLA matrix composites .....	31
<b>1.3 Manufacturing polymer matrix composites</b> .....	<b>33</b>
1.3.1 Filament winding.....	34
1.3.2 Pultrusion .....	35
1.3.3 Compression molding.....	35
1.3.4 Injection molding.....	36
1.3.5 Vacuum infusion .....	37
<b>1.4 Thermoplastic resin transfer molding (TP-RTM)</b> .....	<b>37</b>
1.4.1 Resin flow in resin transfer molding .....	41
1.4.2 Voids in fiber-reinforced composites produced by RTM .....	44
1.4.3 Reactive thermoplastic systems in TP-RTM .....	45
1.4.3.1 Polyamides matrix composites .....	46
1.4.3.2 Poly(methyl methacrylate) matrix composites.....	47
1.4.3.3 Bio-based and biodegradable matrices used in TP-RTM .....	48
1.4.3.3.1 Poly( $\epsilon$ -caprolactone) matrix composites .....	48
1.4.3.3.2 Poly(L-lactide) matrix composites.....	49
1.4.3.4 Poly (butylene terephthalate) matrix composites.....	49
1.4.3.5 Future trends of thermoplastic systems .....	51
<b>1.5 Conclusion</b> .....	<b>54</b>



<b>CHAPTER II: MATERIALS AND METHODS .....</b>	<b>56</b>
<b>2.1 Materials.....</b>	<b>58</b>
2.1.1 Reagents .....	58
2.1.2 Reinforcements .....	58
2.1.3 Mold surface treater and release agent.....	59
2.1.4 TP-RTM apparatus .....	60
2.1.5 TP-RTM Mold .....	61
<b>2.2 Production of composites.....</b>	<b>61</b>
2.2.1 Preparation of reinforcements and mold .....	62
2.2.2 Preparation of reagents .....	62
2.2.3 Injection step .....	63
2.2.4 Polymerization .....	64
2.2.5 Cooling and demolding .....	64
2.2.6 Summary of the production of composites in TP-RTM .....	64
<b>2.3 Physicochemical characterization .....</b>	<b>65</b>
2.3.1 Proton nuclear magnetic resonance spectroscopy ( <sup>1</sup> H NMR).....	65
2.3.2 Size Exclusion Chromatography (SEC) .....	67
2.3.3 Thermogravimetric analysis (TGA) .....	68
2.3.4 Differential scanning calorimetry (DSC) .....	68
<b>2.4 Mechanical testing.....</b>	<b>69</b>
2.4.1 Tensile testing .....	69
2.4.2 Three-point bending testing .....	70
2.4.3 Impact testing .....	71
2.4.4 Cyclic three-point bending test.....	72
<b>2.5 Fiber mass ratio and fiber volume ratio .....</b>	<b>72</b>
<b>2.6 Digital microscopy.....</b>	<b>74</b>
<b>2.7 Accelerated ageing method .....</b>	<b>75</b>
<b>2.8 Conclusion.....</b>	<b>76</b>
<b>CHAPTER III: Glass fabric reinforced composites produced by TP-RTM.....</b>	<b>78</b>
<b>3.1 Study of the viscosity of the reactive thermoplastic system .....</b>	<b>80</b>
<b>3.2 Optimization of polymerization parameters.....</b>	<b>82</b>
3.2.1 Polymerization temperature .....	82
3.2.2 Polymerization time .....	82

3.2.3	Co-monomers over catalyst molar ratio .....	84
<b>3.3</b>	<b>Characterization of glass fabric reinforced composites.....</b>	<b>85</b>
3.3.1	Conversion of monomers and molecular weight of matrices .....	86
3.3.2	Copolymer matrix composition.....	86
3.3.3	Thermal properties of the matrices .....	88
<b>3.4</b>	<b>Characterization of voids in glass fabric reinforced composites .....</b>	<b>92</b>
<b>3.5</b>	<b>Mechanical properties of glass fabric reinforced composites .....</b>	<b>95</b>
3.5.1	Tensile test.....	95
3.5.2	Three-point bending test.....	100
3.5.3	Impact test.....	105
<b>3.6</b>	<b>Optimization of polymerization temperature .....</b>	<b>107</b>
3.6.1	Visual observation of composite plates.....	108
3.6.2	Monomers conversion and molecular weight of PLCL matrices at different polymerization temperatures .....	108
3.6.3	Copolymer composition of PLCL matrices .....	109
3.6.4	Thermal properties of PLCL matrices .....	111
<b>3.7</b>	<b>Mechanical properties of glass fabric reinforced composites produced at various temperatures. ....</b>	<b>112</b>
<b>3.8</b>	<b>Conclusion.....</b>	<b>122</b>
<b>Chapter IV: Carbon fabric reinforced composites produced by TP-RTM .....</b>		<b>123</b>
<b>4.1</b>	<b>Production of carbon fabric reinforced composites (CFRC).....</b>	<b>125</b>
4.1.1	Conversions of monomers and molecular weights of matrices.....	127
4.1.2	Copolymer matrices composition of PLCL/CF composites.....	127
4.1.3	Thermal properties of the matrices .....	128
<b>4.2</b>	<b>Characterization of voids on carbon fabric reinforced composites.....</b>	<b>132</b>
<b>4.3</b>	<b>Three-point bending test of CFRC.....</b>	<b>135</b>
<b>4.4</b>	<b>Conclusion.....</b>	<b>142</b>
<b>CHAPTER V: Biocomposites and accelerated ageing .....</b>		<b>143</b>
<b>5.1</b>	<b>Flax fabric reinforced PLLA composites .....</b>	<b>145</b>
5.1.1	Production of flax fabric reinforced composites.....	145
5.1.2	Thermal stability of flax fabric .....	146
5.1.3	Conversion and molecular weight .....	147
5.1.4	Thermal properties of PLLA matrices.....	148

5.1.5	Characterization of voids on flax reinforced PLLA composites .....	150
5.1.6	Mechanical properties of flax fabric reinforced composites .....	152
5.1.7	Conclusion.....	156
<b>5.2</b>	<b>Ageing of composites .....</b>	<b>156</b>
5.2.1	Investigating the impact of accelerated ageing test on thermal properties, molecular weight, and mechanical performance of composites .....	159
5.2.1.1	Glass fabric reinforced composites (GFRC).....	159
5.2.1.2	Carbon fabric reinforced composites .....	164
5.2.1.3	Flax fabric reinforced composites .....	168
5.2.2	Conclusion.....	172
<b>5.3</b>	<b>General conclusion .....</b>	<b>173</b>
	<b>General conclusion.....</b>	<b>175</b>
	<b>Outlook.....</b>	<b>178</b>
	<b>Appendix .....</b>	<b>218</b>

## ABREVIATIONS

<b>10 PLCL</b>	Poly(L-lactide- <i>co</i> - $\epsilon$ -caprolactone) - Matrix with 10 mol% of $\epsilon$ -CL and 90 mol% of L-LA
<b>10 PLCL/GF</b>	Poly(L-lactide- <i>co</i> - $\epsilon$ -caprolactone)( 10 mol% of $\epsilon$ -CL and 90 mol% of L-LA) matrix composite reinforced with glass fabric
<b><math>^1\text{H NMR}</math></b>	Proton nuclear magnetic resonance
<b>20 PLCL</b>	Poly(L-lactide- <i>co</i> - $\epsilon$ -caprolactone) - Matrix with 20 mol% of $\epsilon$ -CL and 80 mol% of L-LA
<b>20 PLCL/CF</b>	Poly(L-lactide- <i>co</i> - $\epsilon$ -caprolactone)( 20 mol% of $\epsilon$ -CL and 80 mol% of L-LA) matrix composite reinforced with carbon fabric
<b>20 PLCL/GF</b>	Poly(L-lactide- <i>co</i> - $\epsilon$ -caprolactone)( 20 mol% of $\epsilon$ -CL and 80 mol% of L-LA) matrix composite reinforced with glass fabric
<b>30 PLCL</b>	Poly(L-lactide- <i>co</i> - $\epsilon$ -caprolactone) - Matrix with 30 mol% of $\epsilon$ -CL and 70 mol% of L-LA
<b>30 PLCL/CF</b>	Poly(L-lactide- <i>co</i> - $\epsilon$ -caprolactone)( 30 mol% of $\epsilon$ -CL and 70 mol% of L-LA) matrix composite reinforced with carbon fabric
<b>30 PLCL/GF</b>	Poly(L-lactide- <i>co</i> - $\epsilon$ -caprolactone)( 30 mol% of $\epsilon$ -CL and 70 mol% of L-LA) matrix composite reinforced with glass fabric
<b>CBT</b>	cyclic butylene terephthalate
<b><math>\text{CDCl}_3</math></b>	Deuterated chloroform
<b>CF</b>	Carbon fabric
<b>CFRC</b>	Carbon fabric reinforced composites
<b><math>\text{CHCl}_3</math></b>	Chloroform
<b><math>\bar{D}</math></b>	Dispersity
<b>DSC</b>	Differential scanning calorimetry
<b>DTG</b>	Derivative thermogravimetry
<b><math>E_b</math></b>	Bending modulus
<b><math>E_t</math></b>	Tensile modulus
<b>FF</b>	Flax fabric
<b>FFRC</b>	Flax fabric reinforced composites

<b>GF</b>	Glass fabric
<b>GFRC</b>	Glass fabric reinforced composites
<b>LCM</b>	Liquid composite molding
<b>L-LA</b>	L-lactide
<b>MMA</b>	methyl methacrylate
<b>MWCNT</b>	multi-walled carbon nanotubes
<b>PA-6</b>	Polyamide-6
<b>PA-11</b>	Polyamide-11
<b>PA-12</b>	Polyamide-12
<b>PAN</b>	Polyacrylonitrile
<b>PBAT</b>	Polybutylene adipate terephthalate
<b>PBS</b>	Polybutylene succinate
<b>PBT</b>	Poly(cyclic butylene terephthalate)
<b>PCL</b>	Polycaprolactone
<b>PDLA</b>	Poly(D-lactide)
<b>PDLLA</b>	poly(D,L-Lactide)
<b>PET</b>	Polyethylene terephthalate
<b>PHA</b>	Polyhydroxyalkanoate
<b>PLCL</b>	Poly(L-lactide-co- $\epsilon$ -caprolactone)
<b>PLCL/CF</b>	Poly(L-lactide-co- $\epsilon$ -caprolactone) matrix composite reinforced with carbon fabric
<b>PLCL/GF</b>	Poly(L-lactide-co- $\epsilon$ -caprolactone) matrix composite reinforced with glass fabric
<b>PLLA</b>	Poly(L-lactide)
<b>PLLA / CF</b>	Poly(L-lactide) matrix composite reinforced with carbon fabric
<b>PLLA/GF</b>	Poly(L-lactide) matrix composite reinforced with glass fabric
<b>PLLA/TW</b>	Poly(L-lactide) matrix composite reinforced with twill 2/2 flax fabric
<b>PLLA/UD</b>	Poly(L-lactide) matrix composite reinforced with unidirectional flax fabric
<b>PMMA</b>	Poly(methyl methacrylate)
<b>PP</b>	Polypropylene
<b>PS</b>	Polystyrene
<b>ROP</b>	Ring-opening polymerization

<b>RTM</b>	Resin transfer molding
<b>SEC</b>	Size exclusion chromatography
<b>Sn(Oct)<sub>2</sub></b>	Tin octoate
<b>T<sub>g</sub></b>	Glass transition temperature
<b>TGA</b>	Thermogravimetric analysis
<b>THF</b>	Tetrahydrofuran
<b>T<sub>m</sub></b>	Melting temperature
<b>TP-RTM</b>	Thermoplastic resin transfer molding
<b>TW</b>	Twill 2/2 flax fabric
<b>UD</b>	Unidirectional flax fabric
<b>VARTM</b>	Vacuum assisted resin transfer molding
<b>ε-CL</b>	ε-caprolactone
<b>σ<sub>b</sub></b>	Bending strength
<b>σ<sub>t</sub></b>	Tensile strength
<b>ω-LL</b>	ω-lauro lactam



## General introduction

Composites have revolutionized the domain of materials engineering by offering unique properties that combine the strengths of multiple constituent materials. These versatile materials consist of two or more distinct components, each one displaying different physical or chemical properties, working together to create a synergistic whole that surpasses the capabilities of individual constituents.<sup>1</sup> One of the most prominent subsets of composites is fiber-reinforced polymer composites, where strong fibers are associated within a polymer material, resulting in structures that possess exceptional strength-to-weight ratios, durability, and tailored performance characteristics.<sup>2</sup>

Fiber-reinforced polymer composites have been successfully utilized for many decades in numerous engineering applications, such as automotive, aerospace, construction, among others.<sup>3</sup> These composites are undoubtedly the most widely used composites type, notably due to its high strength, lightweight nature and durability.<sup>4</sup> Between 2023 and 2028, the fiber-reinforced polymer composites market is expected to experience a consistent annual growth rate (CAGR) of over 4.5%.<sup>5</sup> The market is consolidated and dominated by major companies (Hexcel Corporation, Teijin Limited, Toray Industries Inc, SGL carbon, Mitsubishi Chemical Carbon Fiber and Composites Inc) with buyers mainly from automotive and aerospace industry.

The production of composite materials has been consistently associated with energy-consuming processes involving mainly non-renewable materials and generating substantial waste. In response to the growing concerns regarding environmental conservation and resource depletion, more sustainable practices have been adopted for composites production.<sup>6</sup>

Several key-aspects must be considered regarding the sustainability of fiber-reinforced polymer composites production:

- **Materials selection:** Sustainable composites production starts with the selection of raw materials. Choosing natural fibers (*i.e* flax, hemp, kenaf...) instead of synthetic ones (*i.e* carbon, glass...) or recycled fibers is an alternative to decrease the carbon footprint of the final part. Wastes from agro-industries, discarded consumer food, co-products generated in industries along with recycled materials, are all categorized as eco-friendly fillers.<sup>7</sup> Bio-based resins are emerging as a substitute to petroleum-based resins, thereby decreasing the dependence on fossil fuel resources.<sup>8,9</sup>



- Clean production: Reducing the energy consumption and the waste of materials are the main goal to the employment of cleaner manufacturing processes.,<sup>10</sup> Additionally, these practices support the use of renewable energy sources and materials, along with sustainable product design. This approach ensures the development of non-toxic products and processes.<sup>11</sup>
- End-of-life management: The end-of-life of composite materials is a critical aspect of their lifecycle management, as it involves the disposal, recycling, or reuse of these materials once they have reached the end of their intended use.<sup>12</sup> Recycling, upcycling and reuse are the best alternatives to be considered in composites end-of-life. Recycling technologies to separate the reinforcement from the matrix have been developed in the last years, contributing to minimizes waste.<sup>13</sup>
- Life cycle assessment: The environmental impact of composites production can be evaluated by life cycle assessment (LCA) and so serving as a decision-guide to optimize the process to reduce the environmental impact.<sup>14</sup>

By combining these sustainable practices, the production of fiber reinforced polymer composites becomes more environmentally friendly. This approach is in line with the global shift towards a more circular and sustainable economy.

Historically, thermoset resins like epoxy and phenolic resins have been widely used in fiber-reinforced composites due to their excellent mechanical properties, high temperature resistance, and good chemical resistance.<sup>4,15</sup> In recent years, the use of thermoplastics as matrices in composites has been increasing. Thermoplastics like polypropylene (PP), polyethylene (PE), polyetheretherketone (PEEK), and polyamide (PA) offer advantages such as improved impact resistance, recyclability, and the ability to be reshaped upon heating.<sup>16</sup>

More and more bio-based and biodegradable polymers (thermosets and thermoplastics) have been employed in composites. Bio-based thermosets, epoxy and benzoxazines, issued from vegetable oils *i.e* castor oil, soybean oil and linseed oil have been extensively investigated in the last years.<sup>17</sup> Regarding bio-based thermoplastics employed in composites, one can cite poly( $\omega$ -undecanamide) (PA-11), poly(hidroxy alcanoate) (PHA), poly(lactic acid) (PLA).<sup>18,19</sup>

In the context of materials selection, poly (lactic acid) also known as polylactide (PLA) has been widely employed as a matrix in fiber reinforced composites once this polymer is bio-based and biodegradable, which contributes to a “greener” production. Traditionally, the manufacturing of PLA matrix composites is made by injection or compression molding, under high pressures to insure the proper impregnation of the reinforcements since molten PLA displays high viscosity.<sup>20,21</sup> These processes can be replaced by less energy-intensive ones *i.e* manufacturing process belonging to the family of Liquid Composite Molding (LCM).

Among them, one can find vacuum infusion process (VI), resin transfer molding (RTM), vacuum assisted resin transfer molding (VARTM). The particularity of these techniques is the use of low viscosity resins which are injected through the reinforcement given rise to composites with low voids content.

More specifically, the RTM process, originally designed for low viscosity thermoset resins, has been used since 1950. In the last 20 years, researchers developed thermoplastic resins for RTM process, to design recyclable polymer composites. Since now, some thermoplastic resins have been employed by manufactures in this technique *i.e* polyamides, polyacrylates, poly(butylene terephthalate).<sup>22</sup> When thermoplastics are utilized in RTM process, it is common to refer to these as Thermoplastic Resin Transfer Molding (TP-RTM). Since the applicability of TP-RTM is limited to low viscosity resins, monomers are used instead of polymers in this technique. Monomers are associated to an activators and/or catalysts and the resulting mixture called “reactive thermoplastic system”, disposes viscosity lower than 1 Pa.s.

Up to date, the only bio-based thermoplastic employed as a composite matrix produced by TP-RTM is poly(L-lactide) (PLLA). In previous works conducted at UMET, PLLA / Glass fabric composites were successfully produced by TP-RTM, in which high monomer conversions along with high molecular weight matrices were reached.<sup>23</sup> Despite its advantages such as its bio-based nature and biodegradability (*i.e.* anaerobic digestion, industrial composting), PLLA is brittle which limit its applications.<sup>24</sup> To transcend this limitation, PLLA is either used as main component in blends with other polymers such as poly( $\epsilon$ -caprolactone) (PCL), either L-lactide is copolymerized with various co-monomers such as ethylene glycol and  $\epsilon$ -caprolactone ( $\epsilon$ -CL) in order to improve its elongation at break.<sup>25,26,27,28</sup> Poly(L-lactide-co- $\epsilon$ -caprolactone) copolymer (PLCL) is mainly used in biomedical fields due to its biodegradability and biocompatibility.<sup>28</sup> Depending on the copolymer composition, the elongation at break of PLCL can be 300 % higher than PLLA.<sup>27</sup>

In this context, the main objective of this thesis work was the production of poly(L-lactide-co- $\epsilon$ -caprolactone) (PLCL) matrix composites by TP-RTM and the evaluation of their chemical, thermal and mechanical properties. The copolymerization of L-LA with  $\epsilon$ -CL with tin octoate ( $\text{Sn}(\text{Oct})_2$ ) as the catalyst was conducted into the mold with pre-disposed reinforcements. In a first approach, glass and carbon fabrics were selected as reinforcements for their inertness to prevent side reactions with the catalyst. In a second part of the present work, fully bio-based PLLA /flax composites were successfully produced by TP-RTM. Regarding the end-of-life management, accelerated ageing test were performed on all composites prepared in this study.

The present manuscript is thus divided in five chapters. The first one gives a general background about composite materials and their manufacturing techniques. A focus is done in TP-RTM process, in which the process parameters and its applicability to thermoplastic polymers are presented. The synthesis, the thermal characterization, and the mechanical properties of PLLA and PLCL (co-)polymers, PLA/PCL blends and PLLA as matrix in composites are discussed.

In the second chapter, the materials and experimental methods employed in this study are provided. All the reagents and raw materials used in the TP-RTM process as so as the different steps of the process are described. Then, characterization methods and accelerated ageing tests are presented, allowing the evaluation of the mechanical properties of the composites produced by TP-RTM.

The third chapter reports the production of glass fabric reinforced composites (GFRC), in which PLLA and PLCL were used as matrices. The monomers conversions, the molecular weights and the thermal properties of the matrices were examined. The mechanical properties (tensile, bending, impact) of these composites are presented and an investigation of the fracture of the composites was done via by microscopy analysis.

In chapter four, the production of carbon fabric reinforced composites (CFRC) by TP-RTM with PLLA and PLCL as matrices was studied. The monomers conversions, the molecular weights and the thermal properties of the matrices were studied as well as their influence on bending properties of composites.

The last chapter deals with the production of flax fabric reinforced composites (FFRC) by TP-RTM, in which PLLA was used as the matrix. Chemical and thermal properties of the matrix and fibers were studied as well the mechanical properties of PLLA / flax composites. Furthermore, accelerated ageing tests were performed on GFRC, CFRC and FFRC to evaluate the impact of accelerated ageing on chemical, thermal and mechanical properties of these composites.

Upon concluding this project, a general conclusion is presented, along with a prospective overview of potential areas for future research within this subject matter.

## **CHAPTER I: LITERATURE REVIEW**

This chapter presents general information on composites, biopolymers, biocomposites and their manufacturing techniques. More specifically, a review on poly (lactic acid) synthesis, its copolymers and blends with other polymers and its applications as composites is proposed. An analysis of the works carried out on thermoplastics used in resin transfer molding process is presented. This literature review will particularly focus on process parameters, and chemical, physical, and mechanical properties of thermoplastic composites produced via this technique. This bibliographic study will allow us to target more particularly the specificities of the use of poly (lactic acid) and poly(L-lactide-co- $\epsilon$ -caprolactone) as matrices in resin transfer molding process and their combination with different reinforcements (glass, carbon, and flax fabrics).



## 1.1 Composite materials

A composite material is a macroscopic combination of two or more materials in which a finite interface is well-defined between them (Figure 1). Consisting of reinforcements – continuous or non-continuous surrounded by a matrix, the composite materials combine the performance of its constituents resulting in a material with performances unattainable by the individual components.<sup>29</sup> The continuous phase – the matrix – can be metallic, mineral, or polymer while the nature of the dispersed phase – the reinforcement is present in the form of particles, flakes, whiskers, short fibers, continuous fibers, or sheets.<sup>1</sup>

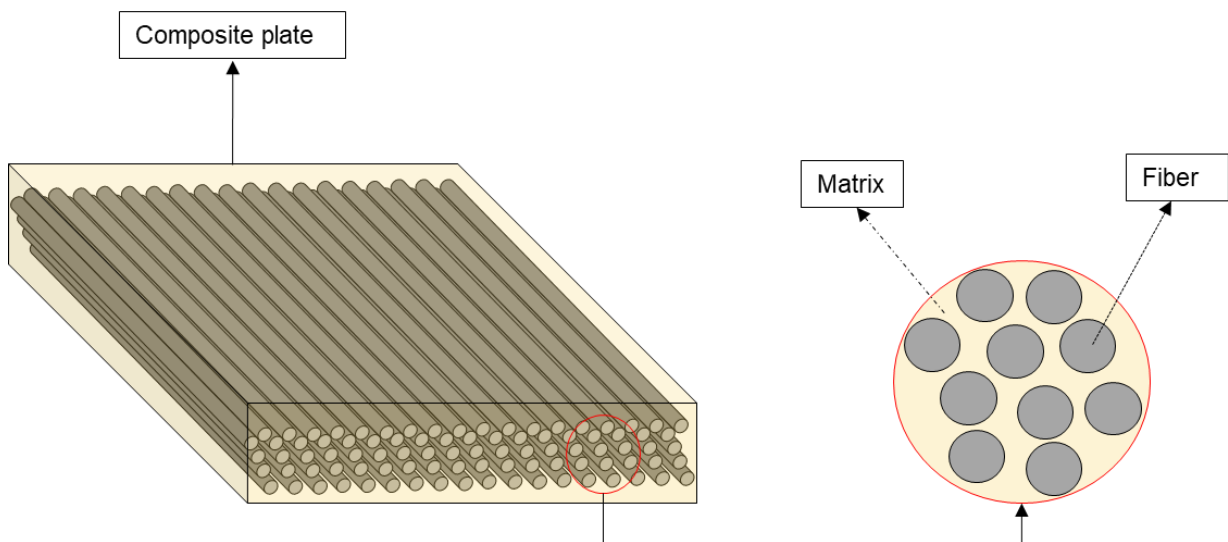


Figure 1: Scheme of composite material with unidirectional fibers.

The association of matrix and reinforcement depends on the chemical compatibility between the phases, the manufacturing process, the mechanical requirements of the final part, the chemical resistance desired, and the cost of the manufacturing process and the raw materials.<sup>16</sup> The role of the reinforcement in a composite is to support the applied load and supply structural properties like strength, stiffness, and thermal stability.<sup>2</sup>

The functions of the matrix are to : ensure the cohesion and the orientation of the reinforcement; maintain desired fiber spacing; transfer the load to the reinforcement; protect the reinforcement from mechanical damages and provide rigidity and shape to the structure.<sup>16</sup>

### 1.1.1 Polymer composite materials

Polymer composite materials are a combination of a polymer – the continuous phase – with a reinforcement to improve the global performances of the resulting material. The polymer matrix can be a thermoplastic or a thermoset, giving rise to composites with unique physical, chemical,<sup>16</sup> and structural properties.

Thermosetting polymers are characterized by an irreversible change in the solidification process. The conversion into a bulk hard solid is initiated by the chemical hardener forming chemical cross-links between the polymer chains. This process is commonly called the “curing process” and once cured, thermosetting resins cannot be melted. The mechanical properties of thermosetting polymers are determined by the molecular units that consist of the cross-linking polymer network, and the length and the crosslinking density. Thermosetting polymers are usually brittle materials with low strain at break due to the tightly bound polymer network.<sup>30</sup>

Generally, thermoset resins display a low viscosity (< 1Pa.s), and due to their characteristics, these resins have been extensively used in composite materials leading to the good impregnation of reinforcements.<sup>15</sup> The most common types of thermosetting resins are unsaturated polyesters and epoxy.

Nowadays, the increasing demand for high-performance composites is confronted with the recyclability at the end-of-life of the thermosetting composites. Because of the high density of cross-links, thermosetting polymers cannot be reprocessed, making the recycling process very complex. In this way, thermoplastic polymers, which can be molten and thus theoretically reprocessed, are more and more investigated to replace thermosetting as matrices in polymer composites.<sup>16</sup> A restricted number of heating and cooling cycles can be performed without any structural or functional effects such as color and shape modification, microstructural alteration, and mechanical dysfunction.<sup>31</sup>

Thermoplastic polymers find application in the composite industry due to their notable attributes, including high ductility, elevated melting temperatures, and robust chemical resistance. In particular, polypropylene (PP)<sup>32</sup>, high-density polyethylene (HDPE)<sup>33</sup> polyethylene terephthalate (PET)<sup>34</sup>, aliphatic polyesters such as polyamide 6 (PA-6)<sup>35</sup> polyamide 66 (PA-66)<sup>36</sup> polylactide (PLA)<sup>37</sup> and polyether ether ketone (PEEK)<sup>38</sup> poly(methyl methacrylate) (PMMA)<sup>39</sup> are the main thermoplastics used in composites.

Compared to thermosetting composites, thermoplastics display some advantages such as recyclability, faster processing cycle without curing stages, facility to demold, and the possibility of post-processing, *i.e.* joining fusion, allowing the production of large composite parts. Due to their advantages, thermoplastic composites are becoming more and more popular and they are being used in many applications such as transportation<sup>40</sup>, military <sup>41</sup>, shipbuilding<sup>42</sup>, and wind energy sector<sup>43</sup> but especially in the automotive industry in parts like spare-wheel pans, door modules, and instrument panel carrier.<sup>44</sup> However, a primary challenge associated with employing thermoplastics in composites is the typically weak interface between the matrix and the reinforcement, along with a notable presence of voids.

This is primarily attributed to the elevated melt viscosity of the polymer. Indeed, this high viscosity makes the impregnation of the reinforcement by the matrix difficult, leading to the formation of voids. Studies have been done to decrease the viscosity of these thermoplastics and to use of molten monomers instead molten polymers in some composite manufacturing techniques.<sup>45,46</sup> Various thermoplastics displaying low viscosity and reactive thermoplastic systems, composed of a mixture of monomer(s) and a catalyst, are presented in Section 1.4.3.1 (p.46).

### **1.1.2 Reinforcement fibers**

The most commonly reinforcements used in polymer composite materials are fibers. They are constituted of thousands of filaments with diameters varying from 5 to 15  $\mu\text{m}$ .<sup>2</sup> These fibers are generally used to produce textiles and they are commercialized as short fibers *i.e* felt, mat, and long fibers *i.e* woven textiles. It exists natural and synthetic fibers and their selection must be done with respect to the envisaged application of the composite material.<sup>1</sup> Textile fibers are often classified according to its origin (Figure 2).<sup>47</sup> Among human-made fibers, undoubtedly the most employed fibers in the composite industry are glass, carbon, and aramid fibers. Flax and hemp fibers are the most used natural fibers.<sup>48</sup>

The filaments assembled in form of fibers can take two forms: continuous or discontinuous and both types can be manufactured in textiles.<sup>2</sup> Continuous fibers can be assembled in yarn or roving (Figure 3). These fibers have a homogeneous structure in their length and also in the final product. On the other hand, discontinuous fibers are not homogeneous along the length, and the final product display imperfections.<sup>3</sup> Before the filament winding, the fibers are submitted to a chemical or physical surface treatment, depending on the nature of the fiber, to improve the adhesion with the matrix and also to decrease the abrasion during the filament winding.<sup>49</sup>



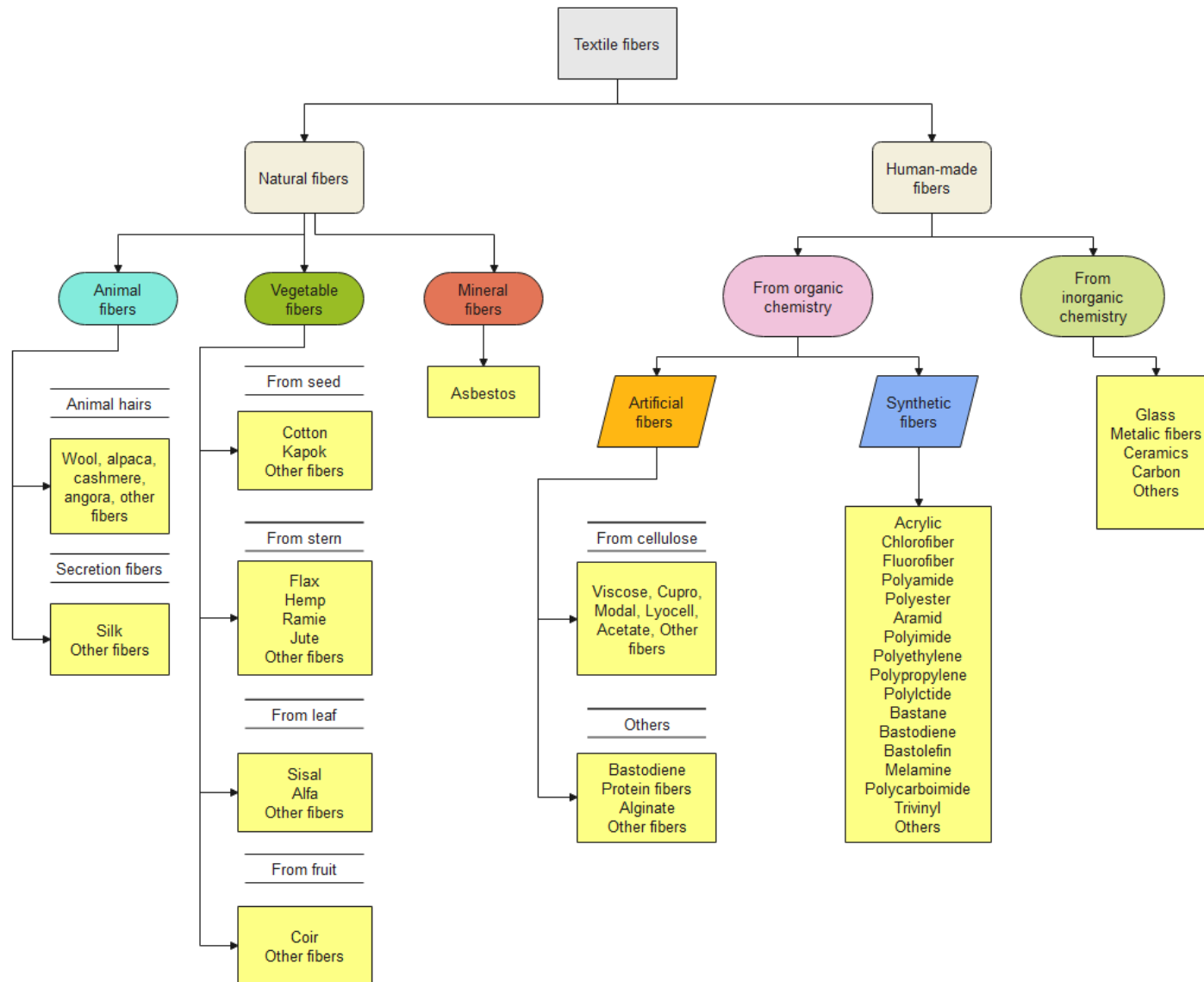


Figure 2: Classification of textile fibers.<sup>50</sup>

The assemblage of fibers to make fiber forms can take unidimensional (unidirectional tows, yarns, or tapes), bidimensional (woven or non-woven fabrics, felt or mats), and multidimensional (3D structures) forms. In general, woven, non-woven fabrics and more recently 3D structures are currently chosen to be used as reinforcement in composite materials.<sup>51</sup>

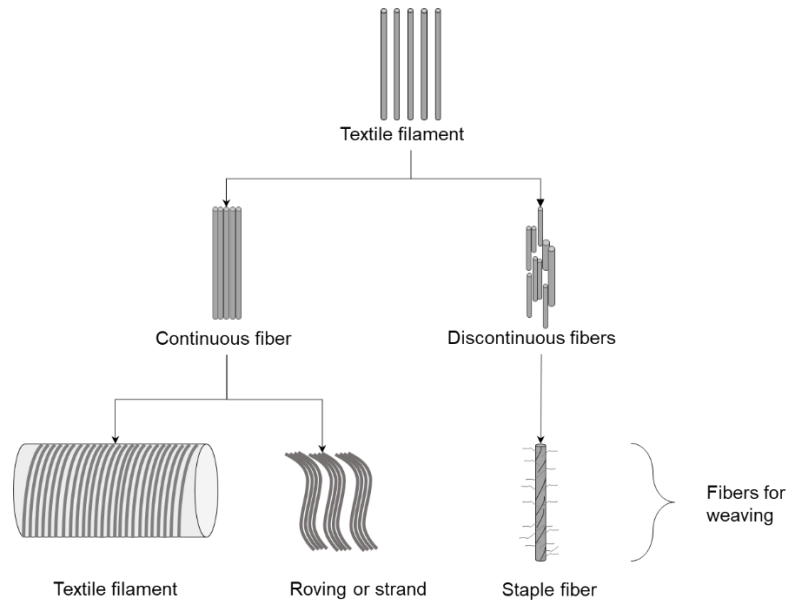


Figure 3: Different forms of fibers.<sup>1</sup>

The woven fabrics are made of fibers assembled in two perpendicular directions where the fill yarns pass over and under the warp yarns to form a pattern. The patterns can take the form of a plain, leno, satin, or twill weave (Figure 4).<sup>52</sup>

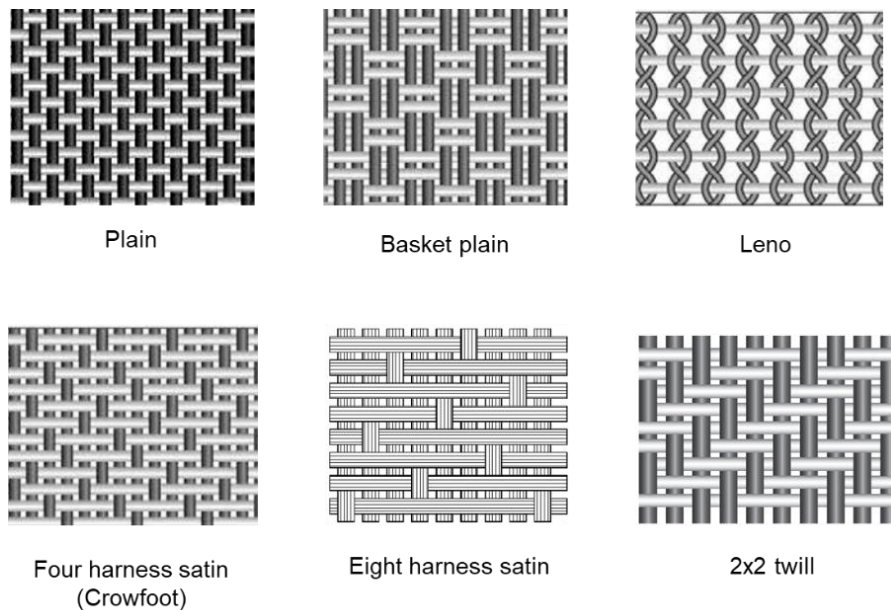


Figure 4: Different forms of patterns of woven fabrics.<sup>53</sup>

The choice of the pattern depends on the geometry of the composite part. For example, plain weave is more rigid than satin, leno, and twill weave, so it is more difficult to lay the fabric in the non-flat parts. However, the manipulation of satin and twill weave is more problematic than plain weave because of the lack of stability of the yarns which are less present in plain weave.<sup>30</sup> The 2x2 twill has the better drapability of all forms of patterns and so more employed in parts with complex geometries.<sup>53</sup>

### 1.1.2.1 Glass fibers

Glass fibers are used in polymer matrix composites particularly in the automobile and wind energy sectors due to their relatively low price, high strength, and fire resistance.<sup>54</sup> Glass fibers are mainly composed of silicon dioxide ( $\text{SiO}_2$ ), calcium dioxide ( $\text{CaO}$ ) and other additives ( $\text{Al}_2\text{O}_3$ ,  $\text{B}_2\text{O}_3$ ,  $\text{K}_2\text{O}$ ,  $\text{Na}_2\text{O}$ ...). The different ratios of these oxides affords glass fibers different physical, chemical, and electrical properties.

The E and S glass fibers are the most employed in composite industry, due to its high strength and they are mainly composed by  $\text{SiO}_2$  and  $\text{Al}_2\text{O}_3$ . A and D glass fibers are used in electrical applications and C and R glass fibers are used in corrosive environments (Table 1).<sup>4</sup>

Table 1: Classification, chemical composition and properties of glass fibers.

Classification	Chemical composition (wt %)							Properties
	$\text{SiO}_2$	$\text{CaO}$	$\text{Al}_2\text{O}_3$	$\text{B}_2\text{O}_3$	$\text{K}_2\text{O}$	$\text{Na}_2\text{O}$	$\text{MgO}$	
A glass	67.5	6.5	3.5	1.5	3.0	13.5	4.5	High durability, strength and electric resistivity
C glass	65.0	13.4	4.1	5.0	0.5	9.6	3.3	High corrosion resistance
D glass	74.0	-	-	22.5	2.0	1.5	-	Low dielectric constant
E glass	52-56	16-25	12-16	8-13	0-1	0-1	0-6	High strength and electrical resistivity
R glass	60.0	9.0	24.0	-	0.1	0.5	6.0	High strength and acid corrosion resistance
S-glass	64-66	-	24-26	-	-	-	9-11	Highest tensile strength

The production of glass fibers starts with melting the raw materials (sand for  $\text{SiO}_2$ , clay for  $\text{Al}_2\text{O}_3$ , colemanite or boric acid for  $\text{B}_2\text{O}_3$ , and limestone or calcite for  $\text{CaO}$ ) in a furnace at around  $1600\text{ }^\circ\text{C}$ .<sup>55</sup> After exiting the furnace, the molten mixture is transported through the forehearth channel, eventually reaching a bushing. When the liquid glass exits the nozzle, it is rapidly cooled by cold air and water spray. It is then passed through the size applicator, a few meters below the bushing, at which point the glass is fully solidified (Figure 5).<sup>49</sup> After this step, the surface of the continuous glass filament is treated and is ready to be woven.

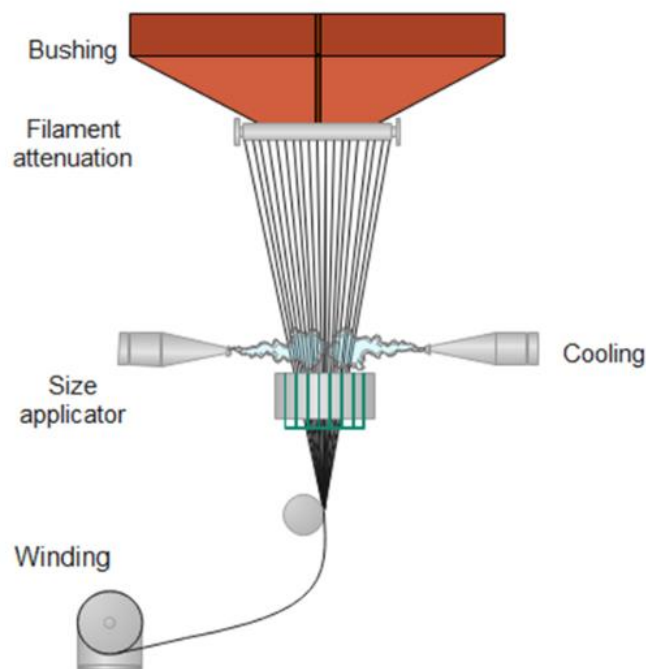


Figure 5: Continuous glass filament forming.

Regarding mechanical properties, glass fibers display a tensile strength between 4-5 GPa, a tensile modulus between 70-80 GPa, and a strain at break of 5%.<sup>18,56</sup> Additionally, glass fibers display a density around  $2.5\text{ g}\cdot\text{cm}^{-3}$ , higher than that of carbon ones ( $1.7\text{ g}\cdot\text{cm}^{-3}$ ).<sup>30</sup> The values presented regarding the mechanical properties of glass fibers are generic and each glass fiber disposes of a characteristic value. High values of ultimate stress are observed in unidirectional roving with a high volume fraction of fibers and, the lowest values of ultimate stress are observed in composites reinforced with mat and cut glass fibers (Figure 6). The mechanical properties of a composite depend not only on the mechanical properties of the reinforcement but also depends on the proportions and form of the reinforcement.<sup>2</sup>

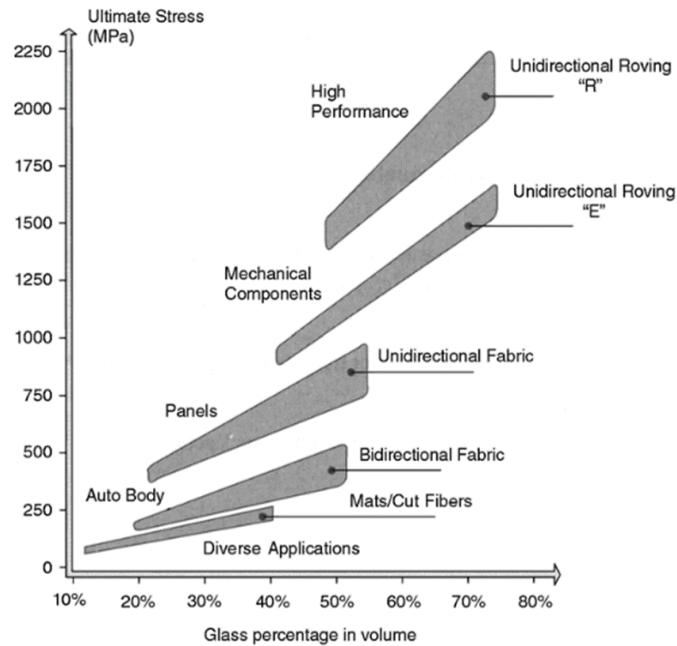


Figure 6: Tensile strength of epoxy/glass composites.<sup>1</sup>

### 1.1.2.2 Carbon fibers

Known for their lightness and high mechanical performance, carbon fibers are traditionally used in lightweight composite parts in the aerospace, defense, and automotive.<sup>1,2</sup> Commercially available carbon fibers are synthesized from polyacrylonitrile (PAN), pitch, or rayon with distinct mechanical properties. The production of carbon fibers starts with the polymerization of the desired precursor, followed by fiber spinning, fiber drawing, stabilization, and carbonization.<sup>57</sup> Following these steps, the fibers are often submitted to a surface treatment in order to improve the interfacial adhesion to enhance the mechanical properties of the composite product.<sup>58</sup> This is usually done with liquid oxidation which involves passing the carbon fiber through an electrolytic bath of nitric acid, sulfuric acid, or ammonium sulfate, with an electric current and a graphitic cathode plate. This treatment leaves the carbon fiber with carbonyl surface groups. Finally, a protective coating to prevent damage during handling and to make it compatible with the matrix material of the composite (epoxy, vinyl ester, urethane, thermoplastic, etc.) is conducted.<sup>57</sup>

PAN-based carbon fibers represent 96% of the market. They display a tensile strength between 3-7 GPa, a tensile modulus between 200-600 GPa and they are the lighter carbon fibers with a density around  $1.5-1.9 \text{ g.cm}^{-3}$ .<sup>58</sup> Pitch-based carbon fibers have a tensile strength around 1-4 GPa and a tensile modulus between 54 to 935 GPa. These fibers have a density higher than the last ones, around  $2 \text{ g.cm}^{-3}$ .

Rayon-based carbon fibers have less performing mechanical properties with tensile properties similar to those of glass fibers and their use is still limited due to production cost and lower mechanical properties.

Concerning the stretchability of PAN and pitch carbon fibers, it can vary from 0.3 to 2.5 %. A correlation of tensile strength and tensile modulus of PAN and pitch carbon fibers are shown in Figure 7, showing that pitch based carbon fibers display tensile modulus higher than PAN-based carbon fibers. However, the last ones have the highest values of tensile strength.<sup>57</sup>

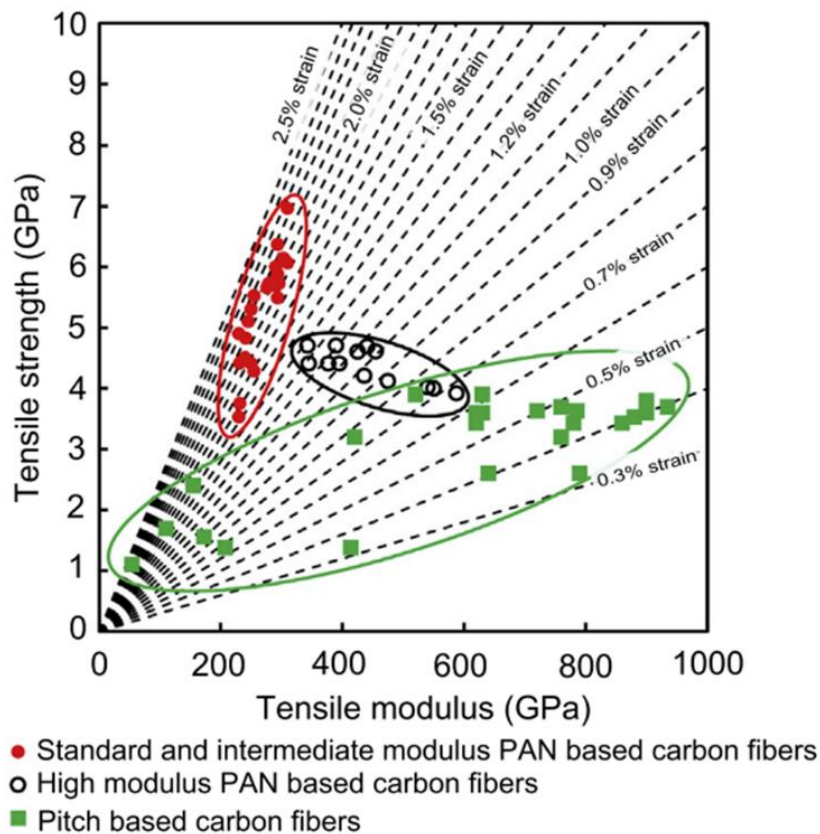


Figure 7: Tensile strength versus tensile modulus of PAN/pitch carbon fibers.<sup>57</sup>

Despite their remarkable mechanical properties, the majority of carbon fibers available in the market are oil-based. Because of the green industrial policy in which a transition towards a low-carbon economy is fixed, the next generation of carbon fibers tends to be issued from renewable resources such as lignin and cellulose.<sup>59,60</sup> Even if alternative routes for the production of “greener” carbon fibers were investigated, the mechanical properties of these fibers attempt only 10% of the theoretical upper limit.<sup>59</sup> In that way, the replacement of synthetic fibers by natural fibers in the composite field are also an alternative to produce eco-friendly materials.

### 1.1.2.3 Flax fibers

Flax fiber is one of the most popular natural fibers used in composites as reinforcement. Thermoplastic and thermosetting polymers can be used as matrices in flax composites, and they can be oil-based or bio-based. However, bio-based polymers are more commonly associated with flax fibers to produce a green composite.<sup>6</sup>

The main components of flax fiber are cellulose (64 – 75 wt %), hemicellulose (2 – 20 wt %), water (2 – 20 wt%), lignin (2.2 – 20.6 wt%), and pectin (1.8 – 2.3 wt%).<sup>61</sup> Cellulose is a semicrystalline polysaccharide, the strongest constituent, and gives stiffness to fiber. This constituent disposes of a large amount of hydroxyl group which gives a hydrophilic nature to this fiber. Hemicellulose is amorphous and is bounded to cellulose via hydrogen bonds. Lignin and pectin are amorphous and act like bonding agents.<sup>62</sup>

The microstructure of flax fiber is relatively complex with two main cell walls (Figure 8). The primary cell wall, the outer one, is only 0.2  $\mu\text{m}$  thick. The secondary cell wall is composed of three layers: S1, S2, and S3. The S1 layer is the outermost layer of the secondary cell wall and is primarily composed of cellulose. It is responsible for providing strength and rigidity to the fiber. The S2 layer is the thickest layer of the secondary wall and is also composed of cellulose, but it has a higher degree of crystallinity than the S1 layer. The S3 layer is the innermost layer of the secondary wall and is composed of lignin and hemicellulose. Due to its amorphous character, it is responsible for providing flexibility and compressibility to the fiber.<sup>62,63</sup>

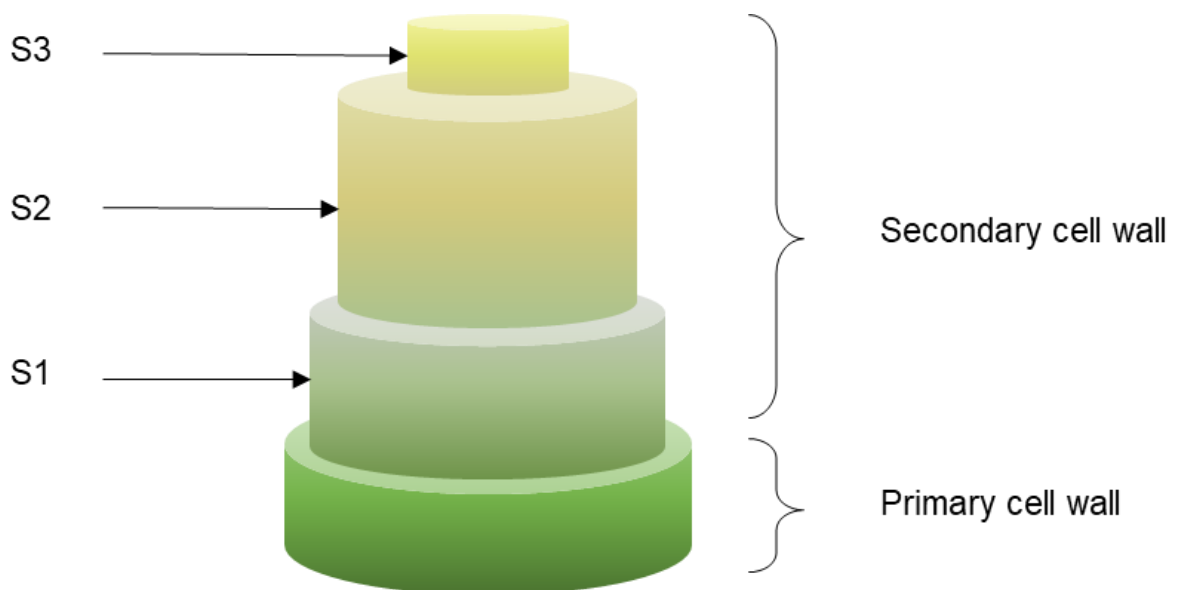


Figure 8: Microstructure of flax fiber cell.

Flax fiber has a lower density of  $1.5 \text{ g.cm}^{-3}$  in comparison to glass fiber ( $2.5 \text{ g.cm}^{-3}$ ).<sup>4</sup> As a result, reinforced polymers with flax fibers display a lightweight structure. Furthermore, flax fiber exhibits a stiffness comparable to that of glass fiber, with a tensile strength ranging from 345-1100 MPa, Young's modulus of 28 GPa, and elongation at break around 3%.<sup>62</sup> Like synthetic fibers, flax fibers can be assembled in different forms to be used in polymer composites: mat, roving, fabric, short fiber, and yarn (Figure 9) and the selection of a suitable manufacturing process adapted to the fiber morphology can improve the mechanical properties of flax composites.

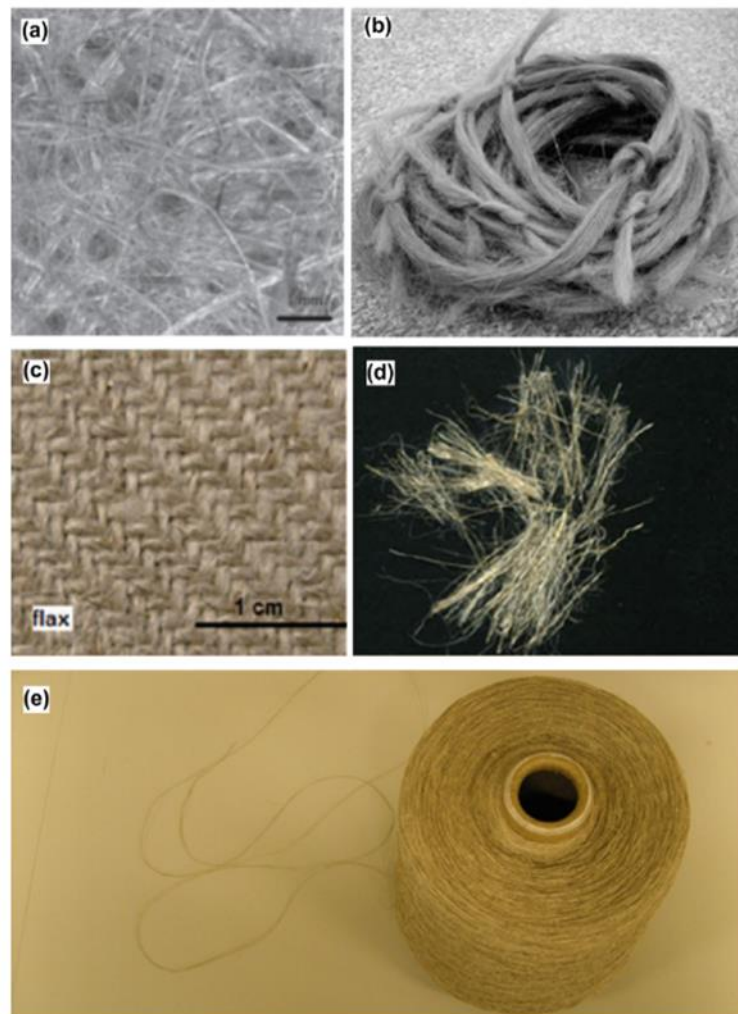


Figure 9: Different forms of flax fibers: (a) mat, (b) roving, (c) fabric, (d) short fibers, (e) yarn.<sup>62</sup>

Flax fibers have specific mechanical properties that make them a viable and cost-effective alternative to glass fibers for composite reinforcement. However, their main disadvantage lies in the inconsistency of their properties. Exposure to environmental factors such as high relative humidity can degrade the tensile properties of flax fibers. To address this, chemical treatments, can enhance the tensile strength and strain of these fibers and also increase the interfacial bonding fiber/matrix.



## 1.2 Biopolymers and biocomposites

The philosophy of eco-designing new materials is becoming a rule driven by the necessity to reduce greenhouse gas emissions and the rampant consumption of plastics. Several laws to reduce the consumption of plastics have been approved in the last ten years around the world, especially in European countries. The majority of the production of plastics is still oil-based and their production contributes to global warming and the contamination of ecosystems with macro and microplastics.<sup>64</sup> This is why biopolymers are seen as an alternative to oil-based polymers. To avoid any confusion, the definition of biopolymers, biodegradable polymers and biocomposites are presented next.

The definition adopted by the scientific community indicates that biopolymers are defined as polymers produced by/or derived from living organisms, such as plants and microbes, rather than from petroleum, the traditional source of polymers.<sup>65</sup>

Biodegradable polymers are materials that can work for a limited time before degrading into readily discarded products through a regulated procedure, they can be either bio- or fossil-based.<sup>48</sup> Biodegradability is not an intrinsic characteristic of biopolymers. Many, but not all biopolymers are biodegradable, nevertheless oil-based polymers can also be biodegradable. Several classifications of the most common biodegradable polymers are proposed by researchers and one of them is proposed in Figure 10. The majority of biopolymers are thermoplastics, but thermoset ones exist.<sup>8</sup>

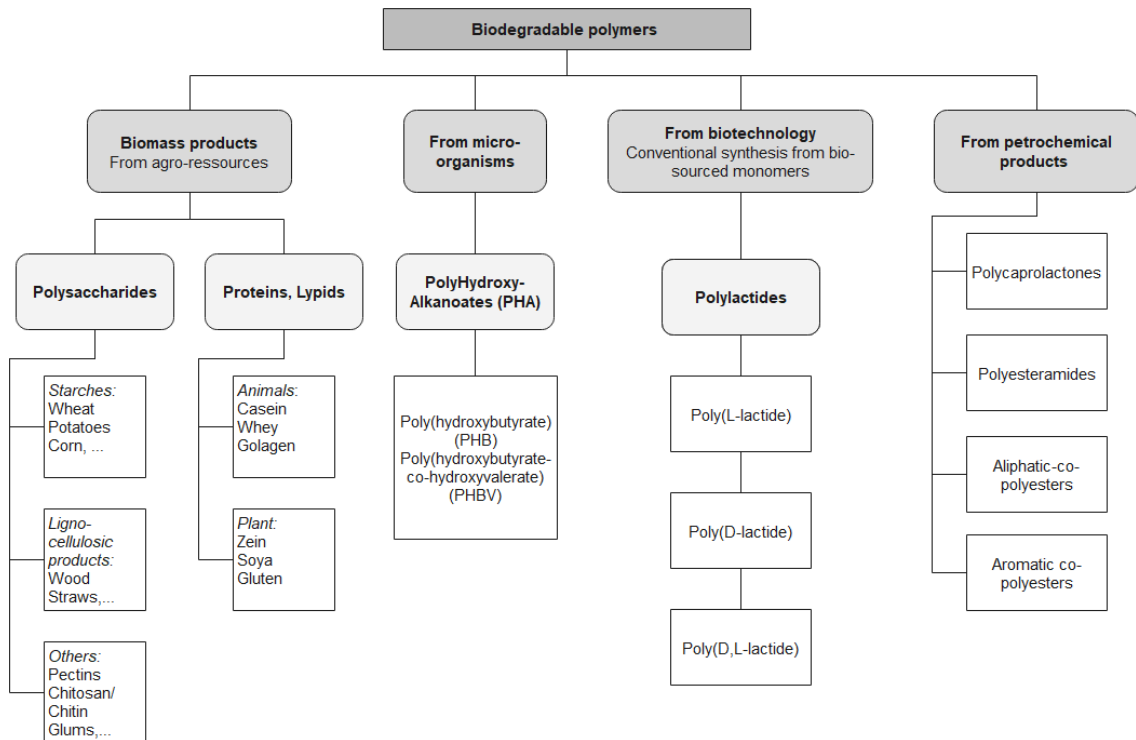
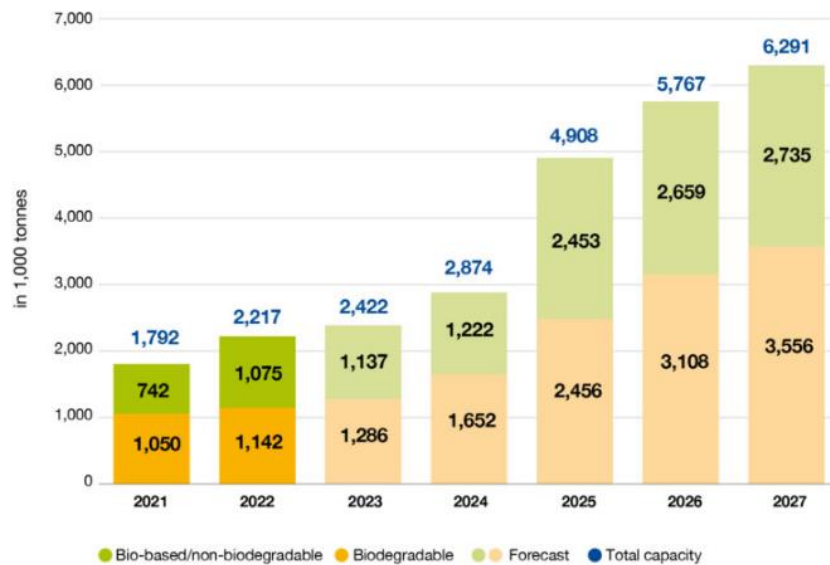


Figure 10: Classification of biodegradable polymers.<sup>66</sup>

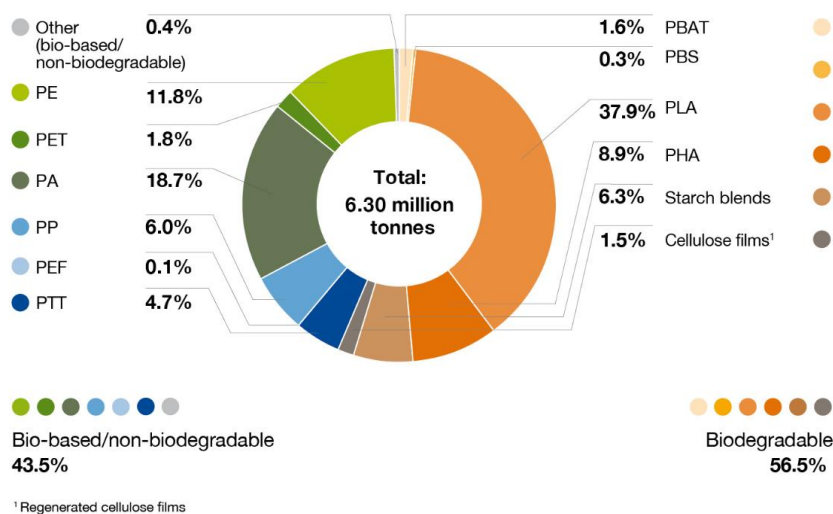
In 2021, the global production of bioplastics amounts to 1.8 million tonnes, and an increase to 6.3 million tonnes capacity in 2027 is expected. (Figure 11). The highest production growth is expected for poly (lactic acid) (PLA) since the industrial production of this biopolymer is mastered and because PLA displays similar physical and mechanical properties to some other oil-based polymers such as PET and can be an alternative for some applications. Its production is mainly concentrated in Asia, followed by Europe, North, and South America.<sup>67</sup>

### Global production capacities of bioplastics



Source: European Bioplastics, nova-Institute (2022). More information: [www.european-bioplastics.org/market](http://www.european-bioplastics.org/market) and [www.bio-based.eu/markets](http://www.bio-based.eu/markets)

### Global production capacities of bioplastics 2027 (by material type)



Source: European Bioplastics, nova-Institute (2022). More information: [www.european-bioplastics.org/market](http://www.european-bioplastics.org/market) and [www.bio-based.eu/markets](http://www.bio-based.eu/markets)

Figure 11: Bio-based polymers – Evolution of worldwide production capacities 2021 to 2027.<sup>67</sup>

Biodegradability can be influenced by a variety of factors, such as temperature, nutrients, oxygen, and microbial activity, which vary from one location to another. To be considered as biodegradable, the polymer must respect some degradation conditions in a specific environment such as a marine environment, fresh water, soil, home composting, landfill, anaerobic digestion, or industrial composting.<sup>68</sup> Even if the biodegradability of the polymer is confirmed, the specific end-of-life of each polymer must be respected.

In general, polymers issued from biomass (*i.e.* cellulose, starch...) or micro-organisms (*i.e.* PHB), display biodegradability in various environments while polymers issued from biotechnology and oil-based display more limited biodegradability conditions. For example, PHB is biodegradable in various environment while PLA is only biodegradable in thermophilic digestion and industrial (Figure 12).<sup>67</sup>

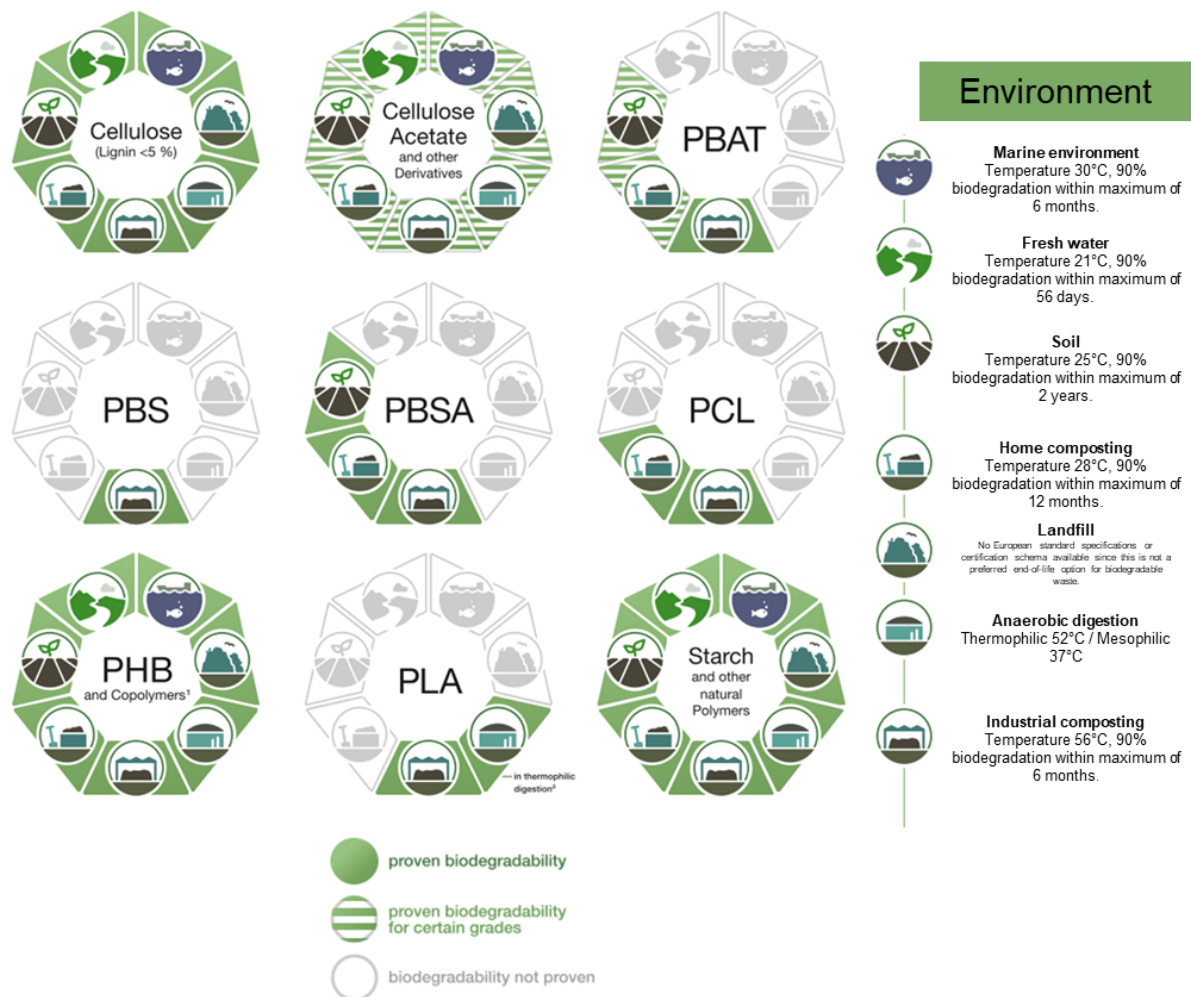


Figure 12: Biodegradability of some polymers in various environments.<sup>67</sup>

Today, there are different definitions for biocomposites. For some researchers, it is considered as a biocomposite if at least one of its component, matrix and/or reinforcement, is naturally derived.<sup>69,70</sup>

In other definitions, the biocomposite must have its two components naturally derived.<sup>71</sup> This diversity in viewpoints highlights the ongoing evolution of the biocomposites field and the need for continued discussion.

The most studied type of biocomposite is the natural-fiber-reinforced biopolymer in which vegetable fibers *i.e* flax, hemp, are associated with a biopolymer matrix. The potential of biopolymers and biocomposites to be a more sustainable and eco-friendly solution in the future is exciting.<sup>69</sup> These materials can reduce CO<sub>2</sub> emissions and eliminate the need for oil, thus decreasing the environmental impact of products.<sup>72</sup>

### 1.2.1 Poly(lactic) acid

Among biopolymers, poly (lactic acid) (PLA), commonly called polylactide, is a bio-sourced, biodegradable and biocompatible aliphatic polyester which finds many applications in particular in biomedical, packaging, and automotive.<sup>73</sup> PLA can be synthesized either by polycondensation of lactic acid (2-hydroxypropanoic acid) (Figure 13), obtained from the fermentation of vegetable-based carbohydrates, or by ring-opening polymerization (ROP) of lactides (3,6-dimethyl-1,4-dioxane-2,5-dione) (Figure 14). Depending on the conformation of the LA monomer, D = S,S, L = R,R or D,L = R,S, three stereoisomers of PLA can be produced poly(L-lactide) (PLLA), poly(D-lactide) (PDLA), and poly(D,L-Lactide)(PDLLA). PLLA and PDLA are semicrystalline polymers with melting temperatures between 140-170 °C whereas PDLLA is usually amorphous.<sup>74</sup> Semi-crystalline PDLLA can be obtained by the use of stereoselective metal-based catalysts.<sup>75</sup>

Theophile-Jules Pelouze and co-workers first developed the synthesis of PLA via polycondensation of lactic acid in 1845. This is much later that, in 1932, Carothers *et al.* reported an innovative technique to polymerize lactide into PLA, which was patented by Du Pont in 1954.<sup>76</sup> By the late 1970s, PLA and its copolymers (*i.e* PDLLA) have been developed as biomedical materials due to their biocompatible nature. Furthermore, the biomedical application of PLA has been extended to tissue engineering, including scaffold materials, as well as biocompatible materials for sutures and prostheses, which use high and low molecular-weight PLAs, respectively.<sup>77</sup> In the early 1990s, a breakthrough was achieved in the production of PLA as Cargill Inc. succeeded in polymerizing high molecular weight PLLA through the process of ring-opening polymerization (ROP) of L-lactide (L-LA) using Sn(Oct)<sub>2</sub> as catalyst at the industrial scale and commercialized the polymer on the mid-1990s. With its high mechanical properties as well as its biodegradable nature, PLLA has been deemed to present an extensive potential for replacing non-degradable oil-based polymers, such as poly (ethylene terephthalate) (PET), polystyrene (PS), and polypropylene (PP).

Nowadays, NatureWorks (Cargill) is the largest world producer of PLLA. Corbion, a multinational company, holds a special position in the polylactide market. They are one of the primary producers of lactic acid (L- and D- isomers) as well as lactides and are a monomer supplier to many polymer producers.

### 1.2.2 PLA synthesis

As previously mentioned, there are two PLA synthesis routes: polycondensation and ring-opening polymerization. The first route will be discussed and the second one will be described in detail as it is the one chosen in the present PhD work.

PLA can be synthesized by polycondensation from two optically active stereoisomers of lactic acid, namely L and D enantiomers (Figure 13). An equimolar mixture of L- and D-lactic acid results in racemic lactic acid. Both enantiomers are obtained from fermentation of sugars made by micro-organisms while the racemic D,L-lactid acid is synthesized by chemical method.<sup>78</sup> In polycondensation, the esterification takes place in an organic solvent in the presence of a catalyst at high temperatures (180 – 200°C) and high pressure (0.13–2.66 kPa) at long reaction times (> 24 h). The polylactides obtained via this route display in general low-molecular-weight leading to a brittle material.<sup>79</sup>

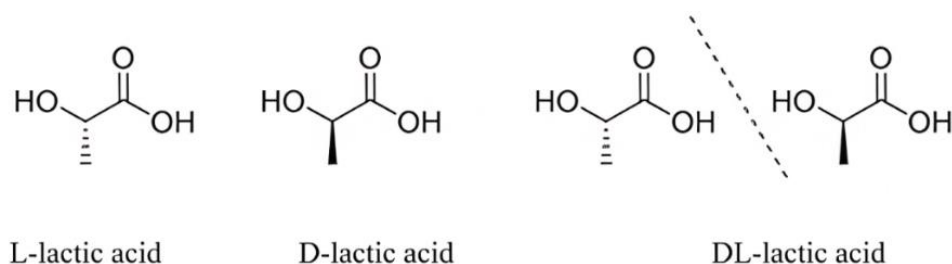


Figure 13: Structures of L-, D- and D,L-lactic acids.<sup>74</sup>

Regarding ROP, the monomer involved is lactide, a cyclic ester, which also exists in different stereoisomeric forms. L- and D-lactides are composed of two S and R asymmetric carbons respectively, while meso lactide displays one R- and one S- asymmetric carbons (Figure 14). Lactides are synthesized through the depolymerization of the corresponding oligo(lactic acid) obtained by polycondensation of lactic acid.<sup>80</sup>

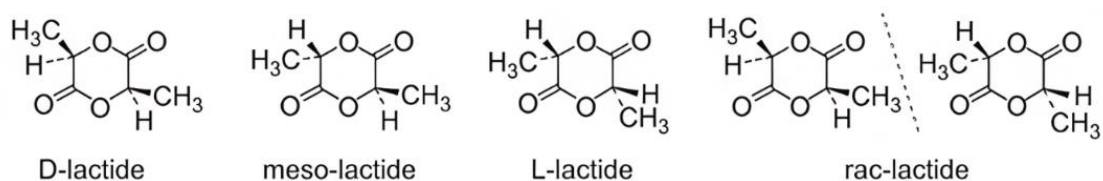


Figure 14: Structure of lactides.<sup>81</sup>

Lactides have different thermal properties which influence the conditions of polymerization reaction. Both L- and D-Lactide have a melting temperature ( $T_m$ ) between 95-98°C, while meso-lactide has a  $T_m$  around 54°C. *Rac*-lactide has the highest  $T_m$ , between 122-126°C.<sup>81</sup> The ROP of lactides can take place in solvent or in bulk (in the absence of solvent) in the presence of catalysts. ROP of lactide can be conducted via several mechanisms, anionic, cationic, coordination-insertion via a metal-based catalyst or organocatalysis.<sup>82</sup> In the case of metal-based catalysts, the resulting polylactides display high molecular weights and good mechanical properties and thus it is the most used way of industrial production of polylactide.<sup>83</sup> A scheme summarizing the different synthesis routes for poly(lactid acid) is shown in Figure 15.

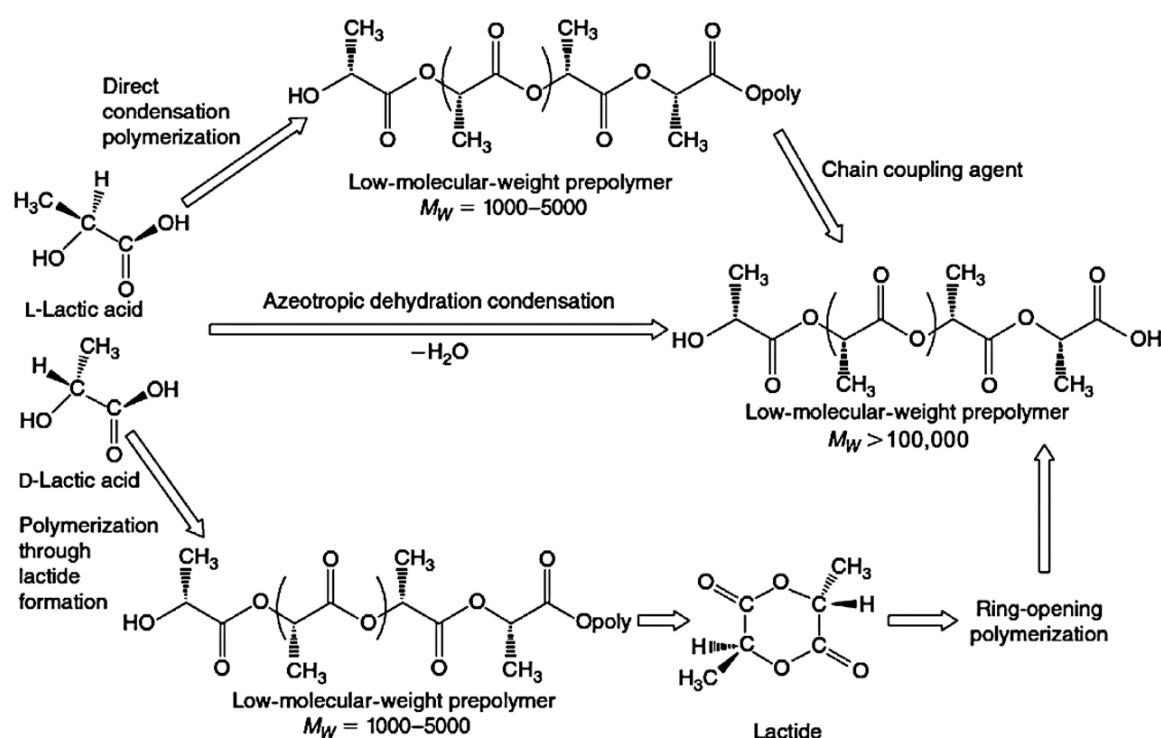
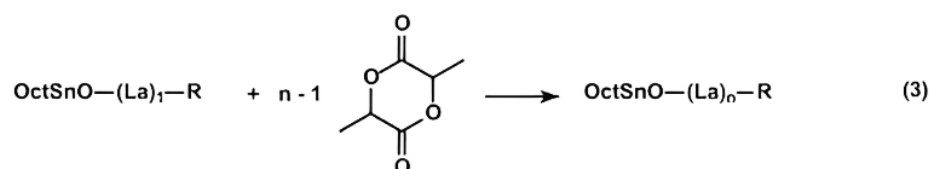
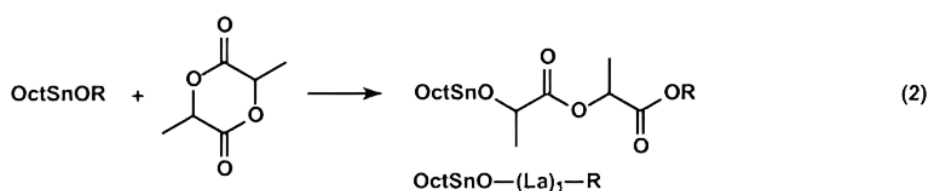
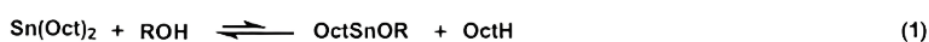


Figure 15: Different routes for synthesis of poly(lactid acid).<sup>77</sup>

Regarding metal-based catalysts, various metal complexes of Al, Mg, Zn, Ca, Sn, Fe, Y, Sm, Lu, Ti, and Zr were studied as catalysts of the ROP of lactide, but the widely used standard catalyst used for lactide polymerization is tin(II) octoate ( $\text{SnOct}_2$ ).<sup>81</sup>  $\text{SnOct}_2$  has been used as a standard catalyst system for the ROP of lactides in scientific research and today it is also used in the industrial processes for the production of PLA.<sup>84</sup> Additionally, this catalyst displays many advantages over other metal-based catalysts such as high stability under air, low cost, good solubility in organic solvents and molten lactide, allowing the polymerization in solution or in-bulk.<sup>77</sup> While permissible in food regulations, the presence of tin octoate is discouraged in materials used for biomedical applications due to its toxic effects.



The polymerization mechanism of lactide catalyzed by tin octoate has been discussed for a long time. The researchers propose that the polymerization can be induced by a “monomer activation mechanism” or by “insertion-coordination mechanism” but the last one is the most accepted by the scientific community. The initiation and propagation stages follow the pathway depicted in Figure 16. It is noteworthy that  $\text{Sn}(\text{Oct})_2$  is not inherently an initiator; rather, it serves as a precursor from which the actual initiator is generated in situ. Reaction (1) in Figure 16 describes the equilibrium established when a protic compound ROH (such as water or alcohol, e.g., butanol) is present in the polymerizing mixture. Reactions (2) and (3) illustrate initiation and propagation, respectively, involving the tin alkoxide groups. The ROP via the coordination-insertion mechanism starts with the coordination of lactide monomer to the metal center.<sup>84</sup> The reaction between ROH and the  $\text{OctSn-}$  end-groups (reaction (4)) results in the formation of propagating species, allowing two polylactide chains to grow from a single Sn atom. Finally, hydrolysis leads to the formation of polylactide chains with terminal -OH groups. This polymerization process affords high yields of high-molecular-weight PLA.



Where R = Bu or H

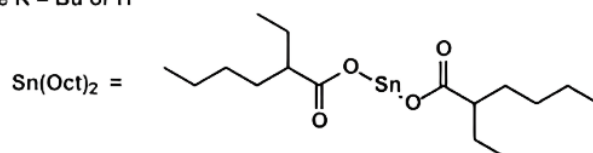


Figure 16: Reactions involved in polymerization of lactides initiated with  $\text{Sn}(\text{Oct})_2/\text{ROH}$  system.<sup>84</sup>

The mechanical properties of PLA rely on several parameters, such as crystallinity, polymer structure (*i.e.* D-isomer content, linear structure...), molecular weight, and material formulation (blends, plasticizers, composites, etc.).



The mechanical properties of PLLA is often compared to the most used petrobased polymers, *i.e* PP, PS, PET, since the PLLA is an alternative to the last ones. PLLA Young modulus is comprised between 3-4 GPa and its tensile strength  $\approx$  50-60 MPa what is to say similar to that of polyethylene terephthalate (PET) and higher than polypropylene (PP) (Table 2).<sup>77</sup> However, PLLA is a brittle material, with low elongation at break and low impact strength, similarly to polystyrene (PS).

Table 2: Comparison of mechanical properties of PLLA vs. PS, PET and PP.<sup>77</sup>

Polymer	Tensile strength (MPa)	Young's modulus (GPa)	Elongation at break (%)	Izod (J/m)
PLLA	50-60	3-4	3-6	20-30
PS	45	3.2	3	21
PET	57	2.8-4.1	300	59
PP	22-35	1-2	10-15	27-130

To improve mechanical properties, in particular the stiffness and the impact strength, PLLA is often:

- mixed with modifiers / plasticizers (lactides, poly (ethylene glycol), citrates...)
- used in blends with other biodegradable polymers and especially with poly(caprolactone) (PCL)<sup>25</sup>, poly(butylene adipate-co-terephthalate)<sup>21</sup> (PBAT), polyhydroxyalkanoates (PHAs)<sup>85</sup>, etc...
- copolymerized with  $\epsilon$ -caprolactone and ethylene glycol<sup>86,28</sup>
- used as a matrix in composites<sup>37,87</sup>

Among the solutions to improve mechanical properties of PLLA, PLA/PCL blends, poly(lactide-co- $\epsilon$ -caprolactone) (PLCL) copolymers, and PLLA-matrix composites have attracted a special interest from the scientific community and publications dealing with the development and study of these materials are still increasing (Figure 17).<sup>88</sup>

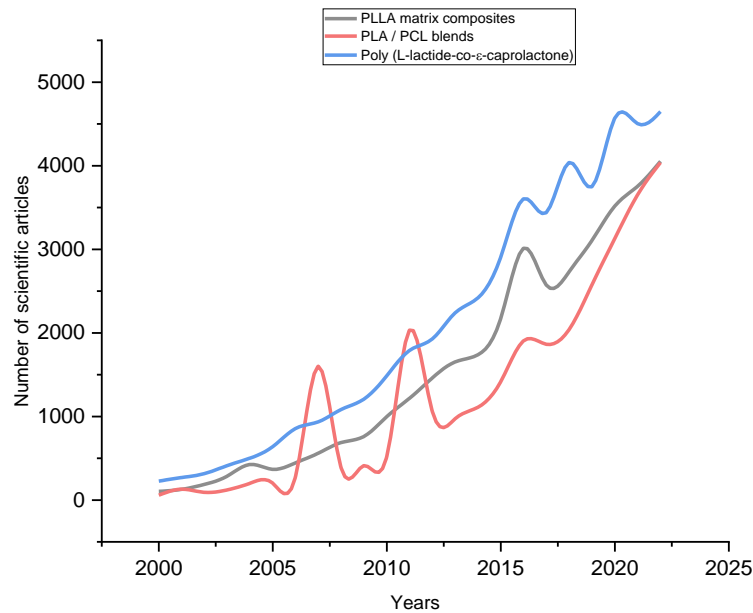


Figure 17: Number of publications per year between 2000-2022 for PLLA matrix composites, PLLA/PLCL blends and poly(L-lactide-co-ε-caprolactone).<sup>88</sup>

In the following, a review of the works carried out on PLLA/PCL blends, poly(L-lactide-co-ε-caprolactone) (PLCL), and PLLA matrix composites is proposed. The following information will be helpful to understand the production and characterization of the PLLA and PLCL matrix based composites presented in this thesis.

### 1.2.3 PLA/PCL blends

PLLA/PCL blends have been studied extensively by researchers because PCL exhibits a rubbery character with an elongation at break close to 600%, which can balance the poor toughness of PLLA.<sup>89</sup> The biodegradability of the blend is assured, once both polymers are biodegradable in similar conditions and both are also biocompatible. The mechanical properties of the blend are influenced by the PLA crystallinity, the PCL particle size, and the presence of modifiers. The primary aim of producing PLA/PCL blends is to increase the toughness of PLA while minimizing any decrease in its stiffness.<sup>26</sup>

PLA and PCL pellets are the raw materials for the production of PLA/PCL blends. Blends are usually elaborated by extrusion and the final part can be produced by thermoforming or injection process for example. The PLA/PCL blend can also be used as a matrix for composites. Since the viscosity of the melt PLA/PCL blend does not permit their use in “liquid composite techniques” composite matrix blends are made by classic manufacturing techniques.

Commercial grades of semi-crystalline PLA display  $T_m$  between 140 and 180°C and  $T_g$  from 55 to 65°C while commercial PCL displays a rubbery amorphous phase at room temperature due to its  $T_g$  around -60°C, and a melting temperature  $T_m$  around 60°C. The  $T_m$  of PLLA/PCL blends is then comprised between the melting temperature of PLLA and PCL and the same for  $T_g$ , depending on the blend composition.<sup>26,90</sup>

Among the various blends compositions, the ratio PLA/PCL 80/20 (80 wt% PLLA and 20 wt% PCL) seems to be the best, regarding the perfect balance between toughness and stiffness. It was reported that the elongation at break of PLA/PCL blends can increase up to 715% for the compositions containing 22.5 wt % of PCL, at the expense of the tensile strength which drops from 64 MPa (pure PLA) to 46 MPa (80/20 PLA/PCL blend).<sup>91</sup> Since the toughness increases with the addition of PCL in PLA, the impact resistance of PLA/PCL blends are supposed to increase compared to pure PLA. Researchers reported an increase in the impact energy of 80/20 PLA/PCL blend 16 times higher than pure PLA (Figure 18).<sup>92</sup>

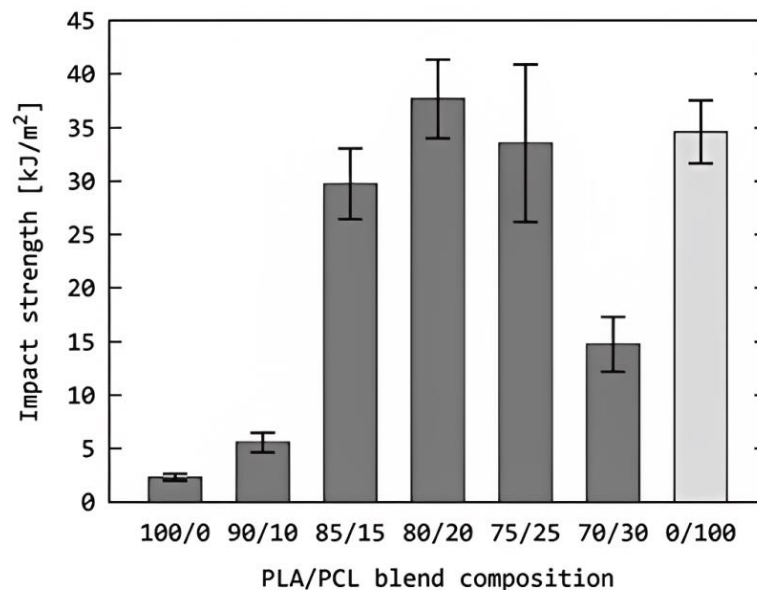


Figure 18: Charpy notched impact strength of PLA/PCL blends.<sup>92</sup>

As seen earlier, in PLA/PCL blends, the toughness is increased but the tensile strength decreases. To settle this problem, PLA/PCL blends are often associated with particles and nanoparticles to obtain PLA/PCL blend matrix composites with better tensile strength.<sup>93</sup> An increase of 26% in tensile strength was reported in nano clay PLA/PLA matrix composites.<sup>94</sup> In another work, Urquijo *et al.* studied the effect of organically modified montmorillonite (OMMT) on the structure and the mechanical properties of PLA/PCL (80/20) blends.<sup>95</sup> They found that the stiffness of PLA/PCL / OMMT nanocomposites increased, while the elongation at break and notched Izod impact strength decreased with the increasing content of OMMT.

The decrease in the elongation at break was from 140% for PLA/PCL (80/20) to 15% for PLA/PCL / OMMT (80/20/6). The Young's modulus of the PLA/PCL / OMMT composite was the highest, reaching 3940 MPa and increasing the modulus of pure PLA by 12%, and the reference 80/20 blend by 29%. The notched Izod impact strength decreased from about 30 J/m for neat blend to about 15 J/m for composite containing almost 6% of OMMT.

Another way to enhance the toughness of PLA is to perform the copolymerization of L-lactide (L-LA) and  $\epsilon$ -caprolactone ( $\epsilon$ -CL) to obtain poly(L-lactide-co- $\epsilon$ -caprolactone). The synthesis and mechanical properties of this copolymer will be discussed in the next section, as one of the main target in this PhD work was to use it as a composite matrix.

#### 1.2.4 Poly(L-lactide-co- $\epsilon$ -caprolactone)

Poly(L-lactide-co- $\epsilon$ -caprolactone) (that we will refer as PLCL all along this manuscript) is a copolyester commonly synthesized by ring-opening-polymerization of L-lactide and  $\epsilon$ -caprolactone using various metal-based catalysts.<sup>28,96</sup> This copolymer has been extensively studied and its applications are until now restricted in biomedical fields due to its biocompatibility, non-toxic degradation products, and drug permeability. PLCL copolymers are often used in tissue engineering scaffolds, surgical sutures, bone fixation, and drug delivery.<sup>97,98,99</sup>

One of the most convenient catalyst to conduct this copolymerization reaction is tin octoate,  $\text{Sn}(\text{Oct})_2$ , it is cheap, air stable and is able to conduct the reaction in bulk conditions. However, an important consideration is the potential toxicity of the residual amount of tin in the material. Even if the catalyst  $\text{SnOct}_2$  is approved by FDA (Food and Drugs Administration) as a food additive, its toxicity *in-vivo* is often questionable.<sup>100</sup> Once this copolymer is employed in biomedical fields, the toxicity of the catalyst must be taken into account and alternatives to  $\text{SnOct}_2$  exists such as biocompatible zinc-based catalysts.<sup>101</sup> In the case of technical applications for PLCL copolymers, the toxicity of the catalyst has minor importance since the material is not placed *in-vivo*.

When the reaction is conducted with  $\text{Sn}(\text{Oct})_2$ , the copolymerization of L-LA and CL generally takes place *in-bulk* at temperatures higher than 140°C.<sup>102</sup> In these experimental conditions, the molten L-LA is completely miscible with  $\epsilon$ -CL once the last one is liquid at room temperature. The influence of polymerization temperature along with the monomers and catalyst ratios have been widely studied. High monomer conversions (> 90%) and molecular weights ( $M_w > 120,000 \text{ g}\cdot\text{mol}^{-1}$ ) are usually obtained with co-monomer over catalyst ratios between 2000 and 3000 wt % with a polymerization temperature of 150 °C.<sup>103</sup>

In the literature, the copolymer composition is often expressed in the molar ratio: [L-LA]/[ $\epsilon$ -CL] *i.e* 90/10 PLCL or 10 PLCL for 90% of L-LA and 10% of  $\epsilon$ -CL.<sup>27,104</sup> Various compositions of PLCL copolymers were reported in the literature, 90/10, 80/20, 70/30, 50/50, etc. Regarding the thermal properties of PLCL copolymer, the  $T_m$  and  $T_g$  vary according to the [L-LA]/[ $\epsilon$ -CL] molar ratio and the polymerization temperature. To illustrate, 80/20 PLCL copolymers synthesized at 150°C display  $T_m=150^\circ\text{C}$  and  $T_g= 30^\circ\text{C}$  while 70/30 PLCL copolymers synthesized at the same temperature display  $T_m=137^\circ\text{C}$  and  $T_g= 16^\circ\text{C}$ .<sup>103,27</sup>

Regarding mechanical properties, PLCL copolymers have elevated elongations at break compared to pure PLLA. Elongations at break higher than 400% were reported for 70/30 PLCL<sup>103</sup> and higher than 700% for 50/50 PLCL.<sup>28</sup> However, the stiffness is drastically affected. It was reported a decrease of 67% in tensile strength for 70/30 PLCL compared to pure PLLA.<sup>27</sup> Many studies about the reinforcement of PLCL with nanoparticles exist and most works are focused on biomedical applications such as tissue engineering, scaffolds, and drug delivery.<sup>105</sup> In this field, PLCL are often mixed with hydroxyapatite<sup>106</sup>, bioactive glass<sup>107</sup>, tourmaline nanoparticles<sup>108</sup>, titanium oxide<sup>109</sup>, etc. However, since now, no technical application for this material was reported yet.

As for the PLA/PCL blends, PLCL copolymers are also associated with particles and more often nanoparticles to increase the tensile properties. Li et *al.* reported an increase 18 times of the tensile strength and an increase 42 times of the tensile modulus for PLCL matrix nanocomposites charged with 37% of nanoporous cellulose gels as compared to neat PLCL.<sup>110</sup> In another study, Amirian et *al.* reported an increase of 49 % in tensile modulus and 70 % in tensile strength for PLCL nanocomposites charged with 2 % of MWCNTs.<sup>111</sup>

Another remarkable property of PLCL is their shape memory effect, depending on its composition. The mechanism of shape recovery was investigated in the last two decades and is well known. In PLCL copolymer with the composition from 10 to 30% of  $\epsilon$ -CL, only the PLLA phase crystallizes and the crystallinity of PLCL decreases with increasing the content of  $\epsilon$ -CL, once PCL phase is complete amorphous.<sup>112</sup> PLLA phase acts like the permanent phase once the crystal or the entanglement of the molecular chains function as physical cross-link points, while the amorphous phase acts as a reversible phase and is responsible for the shape memory effect of PLCL. In that way, the shape recovery rate increases and the shape retention rate decreases with increasing the  $\epsilon$ -CL content.<sup>113</sup>

The shape memory effect was also investigated in PLCL matrix composites. Amirian et *al.* reported an increase of 46% in recovery stress for PLCL / MWCNT composites compared to pristine PLCL using 2 wt% of functionalized MWCNT.<sup>114</sup> Zhang et *al.* studied the shape memory effect in graphene multilayer reinforced PLCL.

As the graphene content increases, the recovery ratio and shape recovery are both enhanced. All composites with graphene can recover their shape completely when exposed to a constant high temperature. Additionally, the shape recovery rate increases with the amount of graphene. The stiffness of the composites is much higher than that of pure polymer, resulting in larger driving forces.<sup>115</sup>

### 1.2.5 PLLA matrix composites

Another strategy to reinforce PLLA and thus to improve its mechanical properties, and in particular its brittleness, is to use it as matrix in composites. PLLA has successfully been associated with fibers and fillers as reinforcements to modify its physical, rheological or optical properties but also to reduce its cost.<sup>116</sup> Fibers and fillers are in general used in PLLA composites for technical applications and in biomedical field. This section, will focus on PLLA composites reinforced with fibers.

Because of its biodegradable and biobased nature, PLLA is often associated with natural fibers, *i.e* flax, hemp, and kenaf to replace oil-based composites reinforced with synthetic fibers. PLLA composites with synthetic fibers *i.e* glass and carbon fibers are also reported in the literature, even to a lower extent.<sup>37</sup>

The use of natural fibers as reinforcement in polymers exhibits a main difficulty due to their inherent hydrophilic nature and their lower thermal stability, usually restricted at 200 °C.<sup>37</sup> These natural fibers, in the same way as synthetic fibers, are generally treated in order to increase the interfacial bonding with the matrix.<sup>117</sup> The natural fibers can be submitted to physical or chemical treatment, the last one being more represented in the literature (*i.e* alkali, acetyl, silane and maleate anhydride grafted coupling agent).<sup>118</sup>

PLLA/flax composites were extensively studied to enhance the mechanical properties of PLLA. Bodros *et al.* investigated the mechanical properties of PLLA/flax composites filled with up to 30 wt% of fibers.<sup>119</sup> For PLLA/flax composites the Young's modulus undergoes a significant increase from 3.3 GPa (for the pure polymer) to 9.5 GPa. Furthermore, the tensile strength also experiences an increase, from 60 to 99 MPa. However, the strain at break shows a decrease of 50%, dropping from 2.4% to 1.5%. A comparison done by the authors with PP/Glass fabric composites reveal that PLLA/flax composites display similar mechanical properties.

Since the problem of brittleness are not solved with adding flax fibers, PLA can be associated with plasticizers. Oksman *et al.* studied the influence of glycerol triacetate into PLA and PLA/flax composites in order to improve the impact properties.<sup>118</sup> However, the addition of plasticizer did not improve the impact properties of PLA/flax composites.

The PLA/flax composite showed an impact resistance of  $12 \text{ kJ.m}^{-2}$  while the pure PLA showed a value of  $18 \text{ kJ.m}^{-2}$ . According to the authors, these negative results are probably due to the poor interfacial adhesion between the flax fibers and the matrix. In contrast, the authors compared the tensile stress of PP/flax and PLLA/flax composites and the last one have higher values of tensile stress. PP/flax showed a value of tensile stress of 30 MPa while PLA/flax showed a value of 43 MPa for composites with 40 wt% of fibers (Figure 19).

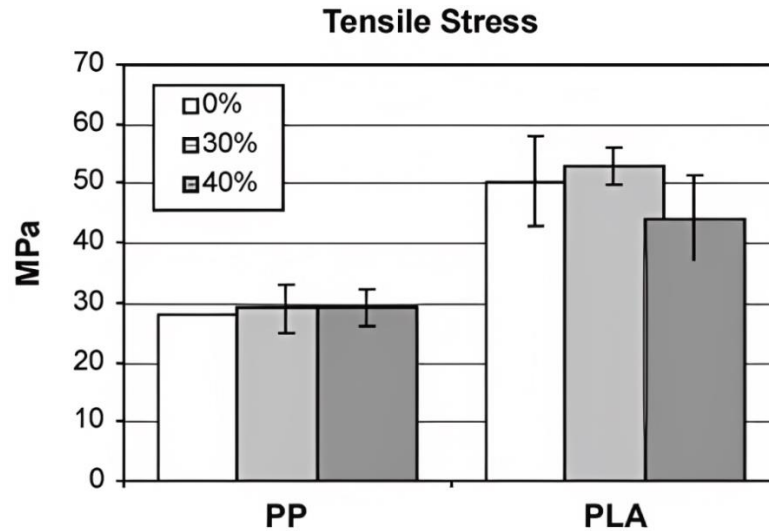


Figure 19: Tensile stress of PLA/Flax composite compared to PP/Flax (30 and 40 wt% of flax fibers).<sup>118</sup>

The study of PLLA/glass fiber composites has not received as much attention as that of PLLA/flax composites. This can be justified by the fact that PLLA is fully biodegradable while glass fibers are not. However, some studies dealing with PLA-glass fiber composites were nevertheless done once glass fibers are the most common and performant reinforcements used in the composite industry.<sup>37</sup> In the study reported by Wang *et al.* the tensile strength and the tensile modulus was increased by a factor two in PLA/glass fiber composites compared to pure PLA when 20 wt% of GF were added.<sup>20</sup> An increase of 3 times in impact strength of PLA/glass fiber composites was also reported. PLA/GF showed an impact strength of  $103 \text{ J.m}^{-1}$  while the pure PLA showed a value of  $31 \text{ J.m}^{-1}$  (Figure 20).

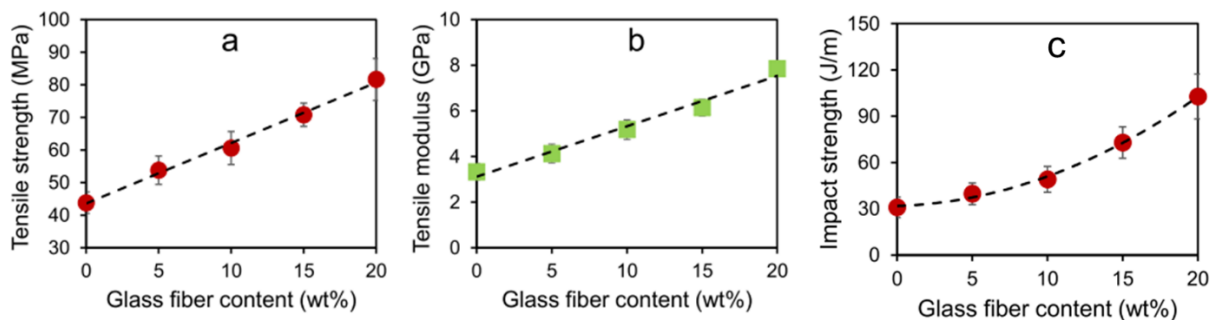


Figure 20: Mechanical properties of the PLA/GF composites: (a) strength, (b) modulus, and (c) impact strength.<sup>20</sup>

Jaszkiewicz et *al.* conducted a comparison between PP and PLLA composites and showed that, despite an equal amount of glass fiber (30 wt%) for both composites, PLLA/glass fibers had a higher tensile modulus of 9.8 GPa in contrast to the PP/glass fiber, which had a tensile modulus of 6.5 GPa.<sup>120</sup> The impact strength of PLLA/glass fibers are approximately 26 % higher than PP/glass fiber composite.

Owing to its high tensile strength and lightness, carbon fibers are usually employed in advanced composite materials. The mechanical properties of 3D printed (Fused deposition molding – FDM) PLLA reinforced with short carbon fibers was investigated by Ferreira et *al.*<sup>121</sup> It was reported that the tensile modulus of PLLA/carbon fibers charged in 15 wt% increased 2.2 times compared to pure PLLA. In another study about the mechanical properties of PLLA/carbon fibers produced via FDM, the tensile strength increases 1.5 times compared to pure PLLA.<sup>122</sup>

Overall, PLLA composites reinforced with natural or synthetic fibers show great potential in various applications, including biomedical implants, packaging materials, and structural parts. The use of natural fibers can offer a more sustainable and environmentally friendly alternative to synthetic fibers, while carbon fibers can provide exceptional mechanical properties. The efficiency of these composites depends on the quality of interfacial adhesion between the fibers and the matrix, which can be enhanced through physical or chemical treatments. Further research is needed to optimize the composite properties and to explore new types of reinforcements and treatments to improve their performance.

### **1.3 Manufacturing polymer matrix composites**

The choice of the elaboration method of polymer based composites must take into account the physical properties of the raw materials, the geometry of the final part, the number of parts, and the cost of production. Moreover, the raw materials are available in different forms: liquid resins, plastic pellets, and pre-pregs.<sup>1</sup> Different classifications of the manufacturing process are proposed in the literature and the most common one is the differentiation between classic composites manufacturing techniques (CCMT) and liquid composite molding (LCM).

In general, pre-pregs, pellets, resins, and films are used in CCMT, whereas only resins are employed in liquid composite molding LCM. CCMT, gathers techniques such as: filament winding, pultrusion, compression molding, and injection molding. In the family of liquid composite molding, we find resin transfer molding (RTM), vacuum infusion bagging, and hand laminating.<sup>123</sup> Different variations of all processes mentioned here exist, but only variations of RTM are cited.<sup>124</sup> The classification depicted in Figure 21 is not an exhaustive list but encompasses the most employed techniques of polymer composite production.



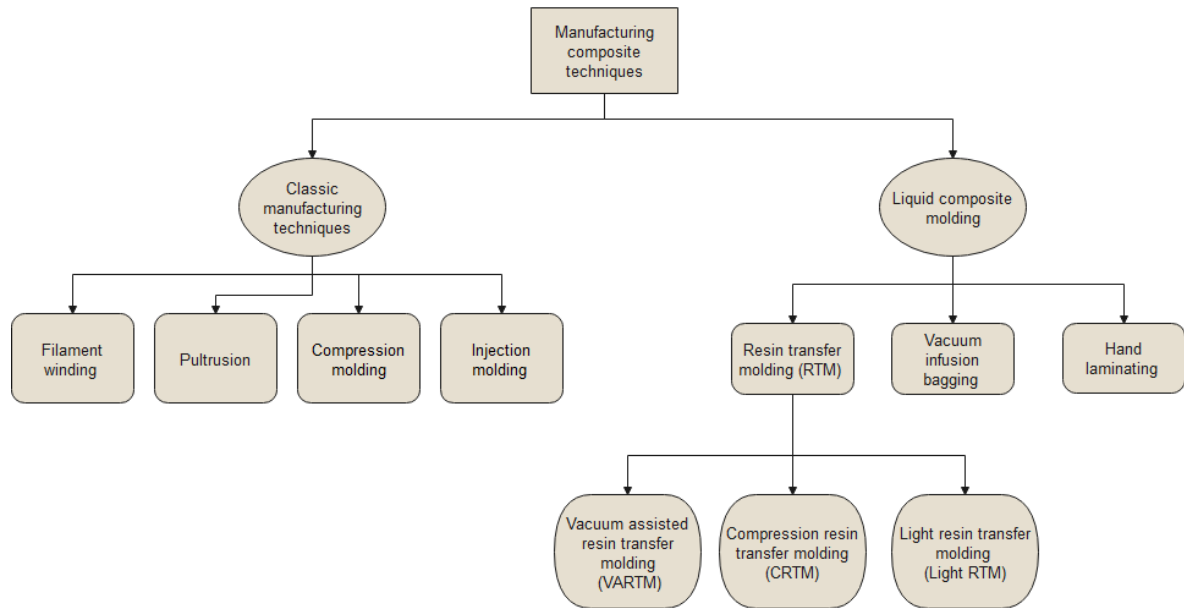


Figure 21: Classification of the principal manufacturing techniques of composites production.

### 1.3.1 Filament winding

In filament winding (Figure 22), a yarn or tow is first wetted by the resin and after wound around a rotating mandrel along a prescribed path. Note that, it is also possible to use pre-pregs (thermoplastics or partially cured thermosets). After winding, the composite part must be heated to cure the thermoset resin or to melt the thermoplastic matrix, promoting the impregnation of the reinforcement. This process is principally used to manufacture pipes for example to produce aircraft fuselage parts. The main advantage of filament winding over other processes is the automation of the process rendering it highly productive. However, the geometry of the feasible parts is limited since it is impossible to wind on negatively curved surfaces.<sup>125,126</sup>

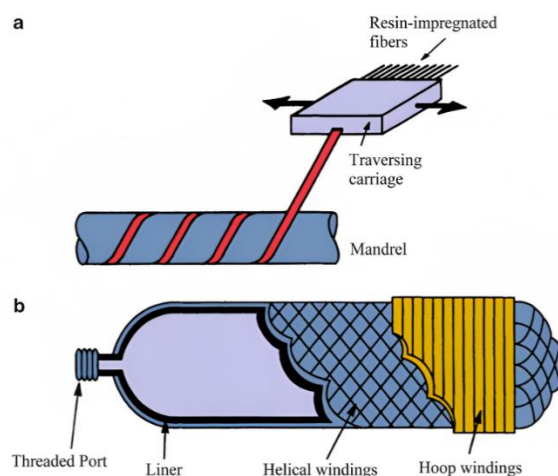


Figure 22: (a) Schematic representation of filament winding (b) Schematic of pressure vessel produced by filament winding.<sup>2</sup>

### 1.3.2 Pultrusion

The pultrusion (Figure 23) is a continuous process in which continuous roving, commingled fibers, or pre-preg tows are pulled through a heated die block, where the curing (thermosetting) or melting process (thermoplastic) takes place.<sup>127</sup> This process produces continuous profiles with a range of shapes and sizes and the profiles are cut to the desired length and post-processed in an oven after the pultrusion process.<sup>128</sup>

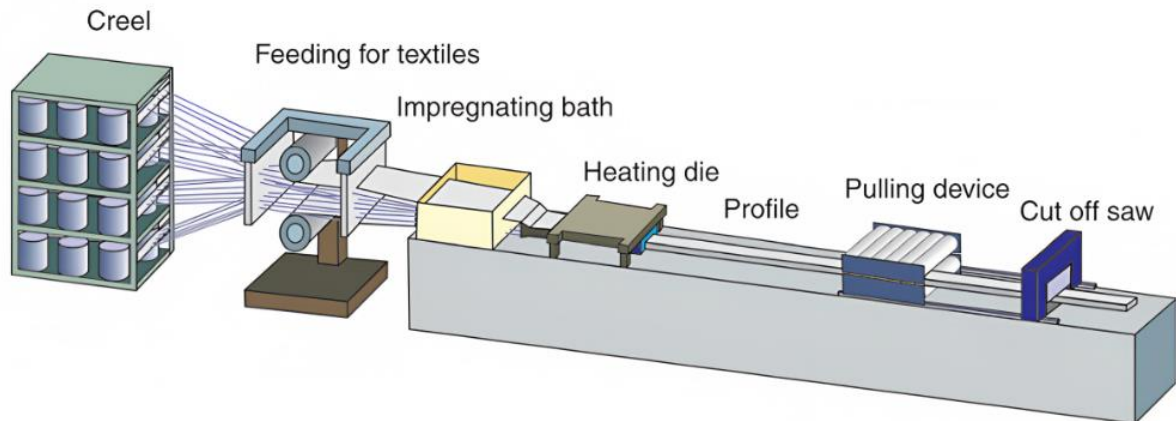


Figure 23: Schematic representation of pultrusion process.<sup>70</sup>

### 1.3.3 Compression molding

Compression molding is the most common thermoset and thermoplastic polymer composite manufacturing process. It is normally used to produce composite components in high production volumes such as automotive components. Short and continuous fibers can be used in this process. For thermosets polymers, semi-cured pre-pregs are used: bulk molding compound (BMC) and sheet molding compound (SMC).<sup>50</sup> For thermoplastic polymers, a mat thermoplastic is normally used as a molding compound. The pre-pregs are placed into the mold, the pressure is applied and the process can be heated or not, depending on the nature of the polymer (Figure 24).<sup>55</sup> Polymer matrices used in this process include polyurethane (PU), vinyl ester, and phenolic resins for thermosets and mainly polypropylene (PP), polyamide (PA), and polyether ether ketone (PEEK) for thermoplastics.

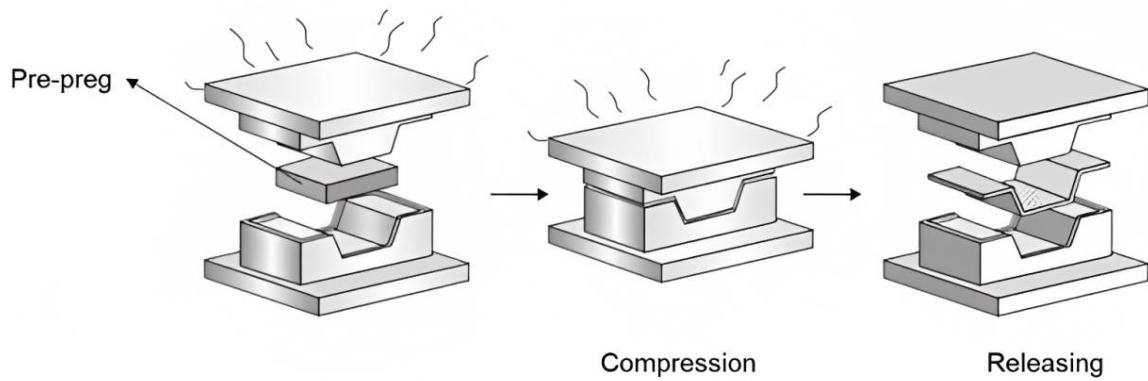


Figure 24: Scheme of the compression molding process.<sup>55</sup>

### 1.3.4 Injection molding

In the injection molding process, short fibers, felts, and mats are the most used reinforcements and thermosetting and thermoplastics can be used as a matrix. This process is composed of a screw-type extrusion machine in which the mold is coupled at the end of the line (Figure 25). The reinforcement and the matrix are placed into the feed hopper and pass through the feed zone, melting zone, and melt-pumping zone. The mixture of reinforcement matrix is then injected into the mold.<sup>129</sup> Depending on the viscosity of the resin, woven fabrics can be placed into the mold to produce long fiber composites. This process is highly productive and allows the production of parts with relatively complex geometries.<sup>1</sup>

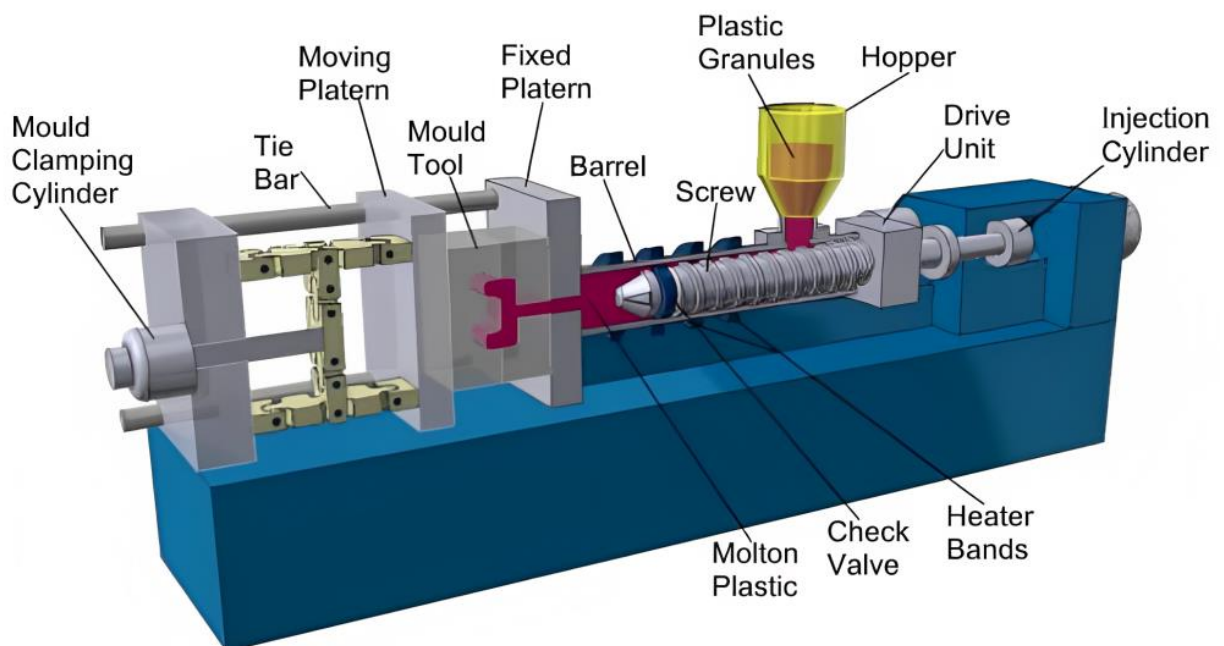


Figure 25: Schematic representation of single-screw injection molding machine.

### 1.3.5 Vacuum infusion

Vacuum infusion is a wet lay-up process that is employed to produce composite laminates, wherein fibers are saturated by liquid resins (thermosetting or thermoplastic resins). A vacuum is utilized to draw resin into the mold, at the same time pressing the bag against the laminate (Figure 26).<sup>130</sup> Vacuum infusion is a low-volume molding process that is suitable for the production of large parts with very high fiber ratios. It exists some variations of the vacuum infusion process, i.e. vacuum bag infusion in which pre-pregs are used instead of fibers. This process can also be executed in an autoclave machine adapted to high-quality structural components containing high fiber volume and low void contents.

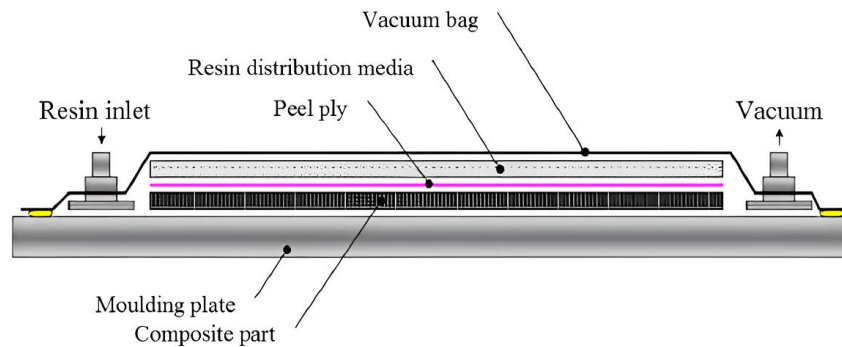


Figure 26: Scheme of the vacuum infusion process.<sup>131</sup>

In the present work, we are going to be interested in the liquid composite technique cited before: Thermoplastic resin transfer molding (TP-RTM) process. A section describing the TP-RTM process and its variants, the types of resins used in this technique, and all thermoplastic composites made by RTM reported since now is presented next.

## 1.4 Thermoplastic resin transfer molding (TP-RTM)

The RTM is a LCM process in which a low-viscosity resin is injected under pressure into a closed mold containing predisposed reinforcements. The polymerization step occurs into the mold to form a matrix. A primal form of RTM was employed in the 1940s by the US Navy to manufacture boats from glass fiber polymer composites.<sup>132</sup> To date, interest in RTM and in the optimization of this technique to obtain parts with higher mechanical performances is growing. A significant development occurred in the 80s with the introduction of structural parts for the aeronautical, automobile, and military industries.<sup>132</sup> The RTM technique is usually employed in the production of thermosetting matrix composites. It also has progressively tended to be used for the conception of thermoplastic-based composites, as these composites display unique properties, thereby allowing for their use when thermosetting plastics are unsuitable, e.g., when a part needs to be welded or recycled, or even when the part must undergo thermoforming processes.

To differentiate the use of thermoplastic resins within the RTM, several authors proposed the use of the terms T-RTM or TP-RTM for thermoplastic resin transfer molding.<sup>133,134,23,135</sup> To note that from a technical point of view there is no difference in RTM or TP-RTM process.

Thermosetting and thermoplastic composites can be produced by the RTM technique by using low-viscosity resins to impregnate the reinforcement.<sup>136</sup> In the case of thermoplastic-based composites produced by RTM, the reagents, called “reactive thermoplastic systems,” are composed of a mixture of monomers and/or oligomers.

They are associated with a catalyst, and in some cases, an additional activator, which are mixed in a chamber and subsequently injected into a mold containing the reinforcement.<sup>137</sup> Afterwards, the polymerization reaction takes place in the mold to form the matrix and provide the composite material in a one-step synthesis.

The RTM and TP-RTM processes essentially follow five stages: reinforcement placement, mold filling, polymerization or curing (term used for thermosetting), cooling, and post-processing. The machine for these processes can be composed of one (Figure 27) or two tanks (Figure 28) where the degassing, melting (if necessary), and mixing of the reagents (resin and activator/catalyst) take place. In specific cases, such as highly reactive systems (e.g., ( $\epsilon$ -CL)/ PA-6), the TP-RTM equipment can comprise different tanks and a mixing head placed between the tanks and mold<sup>138</sup>, where the components can be mixed under high pressure just before injection. The use of several tanks to separate the reagents is necessary in specific cases where the polymerization reaction is too rapid, as this will lead to an increase in the viscosity of the mixture and prevent the injection step. Currently, personalized industrial-scale TP-RTM machines for one or more components with a mixing head have been commercialized by Diatex (France), Tartler (Germany), Krauss Maffei (Germany), and Wolfangel (Germany). Liquid monomers and/or oligomers are injected under pressure through pipes into a mold containing the reinforcement. A press is frequently required to keep the mold parts properly joined during the injection. After the injection, the viscosity of the resin increases as the polymerization reaction occurs, until the resin is fully converted and solidified. The time from the beginning of the polymerization reaction to the complete solidification of the resin is called the polymerization time.

RTM and TP-RTM machines can be assisted by a secondary vacuum pump system placed at the exit of the mold to facilitate the impregnation of the reinforcement. This variation in the RTM process is known as vacuum-assisted resin transfer molding (VARTM). The advantages relative to conventional RTM are (i) a better finish of the composite surface, (ii) a better impregnation of the reinforcement by the matrix, and (iii) a reduction of polymerization time in certain cases.<sup>139</sup>

However, the use of this specific technique can lead to the formation of voids in the final material. In particular, the pressure goes below atmospheric pressure, thereby inducing the sublimation or evaporation of the liquid monomer/oligomer and creating voids.<sup>140,141</sup> In reactive thermoplastic systems, specifically for  $\epsilon$ -CL monomers, the presence of voids is often caused by the presence of water owing to the hygroscopic nature of certain monomers, but also by the gas used during injection, which is generally nitrogen.<sup>142,23</sup>

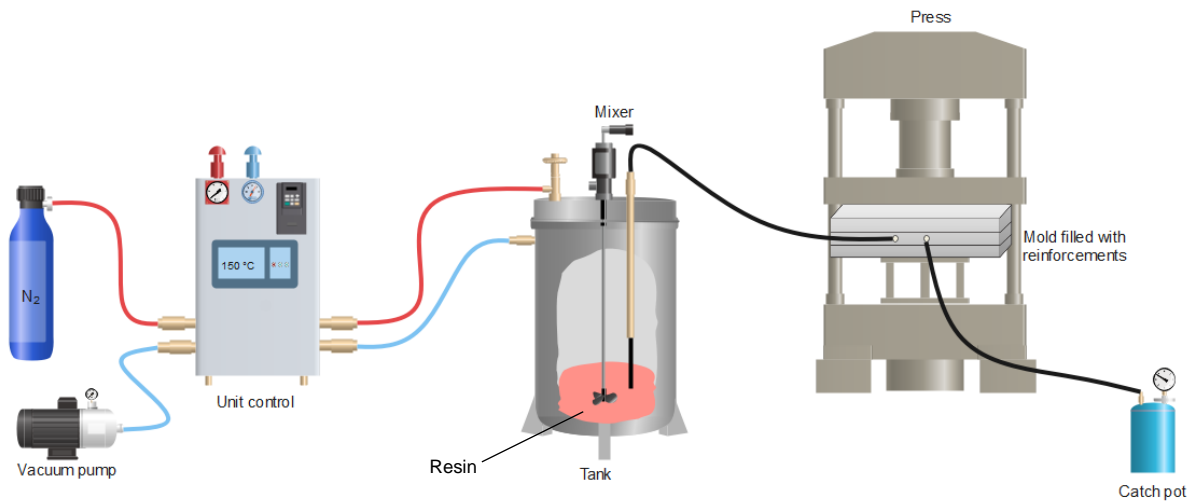


Figure 27: Schematic representation of RTM machine.

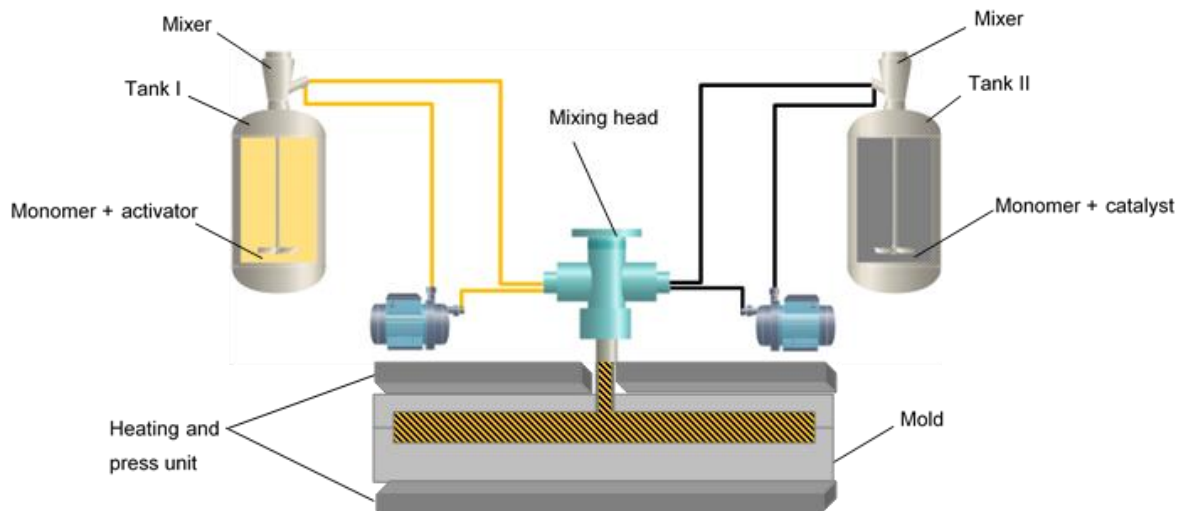


Figure 28: Mixing head used in thermoplastic resin transfer molding (TP-RTM) multi-component machine for highly reactive thermoplastic systems.

The RTM and its variants have basic processing parameters, such as the tank temperature and pressure, stirring speed, injection pressure, filling time, and mold temperature. The tank temperature, stirring time, and tank pressure influence the viscosity of the resin.

A higher tank temperature makes the resin more fluid, and thus, the temperature is considered as a major parameter.

If the resin is sensitive to air, the melting process can take place under a vacuum or inert atmosphere.<sup>137,23</sup> In the case of reactive thermoplastic systems, the stirring time and speed can influence the kinetics of the polymerization reaction, and consequently, the viscosity.<sup>23</sup>

The pressure in the tank can also influence the viscosity. In the case of reactive thermoplastic systems, a high vacuum associated with a high temperature can promote vaporization or sublimation of the monomers in the tank (e.g., in the case of L-LA,  $\epsilon$ -CL, and  $\omega$ -laurolactam, which are in the solid state at room temperature), whereas an overpressure can cause the solubilization of gases into the liquid monomer.<sup>143,144</sup> During the injection step, the pressure must be controlled to avoid fiber distortions related to the permeability of the reinforcement. Usually, high pressures cause reinforcement displacements owing to a high resin flow, and the optimal injection pressure can be predicted using permeability tests and modeling simulation.<sup>145</sup> Ultimately, the mold temperature influences the polymerization time, as in a general manner, higher temperatures accelerate the polymerization kinetics.<sup>146</sup>

The advent of the finite element method has allowed for an understanding of the physical behaviors of the resin in RTM. Simulations of the resin behavior can be conducted using commercially available software exclusively developed for RTM, for example, RTM-Worx by Polyworx and PAM-RTM™ by ESI Group™. These software were designed based on thermosetting resins; therefore, the simulations for thermoplastic resins have not been fully adapted. In fact, the polymerization mechanism (most of the time ring opening polymerization (ROP) or radical polymerization) occurring during the matrix formation is not often considered in the models, but can help in the first approach. Analytical models of the polymerization, crystallization, and rheological behaviors of reactive thermoplastic systems have already been developed experimentally, *i.e.*, for  $\epsilon$ -CL/PA-6<sup>134</sup> and L-LA/PLLA.<sup>147,148</sup> However, a combination of analytical models for the resin flow in a modeling system has not yet been developed.

Compared with other thermoplastic composite manufacturing technologies, TP-RTM displays some advantages, as follows.

- It allows for the use of different types of reinforcements, such as thick fibers, 3D structures, stitched assemblies, and braids.
- The volume of the fibers can be very well-controlled in fixed-cavity tools, resulting in composites with good mechanical properties.
- Composites with a reduced number of voids are obtained when the correct mold design is used, and with meticulous control of parameters such as the injection pressure, injection speed, and curing time.

- Parts with complex geometries can be produced.

It provides better control of the fiber orientation and manufacturing of large parts ( for example, in the aeronautical industry), with short processing times.<sup>132</sup>

#### 1.4.1 Resin flow in resin transfer molding

Owing to the low viscosity of the resin or liquid/melted monomers involved in TP-RTM, good impregnation of the reinforcement by the thermoplastic resin or liquid monomer can be obtained, thereby minimizing empty spaces inside the parts and improving the mechanical performance of the final composites. A perfect balance between the viscosity of the resin and permeability of the fibers allows for optimal impregnation, and reduces the filling time. The impregnation or filling time in TP-RTM is directly proportional to the resin viscosity and inversely proportional to the permeability; this limits the use of highly viscous resins. To improve the permeability and consequently decrease the impregnation time, it is possible to use a second solid phase in the core of the fibers, such as in 3D printed structures.<sup>51</sup> The permeability measurements are not standardized, and different procedures exist. Two experimental setups were developed by Merhi *et al.*<sup>149</sup> and Klunker *et al.*<sup>145</sup> to measure the permeability of fibers. The impregnation time of a resin or melted polymer through the fibers can be estimated using Darcy's Law,<sup>150</sup> assuming a Newtonian fluid in a rigid porous medium. Equation 1 describes the impregnation time for a one-dimensional flow, as follows:

$$t_{imp} = \frac{(1-V_f)\eta L^2}{2K\Delta p} \quad \text{Equation 1}$$

$V_f$  is the fiber volume fraction,  $\eta$  is the fluid viscosity,  $L$  is the impregnation length,  $\Delta p$  is the pressure gradient, and  $K$  is the textile permeability.<sup>35</sup>

The resin injection strategy is crucial for ensuring that the reinforcement is impregnated without air entrapment, allowing for a continuous and homogeneous flow front. For a flat panel with a single injection port, three different injection strategies can be chosen: radial injection, edge injection, and peripheral injection.<sup>151</sup> The direction of the flow front for each injection strategy is indicated by arrows in (Figure 29).



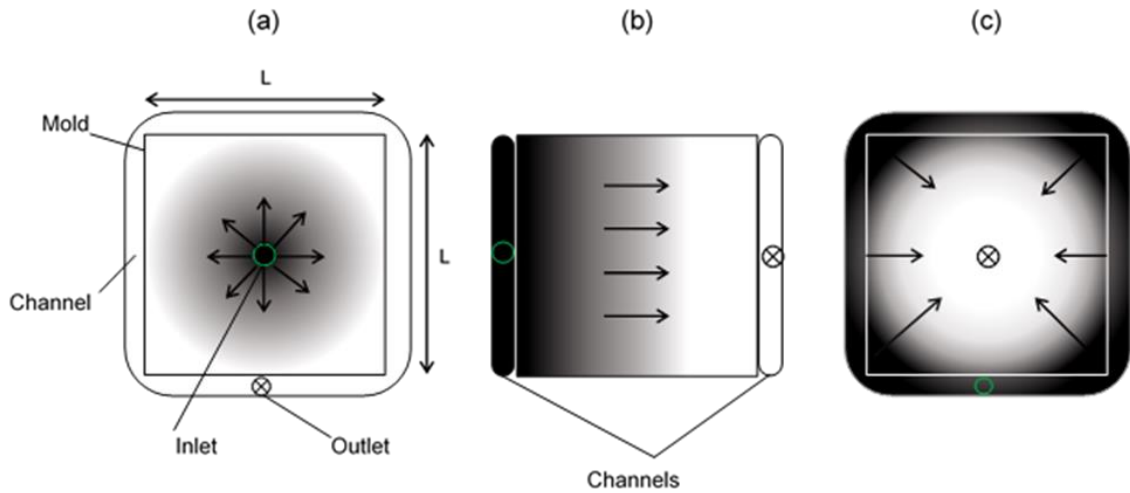


Figure 29: Injection strategies for a square plate in single port with dimensions  $L \times L$ . (a) radial injection (b) edge injection (c) peripheral injection. The flow front starts in the darkest zones in all schemes. The letter "d" corresponds to the diameter of the inlet and outlet.<sup>137,151</sup>

A typical TP-RTM square plate mold is shown in Figure 30. This type of mold is adapted for radial and peripheral injections. The inlet and outlet can be switched depending on the injection strategy. In peripheral injection, the channel around the upper mold is filled with the molten monomer or resin before the impregnation of the fibers into the lower mold. In the case of radial injection, where the inlet is localized at the center of the upper mold, the channel is filled after complete impregnation of the lower mold cavity. To keep the mold properly closed and prevent leaks, the mold disposes of the double silicone seal frequently employed in TP-RTM molds.

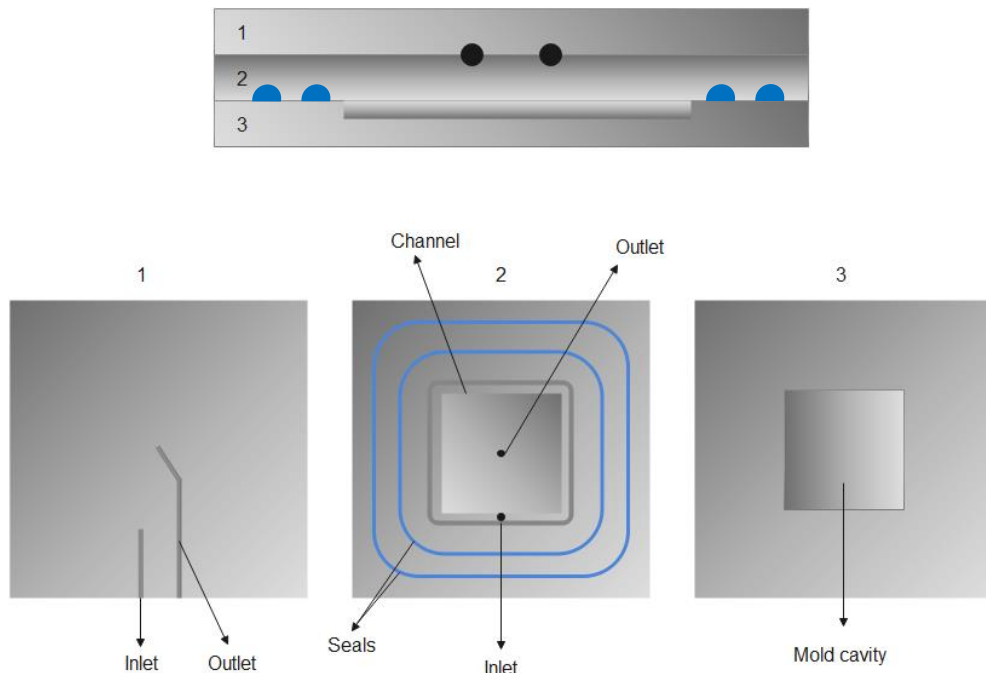


Figure 30: Configuration of TP-RTM square plate mold for peripheral injection strategy. (2) upper mold (3) lower mold.

Depending on the injection strategy, the impregnation time for a one-dimensional flow (Equation 1) can take another form (Equation 2)

$$t_{imp} = C \frac{(1-V_f)\eta L^2}{2K\Delta p} \quad \text{Equation 2}$$

where C is a constant related to the chosen injection type.<sup>151</sup> (Table 3)

Table 3: C values for different injection strategies.

	Radial injection	Edge injection	Peripheral injection
C value	$\frac{1}{16} \left[ \varepsilon^2 + 2 \ln \left( \frac{1}{\varepsilon} \right) \right]$ $\varepsilon = \frac{d}{L}$	$\frac{1}{2}$	$\frac{1}{16}$

The use of peripheral injection leads to the lowest impregnation times, whereas in radial injection, this time is directly related to the diameter of the inlet. However, a very fast impregnation time can cause fiber filling defects. When the resin flows too fast, the fiber bundles are not fully impregnated, resulting in void formation. The speed of resin flow must be controlled to achieve the best impregnation of the reinforcement without defects in the matrix.<sup>151</sup>

Most textile reinforcements exhibit an anisotropic nature, and the flow front is not linear. For a radial or peripheral injection strategy using anisotropic textiles, the flow front exhibits an elliptical shape, whereas for isotropic textiles, the flow front exhibits a linear shape.<sup>152</sup> Minaie *et al.* studied the permeability distribution for the edge injection strategy in anisotropic and isotropic textiles, and a numerical algorithm was proposed to predict the flow front.<sup>153</sup> In this study, an elliptical shape of the flow front for anisotropic textiles could clearly be established (Figure 31). The methodology used to predict the permeability distribution during the RTM process using numerical simulations can also be useful for enhancing the mold filling.

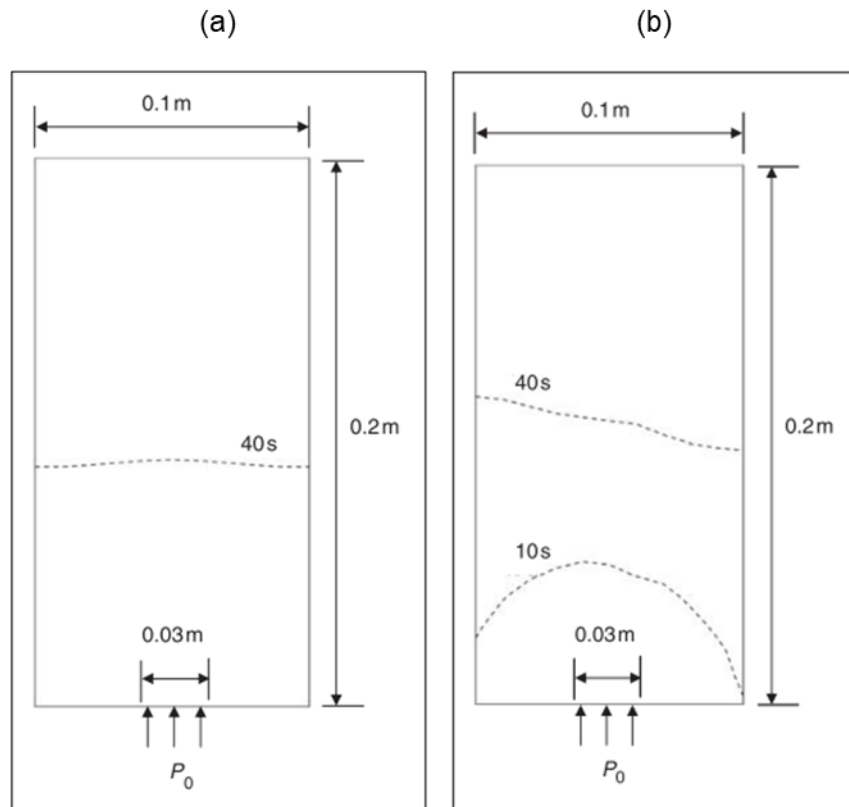


Figure 31: Flow front position in a  $0.1\text{ m} \times 0.2\text{ m} \times 0.01\text{ m}$  resin transfer molding (RTM) mold for (a) isotropic and (b) anisotropic permeability distributions.<sup>153</sup>

#### 1.4.2 Voids in fiber-reinforced composites produced by RTM

In the RTM process, several factors can contribute to the presence of voids in the final thermoset or thermoplastic composites. The main cause is air entrapment during resin flow, generally owing to the inhomogeneity of the textile; this creates a gradient of permeability, resulting in a variation in the resin velocity.<sup>141,154</sup> Owing to the multi-scale nature of reinforcements, voids can be formed at the macro-, meso-, and micro-scales (Figure 32). Macro-voids can be observed with the naked eye in the larger zone of the preform, and meso-voids between the tows and micro-voids are formed between the fiber tow (Figure 33).<sup>141</sup> During the injection step, a competition between the viscous flow and capillary flow is observed, and is governed by the resin velocity. Micro-voids appear between the fiber tows governed by capillary effect, while meso- and macro-voids appear between the tows, as governed by the resin velocity. Other causes of void formation can be considered, such as gas formation owing to chemical reactions, the presence of water in the resin, and incompatibility between the fiber and resin.

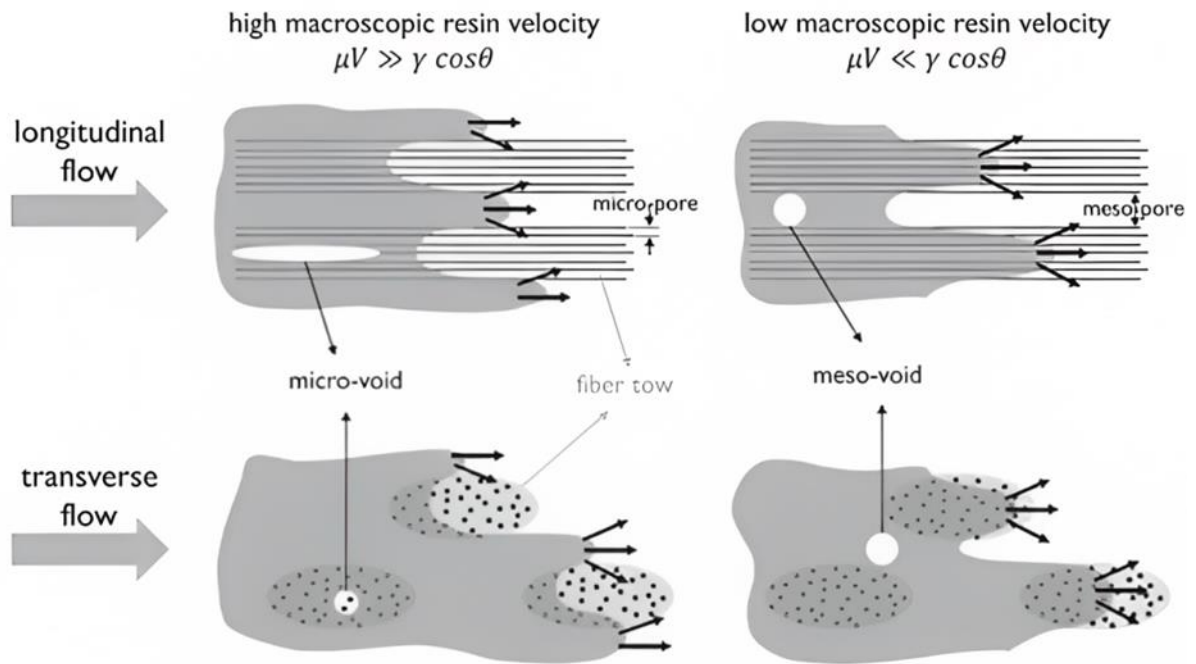


Figure 32: Formation of voids during longitudinal and transverse flow in liquid composite molding.<sup>141</sup>

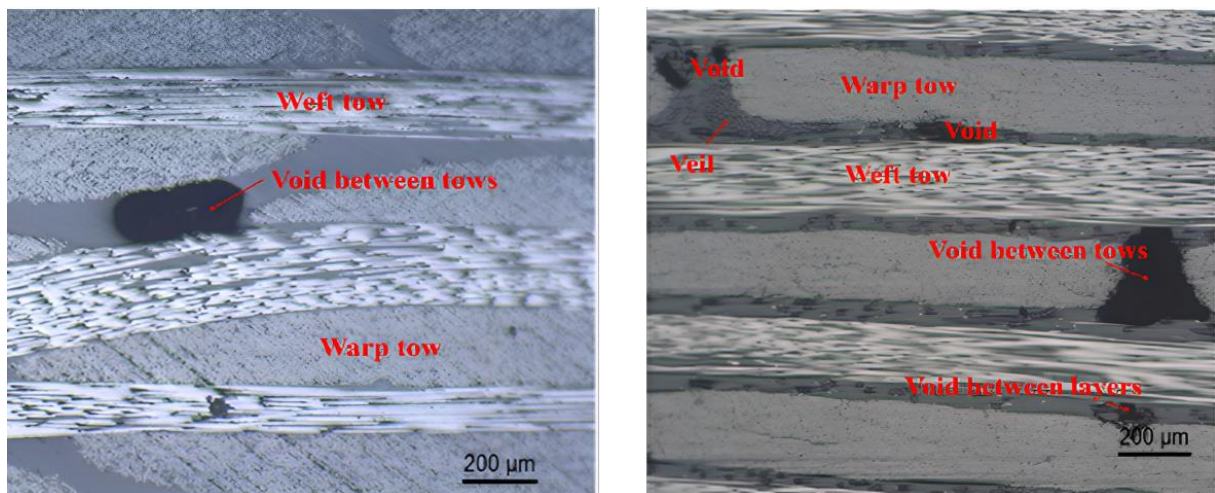


Figure 33: Micrographs of cross-sections of laminates manufactured by a variant of VARTM (*i.e.*, a vacuum-assisted process – (VAP)) under experiment conditions for (a) woven reinforcements and (b) non-crimp reinforcements. (Based on reference <sup>155</sup>)

### 1.4.3 Reactive thermoplastic systems in TP-RTM

To produce thermoplastic composites with good mechanical properties using reactive thermoplastic systems in TP-RTM, the following are required: (i) a high conversion rate of the monomers/oligomers, (ii) a high molecular weight of the resulting polymer matrix, and (iii) no unwanted by-products.<sup>156</sup>

Certain important industrial polymers are produced via ROP, such as polyethylene glycol, polyphosphazene, and polyamides like Nylon<sup>®</sup> 6 which is the most significant in term of volume.<sup>157</sup> Nowadays, some bio-based and biodegradable polymers are industrially produced via ROP, such as Ingeo<sup>™</sup> (polylactide) commercialized by NatureWorks, and Capromer<sup>™</sup> PCL from BASF. The commercial availability of these polymers shows that they can be used in a wide range of applications, particularly for packaging and biomedical applications.

The ROP of cyclic esters is commonly used for the production of thermoplastic composites using TP-RTM. ROP is an efficient synthetic route for the production of engineering plastics with specific and controllable properties (*e.g.*, a high molecular weight) and biodegradable plastics. The ROP mechanism is based on the opening of cyclic ring-shaped molecules via the use of catalysts comprising metal-based systems, organic molecules, or enzymes.<sup>158</sup>

To date, the reported works using thermoplastics in TP-RTM are restricted to polyamides, polyamide-6 (PA-6) and polyamide 12 (PA-12), poly (methyl methacrylate) (PMMA) and some biodegradable polymers such as poly( $\epsilon$ -caprolactone) (PCL), poly(L-lactide) (PLA), and poly (butylene terephthalate) (PBT). Next, the applicability of these polymers in TP-RTM will be presented with a focus on biodegradable polymers.

#### **1.4.3.1 Polyamides matrix composites**

Polyamides are widely used in the industry owing to their excellent mechanical properties, such as high strength, an excellent impact resistance, and a high abrasion resistance. Recently, research has been conducted to develop advanced polyamide-based composites using various reinforcements such as carbon fibers, glass fibers, natural fibers, carbon nanotubes, and graphene.<sup>159</sup> Certain polyamides can be obtained by the anionic ROP of cyclic monomers, allowing for the formation of high-molecular-weight polymer matrices.<sup>46</sup> Nowadays, PA-6 is obtained via the ROP of  $\epsilon$ -caprolactam; this has been commercially exploited by Brüggemann Chemicals.<sup>160</sup>

The production of PA-6 matrix composites via the anionic ROP mechanism by TP-RTM is a viable route owing to the commercial availability of the reagents, low viscosity (3–5 mPa.s) of the reactive system (monomer/activator/catalyst), and fast polymerization rate, thereby enabling its use in industry. However, some disadvantages must be considered, such as the hygroscopic nature of the monomer (which must be stored in vacuum bags or dried before use), and the corrosive nature of the activator and catalyst, which are usually hydroxide salts. Another drawback is the solid nature of the monomer, which must be melted prior to injection. However, these issues seem to be easily bypassed, as the ( $\epsilon$ -Caprolactam) / PA-6 system is the most commonly used reactive thermoplastic system in TP-RTM.

The polyamide -12 are also used in TP-RTM. Some studies have reported PA-12 as a matrix for composite materials produced by TP-RTM via an anionic ROP of the  $\omega$ -laurolactam ( $\omega$ -LL) monomer.  $\omega$ -LL shows a melt shear viscosity ranging from  $4.5 \times 10^{-3}$  Pa.s at 250 °C to  $8 \times 10^{-3}$  Pa.s at 200 °C, which is suitable for injection in TP-RTM.<sup>161</sup> However,  $\omega$ -LL displays a high melt temperature of  $T_m = 154$  °C relative to other monomers used in TP-RTM, such as  $\epsilon$ -CL ( $T_m = 69$  °C) or L-LA ( $T_m = 97$  °C).<sup>148</sup> Thus, the polymerization of  $\omega$ -LL is conducted above the melting temperature of PA-12 ( $T_m = 180$ – $190$  °C). This temperature does not allow for quick demolding (as for PA-6), as crystallization cannot occur during the polymerization reaction.<sup>160</sup> An additional cooling step is required for the solidification of the matrix. This can explain the low number of studies reported on the  $\omega$ -LL/PA-12 system in TP-RTM. In addition, temperatures above 200 °C are required for the polymerization reaction to be initiated, making the process expensive on an industrial scale.

It has been demonstrated that the TP-RTM process is suitable for producing polyamide-based composites. Additionally, various types of reinforcements can be utilized in the process, such as glass fibers, carbon fibers, and nanomaterials. In an industrial approach, an  $\epsilon$ -caprolactam/PA-6 reactive system is more viable in terms of energy than a  $\omega$ -laurolactam/PA-12 system, owing to the high melting temperature of  $\omega$ -laurolactam compared to  $\epsilon$ -CL. Moreover, the production time for PA-12-based composites is longer than that for PA-6 matrix composites, because for PA-12, an additional cooling step is required to allow for demolding. Finally,  $\omega$ -LL monomer and activator systems are no longer commercialized by Arkema (ex-ATOFINA) and EMS-Chemie, which explains the lower interest in PA-12 composites produced via TP-RTM.

#### 1.4.3.2 Poly(methyl methacrylate) matrix composites

PMMA has found numerous applications in optical, electronic, automotive, and biomedical devices.<sup>162</sup> Despite the benefits over thermoset resins already discussed, PMMA displays mechanical properties similar to those of epoxy resins, such as in regards to tensile strength.<sup>163</sup> This polymer can be synthesized by the radical polymerization of methyl methacrylate (MMA), with the use of a peroxide as initiator. Recently, a MMA reactive system called Elium<sup>®</sup> was developed by Arkema for TP-RTM applications, with the resin being available with various viscosities ranging from 100 to 500 mPa.s at 25 °C.<sup>164</sup> The short processing time gives Elium<sup>®</sup> a great advantage in the composite industry, allowing for the production of parts in a very short time. In addition, Elium<sup>®</sup> resins are liquid at room temperature, and do not require melting. Composites produced from Elium<sup>®</sup> exhibit high impact resistance but provide limited use at high temperatures, owing to the low glass transition temperature of PMMA and toxicity of MMA.<sup>162</sup>

### 1.4.3.3 Bio-based and biodegradable matrices used in TP-RTM

Nowadays, the growing interest in biopolymers is justified by the demand for environmentally friendly products, biodegradable materials, and alternative production approaches to petrochemical sources, and because they offer new possibilities in terms of functional properties. The disposal of plastic waste in the environment has severe consequences for biomes, *e.g.*, altering food chains and causing irreparable damage to fauna and flora. It was estimated that world production of polymer resins and fibers increased enormously from the 1950s, jumping from 1.5 Mt in the 1950s to 367 Mt in 2020, with only 9% of these materials being recycled.<sup>165</sup> These data show that the non-biodegradable plastics from petrochemical sources must be increasingly replaced by bio-based and biodegradable polymers to reduce their environmental impacts.

As mentioned earlier, until today, the literature reports the use of only three biodegradable polymers in TP-RTM: poly( $\epsilon$ -caprolactone) (PCL), poly(L-lactide) (PLLA), and poly(butylene terephthalate) (PBT) and the works reporting their use in TP-RTM are presented next.

#### 1.4.3.3.1 Poly( $\epsilon$ -caprolactone) matrix composites

Poly( $\epsilon$ -caprolactone) (PCL) is mostly used in biomedical implants and tissue engineering owing to its biocompatibility and biodegradability, as well as in packaging and microelectronics.<sup>166,167</sup> Corden *et al.*<sup>168</sup> described the production of composites with a biodegradable PCL matrix using a technique inspired by TP-RTM. In this study,<sup>168</sup> composites were prepared by the ROP of  $\epsilon$ -CL (Solvay Interlox, Widnes, UK), with 1,4 butane-diol as the activator, diethyl zinc as the catalyst, and glass fibers as the reinforcement (Vicryl, polyglactin 910 from Ethicon). Notably, a low-molecular-weight oligomer powdered PCL (CAPA 240 Solvay Interlox) was also added. The composite production occurred at the laboratory scale; the tank was composed of a five-necked flask equipped with a mixer, and tubes to transfer the resin into the mold. The reactive system comprising the  $\epsilon$ -caprolactone, PCL oligomer (CAPA 240), and activator was heated at 80 °C under a vacuum. The catalyst (15 wt%) was added to the mixture, which was then injected under nitrogen pressure into the mold. After injection, the mold was maintained at 120 °C for 18 h prior to cooling to room temperature. To compare the laminates produced via TP-RTM, PCL (CAPA 650, Solvay Interlox) powder was used to produce laminates via compression molding. The molecular weight of the PCL matrix obtained via the TP-RTM process was as high as 67300 g.mol<sup>-1</sup>, and was similar to that of commercial PCL (CAPA 650,  $M_n = 60600$  g.mol<sup>-1</sup>). SEM micrographs showed good impregnation of the fibers by the resin, indicating that the TP-RTM process can be used for the production of PCL matrix

composites.<sup>168</sup> Surprisingly, the authors reported that an increase in the molecular weight of the matrix (from 33400 to 67300 g.mol<sup>-1</sup>), which decreases the tensile modulus.

The use of Vicryl fibers did not improve the mechanical properties. One possible reason for the low tensile modulus is the presence of voids, as these may cause an early rupture of the laminate. Unfortunately, the presence of voids was not considered in this study.

Jones *et al.*<sup>169</sup> also prepared PCL matrix composites reinforced with glass fibers using TP-RTM. An  $\epsilon$ -CL monomer was used together with PCL oligomers as the initiator (CAPA 240) and diethyl zinc as the catalyst, via two routes. In the first route, the zinc-based catalyst was dissolved in a toluene solution and mixed with the monomer at 80 °C. The second route was conducted at room temperature with the addition of glycerol and boron trifluoride dimethyletherate to the mixture. The RTM process was associated with the fused deposition modeling technique, which is a rapid prototyping process. The mechanical tests performed were related to the process as a whole, and not only to the composites produced by the RTM. These synthetic routes were unusual as generally, no preformed polymers or oligomers are involved in the RTM process. Since now, no other studies about PCL used as matrix in composites produced by TP-RTM was reported.

#### **1.4.3.3.2 Poly(L-lactide) matrix composites**

The use of a TP-RTM process to produce PLLA-based composites was recently reported by Louisy *et al.*<sup>23</sup> The composites were prepared by a coordination-insertion ROP of L-LA, conducted using tin octoate (SnOct<sub>2</sub>) as the catalyst and glass fabric as the reinforcement. The L-LA and catalyst were mixed together in the TP-RTM tank at 120 °C under a vacuum for 30 min, allowing the monomer to melt. Nitrogen was used to inject the molten L-LA into the mold. The VARTM technique was used in this study, and the injection stage was assisted by a vacuum applied at the exit of the mold, allowing for better impregnation of the glass fabric reinforcement. The resulting PLLA-based composites display high molecular weight matrices up to 78000 g.mol<sup>-1</sup>, with a high monomer conversion of 97 % and crystallinity ranging from 48 to 62%. The good impregnation of the fibers by the matrix was confirmed using optical microscopy. Notably, specific precautions must be taken to conduct the ROP of L-LA in the TP-RTM process.<sup>170</sup> The fibers must be dried prior to use, and a vacuum pump and nitrogen are needed to purge the mold before injection to eliminate residual water.

#### **1.4.3.4 Poly (butylene terephthalate) matrix composites**

Poly(butylene terephthalate) (PBT) is a biodegradable polyester with high strength, stiffness, and low water absorption. It is used in structural applications, the automotive industry, for packaging, and in durable goods. The production of PBT matrix composites by TP-RTM via



the ROP of cyclic butylene terephthalate oligomers (CBTs) in the presence of specific catalysts has been reported in the literature. A CBT has a low processing viscosity of approximately 20 mPa · s, making it suitable for the TP-RTM process.<sup>171,172</sup>

However, CBTs are highly sensitive to water, and a drying step is needed. Another inconvenience is the high melting temperature of CBTs (up to 185 °C), depending on the number of butyl groups in the oligomer mixture.<sup>173,174</sup>

Parton *et al.*<sup>173</sup> investigated the production of glass fiber PBT-matrix composites using the TP-RTM process. A CBT monomer (Cyclics Corporation) was associated with a tin-based catalyst (butylchlorotin dihydroxide, 0.45 wt%) to conduct the polymerization reaction. The resin was then mixed with the catalyst in a container and heated to 190 °C with stirring. The viscosity of the system gradually increased, owing to the polymerization reaction. The resin was then injected into the mold at 190 °C and a polymerization time of 30 min was applied. The composites produced via RTM were compared with PBT specimens fabricated via injection molding without any reinforcements. The PBT in the composite matrix showed crystallinity between 49 and 52% with large and perfect crystals, making them fragile, whereas the pure PBT showed a crystallinity rate of approximately 30%. The authors suggested adjusting the crystallinity to decrease the brittleness of the polymer matrix.

In another study, Parton and Verpoest also studied the production of glass fiber PBT-matrix composites produced by TP-RTM.<sup>175</sup> The methodology used for the production of these composites was the same as in the work mentioned above.<sup>173</sup> Molecular weights up to 66800 g.mol<sup>-1</sup> were obtained with a conversion of the monomer of approximately 90%. Compared with pure PBT, the lower crystallinity rate in the composites was attributed to the presence of the fibers. Despite this, the molecular weights obtained for the composites were close to those of commercial PBTs ( $M_w \approx 85 \text{ kg.mol}^{-1}$ ).

In a study of PBT matrix composites produced via VARTM, Yan *et al.*<sup>174</sup> investigated the rheological properties of CBT. A relationship between the viscosity and catalyst content (butyltin tris(2-ethylhexanoate, 0.1 to 0.6 wt%) at 190 °C and the variations of the viscosity at different temperatures (180 to 210 °C) for the same catalyst content (0.5 wt%) were evaluated (Figure 34). The induction time, *i.e.*, the period in which the solid monomer/oligomer was melted and mixed with the catalyst and during which the mixture exhibited a viscosity lower than 1 Pa.s (optimal for injection), decreased from 25 to 7 min with an increase in the catalyst content (from 0.1 to 0.6 wt%). The authors also reported that increasing the temperature increased the viscosity, and concurrently decreased the induction time. The longest observed induction time was 8 min at 190 °C, and the authors claimed that this time is suitable for the manufacture of large-part thermoplastic laminates. At 180 °C, they observed that the melt

viscosity of the molten oligomer was 200 Pa.s. They indicated that the high viscosity was owing to the high molecular weight of the CBT oligomers, and because the temperature of 180 °C was not sufficient to melt them completely. (Figure 34)

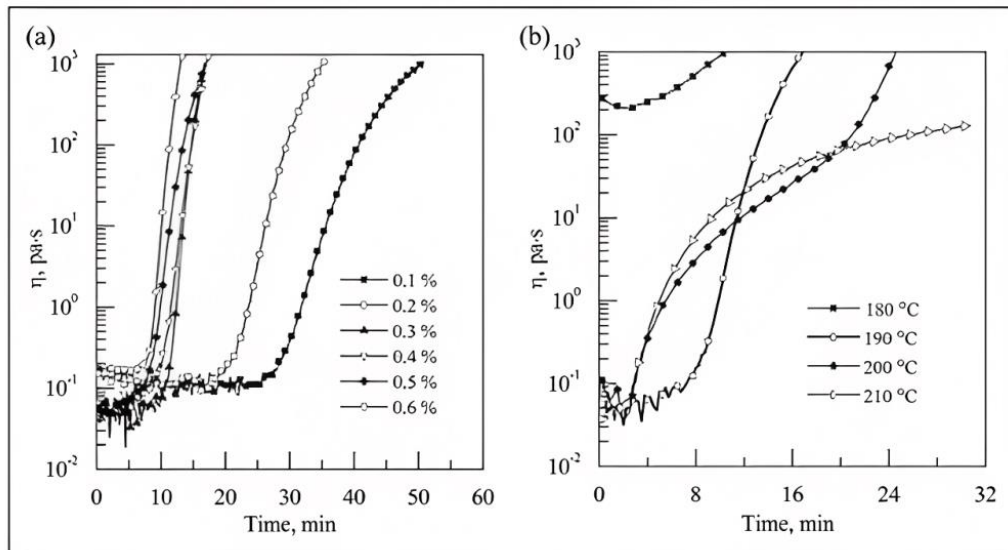


Figure 34: Viscosity of cyclic butylene terephthalate oligomer (CBT) reactive system as function of time in different polymerization conditions. (a) different catalyst contents at 190 °C (b) different polymerization temperatures with 0.5 wt% of catalyst.<sup>174</sup>

For the composite production via VARTM, the CBT was melted at 190 °C under nitrogen with the catalyst (0.5 wt%) in a three-neck round bottom flask, followed by injection into a mold with pre-disposed glass fibers. The injection pressure and vacuum values were not specified. Temperatures ranging from 180 to 210 °C were used to produce the composites. After the injection, the mold was heated for 1 h before being cooled to room temperature. The optimal mechanical properties were obtained for composites produced at 190 °C, with a tensile strength of 549 MPa and flexural strength of 585 MPa.

#### 1.4.3.5 Future trends of thermoplastic systems

Reactive thermoplastic systems can be successfully used in LCM techniques, including TP-RTM, for the production of thermoplastic matrix composites. The low viscosity of the monomers/oligomers involved in these processes leads to a high-quality impregnation of the fibers. The industrial availability of raw materials is a key factor in the manufacturing of thermoplastic-based composites using the RTM technique. In most cases, the monomers involved in reactive thermoplastic systems are cyclic and polymerized by ROP, affording high-molecular-weight matrices. Table 4 summarizes the commercial names, suppliers, viscosity, and polymerization temperatures for all reactive thermoplastic systems in TP-RTM, and the mechanical properties of the resulting matrices.

Currently,  $\epsilon$ -caprolactam/PA-6 is the most employed reactive system in TP-RTM, owing to the good mechanical properties of the resulting composites, its industrial availability, and the low price of the monomer, catalysts, and activators.

Salts of  $\epsilon$ -CL used as a catalyst and activator, generally diisocyanates and both dissolved in  $\epsilon$ -caprolactam, were commercialized by Brüggemann Chemical (Germany) and Rhein Chemie of Lanxess (Germany). Katchem (Czech Republic) commercialized sodium dicaprolactamato-bis-(2-methoxyethoxy)aluminate (Dilactamate<sup>®</sup>) as a solvent-based catalyst. The monomer  $\omega$ -lauro lactam and a carbodiimide-based activator (Grilonit LA), which were commercialized by EMS Chemie (Switzerland), are no longer available; this may explain the low number of studies done in the last few years. MMA-based reactive systems (Elium<sup>®</sup>) were commercialized by Arkema (France) using benzoyl peroxide as the catalyst. A CBT reactive system has been supplied by the Cyclics Corporation, under the trend name Cyclics<sup>®</sup>. Usually, these reactive systems are marketed by only one supplier owing to patent exclusivity, which can increase their prices.

The current development of eco-friendly materials suggests that the production of bio-based composites using TP-RTM should increase progressively in the coming years. The substitution of a thermosetting matrix with thermoplastic materials combined with natural fibers (ramie, hemp, sisal, kenaf, etc.) or recyclable reinforcements is an initial step in the production of green composites. An important challenge in the production of composites is the use of catalysts and activators. The use of metallic compounds such as Sn(Oct)<sub>2</sub> should be reconsidered, as even if this catalyst is approved by the US Food and Drug Administration for use in medical and food applications, it can form toxic Sn(IV)-based compounds. Therefore, alternative biocompatible metal-based catalysts must be considered.

Until now, only one bio-based composite produced by TP-RTM has been reported in the literature; it was created via the ROP of L-lactide.<sup>23</sup> Even though L-lactide (Purac<sup>®</sup>) is commercialized at the industrial scale, one limiting factor for its use in TP-RTM could be its high cost (US\$ 350/kg quotation price in 2023, Corbion, Netherlands), which is almost 200 times higher than the price of  $\epsilon$ -caprolactam (US\$ 1.78/kg quotation price in 2023).<sup>176</sup>

The TP-RTM technique offers the possibility of manufacturing composites with a copolymer matrix, as *in situ* polymerization is possible using this technique. In this framework, the use of copolymers as matrices allows for combinations of the properties (mechanical, chemical, and thermal) of both homopolymers. Generally, the most targeted properties are the modulation of the crystallinity, an improvement of the thermal resistance, and enhancement of the mechanical properties such as toughness and ductility. By selecting new catalysts and varying the co-monomer ratios and experimental conditions, it is possible to synthesize copolymers

with different architectures (block, gradient, and statistical), leading to the production of new advanced materials. Numerous copolymers have been studied in recent years, and their syntheses are well known, *e.g.*, lactam-lactam<sup>177</sup>, lactam-lactone<sup>178</sup>, and lactone-lactone<sup>104</sup>. The production of copolyamides via manufacturing processes such as reactive extrusion<sup>179</sup> and casting<sup>180</sup> has also been reported. To date, only one academic study has been reported on using copolymers as a matrix for the production of composites via TP-RTM.<sup>100</sup>

The transposition of the composite synthesis from lab scale to industrial scale and adapting the copolymerization in bulk using TP-RTM remain challenges, mainly owing to the reproducibility (*i.e.*, allowing manufacturing in a well-controlled and repeatable way). A promising future can be predicted for composites with polymer matrices produced via the TP-RTM. This can be justified not only by the recyclability of the composite parts, but also by the enhanced properties of copolymers and beneficial post-processing features.

The replacement of thermosets with thermoplastic matrices in composites requires adaptation of the RTM process for industrial applications. New multi-component dosing machines with mixing heads have been developed to allow for the injection of highly reactive systems, *e.g.*,  $\epsilon$ -CL/ PA-6, and have been commercialized by KraussMaffei (Germany), Diatex (France), Tartler (Germany), and Wolfangel (Germany). The requirement to use high working temperatures was also an adaptation of RTM to allow for the use of solid monomers such as  $\epsilon$ -caprolactam, L-LA, and  $\omega$ -LL at room temperature. Moreover, the problem of the water content in the reagents was partially solved with the use of a vacuum in the TP-RTM tank, and the possibility of working under an inert atmosphere. However, water and oxygen remain the biggest issues in the ROP of cyclic esters, as they harm the reproducibility of the TP-RTM process. In that context, vacuum pumps have been used and new mold geometries have been designed to eliminate moisture.<sup>135</sup> In addition, an investigation of the moisture adsorption and desorption in the  $\epsilon$ -caprolactam/PA-6 reactive system (as in fibers) has already been conducted, and should be extended to other reactive thermoplastic systems.<sup>181</sup> Owing to extremely low viscosity of some systems, *e.g.*,  $\epsilon$ -caprolactam/PA-6, problems of mold sealing have arisen; nevertheless, the use of double seals can solve this problem.<sup>135</sup>

Mechanical, thermal, and chemical recycling are the main techniques used to recycle thermoplastic composites. Mechanical recycling is the most used technique and allows for the full recovery of the matrix and fibers, whereas thermal and chemical recycling only allow for the recovery of fibers.<sup>13</sup> As the technologies for recovering raw materials by grinding has been extensively investigated and is now well-established,<sup>97,182,183</sup> they can be applied to the recycling of thermoplastic composites manufactured by TP-RTM. Cousins *et al.* proposed a study for recycling a prototypical PMMA-based wind turbine blade produced by TP-RTM using

different techniques such as pyrolysis, grinding, and dissolution.<sup>12</sup> In addition, they recycled wind turbine blade by thermoforming them into other products, such as skateboards.

The most promising recycling technique for maintaining the good mechanical properties of recycled fibers is dissolution. The glass fibers separated by this technique generally show a tensile strength equal to that of virgin samples. Dissolution allows for a complete separation of the fibers from the matrix, but remains expensive and not eco-friendly, as solvents such as methanol and chloroform are used.<sup>12</sup> In term of costs, thermoforming seems to be the most interesting technique for reprocessing large parts and giving new life to composites. Special attention should be paid to PLA-and PCL-based composites, owing to the biodegradable nature of these polymers; thus, investigations of the recyclability and composting of such composites are of interest.

## 1.5 Conclusion

In this chapter, a comprehensive literature review on the properties and applications of composite materials was presented. It covered various topics such as the classification of fibers, the manufacturing process of composite materials, the properties of different types of reinforcements and matrices, and the applications of composite materials in various industries. Additionally, this chapter provided insights into the challenges and opportunities associated with the use of composite materials in different applications.

The use of thermoplastic polymers in LCM techniques are growing, driven by the necessity to become the production of composites more sustainable. The use of bio-based and biodegradable polymers in composite industry is one way to avoid the use of petro-based resins. Among different manufacturing process, the TP-RTM permits the production of polymer reinforced composites with high content of reinforcement with low void content.

In great detail, this chapter also highlighted the production of thermoplastic composites by TP-RTM. Among presented thermoplastics, in this work the focus will be in poly(L-lactide) (PLLA) and poly(L-lactide-co- $\epsilon$ -caprolactone) (PLCL), in which these ones will be used as matrices in composites produced by TP-RTM. The different types of reinforcement presented in this chapter, glass, carbon and flax fibers will be used as reinforcements.

Table 4: Comparison of work temperature and viscosity for all reactive thermoplastic systems used in TP-RTM and mechanical properties for respective matrices.

<b>Reactive system (Monomer/Polymer)</b>	<b>Commercial names</b>	<b>Suppliers</b>	<b>Catalyst/Activator</b>	<b>Viscosity (mPa.s)</b>	<b>Mold temperature (°C)</b>	<b>Tensile strength/Tensile modulus (MPa/GPa)</b>	<b>References</b>
<i>ε-caprolactam/Polyamide-6</i>	Bruggolen®	Brüggemann Chemicals (Germany)	Sodium caprolactam salt/carbodiimide	3 – 5	140 - 180	80 / 3.5	134,184,185
<i>ω-lauro lactam/Polyamide-12</i>		Not marketed in industrial scale	Sodium caprolactam salt /carbodiimide	4.5 – 8	170 - 205	45 / 1.1	161
<i>Methyl methacrylate/Poly(methyl methacrylate)</i>	Elium® C195 Elium® 190	Arkema (France)	Peroxide blends	100	180 - 200	66 / 3.17	186,187
<i>Cyclic butylene terephthalate/ Poly(cyclic butylene terephthalate)</i>	CBT®	Cyclics Corporation (USA)	Tin or titanium - based catalyst	12 – 33	190 - 240	54 / 2.7	188,189
<i>ε-caprolactone/Poly(ε-caprolactone)</i>	Capromer™ Capa® PurasorbC®	BASF (Germany) Ingevity (USA) Corbion (Netherlands)	Zinc or tin-based catalyst	nd	120	4–785 / 0.21– 0.44	166
<i>L-lactide/Poly(L-lactide)</i>	Purasorb®	Corbion (Netherlands)	Tin-based catalyst	nd	185	59 / 3.5	23,190

nd : To date, no studies on the viscosity of ε-caprolactone and L-lactide have been reported

## **CHAPTER II: MATERIALS AND METHODS**

This chapter gathers the description of the raw materials and the experimental techniques used during this study. First, the reagents, the reinforcements, the mold and TP-RTM machine will be presented. Thereafter, the protocol for the production of composites using the TP-RTM machine will be described. Finally, the different techniques used to characterize the composite will be described.



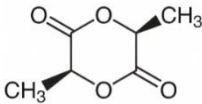
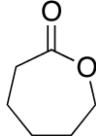
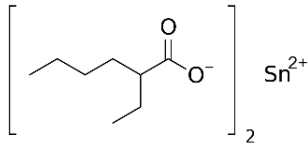


## 2.1 Materials

### 2.1.1 Reagents

L-lactide (L-LA) monomer was purchased from Corbion (Netherlands) was stored in a freezer. L-lactide is a white crystalline solid with melting temperature of 96 °C (Table 5).  $\epsilon$ -caprolactone ( $\epsilon$ -CL) monomer and tin (II) 2-ethylhexanoate ( $\text{Sn}(\text{Oct})_2$ ) were both obtained from AlfaAesar (USA), stored at room temperature and used as received.  $\epsilon$ -CL is a colorless liquid and  $\text{Sn}(\text{Oct})_2$  is a pale yellow liquid at room temperature.

Table 5: Principal characteristics of reagents.

Product	Appearance	Molecular weight (g)	Melting temperature(°C)	Purity (%)	Chemical structure
L-lactide (L-LA)	White crystalline solid	144.126	96	>99.9	
$\epsilon$ -caprolactone ( $\epsilon$ -CL)	Colorless liquid	114.14	-1	>98.5	
tin (II) 2-ethylhexanoate ( $\text{Sn}(\text{Oct})_2$ )	Pale yellow liquid	405.12	0	92.5-100	

### 2.1.2 Reinforcements

Different types of reinforcements were chosen in this work. Among synthetic fibers, glass woven fabric and carbon woven fabric were selected. Regarding natural fibers, two types of flax fibers were chosen as reinforcement: twill 2/2 and cross-stitched unidirectional (Figure 35).

Woven glass fabric (GF), supplied by Hexcel, disposes areal weight of 390 g.m<sup>-2</sup>, Young modulus of 72 GPa and elongation at break of 4%. Woven carbon fabric (Mitsubishi) have areal weight of 210 g.m<sup>-2</sup>, Young modulus of 234 GPa and elongation at break of 1.8 % (Table 6).

Table 6: Principal characteristics of reinforcements used in the production of composites.

Type of reinforcement	Pattern	Areal weight (g.m <sup>-2</sup> )	Density (g.cm <sup>-3</sup> )	Mechanical properties			Supplier
				Young modulus (GPa)	Tensile strength (MPa)	Elongation at break (%)	
Woven glass fabric	Twill 2/2	390	2.50	72	5600	4	Hexcel (USA)
Woven carbon fabric	Twill 3K 2/2	210	1.79	234	4120	1.8	Mitsubishi (Japan)
Woven flax fabric	Twill 2/2	300	1.29	12	113	1.7	Ecotechnilin (France)
	Cross-stitched unidirectional	180	1.33	35	330	0.8	Ecotechnilin (France)

Woven flax fabric twill 2/2 (TW) have areal weight of 300 g.m<sup>-2</sup>, Young modulus of 12 GPa and elongation at break of 1.7 %. Woven flax fabric cross-stitched unidirectional (UD) dispose areal weight of 1.33 g.m<sup>-2</sup>, Young modulus of 35 MPa and elongation at break of 0.8 % (Table 6).

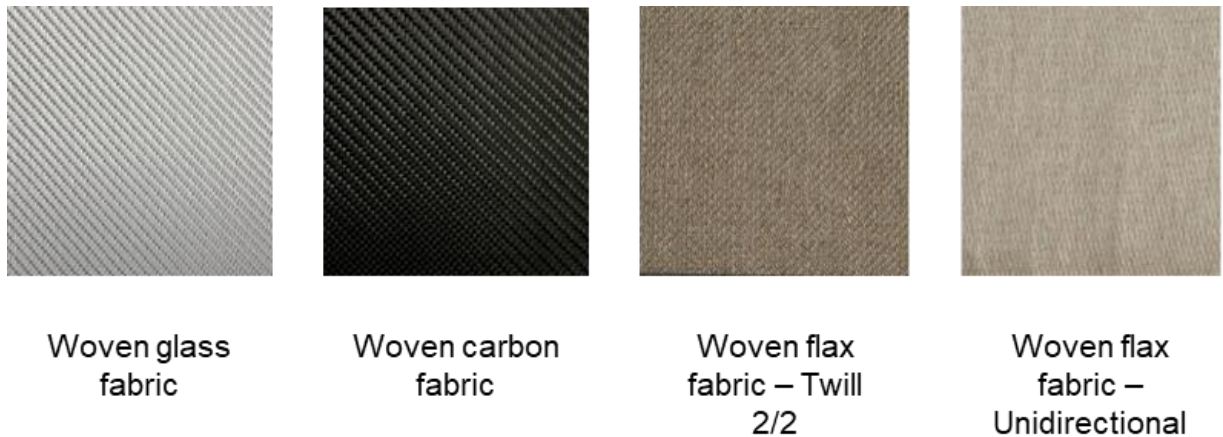


Figure 35: Physical aspect of reinforcements.

### 2.1.3 Mold surface treater and release agent

An aromatic naphtha based surface treater (Sealer GP) purchased from ChemTrend was used to treat the mold surface to prevent abrasion and seal pores.

A release agent (Zyvax® WaterShield™) supplied by ChemTrend was used to facilitate the demold. This release agent is water based and is recommended for releasing epoxies, phenolics, polyester resins, polyamides, polybismaleimides, various rubbers and elastomers.

### 2.1.4 TP-RTM apparatus

A single component TP-RTM machine (CIJECT III) from DIATEX (France) was used in this work (Figure 36). The machine is composed by a 7.5 L high-pressure regulated tank (7 bar) equipped with an air stirrer. The tank can be heated and the injection of the resin into the mold is assisted by PTFE tubes ( $\varnothing$  4mm x  $\varnothing$  6mm) placed in the tank resin outlet. At the right side of the unit control, a vacuum pump is connected to the vacuum inlet, used to degas the tank and the air inlet is connected to a N<sub>2</sub> gas line used for the injection of the resin and also to make work the stirrer. A scale is placed under the tank used to follow the injection step.

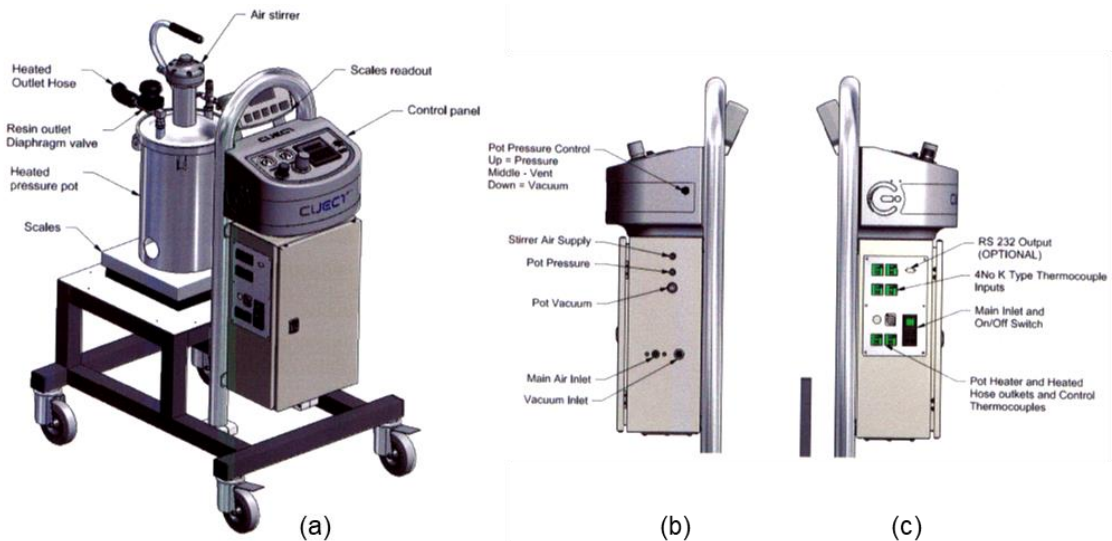


Figure 36: (a) General view of TP-RTM machine; (b) Right and (c) left side of unit control.

Since the tank was originally designed for the injection of high amounts of resin (7.5 L) an aluminum beaker (1 L) was placed in the middle of the tank, in order to allow the injection of lower resin volumes, adapted to the size of the composite plates targeted in this work. To keep it stable, the beaker was surrounded by a support made of aluminum paper (Figure 37).

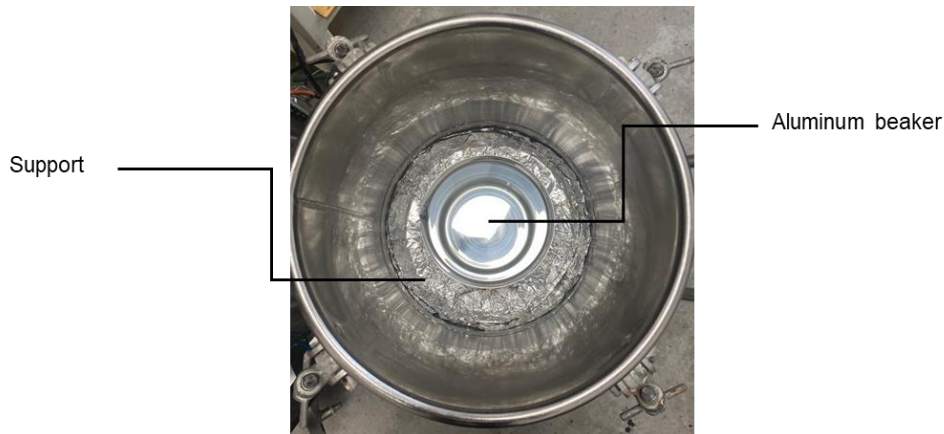


Figure 37: Aluminum beaker placed in the middle of the TP-RTM tank.

### 2.1.5 TP-RTM Mold

An aluminum mold with dimensions 120 x 120 x 5 mm<sup>3</sup> was supplied by Diatex (France). The mold is composed of 3-parts and a peripheral injection was used to fill the mold. To keep the mold hermetically closed and prevent leaks, the mold disposes of the double silicone seal.

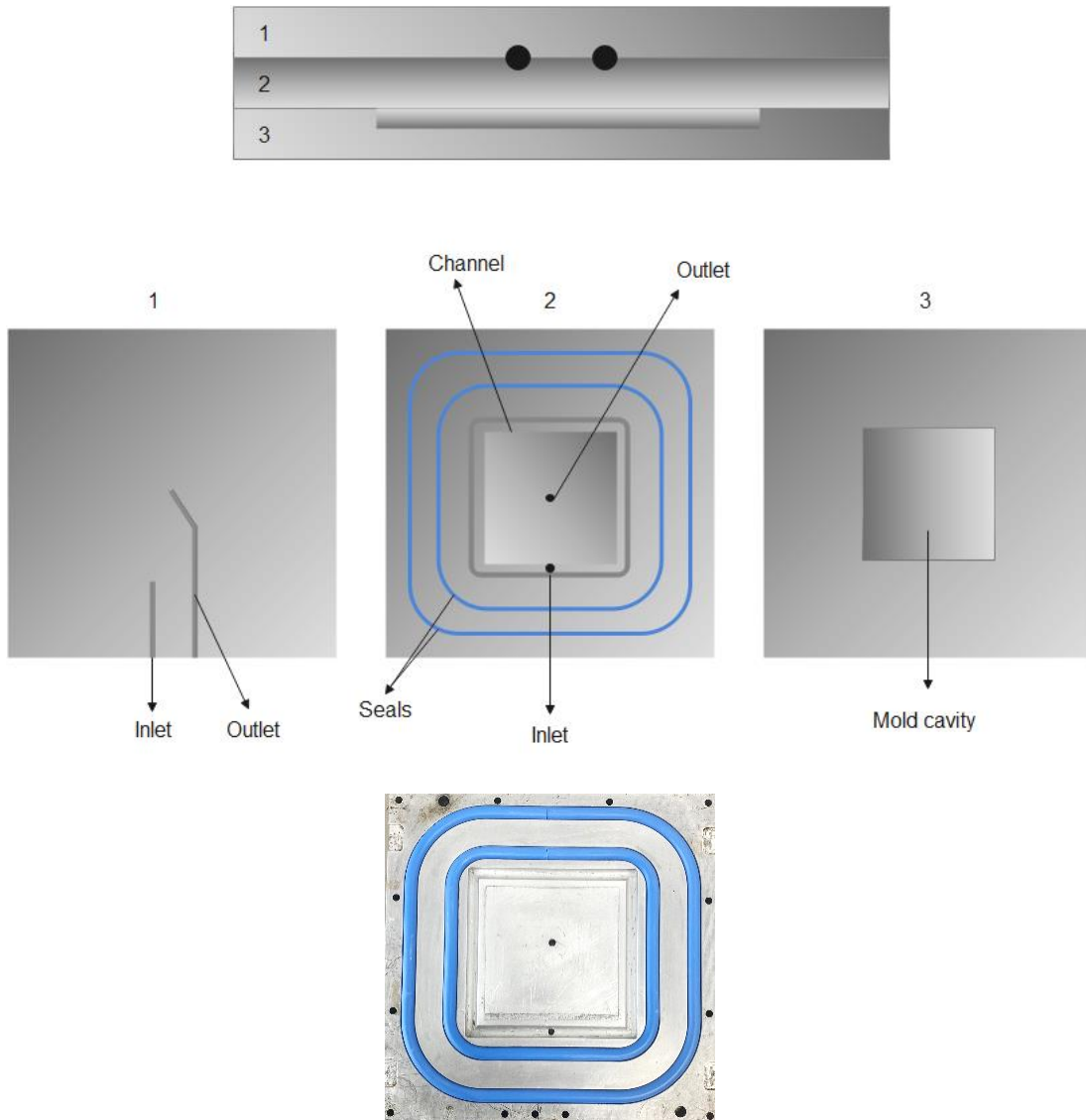


Figure 38: Aluminum mold used to produce composite plates.

## 2.2 Production of composites

The production of PLLA and PLCL matrix composites by TP-RTM was conducted following five steps: (i) preparation of reinforcement and mold, (ii) preparation of reagents and melting, (iii) injection step, (iv) polymerization, (v) cooling/demolding. These five steps will be thoroughly described below and a resume of the production of composites including all TP-RTM parameters is proposed in Section 2.2.6.

### 2.2.1 Preparation of reinforcements and mold

Glass, carbon, and flax fabrics were cut at the same dimensions as the mold cavity using a roll cutter. Following this step, all fabrics were dried at 80°C for 24h prior to use. Before placing the fabrics into the mold, its surfaces were treated with a sealer (Sealer GP) to overcome micro-porosity in the mold surface, and protect the surface of the mold from gases and abrasion, therefore extending the mold life. Four coats were applied with towel paper respecting a minimum of 15 minutes cure time before the application of the next coat. Then, a release agent (Zyvax® WaterShield™) was applied to the surface of the mold to facilitate the demold. Two coats were applied with a minimum of 30 minutes before the application of the next coat.

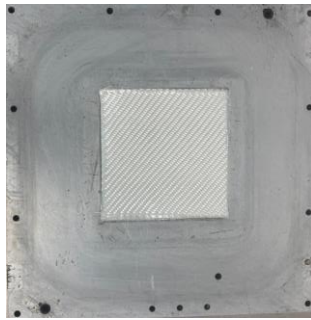


*Figure 39: Mold cavity with pre-disposed glass fabric.*

The layers of the reinforcement were placed into the mold cavity, fully to the edge. Due to the different characteristics of the fibers and the fabrics, a different number of layers were used for each fabric to fully fill the cavity. Besides ten layers of glass, carbon, and unidirectional flax fabric were used while for woven twill 2/2 flax fabric, only five layers were used. Worth noting is that all the fabric layers were placed along the same orientation.

After the surface treatment of the mold and the placement of the reinforcement, the mold was closed and heated using a press. To keep the mold closed, a pressure of 30 kN was applied and different temperatures were chosen (for the polymerization temperatures see Section 2.2.4 (p.64)).

### 2.2.2 Preparation of reagents

To fill the mold cavity completely with the reactive thermoplastic system, a quantity of 200g of reagents was used.<sup>23</sup> Different molar ratios of the two co-monomers L-LA and  $\epsilon$ -CL was used to produce the matrix (Table 7) with a co-monomers over catalyst ratio of 2000 for all compositions, as an example based on our previous results and the literature.<sup>23,27,28</sup>

Table 7: Matrix compositions of composite plates.

<i>Abbreviation of matrix composition</i>	<i>Monomers</i>	
	<i>L-lactide</i> (mol %)	<i>ε-caprolactone</i> (mol %)
Neat PLLA	100	0
10 PLCL	90	10
20 PLCL	80	20
30 PLCL	70	30

Before placing the monomers and the catalyst mixture into the tank, the latter was previously heated at 150°C to allow the melting of L-Lactide ( $T_m = 96^\circ\text{C}$ ), which is then fully miscible with both  $\epsilon$ -caprolactone and  $\text{SnOct}_2$ . Once put into the tank, 30 minutes were necessary to melt all the L-LA in all compositions. During this time, the tank was kept under a dynamic vacuum of 0.5 bar to remove any traces of water.

### 2.2.3 Injection step

Prior to the injection step, the stirring of the mixture, also called “reactive thermoplastic system”, was done into the tank. The stirrer, initially designed for mixing large amounts of resin (7,5 L), is activated via  $\text{N}_2$  pressure. A minimum pressure of 2 bar is required to make the stirrer work, but the rotations per minute (RPM) are unknown since there is no advice in the machine to measure this parameter. Pressures higher than 2 bar are not adapted to mix low contents of resin. In this context, the stirrer was activated with 2 bar for 15 seconds.

After stirring, the injection step takes place in a pre-heated mold. A pressure of 1 bar of  $\text{N}_2$  was applied into the tank to allow the injection of the reactive thermoplastic system into the mold. Since the last one display a water-like viscosity, this low pressure is sufficient to allow its injection in the mold. Once the pressure was applied, the reactive system rises throughout the inlet PTFE tube. When the liquid mixture starts to leave by the outlet PTFE tube, indicating that the mold is filled, the latter was clamped and the injection continues for approximately 10 seconds, allowing the saturation of the reinforcement by the resin. After this time, the inlet PTFE tube was also clamped and the injection step is finished.

### 2.2.4 Polymerization

The polymerization starts after the injection step and the polymerization temperature is the same temperature of the mold. Different polymerization temperatures were tested, 150, 160, 170 and 185°C, and the choice of the optimal temperature depending on the matrix composition will be discussed later in Section (3.6, p.107). Regarding the polymerization time, a time of 120 minutes for PLLA matrix composites was chosen based on the former works.<sup>23</sup> For PLCL matrix composites, different polymerization times were tested, 2, 3, and 5 h, and the discussion of the optimal polymerization time for PLCL matrix composites will be discussed later in Section (3.2.2, p. 82).

### 2.2.5 Cooling and demolding

Once the polymerization is completed, the mold was kept under pressure and cooled down to room temperature, without chiller. The composite plates were then demolded and the polymer present in the channels were cut with scissors (Figure 40).

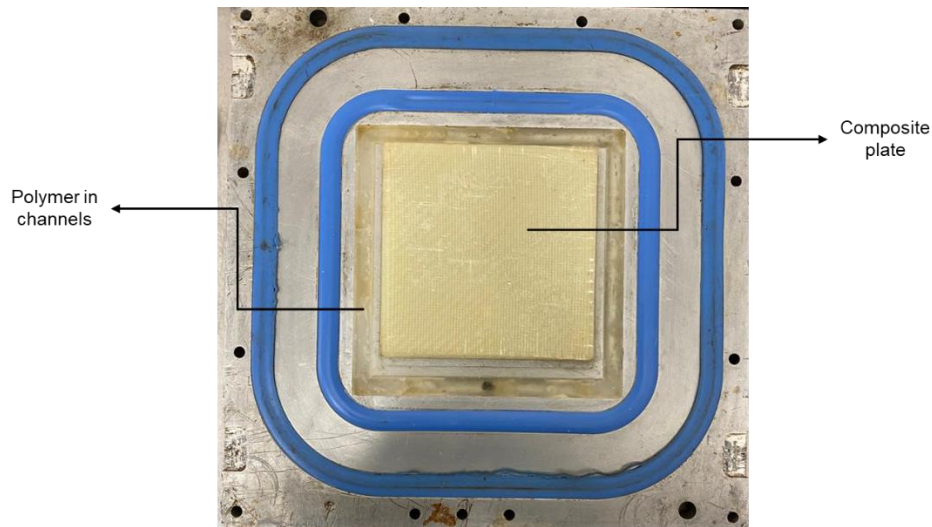


Figure 40: Composite plate before demold, showing the polymer in mold channels.

### 2.2.6 Summary of the production of composites in TP-RTM

The production of composite plates starts with the preparation of the woven fabrics, the mold, and heating the TP-RTM tank (Figure 41). The woven fabrics are placed into the mold cavity; the latter being closed using a press.

The mixture of L-LA,  $\epsilon$ -CL, and  $\text{Sn}(\text{Oct})_2$  is placed into the TP-RTM tank. The melting of L-LA takes place inside the tank, the mixture is stirred and injected into the mold.

Following injection, polymerization takes place inside the mold. Once the polymerization is over, the mold is cooled at room temperature and the composite plate is demolded.

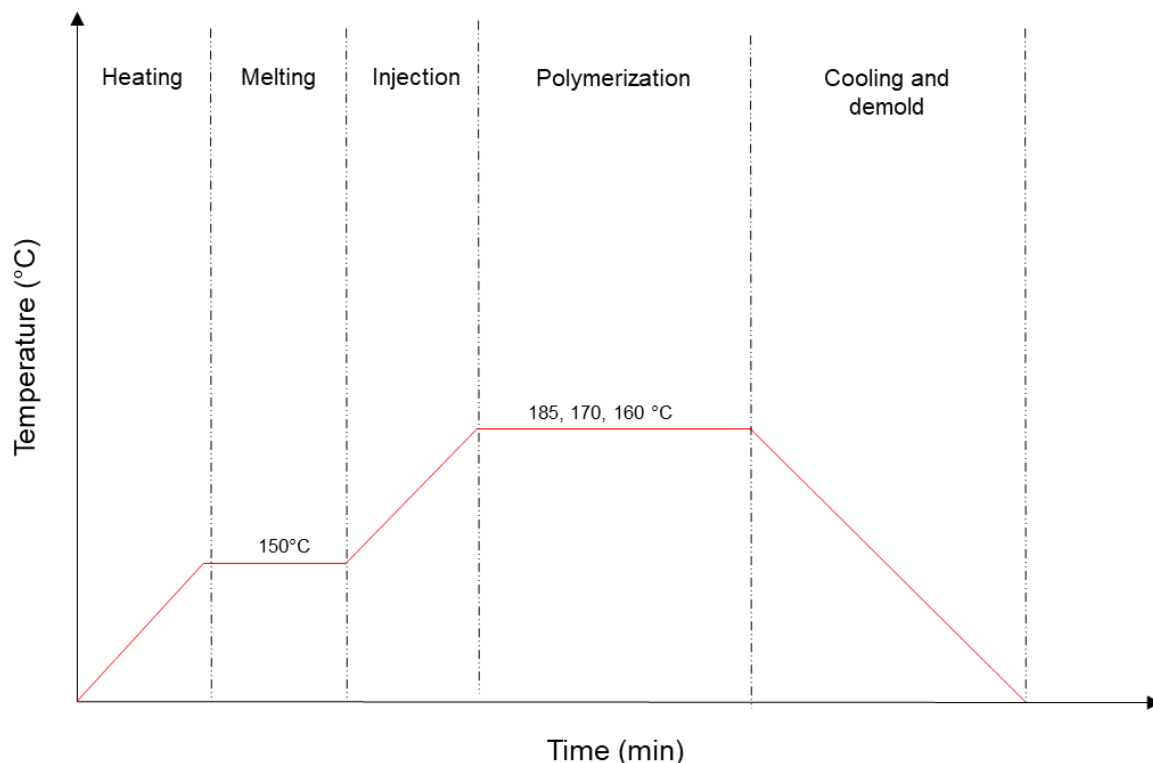


Figure 41: Schematic representation of the temperature process versus time during the production of composite plates in TP-RTM.

## 2.3 Physicochemical characterization

### 2.3.1 Proton nuclear magnetic resonance spectroscopy ( $^1\text{H}$ NMR)

Liquid proton nuclear magnetic resonance was used to determine the conversion of the comonomers to polymer and also to determine the copolymers composition as well as their microstructure. The analyzes were carried out on a Bruker Avance 300 MHz spectrometer. The samples (about 5 to 15 mg) were dissolved in 1 mL of  $\text{CDCl}_3$ , in a 5 mm diameter tube. The number of scans was set to 32 and the delay between each scan was set to 4 s. The calibration of the spectrum was made via the residual pic of  $\text{CHCl}_3$  in the deuterated solvent at 7.26 ppm.

The conversion of L-LA was determined by integrating the methine ( $-\text{CH}$ ) signal of monomer centered at 5.05 ppm and polymer at 5.15 ppm. The conversion of  $\epsilon$ -CL was determined by integrating the signals of the monomer centered at 4.22 ppm and the signals of the polymer which corresponds to the  $\epsilon$  methylene ( $-\text{CH}_2-$ ) around 4.12 and 4.05 ppm (Figure 42).



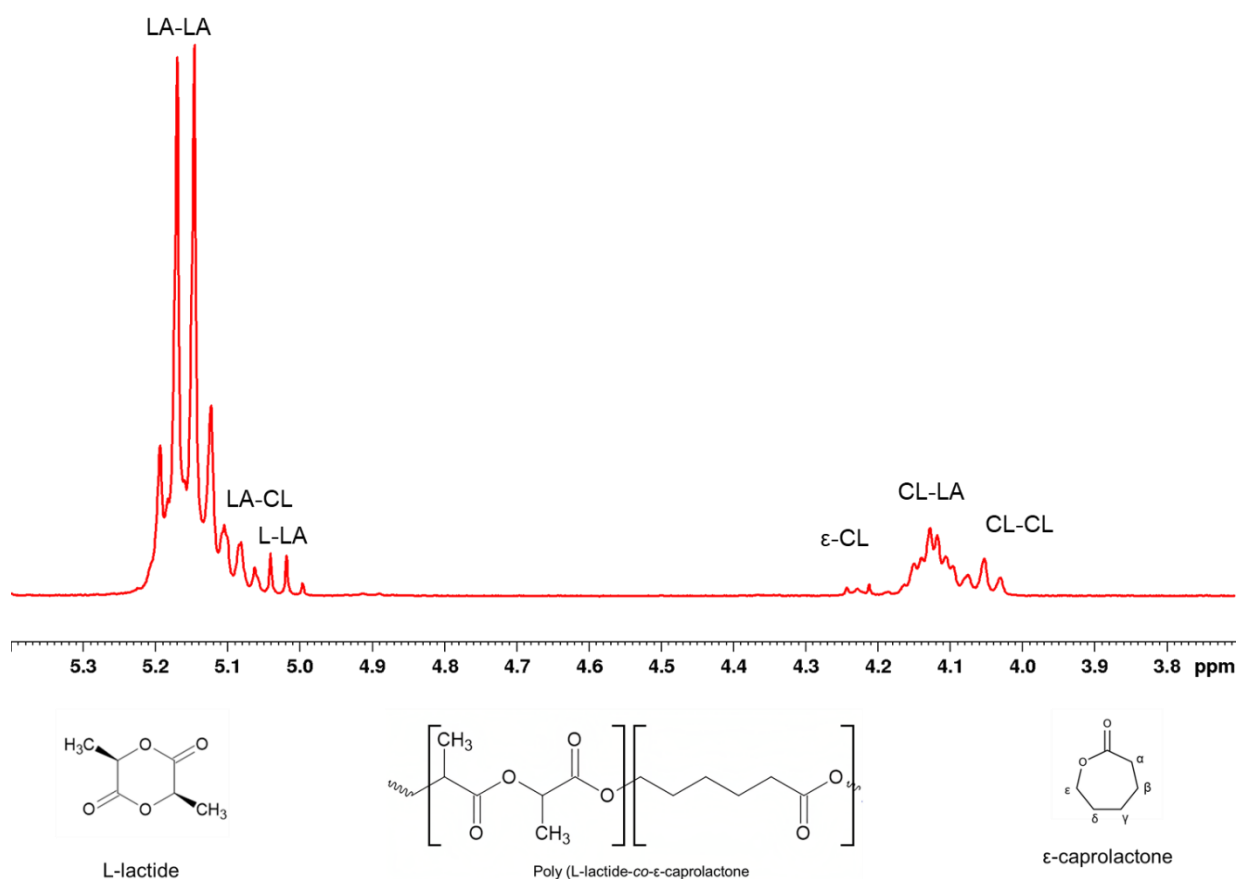


Figure 42: <sup>1</sup>H NMR spectra of 20 PLCL ([L-LA]:[ε-CL] = 80:20) in CDCl<sub>3</sub>.

To determine the copolymer composition and the microstructural magnitudes of copolymers the average dyad relative molar fractions were resolved by <sup>1</sup>H NMR integrating the peak areas. Regarding CL unit signals, the peak at 4.05 ppm correspond to the CL – CL dyad and the peak centered at 4.12 correspond to the CL – LA dyad. In the matter of LA unit signals, the peaks corresponding to LA – LA and LA – CL are overlapped at 5.16 ppm. Considering that the LA – CL dyad contribution to the LA methine signal has the same relative molar fraction obtained for CL – LA dyad, the integration of ε methylene corresponds to the total relative molar fraction of the CL – LA dyad.

The number-average sequence lengths of LA ( $l_{LA}$ ) and CL ( $l_{CL}$ ) building blocks (Equation 3) the Bernoullian random number-average sequence lengths (Equation 4) and the randomness character (R) (Equation 5) were calculated based on the Bernoullian model, where (LA) and (CL) are the comonomer molar fractions and (LA – CL) is the LA – CL average dyad relative molar fraction.<sup>191</sup>

$$l_{LA} = \frac{2(LA)}{(LA-CL)}; l_{CL} = \frac{2(CL)}{(LA-CL)} \quad \text{Equation 3}$$

$$(I_{LA})_{Random} = \frac{1}{(CL)}; (I_{CL})_{Random} = \frac{1}{(LA)} \quad \text{Equation 4}$$

$$R = \frac{(I_{(LA)Random})}{I_{LA}} = \frac{(I_{(CL)Random})}{I_{CL}} = \frac{(LA-CL)}{2(LA)(CL)} \quad \text{Equation 5}$$

### 2.3.2 Size Exclusion Chromatography (SEC)

Size exclusion chromatography (SEC) was used to determine the number average molecular mass ( $M_n$ ), the weight average molecular weight ( $M_w$ ) and the dispersity ( $\mathcal{D}$ ) of the poly(L-lactide) (PLLA) and poly(L-lactide-co- $\epsilon$ -caprolactone) (PLCL) matrices. The samples were prepared with a concentration of 1 mg. mL<sup>-1</sup>, using chloroform (CHCl<sub>3</sub>) as solvent for PLLA and tetrahydrofuran (THF) for PLCL and filtered through a 0.45  $\mu$ m pore-size membrane. Given the widely acknowledged tendency of polystyrene-calibrated SEC measurements to overestimate the real molecular weights values of aliphatic polyesters, attributed to the relatively smaller hydrodynamic volume of polystyrene, the molecular weights of PLLA and PLCL were corrected using PLLA and PCL Mark-Houwink coefficient in the corresponding solvent.

Measurements of molecular weights of PLLA matrices were performed at UMET on an Agilent system (1260 Infinity II LC System) equipped with three columns (Shodex K-802.5, 803 et 804) placed in series and coupled with a differential refractometer (Wyatt Optilab). The PLLA samples were analyzed at 25 °C in CHCl<sub>3</sub> and flow rate of 1 mL.min<sup>-1</sup>. It was established that both  $M_n$  and  $M_w$  would be corrected by a factor of 0.68.<sup>192,193</sup>

The molecular weights of PLCL matrices were measured at UMET on an Agilent system (1260 Infinity II LC System) equipped with three columns (Waters HR1, HR3 et HR4) placed in series and coupled with a differential refractometer (Wyatt T-REX). The PLCL samples were analyzed at 35 °C using THF as solvent and flow rate of 1 mL.min<sup>-1</sup>. The molecular weights ( $M_n$  and  $M_w$ ) of PLCL were corrected combining the correction factors of PLLA and PCL in THF, according to the ratio of co-monomers in the PLCL matrix. The correction factor used for the PLLA is 0.58 and 0.56 for PCL.<sup>194,195</sup> The correction factor applied to PLCL matrices was then: [0.58 x wt % LA units + 0.56 x wt % CL units].<sup>196</sup>

Due to the lack of availability of SEC apparatus at UMET, the first measurements of molecular weights presented in Section 3.2 (p.82) were conducted at IMP Lyon. The analysis were performed in a Perkin Elmer system (Series 200), equipped with three columns (Agilent PLgel MIXED-E, 7.5 x 300 mm) coupled with a multi-angle light scattering (Wyatt TREOS) and with a differential refractometer (Shimadzu RID 10A). The analysis were conducted in CHCl<sub>3</sub> at 30 °C for both PLLA and PLCL matrices. Due to the triple detection system, the molecular weights were not corrected.

For the sake of comparison, the molecular weight of a commercial PLA (4032D - NatureWorks) was assessed using the SEC apparatus at UMET. The measurements were conducted in  $\text{CDCl}_3$ , resulting in a  $M_n$  of  $93,600 \text{ g}\cdot\text{mol}^{-1}$  and an  $M_w$  of  $137,300 \text{ g}\cdot\text{mol}^{-1}$  for the PLA sample. These values were corrected by a factor of 0.68.

### 2.3.3 Thermogravimetric analysis (TGA)

TGA measurements were performed in a TG 209 F1 Libra<sup>®</sup>. The samples were prepared using only the matrices without reinforcement. Approximately 10 mg of samples were placed in open silica pans and submitted to an isotherm at  $50 \text{ }^\circ\text{C}$  for 10 minutes followed by a heating ramp of  $10 \text{ }^\circ\text{C}/\text{min}$  until  $800 \text{ }^\circ\text{C}$  under  $\text{N}_2$ , with purge flow rates set at 15 and  $100 \text{ mL}\cdot\text{min}^{-1}$ .

### 2.3.4 Differential scanning calorimetry (DSC)

The glass transition temperature ( $T_g$ ), the melting temperature ( $T_m$ ) and the melting enthalpy ( $\Delta H_m$ ) of the matrices were determined by differential scanning calorimetry (DSC). Analyses were performed on a TA Instrument Discovery DSC operated with Trios software. The samples were prepared using 5 - 10 mg of polymer or copolymer placed in a standard aluminum sample crucible.

The samples were exposed to two cycles of cooling and heating under a nitrogen atmosphere. During the analysis, the samples were twice cooled from room temperature to  $-80 \text{ }^\circ\text{C}$  at  $10 \text{ }^\circ\text{C}/\text{min}$  and heated at  $200 \text{ }^\circ\text{C}$  at  $10 \text{ }^\circ\text{C}/\text{min}$  (Figure 43). The first scan was used to determine the  $T_m$  and the  $\Delta H_f$ . The second scan permits to measure the  $T_g$ .

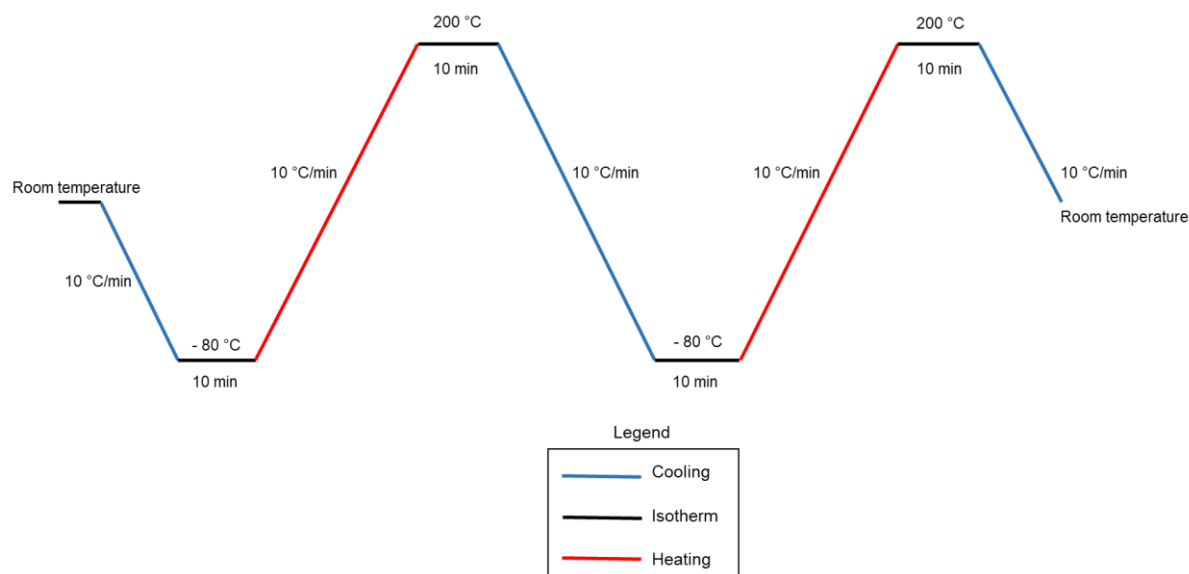


Figure 43: Cycles of heating and cooling used in DSC analysis.

The crystallinity ( $\chi_c$ ) in % of the PLLA matrix was calculated from Equation 6,

$$\chi_c = \frac{100 \Delta H_f}{\Delta H_f^0} \quad \text{Equation 6}$$

where  $\Delta H_f^0 = 93.1 \text{ J.g}^{-1}$  is the enthalpy of fusion of 100% crystalline PLLA.<sup>197</sup>

The crystallinity of PLLA into the PLCL matrix was determined from Equation 7, assuming that only the lactide units crystallize, where ( $LA^*$ ) is the actual lactide mass fraction in the copolymer.<sup>27</sup>

$$\chi_c = \frac{100 \Delta H_f}{\Delta H_f^0 \cdot (LA^*)} \quad \text{Equation 7}$$

## 2.4 Mechanical testing

The composites underwent three types of mechanical tests: uniaxial tensile test, three-point bending, and impact test. The specimens of each test were cut from the composite plates using a waterjet cutting machine (BP-H 3015 TCI Cutting Waterjet & Laser systems).

### 2.4.1 Tensile testing

Tensile tests were conducted for the determination of tensile properties of fiber-reinforced plastic composites: Young modulus ( $E$ ), tensile strength ( $\sigma_t$ ), and elongation at break ( $\epsilon$ ). An Instron 4466 machine was used with a 10kN load cell and the specimens (Figure 44) were tested at 10 mm/min. The dimensions of the specimens (Table 8) for the tensile test were based on the ISO 527-4 standard (Tensile Properties of Isotropic and Orthotropic Fiber-Reinforced Plastic Composites). Five specimens for each composition with different reinforcements were tested.

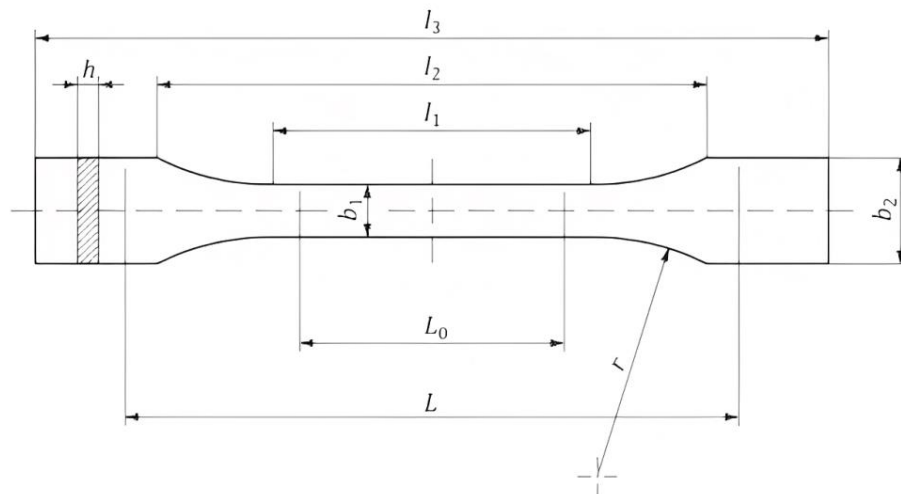


Figure 44: Type 1B specimen.

Table 8: Dimensions of type 1B specimen used in tensile test.

Symbol	Name	Dimensions (mm)
$l_3$	Overall length	100
$l_1$	Length of narrow parallel-sided portion	30
$r$	Radius	120
$b_2$	Width at ends	10
$b_1$	Width of narrow portion	5
$h$	Thickness	5
$L$	Initial distance between grips	$100 \pm 1$

### 2.4.2 Three-point bending testing

Three-point bending test was used to determine the flexural strength ( $\sigma_f$ ) and the bending modulus ( $E_B$ ). A universal testing machine (Instron 5867) was used and the specimen was placed on two support anvils and bending it through an applied force at 10 mm/min. (Figure 45). Five test specimens with valid failures were tested.



Figure 45: Instantaneous moment of performing the three-point bending test.

The dimensions of the specimens were adapted from ISO 14125 standard (Fiber-reinforced plastic composites – Determination of flexural properties), with length of 60 mm, width of 15 mm and thickness of 5 mm.

The flexural strength ( $\sigma_f$ ) is given by the following equation:

$$\sigma_f = \frac{3FL}{2bh^2} \quad \text{Equation 8}$$

where

$\sigma_f$  is the flexural strength, in megapascal (MPa)

F is the load, in newton (N)

L is the span, in millimeters (mm)

h is the thickness of the specimen, in millimeters (mm)

b is the width of the specimen, in millimeters (mm)

The bending modulus was calculated between  $\varepsilon_f' = 0.0005$  et  $\varepsilon_f'' = 0.0025$ .

### 2.4.3 Impact testing

Charpy impact test was carried out according to the ISO 179-1 standard (Plastics – Determination of Charpy impact properties) to determine impact strength ( $\alpha_{CU}$ ). Tests were performed with unnotched specimens with dimensions 80 x 15 x 5 mm<sup>3</sup> using a 50 J hammer on a pendulum impact testing machine (CEAST 9050 – Instron®). The specimens were positioned edgewise to the blow and five specimens were tested (Figure 46).

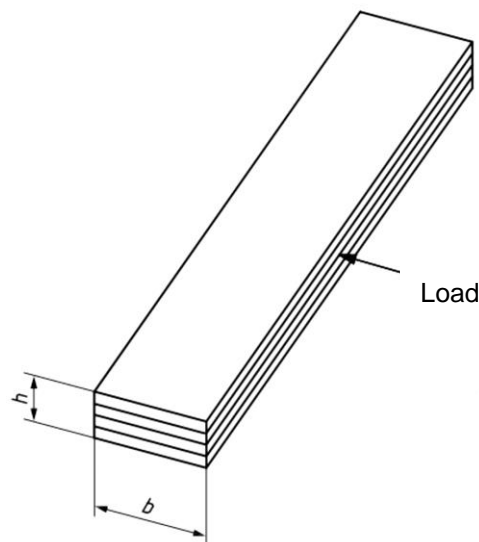


Figure 46: Scheme of designation describing the direction of blow.

The Charpy impact strength of unnotched specimens ( $\alpha_{cU}$ ), expressed in kilojoules per square meter, were calculated using the following equation:

$$\alpha_{cU} = \frac{E_c}{h.b} \times 10^3 \quad \text{Equation 9}$$

where,

$E_c$  is the energy, in joules, absorbed by breaking the specimen;

$h$  is the thickness, in millimeters, of the test specimen;

$b$  is the remaining width, in millimeters, of the test specimen.

#### 2.4.4 Cyclic three-point bending test

In order to investigate the shape recovery of the composites, preliminary tests were conducted.<sup>238</sup> Cyclic three-point bending test was performed on 30 PLCL/CF composites produced at various polymerization temperatures (160 °C, 170 °C and 185 °C). A load (5 mm.min<sup>-1</sup>) was applied to the specimens until 5 mm of deformation followed by an unload at 0.5 mm.min<sup>-1</sup>. This cycle was repeated 5 times and the shape recovery ( $R_r$ ) of composites was calculated according to the equation below:

$$R_r = \frac{\Delta U_d}{\Delta L_d}$$

Where:

$\Delta U_d$  is the displacement (mm) measured at unload

$\Delta L_d$  is the displacement (mm) measured at load

The results of cyclic three-point bending test are presented in Section 6 (p.178)

### 2.5 Fiber mass ratio and fiber volume ratio

The fiber mass ratio (FMR) is defined as the ratio of the mass of fibers present in the composite plate with regards to the total mass of the composite. In that way, the fiber volume ratio (FVR) is the ratio of the volume of fibers present in the composite plate. The fiber mass content and the reinforcement volume content are calculated below:

$$M_f \% = \frac{M_f}{M_f + M_m} \quad \text{Equation 10}$$

$$V_f \% = \frac{V_f}{V_f + V_m} \quad \text{Equation 11}$$

where,

$M_f$  = mass of fiber

$M_m$  = mass of matrix

$V_f$  = volume of fiber

$V_m$  = volume of matrix

The previous equations can be expressed in function of volumetric mass of fiber ( $\rho_f$ ) and volumetric mass of matrix ( $\rho_m$ ):

$$FMR \% = \frac{V_f\%}{V_f\% + \left(\frac{\rho_m}{\rho_f}\right)(1 - V_f\%)} \quad \text{Equation 12}$$

$$FVR \% = \frac{M_f\%}{M_f\% + \left(\frac{\rho_f}{\rho_m}\right)(1 - M_f\%)} \quad \text{Equation 13}$$

$M_f$  % was calculated using Equation 10 and  $V_f$  % was calculated using Equation 12. However, to calculate  $V_f$  % it is necessary to know the values of  $\rho_f$  and  $\rho_m$ . The values of  $\rho_f$  were provided by the suppliers while the values of  $\rho_m$  were measured thanks to the hydrostatic weighing technique. An approximately 10g of the polymer matrix without fibers was put into a recipient underwater (Figure 47) and the underwater weight was measured.

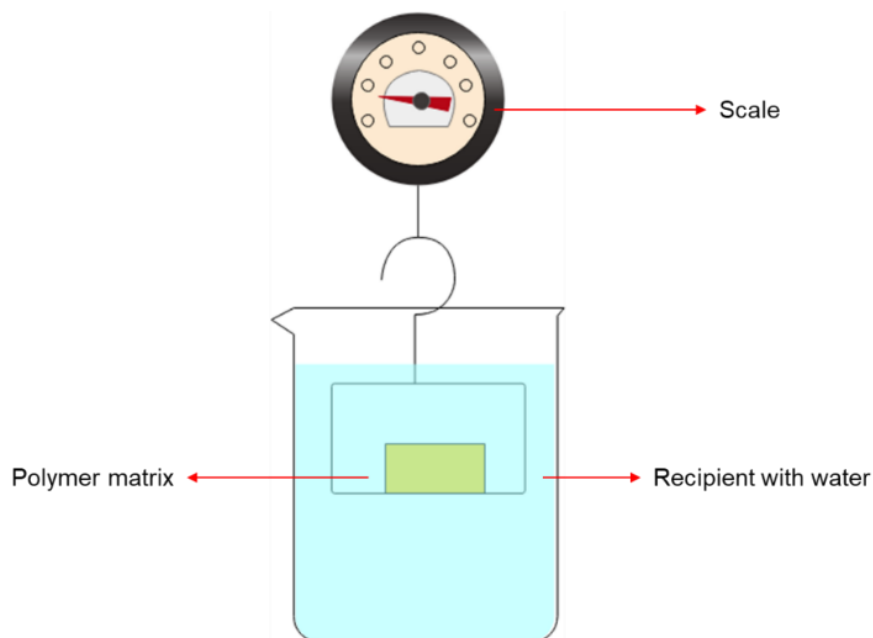


Figure 47: Scheme of hydrostatic weighing technique used to calculate the values of volumetric masses of polymer matrices.



Table 9: Volumetric mass of matrices and reinforcements.

	<b>Sample</b>	<b>Volumetric mass (g.cm<sup>-3</sup>)</b>
<i>Matrices</i>	PLLA	1.24
	10 PLCL	1.22
	20 PLCL	1.22
	30 PLCL	1.22
<i>Reinforcements</i>	Glass woven fabric	2.54
	Carbon woven fabric	1.79
	Flax fabric twill 2/2	1.29
	Flax fabric unidirectional	1.30

## 2.6 Digital microscopy

Digital microscopy (Keyence VHX-7000 series) was used to investigate the quality of the impregnation of the matrix through the reinforcements, to analyze the presence and the morphology of the voids, and to analyze the morphology of the fractures in the specimens tested in traction, three-point bending, and impact.

The morphology of the fractures was evaluated directly in the specimen but samples were prepared for the investigation of the impregnation and the voids characterization. Cross sections between 25 x 5 x 5 mm<sup>3</sup> and 10 x 5 x 5 mm<sup>3</sup> were cut from 120 x 120 x 5 mm<sup>3</sup> composite plates using a bandsaw. The cross sections were cold mounted into a 30 mm diameter mold, ground with abrasive papers and flushed with water (P80, P180, P600, P1200), and polished with silicon carbide papers (800/P2400 and 1200/P400).



Figure 48: Example of mounted sample of PLLA matrix composite.

## 2.7 Accelerated ageing method

The accelerated ageing of composite plates was performed in an accelerated weathering tester chamber (QUV Q-Lab) (Figure 49-a). The specimens for the bending test were used to investigate the ageing and placed in holders (Figure 49-b). The weathering conditions chosen are from the ISO 4892-3 standard (Plastics — Methods of exposure to laboratory light sources — Part 3: Fluorescent UV lamps). The samples were exposed to a UVA irradiation (UVA-351 lamp) at 50°C with no moisture or condensation in 24h cycles, with a total test duration of 720h. These conditions simulate the UV solar radiation behind window glass. The conditions in the accelerated weathering chamber are summarized in Table 10.



(a)



(b)

Figure 49: (a) QUV tester chamber (b) bending specimens placed in holders.

In order to evaluate the influence of UVA irradiation and the temperature in composite plates, DSC, SEC, and RMN were conducted after 336 h, 504 h and 720 h. Three-point bending test was performed after 720 h.

Table 10: Artificial accelerated weathering with UVA-351 lamps.

<b>Exposure period</b>	<b>Lamp type</b>	<b>Irradiance</b>	<b>Temperature</b>	<b>Total duration of the test</b>
24 h dry (no moisture)	UVA-351	0.76 W·m <sup>-2</sup> nm <sup>-1</sup> at 340 nm	50 °C ± 3 °C	720h

## **2.8 Conclusion**

In this chapter, the discussion has centered around the raw materials and experimental techniques employed in the production of composites using the TP-RTM machine. The injection and polymerization stages were explored, encompassing the various temperatures and polymerization times that were experimented with to attain optimal outcomes. Furthermore, details were furnished regarding the reagents, reinforcements, mold, and TP-RTM machine that were applied throughout this research. The characterization of the composite was also presented. In summary, this chapter offers a comprehensive outline of the materials and methods utilized within this study, thus establishing the groundwork for the following chapters.



## **CHAPTER III: Glass fabric reinforced composites produced by TP-RTM**

This chapter focuses on the production and characterization of poly(L-lactide) / glass fabric (PLLA/GF) and poly(L-lactide-co- $\epsilon$ -caprolactone)/glass fabric (PLCL/GF) composites. The optimization of polymerization parameters is discussed, including monomers over catalyst molar ratios and polymerization time and temperature. The viscosity of the reactive thermoplastic system is also studied to better understand its impact on composite production. The full characterization of the PLLA and PLCL matrices was conducted, including the monomers conversions, the molecular weights and the microstructure of the PLCL copolymer. Also, thermal properties of composites are evaluated. Voids in composites were characterized by optical microscopy. Finally, mechanical properties of composites were tested using tensile, three-point bending and impact tests. Overall analysis and evaluation of the production process and resulting composite materials are provided. In conclusion, this chapter provides a comprehensive overview of the production process of PLLA/GF and PLCL/GF composites using TP-RTM.



### 3.1 Study of the viscosity of the reactive thermoplastic system

The production of glass fabric reinforced composites (GFRC) was done with two different matrices: poly(L-lactide) (PLLA) and poly(l-lactide-co- $\epsilon$ -caprolactone) (PLCL). The PLCL matrix composites were produced with the following compositions: 10 PLCL (10 mol% of  $\epsilon$ -CL), 20 PLCL (20 mol% of  $\epsilon$ -CL) and 30 PLCL (30 mol% of  $\epsilon$ -CL). The PLLA/GF composite was used as standard. Before the composites production, a study regarding the viscosity of the reactive mixture was done.

The major parameter influencing the injection step in TP-RTM is the viscosity of the reactive thermoplastic system (mixture of monomers and catalyst). If the reactive system reaches a viscosity higher than 1 Pa.s its injection becomes impossible.<sup>134</sup> Since the L-lactide is solid at room temperature ( $T_m = 96\text{ }^\circ\text{C}$ ), it is necessary to add a melting step before the injection.<sup>80</sup> The viscosity of both molten L-LA and  $\epsilon$ -CL decreases when temperature increases. For lactide, viscosity reaches the value of 1.88 mPa.s at 130  $^\circ\text{C}$  (Figure 50).<sup>80</sup> The  $\epsilon$ -CL does not need to be melted as it is liquid at room temperature with a viscosity of 5.73 mPa.s and its viscosity also decreases with increasing temperature.<sup>198</sup>

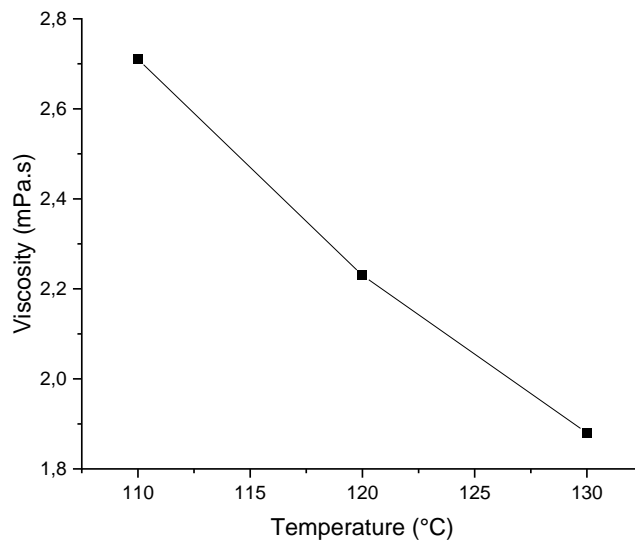


Figure 50: Viscosity of molten L-lactide at different temperatures.<sup>80</sup>

In a previous work, a time of 30 min at 120  $^\circ\text{C}$  was reported to full melt a quantity of 100 g of L-LA in TP-RTM tank under vacuum.<sup>199</sup> In order to determine the optimal melting time of L-LA in the presence of  $\epsilon$ -CL, a study was done.

Since the ring-opening polymerization (ROP) of L-LA/ $\epsilon$ -CL is sensitive to air and as no device allowing the study of the viscosity in low-pressures (the same environment as in the TP-RTM tank) was available at the laboratory, the study was based on the conversion of L-LA.

The viscosity increases as the polymerization reaction progresses in the tank, thus the monomer conversion was used to study indirectly the viscosity of the reactive mixture.

A quantity of 200 g of a reactive system containing 20 mol% of  $\epsilon$ -CL was put into the TP-RTM tank at 150°C and aliquots were taken after 30, 40, 45, and 60 minutes and analyzed by  $^1\text{H}$  NMR. Co-monomers over catalyst molar ratio of 2000 was used, based on previous work.<sup>200</sup> It had to be mentioned that after 15 and 20 minutes, L-LA was not completely melted (visual observation).

At the melting time of 30 minutes, the L-LA reached a conversion of 5 %, the  $\epsilon$ -CL a conversion of 0% and the reactive system had visually water-like viscosity. After 40 minutes, L-LA displays a conversion of 7 % and no conversion for  $\epsilon$ -CL was observed and the reactive mixture displays a water-like viscosity (Figure 51). At 45 minutes, the conversion of L-LA reach 21 % whereas the polymerization of  $\epsilon$ -CL has not started yet but the viscosity of the whole reactive mixture has changed, becoming visually more viscous. After 60 minutes, the L-LA is converted by 80 % and the  $\epsilon$ -CL started to polymerize, with 10 % of conversion (Figure 51). However, at this melting time, the reactive system is too viscous (visual observation) and the injection was impossible. It can be inferred that after 60 minutes, the viscosity of the reactive mixture reached a viscosity higher than 1 Pa.s.

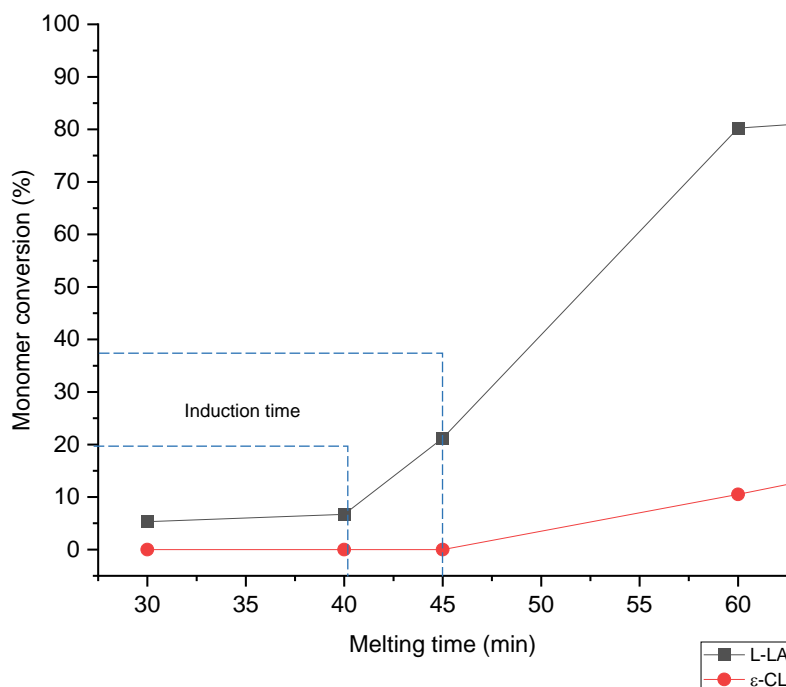


Figure 51: Evolution of monomers conversion and the melting time.



The increase of the viscosity of the reactive system at different melting times are corroborated with the  $^1\text{H}$  NMR spectra (Annexes - Figure 120). As the melting time increases, the signal corresponding to L-LA decreases and that corresponding to PLLA increases, indicating that the ROP of L-LA starts before that of  $\epsilon$ -CL. In the copolymerization of L-LA and  $\epsilon$ -CL with  $\text{Sn}(\text{Oct})_2$ , the L-LA display a higher reactivity towards  $\epsilon$ -CL due to its higher value of polymerization enthalpy.<sup>201</sup>

The study of co-monomers conversion makes it possible to establish an optimal melting time of 30 minutes. The induction time, defined as the time when no change in viscosity is observed, was determined to be 40 minutes. After this time, the polymerization reaction accelerates significantly and the viscosity increases, preventing the injection. The processing window was determined experimentally based on the conversion of monomers and indirectly by the observation of the viscosity of the resin and so fixed at 45 minutes. After this time, the injection of the reactive mixture becomes impossible. The melting time of 30 minutes at 150 °C was applied to the compositions of PLLA, 10 PLCL, 20 PLCL, 30 PLCL and it was enough to melt all L-LA and kept the viscosity of the reactive system as low as possible allowing the injection of the mixture in the mold.

## 3.2 Optimization of polymerization parameters

After determining the melting time, the production of glass fabric reinforced composites (GFRC) was done according to process described in Section 2.2 (p.61). To determine the optimal reaction parameters for the composite production, polymerization temperature, polymerization time and the co-monomers over catalyst molar ratio will be presented hereafter. All GFRC was produced with ten layers of glass fabric, reaching values of fiber mass ratio between 45-48 %.

### 3.2.1 Polymerization temperature

The choice of polymerization temperature for poly(L-lactide)/glass fabric composite (PLLA/GF) produced by TP-RTM was 185 °C. This value was reported in the previous works done at UMET.<sup>200</sup> At this point, for the poly(L-lactide-co- $\epsilon$ -caprolactone)/glass fabric composites (PLCL/GF), it was decided to use the same polymerization temperature (185°C), to compare the copolymer based composite with the standard PLLA/GF. The influence of the polymerization temperature for PLCL/GF composites will be discussed in Section 3.6 (pag.107).

### 3.2.2 Polymerization time

Based on previous work, the conditions of polymerization for PLLA/GF produced by TP-RTM is 2 h using  $\text{Sn}(\text{Oct})_2$  as the catalyst with the ratio of  $[\text{L-LA}]/[\text{Sn}] = 2000$ .<sup>200</sup>

To study the influence of the time of polymerization on the PLCL/GF composites, it was decided to use the same co-monomers over catalyst ratio. The influence of  $[L-LA] + [\epsilon-CL]/[Sn]$  is studied in Section 3.2.3 (p.84).

Polymerization times of 2, 3.5, and 5 h were selected with a composition of  $[L-LA]/[\epsilon-CL]$  of 80/20 (20 PLCL). The parameter used to select the optimal polymerization time was the conversion of both monomers, L-LA and  $\epsilon$ -CL (Table 1).

Table 11: Conversion of L-LA and  $\epsilon$ -CL in composites matrices at different polymerization times.

Sample <sup>a</sup>	Matrix	Polymerization time (h)	L-LA (%) <sup>b</sup>	$\epsilon$ -CL (%) <sup>b</sup>
1	PLLA	2	97	-
2	20 PLCL	2	96	56
3		3.5	97	77
4		5	97	95

<sup>a</sup> Experimental condition: Polymerization in TP-RTM at 185°C, Sn(Oct)<sub>2</sub> as the catalyst,  $[L-LA + \epsilon-CL] / [Sn] = 2000$ , fiber mass ratio 46%. <sup>b</sup> Determined by <sup>1</sup>H NMR in CDCl<sub>3</sub>.

With these experimental conditions, after 2 h of polymerization, a conversion of 97 % of L-LA was reached for the standard PLLA matrix, which corroborate the previous results.<sup>200</sup> Regarding the conversions of L-LA and  $\epsilon$ -CL in the PLCL matrix one can conclude that at 185 °C the best polymerization time for the production of 20 PLCL/GF composites in TP-RTM is 5 h, allowing to reach conversions as high as 97 and 95 % respectively .

The conversion of L-LA and  $\epsilon$ -CL was evaluated by <sup>1</sup>H NMR (Annexes - Figure 121). For the pure PLLA matrix, the conversion is calculated by integrating the signals centered at 5.05 and 5.16 ppm corresponding to the methine of L-LA and PLLA respectively. The signals centered at 4.23 and 4.11 ppm corresponding to the  $\epsilon$ -methylenes of CL – CL dyad and  $\epsilon$ -caprolactone respectively, varies with the polymerization time. Also, it can be inferred that the conversion of L-LA is faster than the  $\epsilon$ -CL because after 2 h its conversion reaches almost 97 %, against only 56 % for  $\epsilon$ -CL. Since a polymerization time of 5 h leads to the best monomers conversions for the PLCL with 20 mol% of  $\epsilon$ -CL, the same time was used for the reaction of L-LA with  $\epsilon$ -CL at 10 and 30 mol%. In all cases the conversions are higher than 95 % for both monomers (Table 12).

Table 12: Conversion of co-monomers for different molar compositions.

Sample <sup>a</sup>	Matrix <sup>a</sup>	Monomer conversion (%)	
		L-LA <sup>b</sup>	$\epsilon$ -CL <sup>b</sup>
1	PLLA	97	-
5	10 PLCL	96	96
6	20 PLCL	97	95
7	30 PLCL	96	95

<sup>a</sup> Experimental condition: Polymerization in TP-RTM at 185°C, Sn(Oct)<sub>2</sub> as the catalyst, [L-LA +  $\epsilon$ -CL] / [Sn] = 2000, fiber mass ratio 46%. <sup>b</sup> Determined by <sup>1</sup>H NMR in CDCl<sub>3</sub>.

### 3.2.3 Co-monomers over catalyst molar ratio

The choice of a co-monomers over catalyst molar ratio of 2000 was based on the previous work on the production of PLLA/GF composite in TP-RTM.<sup>23</sup> Even if the ratio of 2000 is also reported for the copolymerization of L-LA and  $\epsilon$ -CL *in-bulk* at lab-scale in a flask,<sup>28,27,202,103</sup> a study in TP-RTM to choose the optimal ratio used for the production of PLCL / GF composite was conducted. The co-monomers composition of [L-LA]/[ $\epsilon$ -CL] = 80/20 (20 PLCL) was selected to study the influence of the co-monomers loading, and ratios of 2000, 3000 and 4000 were tested. The choice of the optimal co-monomers over catalyst molar ratio for PLCL matrix was based on the results of monomers conversion and the molecular weight of the resulting matrices (Table 3).

Table 13: Conversion and molecular weight of 20 PLCL matrix at different co-monomers over catalyst ratios.

Sample	Matrix	Co-monomer over catalyst ratio [L-LA + $\epsilon$ -CL] / [Sn]	Monomer conversion		Molecular weight		
			L-LA <sup>a</sup> (%)	$\epsilon$ -CL <sup>a</sup> (%)	$M_n$ <sup>b</sup> (g.mol <sup>-1</sup> )	$M_w$ <sup>b</sup> (g.mol <sup>-1</sup> )	$\bar{D}$
8	20 PLCL	2000	97	96	62,000	92,300	1.4
9		3000	94	93	48,260	83,750	1.7
10		4000	96	91	17,600	32,700	1.4

<sup>a</sup> Determined by <sup>1</sup>H NMR in CDCl<sub>3</sub> <sup>b</sup> Determined by SEC in CHCl<sub>3</sub> at 30°C, triple detection.

Looking at the results (Table 13), it is clear that the highest conversions of L-LA and  $\epsilon$ -CL as well as the highest molecular weight were obtained with the co-monomers over catalyst molar ratio of 2000, in which  $M_w$  of 92,300 g.mol<sup>-1</sup> was reached with conversions higher than 96 % for L-LA and  $\epsilon$ -CL. With the co-monomers over catalyst molar ratio of 3000,  $M_w$  of 83,750 g.mol<sup>-1</sup> was reached with conversions of 94 % for L-LA and 93 % for  $\epsilon$ -CL. Finally, with the ratio of 4000,  $M_w$  of 32,700 g.mol<sup>-1</sup> was reached with conversions of 96 % for L-LA and 91 % for  $\epsilon$ -CL.

This ratio of 2000 was then applied to the other co-monomers compositions (Table 14). The results show that conversions higher than 95 % were obtained for the compositions containing 10 and 30 mol% of  $\epsilon$ -CL, similarly to the conversions obtained with 20 mol %  $\epsilon$ -CL. Also, the results of molecular weight were satisfactory with  $M_w$  reaching 90,600 g.mol<sup>-1</sup> for the 10 PLCL matrix and 71,500 g.mol<sup>-1</sup> for the 30 PLCL matrix.

Table 14: Conversion rate and molecular weight of PLLA and PLCL matrices in optimal polymerization conditions.

Sample	Matrix	Monomer conversion <sup>a</sup>		Molecular weight <sup>b</sup>		
		L-LA (%)	$\epsilon$ -CL (%)	$M_n$ (g.mol <sup>-1</sup> )	$M_w$ (g.mol <sup>-1</sup> )	$\bar{D}$
11	PLLA	96	-	88,000	121,200	1.4
12	10 PLCL	97	96	71,100	90,600	1.3
13	20 PLCL	96	95	43,200	61,300	1.4
14	30 PLCL	97	95	53,200	71,500	1.3

Experimental conditions: Polymerization in TP-RTM at 185°C, Sn(Oct)<sub>2</sub> as the catalyst, [L-LA +  $\epsilon$ -CL] / [Sn] = 2000, polymerization time of 2 h for PLLA and 5h for PLCL. Fiber mass ratio 46% <sup>a</sup> Determined by <sup>1</sup>H NMR in CDCl<sub>3</sub> <sup>b</sup> Determined by SEC in CHCl<sub>3</sub> at 30°C, triple detection.

### 3.3 Characterization of glass fabric reinforced composites

With the optimal polymerization parameters *i.e.* polymerization temperature of 185°C, residential time in the tank during 30 min, co-monomers over catalyst ratio 2000, composites of pure PLLA and copolymers with 10, 20 and 30 mol%  $\epsilon$ -CL were produced with ten layers of glass woven fabric, reaching fiber mass ratio between 45 – 48 %. These composites were then fully characterized: conversion of monomers, molecular weight, microstructure of copolymers, thermal properties and mechanical properties.

### 3.3.1 Conversion of monomers and molecular weight of matrices

Conversions of L-LA higher than 96 % was measured for the PLLA matrix. The conversions of both monomers (L-LA and  $\epsilon$ -CL) were higher than 95 % for all compositions of PLCL matrices. (Table 15). The  $^1\text{H}$  NMR spectra used to calculate the conversion of monomers for all samples are presented in Appendix 6.8 (p.218).

Regarding the molecular weights,  $M_w$  higher than 89,800  $\text{g}\cdot\text{mol}^{-1}$  was measured for the PLLA matrix. Values higher than 83,700  $\text{g}\cdot\text{mol}^{-1}$ , was measured for 10 PLCL matrix. The 20 PLCL and 30 PLCL matrices showed values of  $M_w$  higher than 49,900  $\text{g}\cdot\text{mol}^{-1}$  and 40,700  $\text{g}\cdot\text{mol}^{-1}$  respectively.

Table 15: Conversion of the monomers and molecular weight of the matrices .

Sample	Matrix	Feed molar ratio	Conversion <sup>a</sup>		Molecular weight <sup>b</sup>		
		L-LA: $\epsilon$ -CL (mol%)	L-LA (%)	$\epsilon$ -CL (%)	$M_n$ ( $\text{g}\cdot\text{mol}^{-1}$ )	$M_w$ ( $\text{g}\cdot\text{mol}^{-1}$ )	$\bar{D}$
1-X	PLLA	100:0	96	-	38,000	90,900	2.39
2-X			97	-	35,900	89,800	2.50
3-X			96	-	33,900	91,300	2.69
1-A	10 PLCL	90:10	95	97	43,100	88,760	2.05
2-A			97	96	33,400	83,700	2.50
3-A			96	97	48,200	90,600	2.96
1-B	20 PLCL	80:20	96	96	41,300	79,300	1.87
2-B			96	96	23,500	49,900	2.12
3-C			95	95	34,500	60,200	1.74
1-C	30 PLCL	70:30	96	98	19,000	46,900	2.46
2-C			97	98	16,300	40,700	2.49
3-C			97	95	20,500	41,100	2.00

Experimental conditions: Polymerization in TP-RTM at 185°C,  $\text{Sn}(\text{Oct})_2$  as the catalyst,  $[\text{L-LA} + \epsilon\text{-CL}] / [\text{Sn}] = 2000$ , 2 h for PLLA and 5h for PLCL matrices. <sup>a</sup> Determined by  $^1\text{H}$  NMR in  $\text{CDCl}_3$ , <sup>b</sup> determined by SEC in  $\text{CHCl}_3$  for PLLA matrix and in THF for PLCL matrices.  $M_n$  and  $M_w$  corrected by a factor of 0.68 for PLLA and  $[0.58 \times \text{wt \% LA units} + 0.56 \times \text{wt \% CL units}]$  for PLCL matrices.

### 3.3.2 Copolymer matrix composition

$^1\text{H}$  NMR was used to determine the copolymer composition and to assess the microstructure of the matrix of PLCL/GF composites (Table 16). The number-average sequence lengths of L-LA ( $I_{LA}$ ) and  $\epsilon$ -CL ( $I_{CL}$ ), the Bernoullian random number-average sequence lengths random and the randomness character (R) was calculated according Equations 3, 4 et 5 (Section 2.3.165).

### Chapter III: Glass fabric reinforced composites

Table 16: <sup>1</sup>H NMR characterization of PLCL copolymers of different co-monomers compositions synthesized at 185°C.

Sample	Matrix	L-LA:ε-CL (wt%)	L-LA (%)	ε-CL (%)	Average dyad relative molar fractions			Microstructural magnitudes of the copolymers				
					(LA-LA)	(LA-CL)	(CL-CL)	I <sub>LA</sub>	I <sub>CL</sub>	(I <sub>LA</sub> ) <sub>Random</sub>	(I <sub>LA</sub> ) <sub>Random</sub>	R
1-A	10 PLCL	90:10	88,9	11.1	0.8111	0.1560	0.0329	11.40	1.42	9.02	1.12	0.79
2-A			89.7	10.3	0.8192	0.1565	0.0243	12.16	1.31	9.75	1.11	0.85
3-A			90.6	9.4	0.8362	0.1394	0.0244	12.99	1.35	10.63	1.10	0.82
1-B	20 PLCL	80:20	80.8	19.2	0.6802	0.2548	0.0650	6.34	1.51	5.20	1.24	0.82
2-B			79.0	21.0	0.6613	0.2583	0.0804	6.12	1.62	4.77	1.27	0.78
3-B			81.3	18.7	0.6877	0.2512	0.0612	6.40	1.49	5.35	1.23	0.83
1-C	30 PLCL	70:30	70.7	29.3	0.5436	0.3263	0.1301	4.33	1.80	3.41	1.41	0.79
2-C			71.4	28.6	0.5513	0.3258	0.1228	4.38	1.75	3.50	1.40	0.80
3-C			71.3	28.7	0.5454	0.3346	0.1200	4.26	1.72	3.48	1.40	0.82

For all the compositions, the copolymer composition is almost the same as the feed molar ratio (Table 16). The average sequence lengths of L-LA and  $\epsilon$ -CL changes with the copolymer composition (Figure 52). The  $I_{LA}$  decreases with the decrease of L-LA content while the  $I_{CL}$  increases with increasing the  $\epsilon$ -CL content. For the 10 PLCL copolymer, the  $I_{LA}$  is around 12.0 and the  $I_{CL}$  around 1.3. For the 20 PLCL, the  $I_{LA}$  decreases at 6.0 and the  $I_{CL}$  slightly increases at 1.5. The last one, the 30 PLCL, shows a  $I_{LA}$  around 3.0 and  $I_{CL}$  around 2.0.

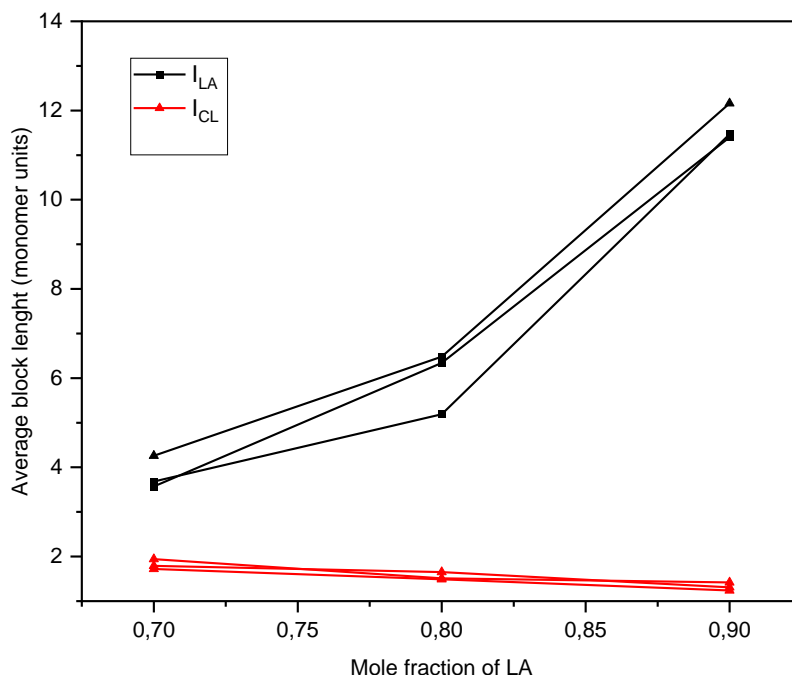


Figure 52: Evolution of the average sequence lengths of different copolymer compositions.

The randomness character ( $R$ ) is used to define the microstructure of copolymers. A pure block copolymer corresponds to a  $R$  close to 0 while a random copolymer corresponds to a  $R$  value is close to 1. All copolymer matrices show  $R$  values close to 0.80, showing a random character (Table 16). These results were expected, as higher temperatures or longer reaction times lead to intermolecular transesterification reactions, further increasing the randomization of the PLCL copolymer chain.<sup>27,203</sup>

### 3.3.3 Thermal properties of the matrices

The thermal degradation of matrices was studied by Thermogravimetry analyses (TGA). Data collected from the TGA of PLLA and PLCL matrices, were: the onset temperature ( $T_{5\%}$ ), the endset temperature ( $T_{95\%}$ ), the temperature at the maximum degradation rate, and the residual weight at 800 °C, (Table 17, Figure 53, Figure 54). A commercial PCL (CAPA™ 6500) was also analyzed to compare the thermal properties with the matrices.

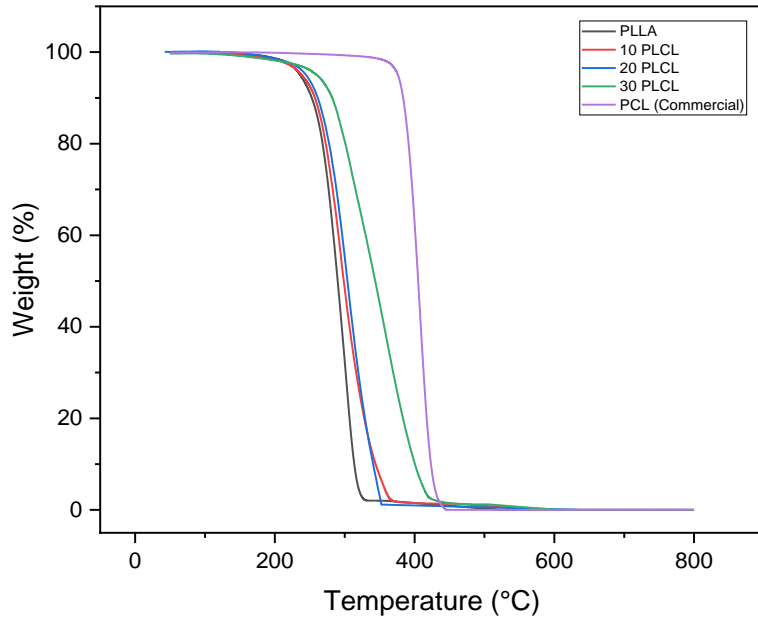


Figure 53: TGA curves of PLLA and PLCL matrices ( $10^{\circ}\text{C}\cdot\text{min}^{-1}$  under  $\text{N}_2$ )

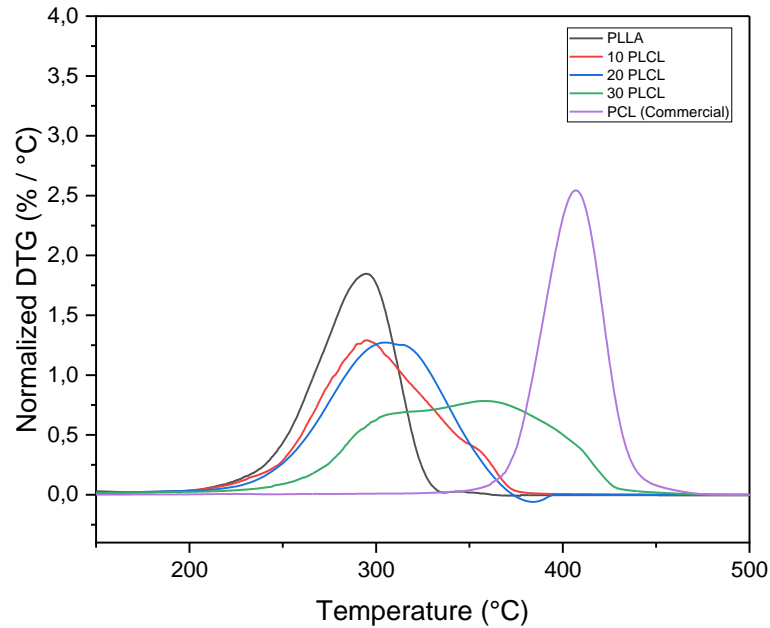


Figure 54: Normalized DTG curves of PLLA and PLCL matrices thermal degradation at heating rate of  $10^{\circ}\text{C}\cdot\text{min}^{-1}$ .

The PLLA matrix degradation starts at  $237^{\circ}\text{C}$  and shows a maximum at  $294^{\circ}\text{C}$  with no residues at  $800^{\circ}\text{C}$ . Regarding the PLCL matrix, the degradation temperature increases when  $\epsilon\text{-CL}$  content increases (Figure 53). The  $T_{5\%}$  increases by 2, 7, and  $25^{\circ}\text{C}$  for 10, 20, and 30 PLCL matrices respectively compared to PLLA matrix.



The maximum DTG observed for PLLA matrix is 294 °C, and this value is increased by 4, 10, and 63 °C for 10, 20, and 30 PLCL matrices respectively (Table 17). The  $T_{95\%}$  also increases with an increase of  $\epsilon$ -CL content going from 314 °C for PLLA matrix to 406 °C for 30 PLCL matrix. The pure PCL display  $T_{10\%}$  at 384 °C.

In summary, as the  $\epsilon$ -CL content rises, PLCL matrices exhibit a reduced degradation rate, resulting in an increase in their maximum DTG. To illustrate, the 10 PLCL matrix degraded at 1.84 % weight °C.min<sup>-1</sup> and its max DTG was 298 °C, while the degradation of the 30 PLCL was 0.78 % weight °C.min<sup>-1</sup> and its max DTG was 358 °C (Table 17).

Table 17: TGA data of PLLA and PLCL matrices (10 °C.min<sup>-1</sup> under N<sub>2</sub>).

Sample	Matrix	$T_{5\%}$ (°C)	$T_{95\%}$ (°C)	Max DTG (°C)	Slope (% weight °C.min <sup>-1</sup> )	Residual weight (%)
1-X	PLLA	237	314	294	-1.84	0
1-A	10 PLCL	239 (+2)	336 (+22)	298 (+4)	-1.29	0
1-B	20 PLCL	244 (+7)	347 (+33)	305 (+10)	-1.26	0
1-C	30 PLCL	262 (+25)	406 (+92)	358 (+63)	-0.78	0
Commercial PCL	PCL	377	425	408	-2.44	0

These results are in agreement with previous works, indicating that the PCL exhibits greater resistance to thermal degradation compared to PLLA, and that their copolymers exhibit intermediate thermal stability characteristics.<sup>27</sup> The values of  $T_{95\%}$  for PLCL copolymers with 10 mol%, 20 mol%, and 30 mol% of  $\epsilon$ -CL were reported as 336 °C, 347 °C, and 406 °C, respectively. Additionally, this works also reported a decrease in the degradation rate with an increasing  $\epsilon$ -CL content.<sup>27,204</sup>

In the normalized DTG curves, the peaks of PLLA are slightly different from PLCL ones (Figure 54). Once PLLA show a single thin peak, PLCL shows a large peak or two peaks with high  $\epsilon$ -CL content of 30%. At 250 °C the L-LA-rich sequences with low thermal stability starts to degrade and the  $\epsilon$ -CL-rich ones which are less sensitive to heat are degraded at 350 °C.<sup>205</sup>

Regarding the thermal degradation mechanisms, the PLLA and PCL degrade both by random chain scission and specific chain-end scission mechanisms.<sup>206,207</sup> The random chain scission occurs at lower temperatures than chain-end scission. In random chain scission, the molecular weight of the polymer steadily reduces without any significant alteration in its mass.

In contrast, during specific chain scission, the mass continuously decreases while its molar concentration remains unchanged. Based on the literature, the activation energies for the random chain scission of PLA and PCL are 10.0 and 18.5 kcal.mol<sup>-1</sup> respectively and the correlate energies for the specific chain scission are 25.2 and 55.5 kcal.mol<sup>-1</sup>.<sup>207</sup> These values of activation energies justify the difference of the degradation temperatures between PLLA and PLCL matrices.

The evaluation of glass transition temperature ( $T_g$ ), melting temperature ( $T_m$ ), and crystallinity ( $\chi$ ) was done by DSC analysis (Table 18 and curves in Appendix 6.11). For PLLA,  $T_g$  is observed at 53 °C,  $T_m$  around 168 – 170 °C and crystallinity of 55% which are in agreement with the literature.<sup>208,209</sup>

Table 18: Thermal properties of the matrices of GFRC.

Sample	Matrix	$T_g$ (°C)	$T_m$ (°C)	$\Delta H_f$ (J.g <sup>-1</sup> )	$\chi$ (%)
1-X	PLLA	53	168	45.2	48.6
2-X		53	169	51.4	55.3
3-X		55	170	54.0	57.1
1-A	10 PLCL	39	143	15.8	18.9
2-A		42	142	20.9	25.0
3-A		38	144	20.4	24.4
1-B	20 PLCL	30	-	-	-
2-B		32	135	1.4	1.9
3-B		29	-	-	-
1-C	30 PLCL	17	-	-	-
2-C		21	-	-	-
3-C		21	-	-	-

Regarding the copolymers,  $T_g$  and  $T_m$  decrease as the  $\epsilon$ -CL content increases (Table 18). The matrix with 10% of  $\epsilon$ -CL displays  $T_g$  around 40°C and  $T_m$  about 142 °C. For 20% of  $\epsilon$ -CL, the  $T_g$  decreases at 30 °C, and only one sample presented  $T_m$  at 135 °C. The other two PLCL samples did not show any  $T_m$ . Finally, the matrix with 30 % of  $\epsilon$ -CL displays a  $T_g$  of 20°C.

The decrease of  $T_g$ ,  $T_m$  and crystallinity are directly connected with the microstructure of copolymers. In PLCL copolymers in which L-LA is the main component, only L-LA-units crystallizes, and the crystallinity is directly related to the number of “pure” L-LA sequences. ( $I_{LA}$ ).

For example, 10 PLCL with  $I_{LA}$  about 12 display crystallinities between 19 and 25% (Table 16 and Table 18). The 20 and 30 PLCL samples have their  $I_{LA}$  divided by 2 and 4 respectively (20 PLCL  $I_{LA} = 6$ , 30 PLCL  $I_{LA} = 3$ ) and no crystallinity was observed. For these two materials one can assume that the “pure” L-LA sequences are no longer enough to allow the formation of a PLA crystal. Regarding  $\epsilon$ -CL units, their length was insufficient to allow their crystallization. Even if the  $I_{CL}$  slightly increases with increasing the  $\epsilon$ -CL content in the matrix, no crystallization was observed in these matrices.

### 3.4 Characterization of voids in glass fabric reinforced composites

Manufacturing defects are one of the principal factors that influences the mechanical properties of composites. Defects are differing from damages since the latter appear after loading of the composite inducing damages such as delamination, fiber pull out, etc. Defects are usually classified based on their location (i.e. into the fibers, at the interface between the fibers and the matrix or into the matrix). Fiber defects are caused by broken fibers, waviness and misalignment while interface defects include the initial debonding between the fiber and the matrix and also initial interlaminar delamination. Regarding matrix defects, they are generated by the incomplete matrix curing and/or by the presence of voids. Compared to the other defects, voids have a major impact on the mechanical properties since they can act as stress concentrators.<sup>141</sup>

The presence of voids was evaluated by digital microscopy and observed in all composites. Owing to the dual-scale nature of these composites, some different types of voids could appear at different scales *i.e.* macro, meso and micro, but only macro and meso-voids were observed in composite plates. The presence of macro and meso-voids occurs as a result of air entrapment during resin flow. This is caused by the inhomogeneous fiber architecture leading to non-uniform permeability of the fiber. As a consequence, there are differences in resin velocity at the local level, leading to variations. The space between the bundles contributes to the variation of the resin velocity during injection (Figure 55). The space between the bundles are clearly identified where the light transmitted through the glass fabric reveals the different sizes of the spaces (Figure 55).

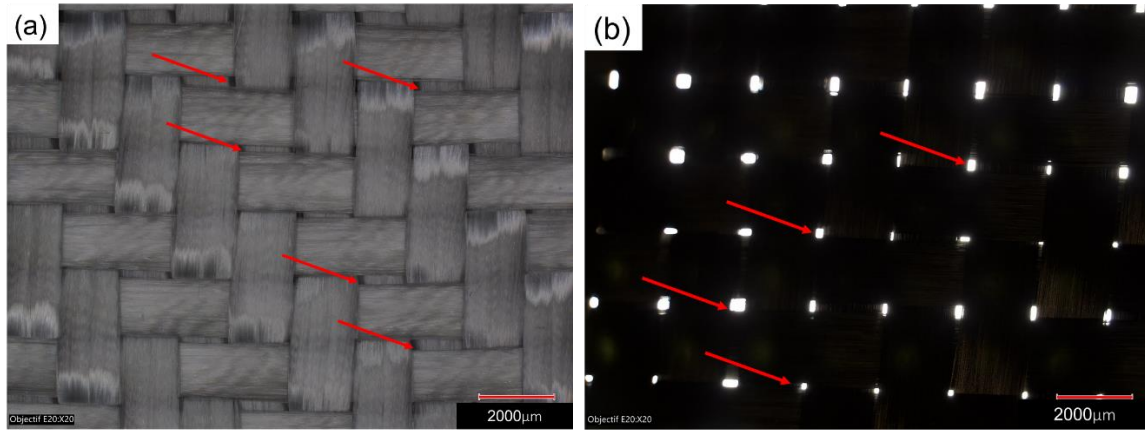


Figure 55: Digital micrograph (a) in reflection and (b) in transmission of glass fabric showing the spaces between the fiber tows.

Macro-voids or “dry spot” have been identified in some composite plates (Figure 56). These type of voids can be identified by naked eye and in general have no characteristic shape, unlike to meso and micro voids which display a circular shape.

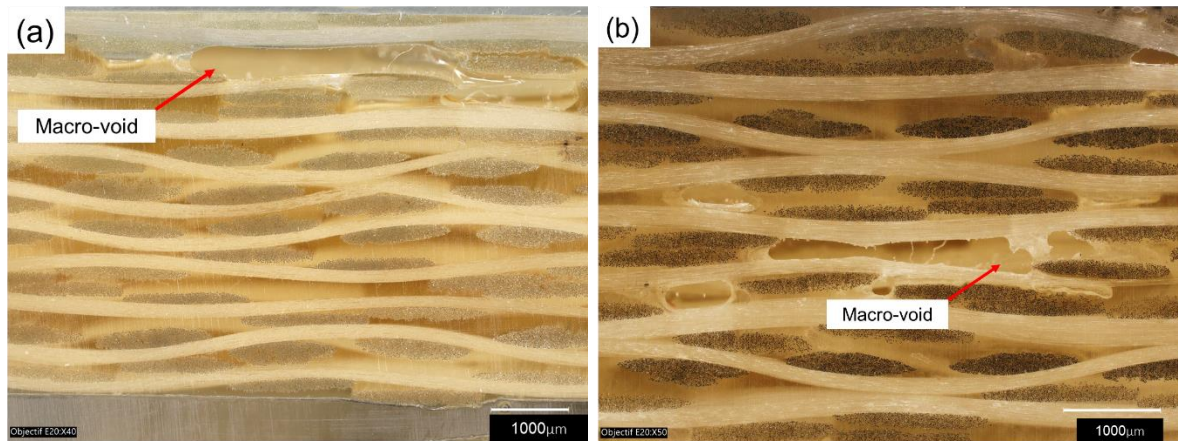


Figure 56: Digital micrographs showing macro-voids in (a) 10 PLCL/GF and (b) 30 PLCL/GF composites.

The formation of meso and micro-voids is controlled by competition between resin viscous flow and capillarity flow. The resin viscous flow is controlled by the hydrodynamic forces between the bundles, while the capillarity flow is driven by the surface tension of the fibers. The dominant factor driving the resin flow between the bundles are the resin viscous flow whereas the capillarity flow drives the resin flow between the fibers. A balance between these forces must be established to obtain composites with a minimum void content. Digital micrographs confirm the presence of meso-voids in composite plates. The inter-bundles meso-voids are present in the 20 PLCL/GF composite plate and display circular shape (Figure 57).

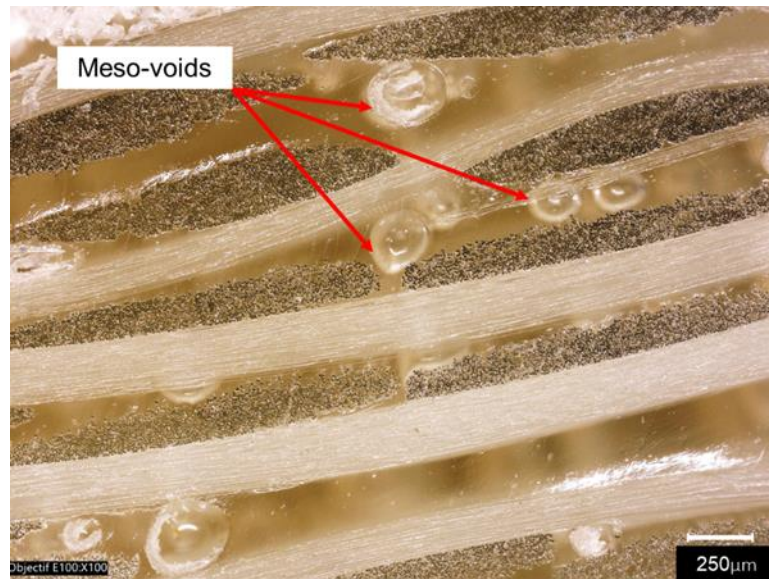


Figure 57: Digital micrograph of 20 PLCL/GF composite plate showing the meso-voids between the bundles.

In a more detailed micrograph (Figure 58), it is possible to observe the interface between the matrix and the meso-void. The meso-void are entirely located between the bundles where the matrix ensures the cohesion between the layers of the fabric.

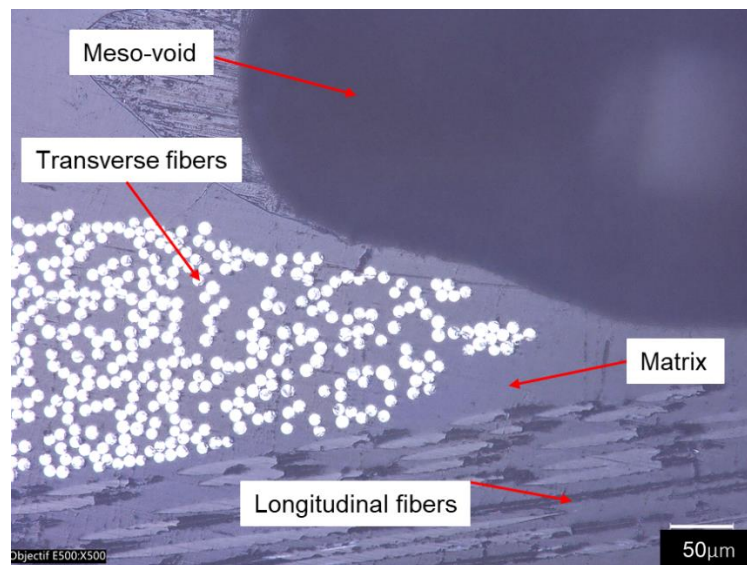


Figure 58: Digital micrograph of 20 PLCL/GF composite plate showing the interface between the matrix and the meso-void.

Micro-voids were not observed in the composites samples. High resin velocity enables the formation of micro-voids as the flow in the channel between the bundles is faster than in between the fibers in a bundle due to capillarity effect.<sup>154</sup> In this way, it can assumed that the resin flow obtained with 0.5 bar of N<sub>2</sub> during injection is appropriated to avoid the formation of micro-voids in the composite. The quality of the impregnation by the matrix into the bundles of fibers and the lack of micro-voids are shown in Figure 59.

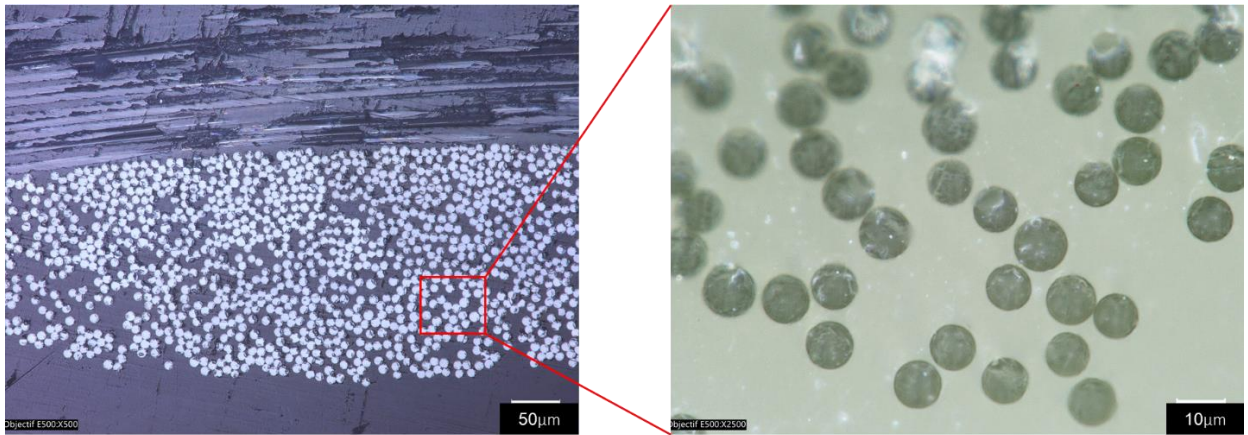


Figure 59: Digital micrograph of 20 PLCL/GF composite with absence of micro-voids intra-bundles.

### 3.5 Mechanical properties of glass fabric reinforced composites

To evaluate the mechanical behavior of glass fabric reinforced composites (GFRC), three tests were conducted, *i.e* tensile, bending and impact tests. The mechanical properties measured from these tests and the analysis of the fracture of the broken specimens is presented in the following session.

#### 3.5.1 Tensile test

All the composite plates have a fiber mass ratio of approximately 46 %, making it possible to compare their mechanical properties (Table 19). The composite plates PLLA/GF, 10 PLCL/GF, and 20 PLCL/GF showed  $E$  varying from 6.40 to 6.53 GPa,  $\sigma_t$  varying from 250 to 275 MPa, and elongation at break between 6 and 7%. Regarding the standard deviation of these values, it can be concluded that PLLA/GF, 10 PLCL/GF, and 20 PLCL/GF with the same fiber volume ratio display similar mechanical properties in tension. Regarding 30 PLCL/GF the Young modulus and the tensile strength are about 1.8 times lower than in the PLLA/GF composite. The elongation at break is like the other samples (Table 19).

Table 19: Tensile properties of GFRC.

Sample	Composite	Young modulus (GPa)	Tensile strength (MPa)	Elongation at break (%)	FMR (%)	FVR (%)	$\chi$ (%)	$T_g$ (°C)
1-X	PLLA/GF	6.40 ± 0.23	250 ± 9	6.26 ± 0.38	46.8	29.2	48.6	52.0
1-A	10 PLCL/GF	6.50 ± 0.16	275 ± 10	6.93 ± 0.47	46.0	28.4	18.9	39.0
1-B	20 PLCL/GF	6.53 ± 0.19	253 ± 6	6.93 ± 0.20	45.9	28.6	-	30.0
1-C	30 PLCL/GF	3.48 ± 0.47	135 ± 10	6.20 ± 0.12	46.6	28.8	-	17.1

The mechanical properties are often related to the crystallinity of a material, since high crystallinity generally provides better mechanical properties. In that way, it was expected that tensile properties ( $E$  and  $\sigma$ ) would decrease while increasing the  $\epsilon$ -CL content since the crystallinity is related with tensile properties. However, in this case the tensile properties do not decrease with the decrease of crystallinity as it would have been expected. Only samples PLLA/GF and 10 PLCL/GF present crystallinity of 48.6 and 18.9 % respectively, and both present similar properties to the sample 20 PLCL/GF which is completely amorphous. It can be supposed that the glass fabric play a more important role than the crystallinity regarding the tensile properties, notably the elongation at break.

In contrast,  $T_g$  seems to have more influence on tensile properties than crystallinity. The composite plates PLLA/GF, 10 PLCL/GF, and 20 PLCL/GF display  $T_g$  above room temperature. However, 30 PLCL/GF shows a low  $T_g$  value of 16 °C. This means that at the testing temperature, the matrix undertake its glass transition to the rubbery state leading to the observed decrease of  $E$  and  $\sigma_t$ .<sup>210</sup>

To summarize, PLLA/GF, 10 PLCL/GF, and 20 PLCL/GF composites display similar values of  $E$  and  $\sigma_t$ , with strain – stress curves with similar shape (Figure 60). In contrast, 30 PLCL/GF composite has its tensile properties divided by almost 2 times compared to other samples (Figure 60). Regarding the elongation at break, the values of all composite plates are between 6 and 7%, and the breaking of the sample is governed by the fiber part of the composite.

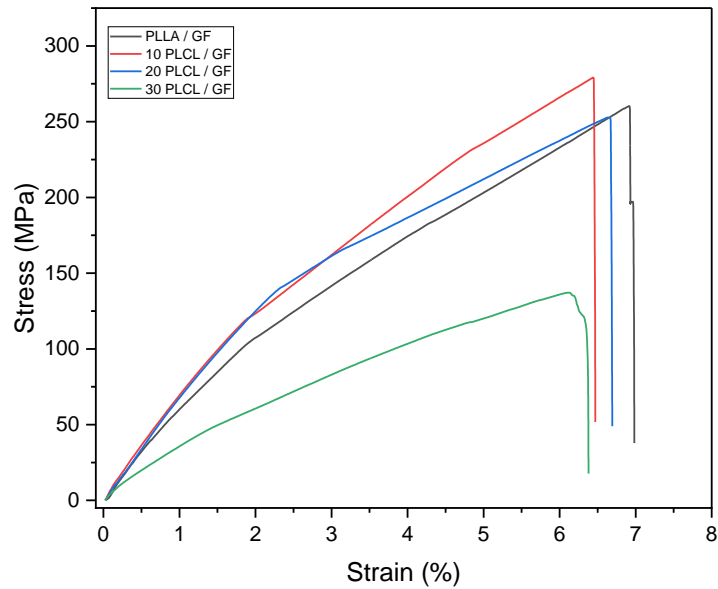


Figure 60: Strain x stress curve in tensile test of PLLA/GF, 10 PLCL/GF, 20 PLCL/GF and 30 PLCL/GF composites.

After tensile test, the specimens were analyzed by digital microscopy to determine the type of failure and the morphology of the fracture. The specimens of PLLA/GF, 10 PLCL/GF, 20 PLCL/GF broke in two parts whereas the specimen 30 PLCL/GF remained in one piece after testing (Figure 61).

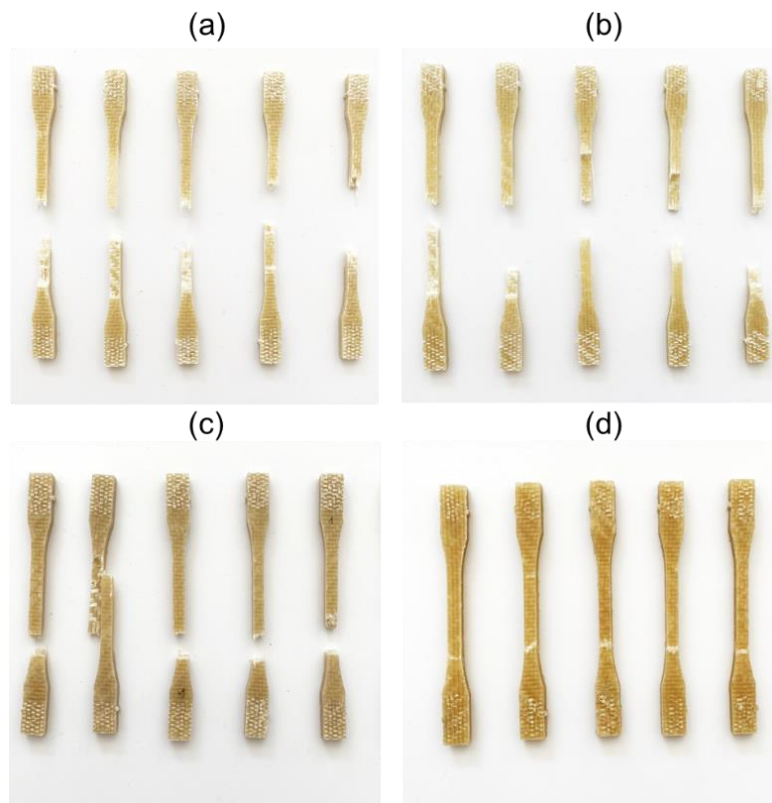


Figure 61: Specimens after tensile test (a) PLLA/GF (b) 10 PLCL/GF (c) 20 PLCL/GF (d) 30 PLCL/GF.



Representative pictures of the surface of the fractures for all specimens are shown in Figure 62. The fibers and the matrix have different values of strain at break. If the fragile component, such as a brittle fiber or matrix with low breaking strain, fractures first, the other component bears the load. The composites display multiple fractures in the fragile component if the component with a higher strain at fracture can handle the extra load. If the fiber fracture strain is lower than that of the matrix, the composite will show a single fracture. On the other hand, if the fiber display strain at fracture higher than the matrix, the composite will exhibit multiple fractures.<sup>2</sup>

All specimens showed multiple fractures after the tensile test. The specimen PLLA/GF and 10 PLCL/GF exhibit an interlaminar delamination, intralaminar matrix cracks, and fiber pull out. As expected, the PLLA/GF specimen shows a brittle character, due to the brittle nature of the matrix and the reinforcement, which facilitate the delamination as well the fiber pull-out (Figure 62 (a), Figure 63 (a)). The addition of 10% of  $\epsilon$ -CL was not sufficient to reduce the brittleness of the matrix, since the 10 PLCL/GF specimen has the same types of failures and similar values of young modulus and tensile strength as the PLLA/GF (Figure 62 (b), Figure 63 (b)).

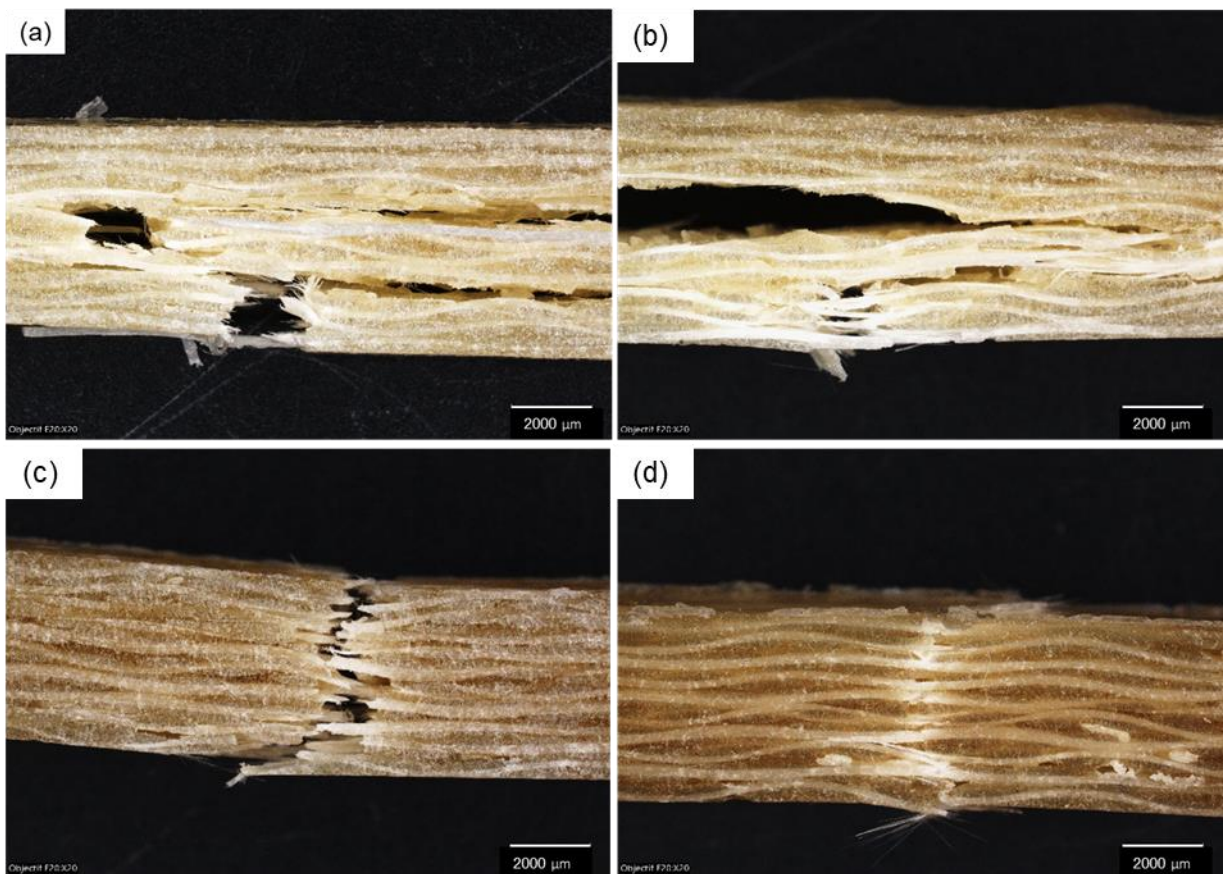


Figure 62: Micrographs of the surface of the fracture after tensile test (a) PLLA/GF (b) 10 PLCL/GF (c) 20 PLCL/GF (d) 30 PLCL/GF specimens.

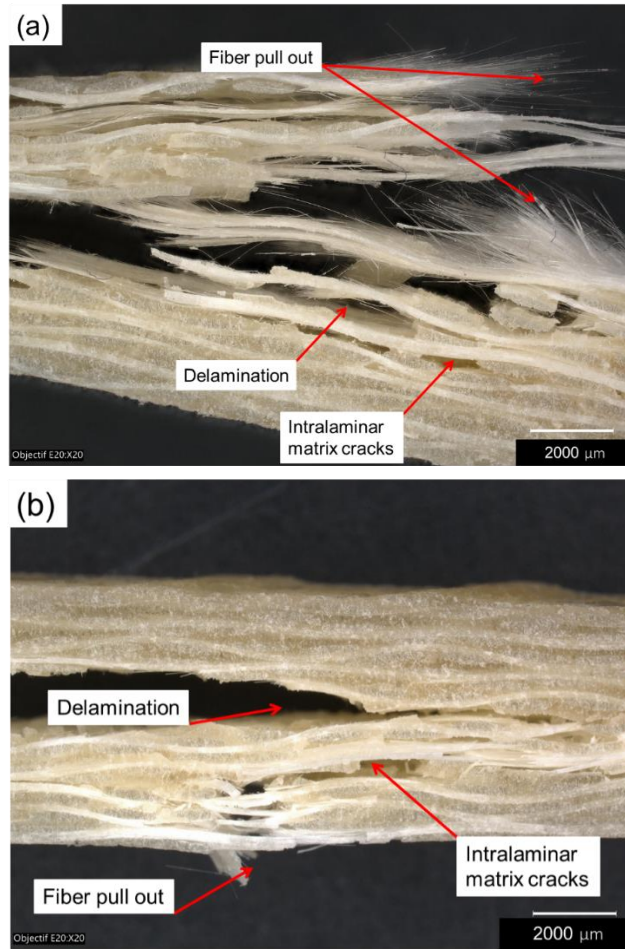


Figure 63: Detailed micrographs of (a) PLLA/GF and (b) 10 PLCL/GF specimens showing different types of fracture.

The 20 PLCL/GF specimen did not show a delamination fracture. However, a translaminar crack, intralaminar matrix crack and a small fiber pull out are observed (Figure 62, Figure 64). The presence of 20% of  $\epsilon$ -CL decreases the brittleness of the matrix with reducing its crystallinity, increasing the interaction between the matrix and the fibers, thus avoiding a premature fracture by delamination.

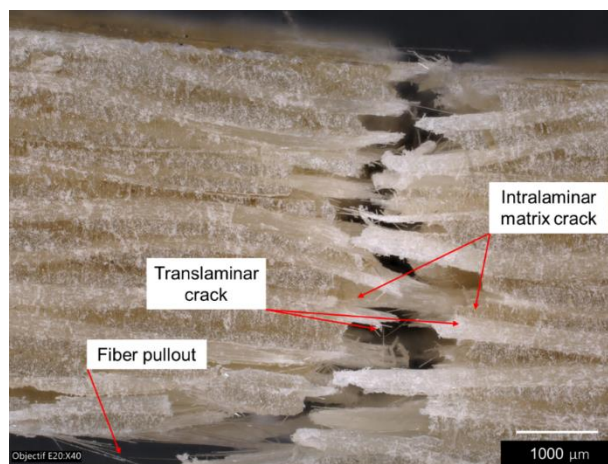


Figure 64: Detailed micrograph of 20 PLLA/GF specimen showing different types of fracture.

The major failure observed in the 30 PLCL/GF plate is the intralaminar matrix crack throughout the longitudinal part of the specimen. A minor fiber pull out can be observed in the bottom of some specimens and some translaminar cracks are also observed (Figure 65). However, these two last ones have a minor impact in the general failure as 30 PLCL/GF specimen did not separate in two distinct parts after the tensile test due to the cohesion of translaminar fibers. A cumulative intralaminar matrix crack caused the failure of the specimen (Figure 65).

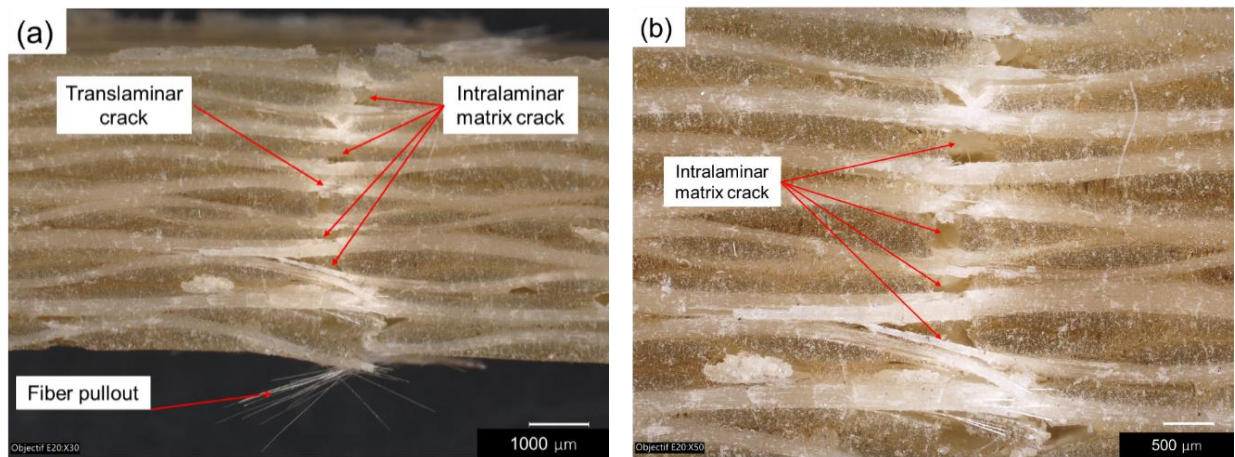


Figure 65: Detailed micrographs of 30 PLCL/GF specimen showing (a) different types of fracture and (b) intralaminar matrix crack.

### 3.5.2 Three-point bending test

Both the bending modulus and the bending strength display the same trend previously observed in the tensile tests, both of them decrease with the increase of  $\epsilon$ -CL content (Table 20). The highest value for bending modulus ( $E_B = 10.34$  GPa) and flexural strength ( $\sigma_B = 273$  MPa) was obtained for PLLA/GF and 10 PLCL/GF showing values of  $E_B = 9.93$  GPa and  $\sigma_B = 256$  MPa closer to the standard. For the 20 PLCL/GF 20 composite, the values begin to drop drastically with  $E_B = 3027$  MPa and  $\sigma_B = 81$  MPa until  $E_B = 301$  MPa and  $\sigma_B = 23$  MPa for 30 PLCL/GF composite. The strain – stress curves in bending are presented in Annexes 6.15 (p.242).

Table 20: Bending properties of GFRC.

<b>Sample</b>	<b>Composite</b>	<b>Bending modulus (GPa)</b>	<b>Bending strength (MPa)</b>	<b>Bending strain (%)</b>	<b>FMR (%)</b>	<b>FVR (%)</b>	<b>T<sub>g</sub> (°C)</b>	<b>χ (%)</b>
2-X	PLLA/GF	10.34 ± 0.20	273 ± 13	3.45 ± 0.10	45.8	28.8	52.2	55.3
2-A	10 PLCL/GF	9.93 ± 0.51	256 ± 10	3.53 ± 0.01	46.9	29.3	42.5	25.0
2-B	20 PLCL/GF	3.02 ± 0.64	81 ± 6	21.93 ± 2.65	46.9	29.3	32.1	3.3
2-C	30 PLCL/GF	0.30 ± 0.03	21 ± 1	22.22 ± 2.13	46.8	29.2	20.7	-

The decrease of 2.2 times of the crystallinity from PLLA/GF to 10 PLCL/GF does not seem to influence drastically the bending properties even if a small decrease of  $E_B$  and  $\sigma_B$  was observed. However, the samples 20 PLCL/GF and 30 PLCL/GF showing crystallinity of 3.3 and 0 % respectively, showed a drastic decrease of  $E_B$  and  $\sigma_B$ . The lowest values of  $E_B$  and  $\sigma_B$  observed for 30 PLCL/GF can be justified either by the lack of crystallinity of the matrix but also by the glass transition temperature below the room temperature (17°C).

The shape of strain – stress curves of PLLA/GF and 10 PLCL/GF shows that a brittle fracture takes place (Figure 66). Regarding 20 PLCL/GF and 30 PLCL/GF, the shape of the strain – stress curve is similar, and no fracture is observed in the strain range tested, even if the values of  $E_B$  and  $\sigma_B$  differ.

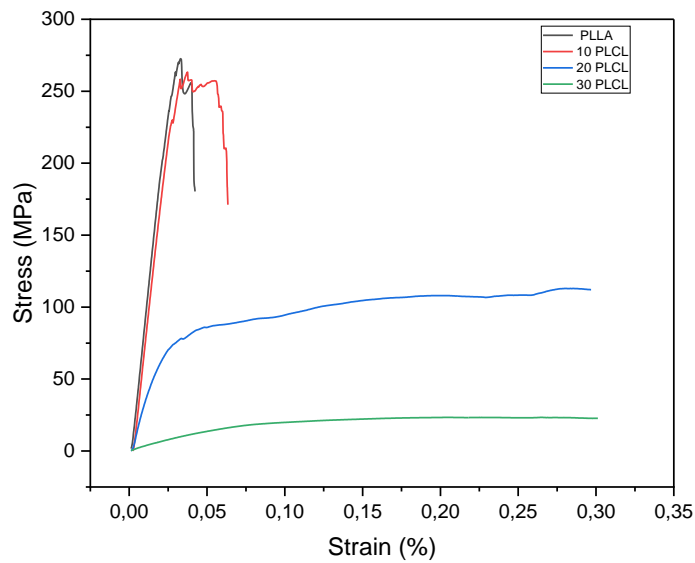


Figure 66: Strain– stress curve in three point bending test of PLLA/GF, 10 PLCL/GF, 20 PLCL/GF, and 30 PLCL/GF composites.

After the bending test, the specimens were analyzed by digital microscopy to determine the type of failure and the morphology of the fracture. The specimens of PLLA/GF and 10 PLCL/GF kept a V shape after the test while the 20 PLCL/GF and 30 PLCL/GF returned to their initial shape. Preliminary studies about the shape recovery of this composites will be presented in Section 0 (p. 178).

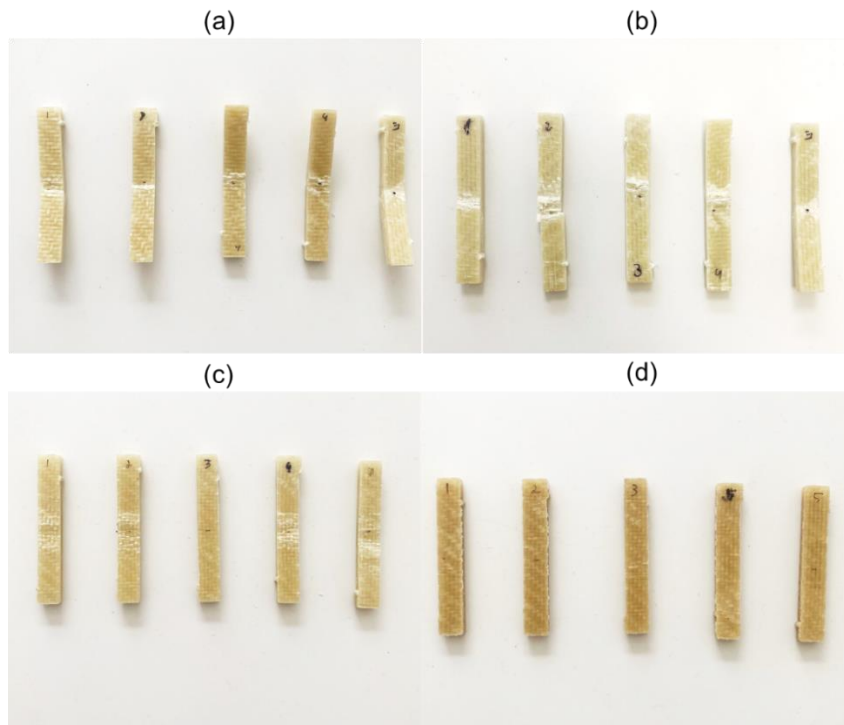


Figure 67: Specimens after three point bending test (a) PLLA/GF (b) 10 PLCL/GF (c) 20 PLCL/GF (d) 30 PLCL/GF.

The PLLA/GF specimens showed different types of failure: compressive fracture (Figure 68 – a), tensile fracture of fiber (Figure 68 – b) and tensile fracture (Figure 68 – c).

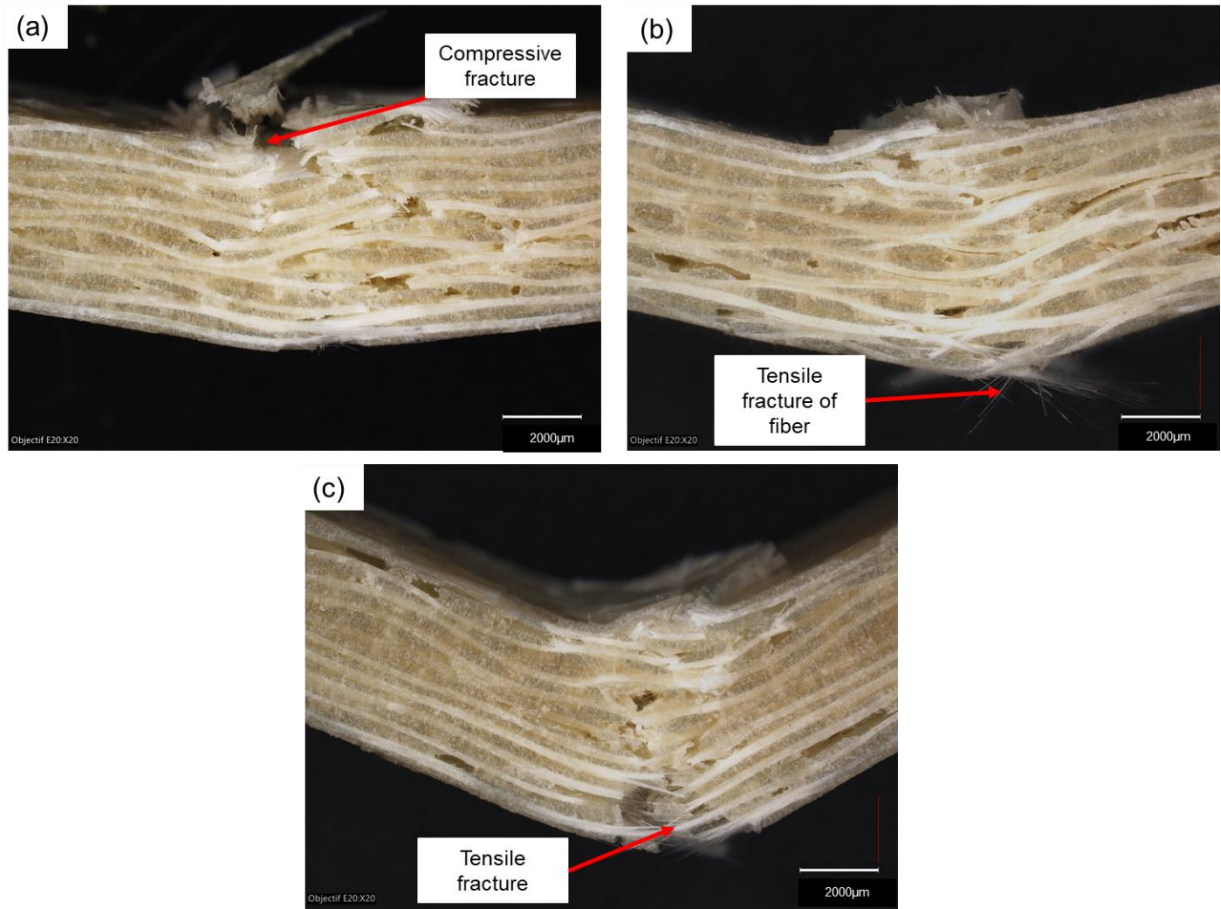


Figure 68: Digital micrographs showing the different types of failure observed in the PLLA/GF specimen.

All 10 PLCL/GF specimens showed tensile fracture and in some cases tensile fracture of the fiber. These specimens showed the same V shape that the PLLA/GF specimen after bending test.



Figure 69: Digital micrograph showing the failure observed in the 10 PLLA/GF specimen.

Taking into account the strain – stress curves of PLLA/GF and 10 PLCL/GF, three different regions can be identified: (i) linear region, (ii) small drop in linear region, and (iii) final failure ( Figure 70).<sup>211</sup> These detailed curves help to understand the failure mechanism of composites in bending test. For both materials, the stress increases linearly in the linear region. The small load drop is observed first in PLLA/GF specimen and later in 10 PLCL/GF, which could correspond to the first failures into the reinforcement or due to manufacturing defects, *i.e.* voids. In the transition region, a sequence of load drops is observed which could correspond to the failure of the various layers of glass fabric. At a bending strength of 3.3 %, PLLA/GF undergoes a catastrophic failure, while an almost linear region appears in the 10 PLCL/GF specimen. In this region, the load drops when a layer of glass fabric is damaged and then, the load increases due to its transfer to the matrix and then to the other undamaged layers. At bending strength of 5.5 % the final failure of the 10 PLCL/GF occurs. The average bending strength of 10 PLCL/GF was 2.3 % higher than that of PLLA/GF, justified by the less brittle character of the matrix.

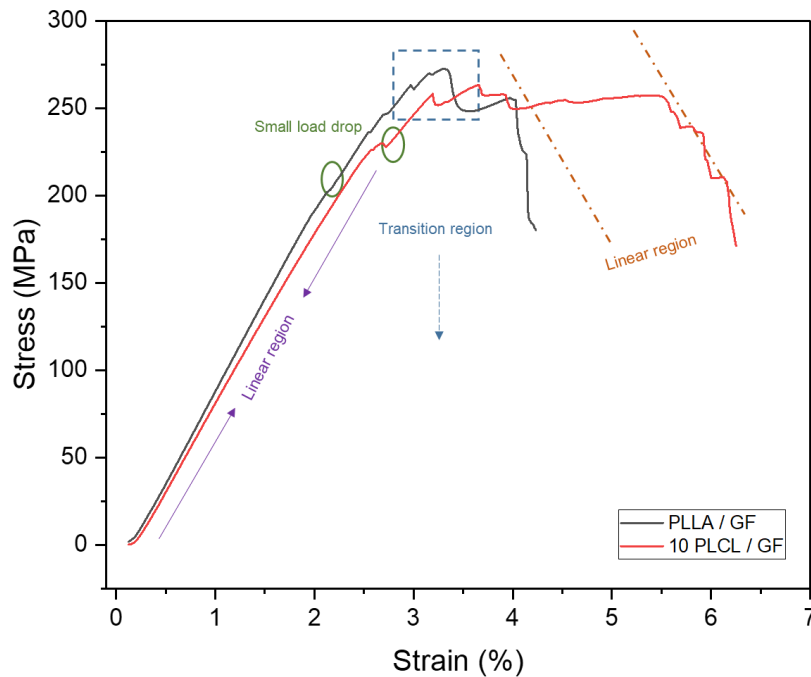


Figure 70: Representative stress-strain graphs for PLLA/GF and 10 PLCL/GF.

No failure was observed in the 20 PLCL/GF and 30 PLCL/GF specimens. In the 20 PLCL/GF specimens, only a compressive damage centered in the first four out layer is observed, visible to the naked eye. This damage was caused by the central loading member. The micrograph of the cross section of the specimen shows the damage in longitudinal fibers, where these ones became whitish (Figure 71-a).

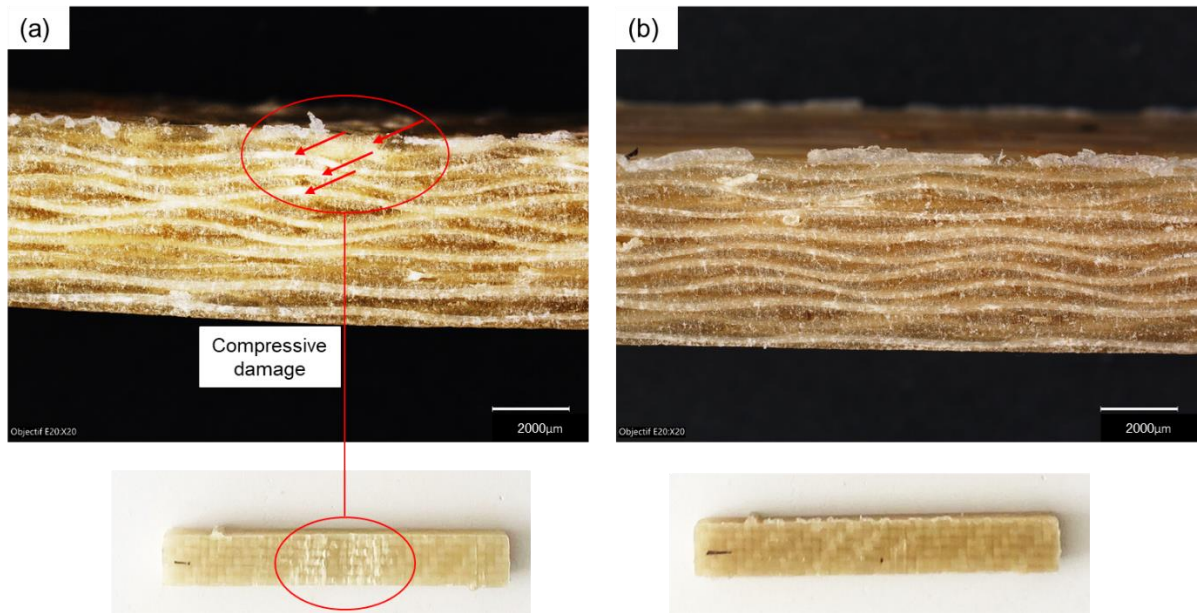


Figure 71: Digital micrographs of the 20 PLCL/GF and 30 PLCL/GF specimens.

### 3.5.3 Impact test

The values of impact strength ( $\alpha_{Cu}$ ) of all composite plates were determined (Table 21). In opposition to the previous mechanical tests, the impact strength of composite plates increases with the increase of  $\epsilon$ -CL content into the matrix. Indeed, an increase of 90 % is observed between the PLLA/GF ( $\alpha_{Cu} = 138.2 \pm 8.3 \text{ kJ/m}^2$ ) and the 30 PLCL/GF ( $\alpha_{Cu} = 262.3 \pm 16.4 \text{ kJ/m}^2$ ). The fiber mass ratio (FMR) measured is approximately of 46 % for all samples, thus, the nature of the matrix is responsible for the differences of absorption energies observed in the impact test.

Table 21: Values of impact strength of composites.

Sample	Composite	FMR (%)	FVR (%)	Impact strength – $\alpha_{Cu}$ (kJ.m <sup>2</sup> )
3-X	PLLA/GF	46.8	29.5	138.2 ± 8.3
3-A	10 PLCL/GF	45.6	28.2	169.6 ± 9.0
3-B	20 PLCL/GF	46.8	29.2	184.2 ± 9.8
3-C	30 PLCL/GF	46.6	29.1	262.3 ± 16.4



After impact test, the specimens PLLA/GF, 10 and 20 PLCL/GF were divided into a hinge shape, while 30 PLCL/GF one kept its initial bar shape (Figure 72).

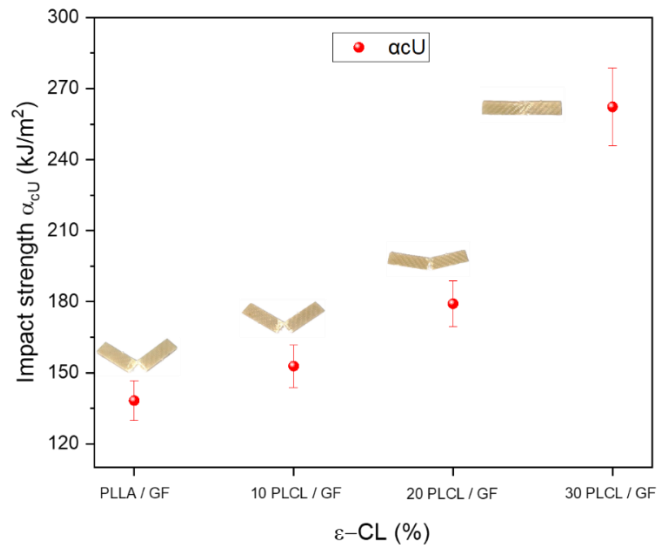


Figure 72: Impact strength of GFRC.

The failure of damaged composite specimens was evaluated for front (impacted) side and back (non-impacted) side by digital microscopy. The failure observed after the impact test in PLLA/GF and 10 PLCL/GF specimens was a hinge break with tensile fracture (Figure 73). In both samples, the impacted surfaces (Figure 73 – a-I – b-I) show damage caused by compression, and the opposed surfaces (Figure 73 – a-II – b II) are fractured by tension.

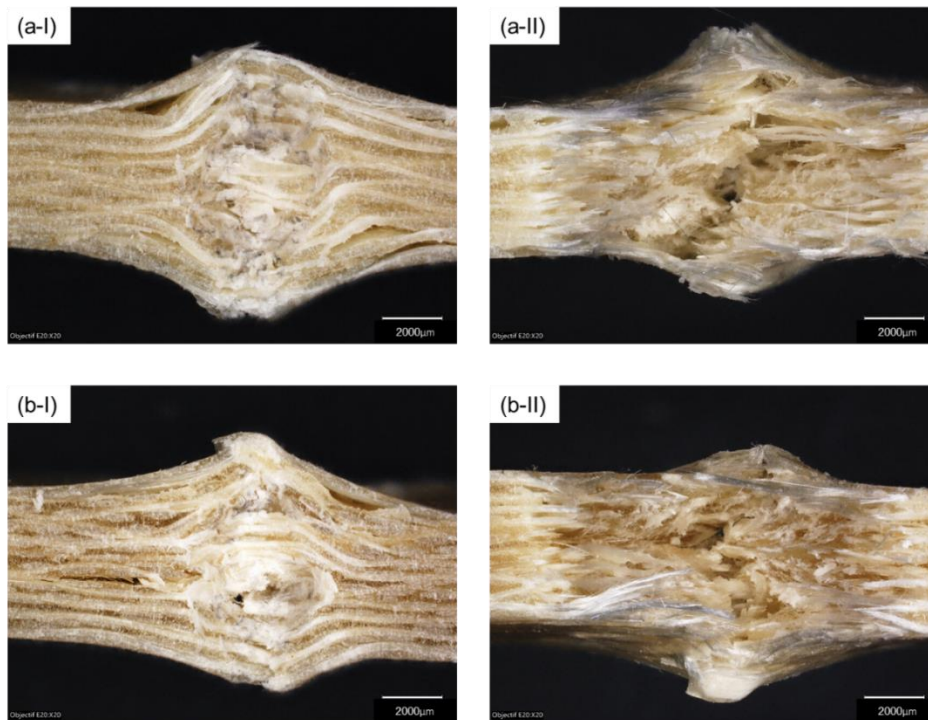


Figure 73: Digital micrograph showing the failure observed in the impacted surface of PLLA/GF (a-I), 10 PLCL/GF (b-I) and opposed impact surfaces of PLLA/GF (a-II) and 10 PLCL/GF (b-II) specimen.

The 20 PLCL/GF specimens exhibit a partial break with tensile fracture while the 30 PLCL/GF ones showed a non-break failure with buckling damage and some fiber pull out (Figure 74).

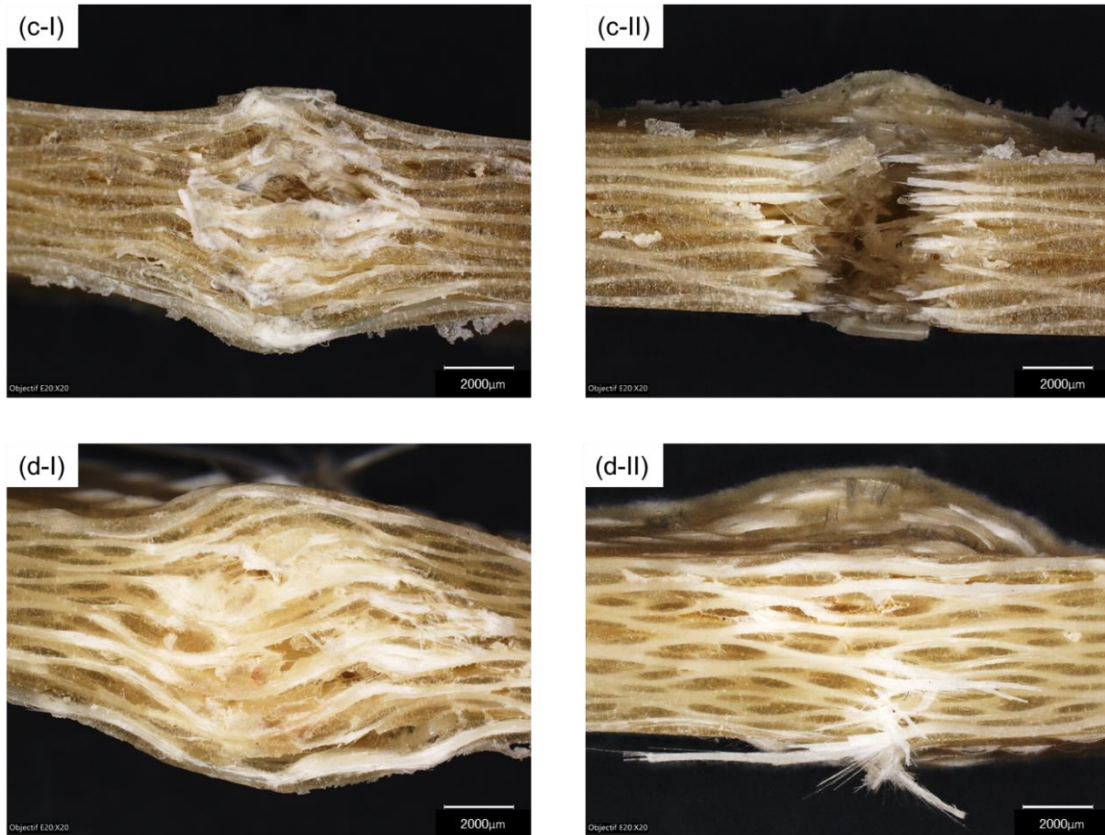


Figure 74: Digital micrograph showing the failure observed in the impacted surface of 20 PLCL/GF (a-I), 30 PLCL/GF (b-I) and opposed impact surfaces of 20 PLCL/GF (a-II) and 30 PLCL/GF (b-II) specimen.

### 3.6 Optimization of polymerization temperature

The successful production of PLLA and PLCL matrix composites using TP-RTM at a temperature of 185 °C has been accomplished. The optimal polymerization temperature of 185 °C for PLLA/GF composites was proved to promote high conversion of L-LA and the obtaining PLLA with high molecular weight. The previously results align with the conversion values reported in the literature.<sup>199,200</sup>

Concerning PLCL/GF composites, the optimization of polymerization temperature in TP-RTM has not been reported to date. As a result, the decision was made to experiment with varying polymerization temperatures. The investigation focused on how the polymerization temperature affects the reaction kinetics, molecular weight, and microstructure of the resulting matrices. Polymerization temperatures of 150, 160, and 170 °C were chosen, and tested for compositions with 20 and 30 mol % of  $\epsilon$ -CL. The choice of temperatures was based on previous works done for the co-polymerization of L-LA and  $\epsilon$ -CL in a flask.<sup>27,212</sup>

The optimal polymerization temperature for pure PLLA matrix is 185 °C as already established previously.<sup>199</sup> The polymerization time was kept at 5 h as for previous experiments conducted at 185°C for the sake of comparison. As PLLA/GF and 10 PLCL/GF composites display similar mechanical properties in traction, bending, and impact and that no significant changes were observed with 10 % of  $\epsilon$ -CL, the 10 PLCL/GF sample was not studied. Samples 2-B (20 PLCL/GF) and 2-C (30 PLCL/GF) already presented and both produced at 185 °C will be set as the standards.

### 3.6.1 Visual observation of composite plates

The numerical pictures of composites clearly show a color change with the variation of polymerization temperature (Figure 75). The variation of color observed was the same for the 20 PLCL/GF and 30 PLCL/GF composites. The plates produced at 185 °C shows a brown color and the plates loss this color tone with the decrease of polymerization temperature, becoming more whitish. At 150 °C, the plates showed a tanned brown color. This variation of color can be ascribed to the degradation of the copolymers.

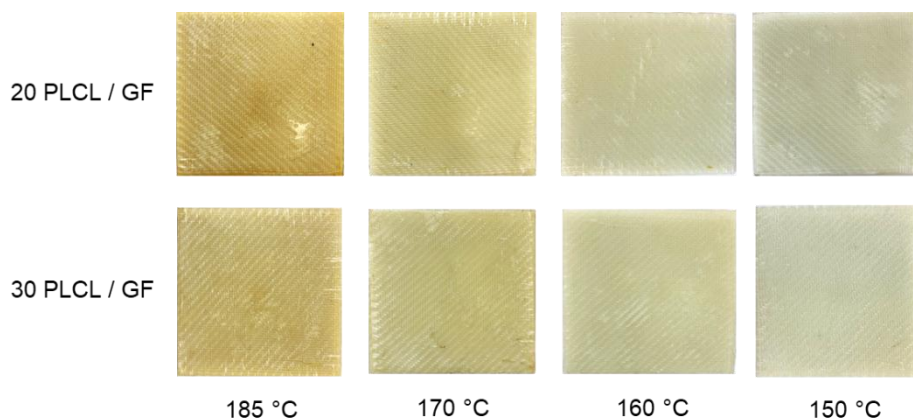


Figure 75: Variation of color of the composite plates.

### 3.6.2 Monomers conversion and molecular weight of PLCL matrices at different polymerization temperatures

The conversion of L-LA in both compositions was higher than 96 % for all the temperatures. However, the conversion of  $\epsilon$ -CL is dependent of the temperature and so is the limiting factor to find the optimal polymerization temperature. In 20 PLCL/GF produced at 170 °C, the conversion of  $\epsilon$ -CL decreases by 3% compared to the same sample produced at 185 °C. A dramatic decrease of 28 and 24 % is observed for 20 PLCL/GF samples produced at 150 and 160 °C respectively (Table 22).

Table 22: Conversion of monomer at different copolymer compositions at different polymerization temperatures.

Sample <sup>a</sup>	Matrix composition	Polymerization temperature (°C)	Conversion		Molecular weight <sup>b</sup>		
			L-LA (%)	ε-CL (%)	M <sub>n</sub> (g.mol <sup>-1</sup> )	M <sub>w</sub> (g.mol <sup>-1</sup> )	D
2-B	20 PLCL	185	96	96	23,500	49,900	2.1
1-D		170	96	93	51,100	115,300	2.2
2-D		160	96	73	92,600	172,300	1.8
3-D		150	98	69	73,150	170,600	2.3
2-C	30 PLCL	185	97	98	16,300	40,700	2.4
1-E		170	97	98	47,100	86,700	1.8
2-E		160	97	95	89,000	100,100	1.7
3-E		150	96	80	51,400	112,800	2.1

<sup>a</sup> Polymerization condition in TP-RTM: PLCL, 5 h, [L-LA + ε-CL] / [Sn] = 2000. <sup>b</sup> Determined by size exclusion chromatography in THF. M<sub>n</sub> and M<sub>w</sub> corrected by a factor of [0.58 x wt % LA units + 0.56 x wt % CL units].

In 30 PLCL/GF composites, the decrease of the conversion of ε-CL was less pronounced than in the 20 PLCL/GF. At 170 °C, the conversion was almost the same than at 185 °C *i.e.* around 98 %. The conversion of ε-CL decreases down to 95 and 80 % at 160 and 150 °C respectively (sample 2-E and 3-E), compared to the standard.

Generally, it was observed that the molecular weight increase when decreasing the polymerization temperature. This trend was expected at 185 °C the matrices could degrade more inducing a decrease of the molecular weight. The highest values of M<sub>w</sub> for 20 PLCL/GF and 30 PLCL/GF were obtained at 160 °C, reaching 172,300 and 100,100 g.mol<sup>-1</sup> respectively (samples 2-D and 3-E).

### 3.6.3 Copolymer composition of PLCL matrices

The copolymer composition and the microstructural magnitudes of the matrices of PLCL/GF composites was determined as previously. The copolymer composition, the number-average sequence lengths of LA (I<sub>LA</sub>) and CL (I<sub>CL</sub>), the Bernoullian random number-average sequence lengths random and the randomness character (R) is presented in (Table 23).

The copolymer composition varies depending on the polymerization temperature for both compositions. The conversion of ε-CL decreases with lowering the polymerization temperature, resulting in the incorporation of more L-LA units into the copolymer chain.

Consequently, the molar lactide composition increases. As an illustration, the molar lactide composition in 20 PLCL/GF (sample 3-D), produced at 150 °C was 85 mol %, while the feed molar ratio was 80 mol % of L-LA. The same tendency is observed for the composition 30 PLCL (sample 3-E), with molar lactide composition of 74.6 mol % with feed molar ratio of 70 % of L-LA. These results are already reported in the literature.<sup>27,103</sup>

Table 23: <sup>1</sup>H NMR characterization of PLCL copolymers synthesized at various temperatures.

Sample	Feed molar ratio L-LA:ε-CL (mol%)	Copolymer composition		Average dyad relative molar fractions			Microstructural magnitudes of the copolymers				
		L-LA (%)	ε-CL (%)	(LA-LA)	(LA-CL)	(CL-CL)	I <sub>LA</sub>	I <sub>CL</sub>	(I <sub>LA</sub> ) <sub>Random</sub>	(I <sub>LA</sub> ) <sub>Random</sub>	R
2-B	80 : 20	79.0	21.0	0.6613	0.2583	0.0804	6.12	1.62	4.77	1.27	0.78
1-D		81.5	18.5	0.7054	0.2194	0.0752	7.43	1.69	5.41	1.23	0.73
2-D		82.9	17.1	0.7363	0.1863	0.0774	8.91	1.83	5.86	1.21	0.66
3-D		85.1	14.9	0.7816	0.1397	0.0787	12.19	2.13	6.73	1.17	0.55
2-C	70 : 30	71.4	28.6	0.5513	0.3258	0.1228	4.38	1.75	3.50	1.40	0.80
1-E		69.1	30.9	0.5252	0.2320	0.2427	5.53	2.50	3.21	1.45	0.58
2-E		71.2	28.8	0.5954	0.2325	0.1722	6.12	2.48	3.47	1.41	0.57
3-E		74.6	25.4	0.6454	0.2021	0.1525	7.39	2.51	3.94	1.34	0.53

The number – average sequence lengths of LA (I<sub>LA</sub>) increases with the decrease of polymerization temperature for both compositions. The I<sub>LA</sub> of 20 and 30 PLCL/GF produced at 150 °C is twice higher than the respective samples produced at 185 °C. A small increase of I<sub>CL</sub> is also observed when decreasing the polymerization temperature for both samples.

The randomness character (R) of both samples decrease with decreasing the polymerization temperature (Figure 76). At a temperature of 185°C, both copolymers exhibited a random distribution with an R value close to 0.8. As the polymerization temperature decreased, the level of randomness in the copolymers also decreased, reaching values of R around 0.50 for both copolymers produced at 150 °C, indicating a moderate blocky character. The reduction

in the level of randomness is particularly noticeable in 30 PLCL/GF composites. The value decreases from 0.80 for the composite produced at 185 °C to 0.58 for the composite produced at 170 °C. This decrease is less pronounced in 20 PLCL/GF composites, where the randomness character decreases from 0.78 to 0.73, for polymerization temperatures of 185°C and 170 °C respectively. In that way, it can be concluded that the polymerization temperature directly influences the microstructure of the copolymers.

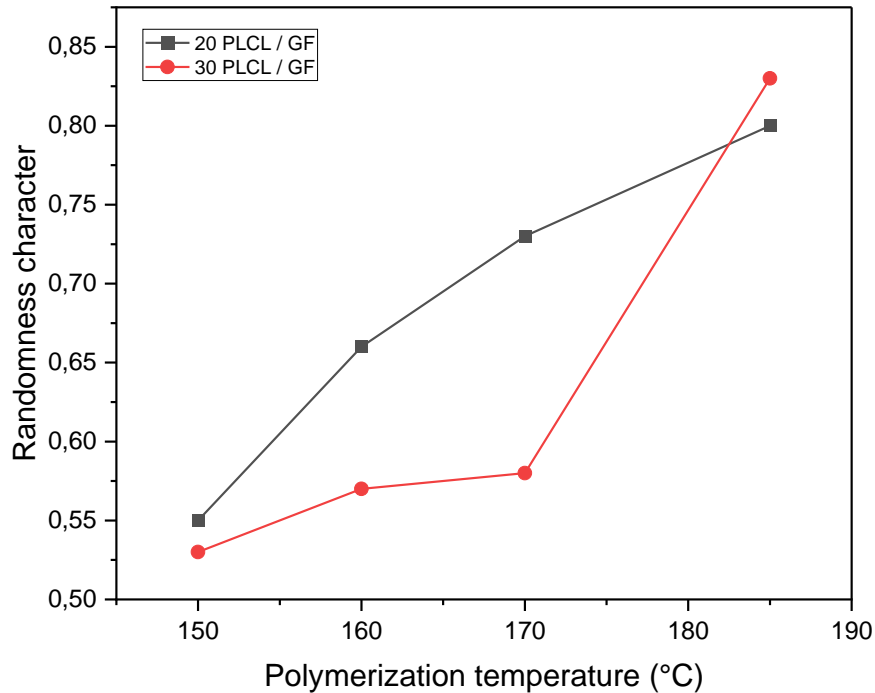


Figure 76: Randomness character vs. polymerization temperature for 20 PLCL/GF and 30 PLCL/GF composites..

### 3.6.4 Thermal properties of PLCL matrices

An increase of the glass transition temperature and melting temperature of the 20 PLCL matrix is observed while decreasing the temperature (Table 24, Annexes 6.11). For instance, the  $T_g$  increased from 32.1°C to 37.9 °C for 20 PLCL matrix produced at 185°C and 150°C respectively (samples 2-B and 3-D). Additionally, at a polymerization temperature of 185 °C, the 20 PLCL matrix (sample 2-B) exhibited a melting temperature of 135 °C, while at polymerization temperatures of 170 °C, 160 °C and 150 °C the melting temperature measured was 133 °C, 139 °C and 145 °C respectively. This increase in melting temperature can be attributed to the increase of molecular weight.

Table 24: Thermal properties of 20 PLCL and 30 PLCL matrices produced at different polymerization temperatures.

Sample	Matrix composition	Polymerization temperature (°C)	$T_g$ (°C)	$T_m$ (°C)	$\Delta H_f$ (J.g <sup>-1</sup> )	$X$ (%)
2-B	20 PLCL	185	32	135	1.4	1.9
1-D		170	29	133	2.7	3.6
2-D		160	35	139	9.6	12.9
3-D		150	38	145	15.6	20.9
2-C		185	21	-	-	-
1-E	30 PLCL	170	18	133	0.1	0.1
2-E		160	17	133	8.8	13.5
3-E		150	17	144	18.4	28.3

The  $T_g$  of the 30 PLCL matrices decreases with the decrease of the polymerization temperature. The melting temperature of 30 PLCL matrices increase with decreasing the polymerization temperature. Compared to the amorphous 30 PLCL matrix produced at 185 °C, the  $T_m$  increase at 133 °C, 133.4 °C and 144°C, at respective polymerization temperatures of 170, 160 and 150 °C.

The crystallinity of both matrices, 20 and 30 PLCL, increase with decreasing the polymerization temperature. The 20 and 30 PLCL matrices (samples 2-B and 2-C) produced at 185 °C was completely amorphous and they reach a crystallinity of 20.9 and 28.3 % respectively at polymerization temperature of 150 °C (samples 3-D and 3-E).

The increase of the crystallinity is related with the number of  $I_{LA}$  and  $I_{CL}$ , both increasing with the decrease of polymerization temperature. The samples with a moderate block character ( $0.8 < R$ ) display  $I_{LA}$  values higher than the sample with statistic character, allowing the crystallization of polylactides.

### 3.7 Mechanical properties of glass fabric reinforced composites produced at various temperatures.

To evaluate the mechanical behavior of the composites, the three-point bending test was selected due to the facility to perform this test. The values of bending modulus ( $E_B$ ) and bending strength ( $\sigma_B$ ) correspond to the average of the five specimens tested for each composition. All composite plates display fiber mass ratio around 46 % and fiber volume ratio near to 28 %.

The bending modulus and the bending strength increase with the decrease of polymerization temperature for both samples (Table 25, Annexes 6.14). The 20 PLCL/GF composite (sample

2-B) produced at 185 °C, showed  $E_B = 3.09$  GPa, while this value increased down to 3.39, 6.05, and 6.91 GPa at polymerization temperatures of 170, 160, and 150 °C respectively. The same trend is observed for the bending strength, with the highest value of 211 MPa measured for the composite produced at 150 °C (sample 3-D).

Table 25: Bending properties of 20 PLCL/GF and 30 PLCL/GF composites at various polymerization temperatures.

Sample	Matrix composition	Polymerization temperature (°C)	Bending modulus (GPa)	Bending strength (MPa)	Bending strain (%)	FMR (%)	FVR (%)	$T_g$ (°C)	$X$ (%)
2-B	20 PLCL	185	3.02±0.43	81 ± 11	22 ± 2.1	45.9	28.49	30.0	-
1-D		170	3.39 ± 0.30	111 ± 13	21 ± 1.0	45.3	27.9	28.8	3.6
2-D		160	6.05 ± 0.12	175 ± 3	5.3 ± 0.2	45.7	28.2	35.3	12.9
3-D		150	6.91 ± 0.17	211 ± 13	5.3 ± 0.2	45.6	28.5	37.9	20.9
2-C	30 PLCL	185	0.39 ± 0.05	29 ± 2	17 ± 3	46.8	29.2	17.1	-
1-E		170	0.75 ± 0.05	38 ± 4	22 ± 1	47.4	29.7	16.3	0.1
2-E		160	3.44 ± 0.25	107 ± 2	9 ± 1	45.7	28.3	17.1	13.5
3-E		150	2.19 ± 0.10	71 ± 5	13 ± 1	47.6	29.9	15.8	28.3

The 30 PLCL/GF composite, also showed an increase of  $E_B$  with decreasing the polymerization temperature until 160°C. The  $E_B$  jumps from 0.39 GPa (sample 2-C) to 3.44 GPa for the sample produced at 160°C (sample 2-E). An increase of  $\sigma_B$  is also observed until 160°, where the bending strength reach 107 MPa (sample 2-E). However, the 30 PLCL/GF composite produced at 150 °C, showed a decrease of bending properties compared to the one produced at 160 °C. At this polymerization temperature, the bending modulus reached 2.19 GPa and bending strength of 71 MPa, values nearly 35 % lower compared to the composite produced at 160 °C.

The increase in bending properties can be directly related to the molecular weight of the matrices (Figure 77). The 20 PLCL/GF composite produced at 185 °C displays  $M_w$  of 49,900 g.mol<sup>-1</sup>, whereas this value increased down to 115,300 g.mol<sup>-1</sup> and 172,300 g.mol<sup>-1</sup> for the composites produced at 170 °C and 160 °C respectively. The composite produced at 150 °C exhibits a slight decrease in molecular weight, reaching 170,600 g.mol<sup>-1</sup>, but has the highest measured bending modulus of 6.91 GPa.



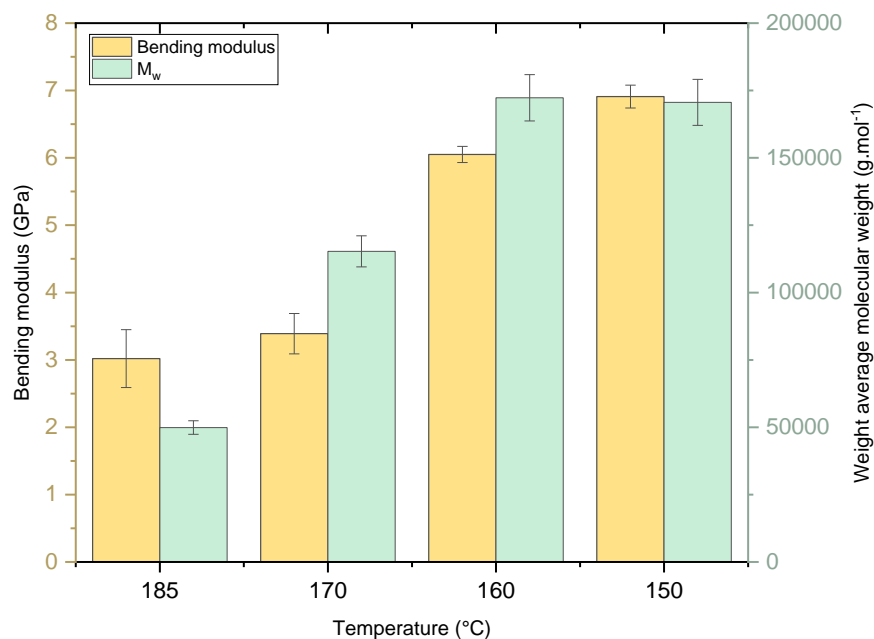


Figure 77: Bending modulus vs  $M_w$  of 20 PLCL/GF composites produced at various temperatures.

The variation in bending modulus values can also be linked to the crystallinity, as discussed in Section 1.3.2. Despite sample 2-D has the highest molecular weight, its crystallinity is nearly half that of sample 3-D. This discrepancy justifies the lower bending modulus observed in sample 2-D compared to sample 3-D, even if the last one displays of the lowest  $M_w$ .

A similar trend is observed for the 30 PLCL/GF composite, where the bending modulus increases with the molecular weight (Figure 78). The sample produced at 185 °C exhibits  $M_w$  of 40,700 g.mol<sup>-1</sup>, while it increases up to 86,700 g.mol<sup>-1</sup>, 100,100 g.mol<sup>-1</sup>, and 112,800 g.mol<sup>-1</sup> for the samples produced at 170 °C, 160 °C, and 150 °C, respectively. The highest measured bending modulus was 3.44 GPa for the composite produced at 160 °C (sample 2-E). The composite (sample 3-E) produced at 150 °C was expected to have the highest bending modulus as it has the highest  $M_w$ . However, a significant decrease of 36% is observed compared to the composite produced at 160 °C (sample 2-E). This decrease can be attributed to the presence of 20 mol% residual  $\epsilon$ -CL in the matrix, which acts as a plasticizer, causing a reduction in the bending properties.

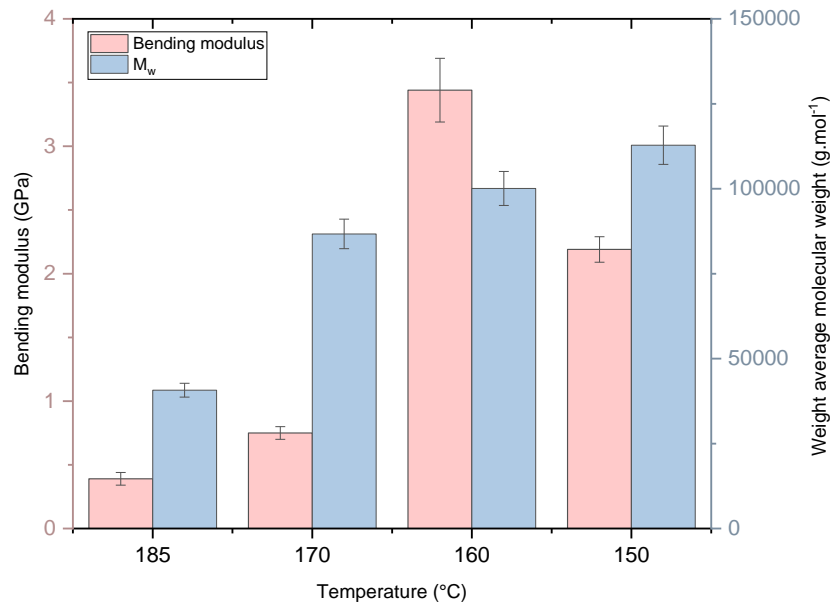


Figure 78: Bending modulus vs  $M_w$  of 30 PLCL/GF composites produced at various temperatures.

The composite produced at 170 °C (sample 1-D) exhibits similar bending properties than the composite produced at 185°C (sample 2-B.) Both specimens display strain-stress curves with a similar shape and show no signs of failure, with a bending strain of approximately 22 % in both cases. However, the sample 1-D shows a higher bending strength of 111 MPa, which is 37% greater than that of sample 2-B. This increase in bending strength can be attributed to the higher molecular weight of the sample 1-D. Interestingly, in this case, crystallinity does not appear to influence the bending properties since sample 1-B only exhibits 3% crystallinity, while sample 2-B is completely amorphous.

The strain-stress curves of samples 2-D and 3-D, produced at 160 °C and 150 °C respectively, exhibit distinct shapes, characterized by a decrease in bending strain to approximately 5% for both specimens. These samples possess the highest bending strength values, of 175 MPa and 211 MPa for samples 2-D and 3-D, respectively. The shape of these curves bears resemblance to the strain-stress curves of PLLA/GF and 10 PLCL/GF composites (Figure 66 – a). Notably, catastrophic failure occurs at a strain of approximately 5% for samples 2-D and 3-D, indicative of a brittle material behavior.

The difference in bending properties can be attributed to two factors: the distinct microstructure of the copolymers and their molecular weight. Samples 1-D ( $R = 0.80$ ) and 2-B ( $R = 0.73$ ) display statistical distribution while sample 2-D ( $R = 0.66$ ) and 3-D ( $R = 0.55$ ) have a marked block character.

In general, the physical and mechanical properties of block copolymers are superior to those of random copolymers as a block copolymer can display properties characteristic of each of the homopolymers from which it is derived as well as a set of properties due to the polymer structure as a whole.<sup>213</sup> In the other way, statistical copolymers do not display the characteristics of their homopolymers in a straightforward manner because the arrangement of the monomers in the polymer chain is random. This means that the properties of a statistical copolymer are determined by a combination of the properties of each monomer unit, but not necessarily in a linear fashion. This corroborates the fact that samples 2-D and 3-D are more resistant to bending than samples 1-D and 2-B.

The other reason which could justifies the resistance to bending of the samples 2-D and 3-D is their elevated molecular weight. Samples 2-D and 3-D display  $M_w$  higher than 170,000 g.mol<sup>-1</sup> and it can be inferred to the copolymer chains that are more entangled to drastically increase the bending properties, since the increase of the molecular weight increases the number of entanglement per chain.<sup>210</sup>

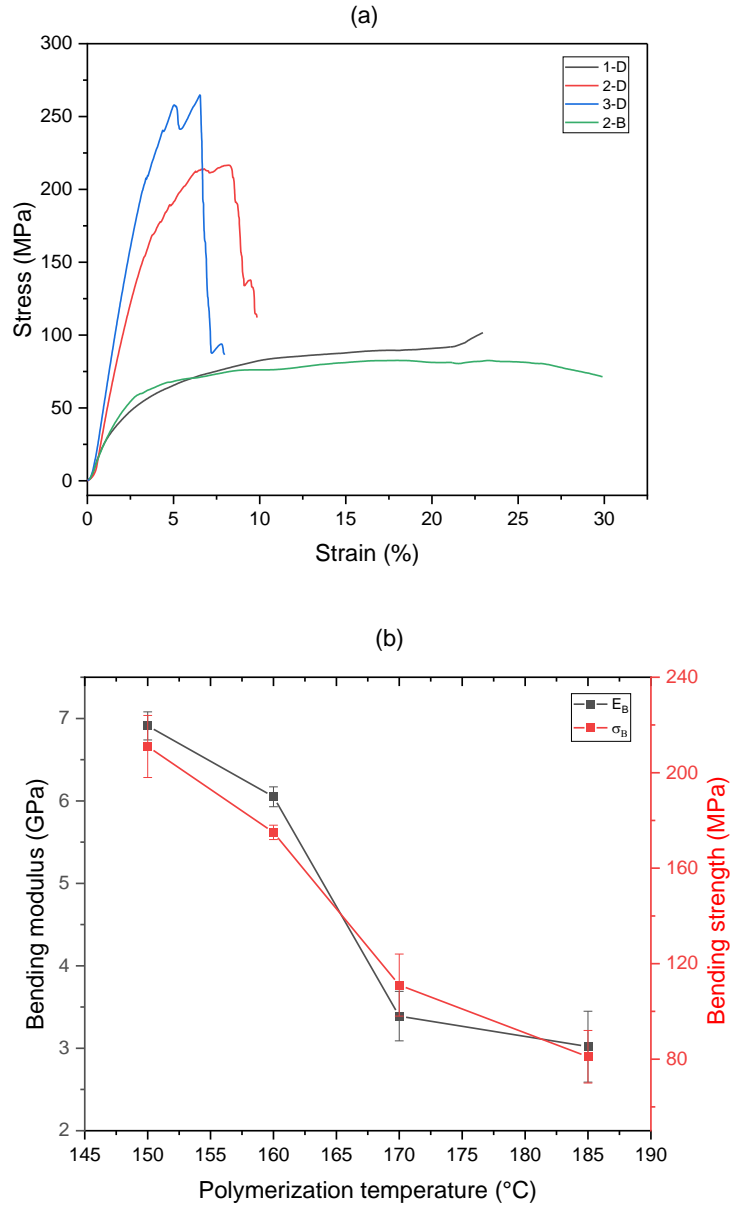


Figure 79: (a) Strain x stress curve in three-point bending test for 20 PLCL/GF composites produced at various temperatures, (b) comparison of bending properties of 20 PLCL/GF composites produced at various temperatures.

After bending tests, the specimens were analyzed by digital microscopy to determine the type of failure and the morphology of the fracture. Specimens 1-D and 2-B returned to their initial shape after the test, whereas specimens 2-D and 3-D kept a V shape after the test. The compressive damage caused by the central loading member are visible in all specimens (Figure 80 – a).

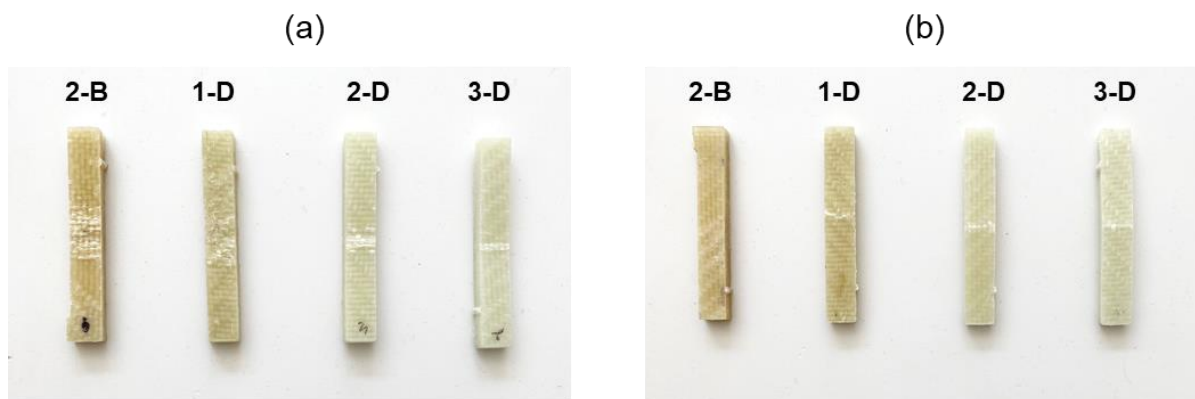


Figure 80: Specimens of 20 PLCL/GF composites after three point bending test. View from (a) central loading member and (b) opposite to loading member.

Digital micrographs showing the cross-section and the opposite direction to the load of the specimens are presented in Figure 81. Only a tensile fracture at the outermost layer of samples 1-D, 2-D, and 3-D are observed, while the standard (2-B), did not show any failure.

Sample 1-E, produced at 170 °C, exhibits similar bending properties than sample 2-C, produced at 185°C (Figure 82). Both samples display strain-stress curves with a similar shape and show no signs of failure, with a bending strain of approximately 20% in both cases. However, sample 1-E demonstrates bending strength of 38 MPa, which is 31 % greater than that of sample 2-C. This increase in bending strength can be attributed to the higher molecular weight of the sample 1-E ( $M_w = 86,700 \text{ g.mol}^{-1}$ ) compared to sample 2-C ( $M_w = 40,700 \text{ g.mol}^{-1}$ ). The crystallinity does not influence the mechanical properties in these case since both samples are amorphous.

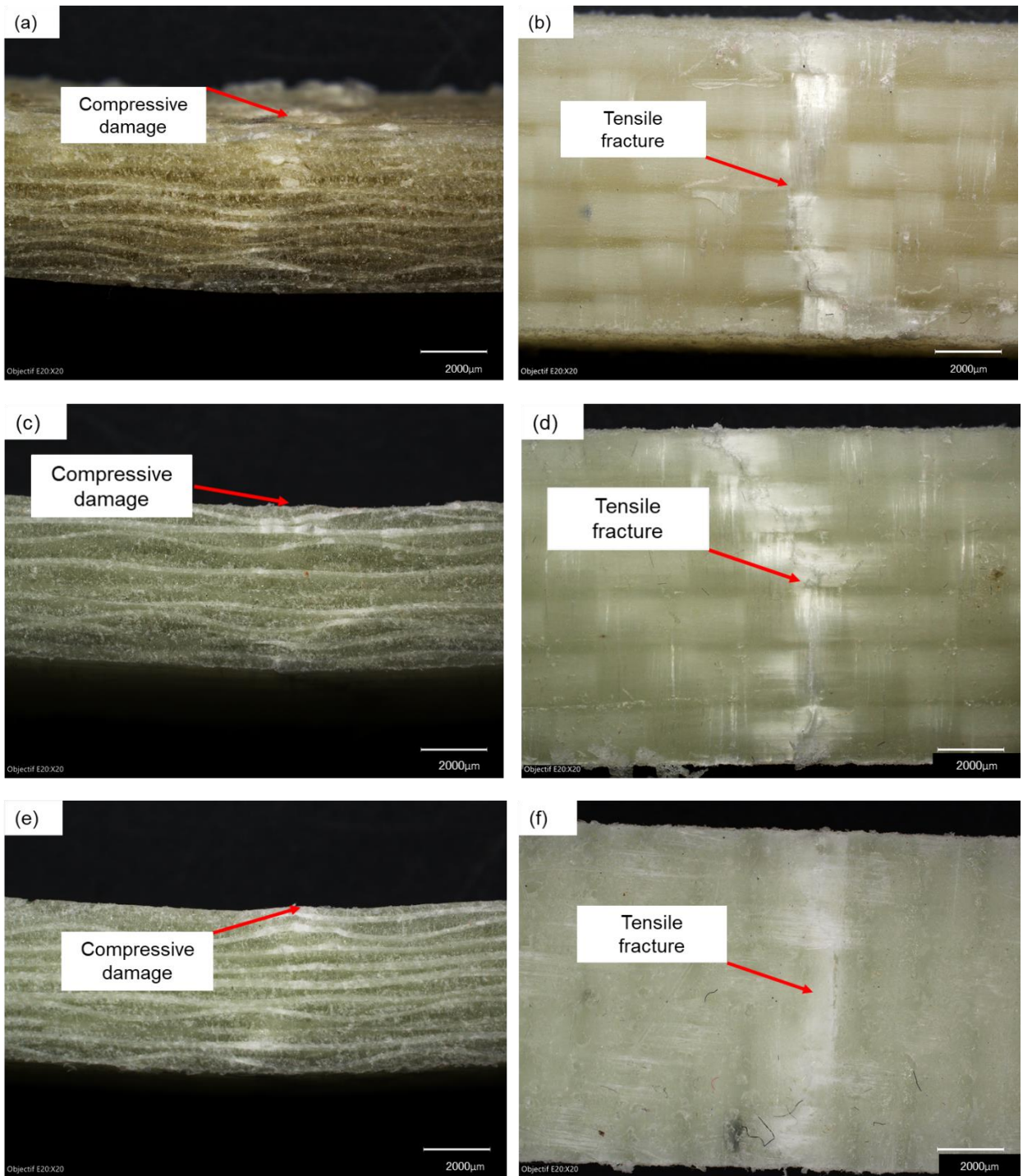


Figure 81: Digital micrograph showing the failure observed in the 20 PLLA/GF specimens produced at various temperatures: (a-b) 170 °C, (b-c) 160 °C, (e-f) 150 °C.

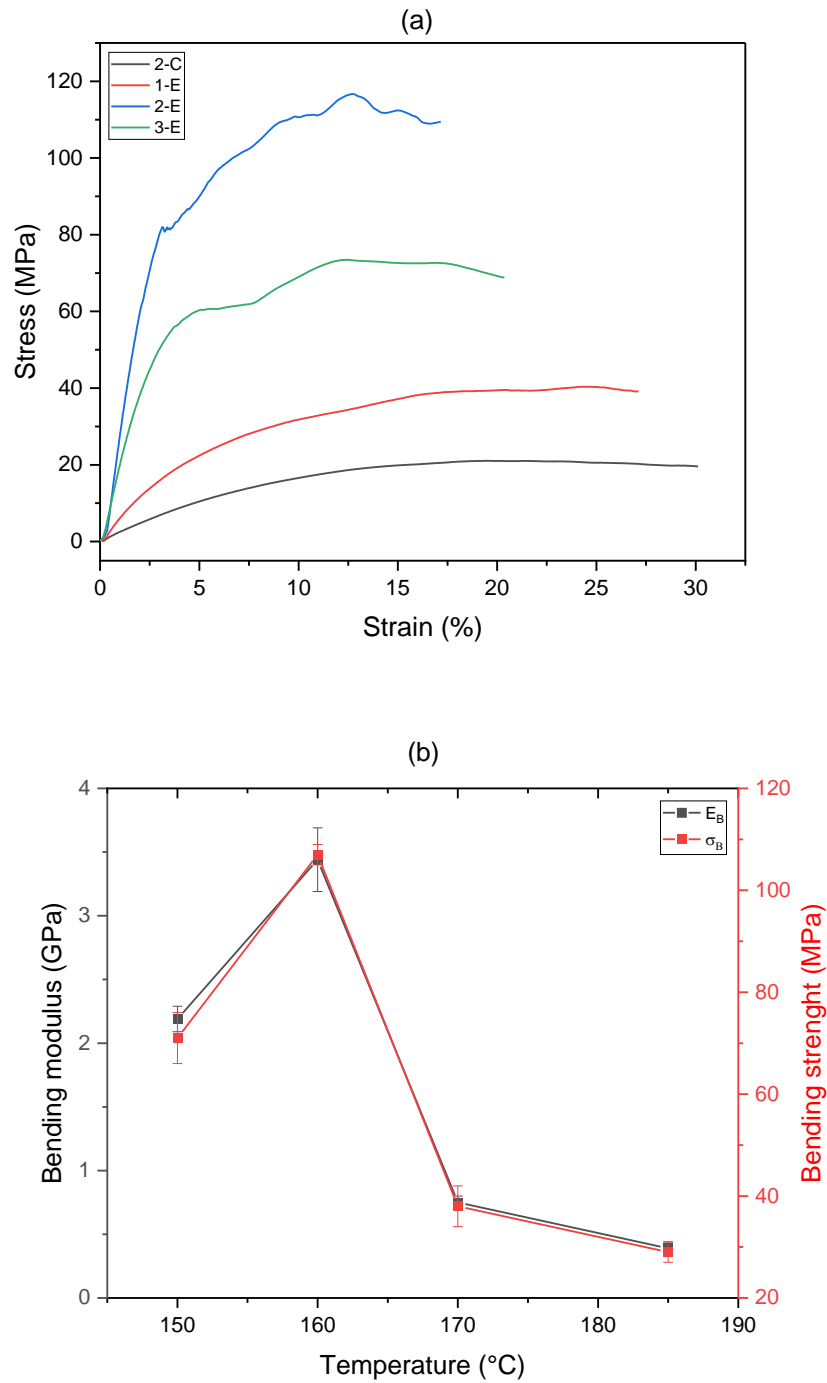


Figure 82: (a) Strain x stress curve in three-point bending test for 30 PLCL/GF composites produced at various temperatures, (b) comparison of bending properties of 30 PLCL/GF composites produced at various temperatures.

The strain-stress curves of samples 2-E and 3-E exhibit distinct shapes compared to the other samples, with bending strains of 9% and 13% respectively. Sample 2-E, produced at 160°C, demonstrates the highest bending strength among all the composites, reaching a value of 107 MPa. Surprisingly, sample 3-E, produced at 150°C, has a lower bending strength than the previous sample, measuring 71 MPa.

As mentioned earlier, despite having the highest molecular mass ( $M_w = 112\,800$ ), sample 3-E is affected by its residual  $\epsilon$ -CL content (20 mol %), which acts as a plasticizer and decreases the bending strength.

In the 30 PLCL/GF composites, only samples 2-E and 3-A exhibited compression damage, while no failure was observed (Figure 83). All specimens regained their initial shape after the bending test, and no V-shaped deformations were reported.

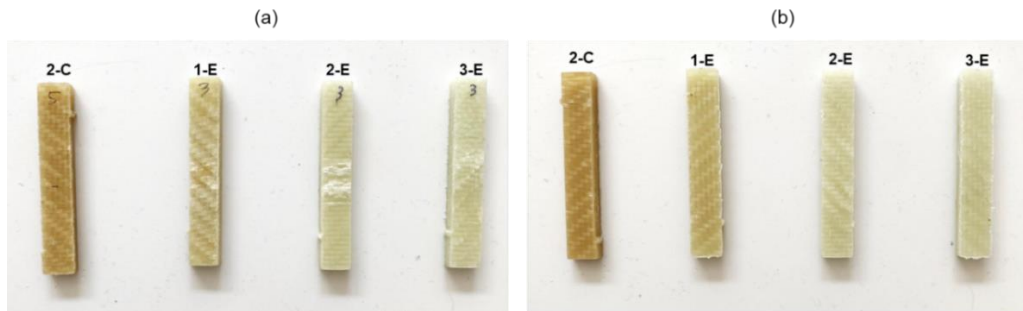


Figure 83: Specimens of 30 PLCL/GF composites after three-point bending test. View from (a) central loading member and (b) opposite to loading member.

Digital micrographs confirm that no failure is present in composites after bending test (Figure 84). However, it is possible to identify some damages in longitudinal fibers of samples 2-E (Figure 84 – b) and 3-E (Figure 84 – c), where these ones became whitish, caused by the compressive load. Nonetheless, the presence of these damages was not enough to cause the failure of the specimen.

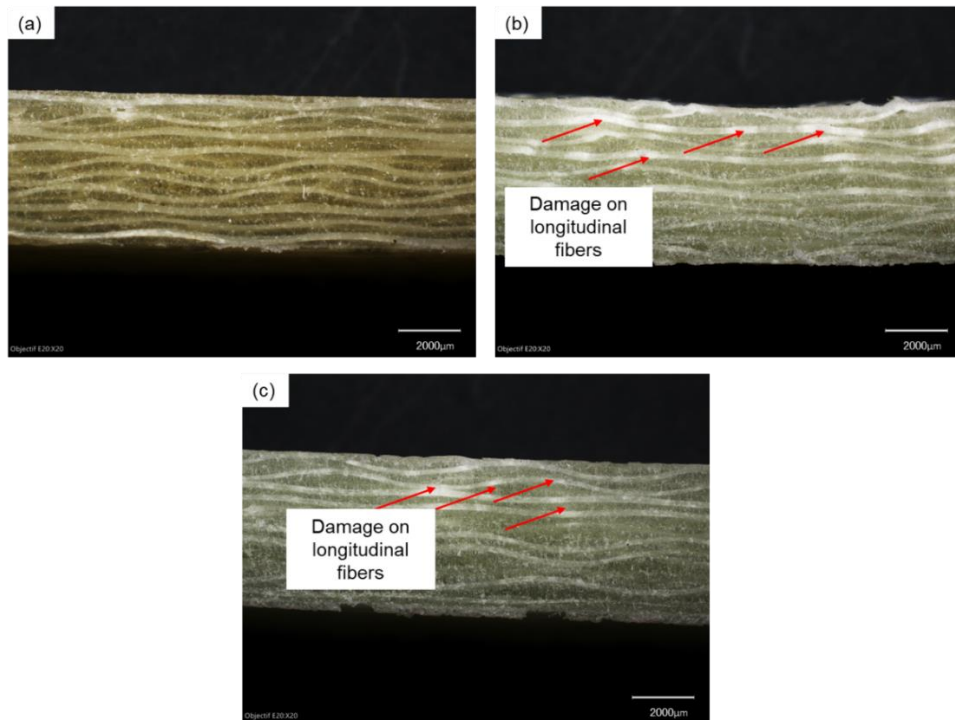


Figure 84: Digital micrographs showing the damage observed in the 20 PLLA/GF specimens produced at various temperatures: (a) sample 1-E, (b) 2-E, (e) 3-E.



### 3.8 Conclusion

In conclusion, the production of poly(L-lactide-co- $\epsilon$ -caprolactone)/glass fabric (PLCL/GF) composites via TP-RTM is a complex process that requires careful consideration of various factors. The optimization of polymerization parameters, including temperature, time, and co-monomers over catalyst ratio, is critical to achieving high-quality composite materials with full conversion of the co-monomers and high  $M_w$ . The viscosity of the reactive thermoplastic system also plays an important role in composite production. In the optimal polymerization conditions, the conversion of both monomers was higher than 95% along with  $M_w$  up to 100,000 g.mol<sup>-1</sup>. Physicochemical characterization of PLLA/GF and PLCL/GF composites is essential to understand their properties and behavior. Thermal properties of these composites were evaluated to determine their suitability for various applications. In particular, the thermal stability of the copolymer matrix composites was improved compared to pure PLLA.

Finally, mechanical properties of all composites were tested using various methods to evaluate their strength and strain. The tensile strength and modulus were found to decrease with increasing the  $\epsilon$ -CL content. The bending modulus and strength follow the same trend. Regarding the impact resistance, the highest values were measured for the composite containing 30 wt% of  $\epsilon$ -CL, and the absorbed energy was found 80% higher than that of pure PLLA composite.

## **Chapter IV: Carbon fabric reinforced composites produced by TP-RTM**

This chapter deals with the production and characterization of poly(L-lactide)/carbon fabric (PLLA/CF) and poly(L-lactide-co- $\epsilon$ -caprolactone)/carbon fabric (PLCL/CF) composites. The conversions and molecular weight of the matrices were determined, along with thermal and mechanical properties of the resulting composites. The influence of the experimental parameters on the composites production was studied and discussed. In particular, it was observed that the polymerization temperatures affected the mechanical properties of the composites. The three-point bending test was used to evaluate the mechanical properties. The study of the failure of the carbon fabric reinforced composites provides valuable insights into the production and characterization of these composites. These carbon fabric reinforced composites (CFRC) were compared to the glass fabric reinforced composites (GFRC) synthesized in the previous chapter.



#### 4.1 Production of carbon fabric reinforced composites (CFRC)

The decision to use carbon fabric (CF) for composite production was motivated by their exceptional mechanical properties and lightweight nature. However, the primary reason behind this choice was the chemical inertness of these fibers.<sup>2,214</sup> This key characteristic should not affect the *in-situ* polymerization of the matrix in the presence of carbon fibers.

As for the glass fibers, carbon fibers are also sized. The manufacturer used a generic epoxy resin, accounting for 1.2 wt % of the sizing, without specifying its exact nature. Prior to their use, the thermal stability of carbon fabric was examined using TGA (Figure 85). A weight loss begins at 100 °C, with a maximum weight loss of 1.5%. This weight loss is consistent with the quantity of sizing agent present in the carbon fibers.

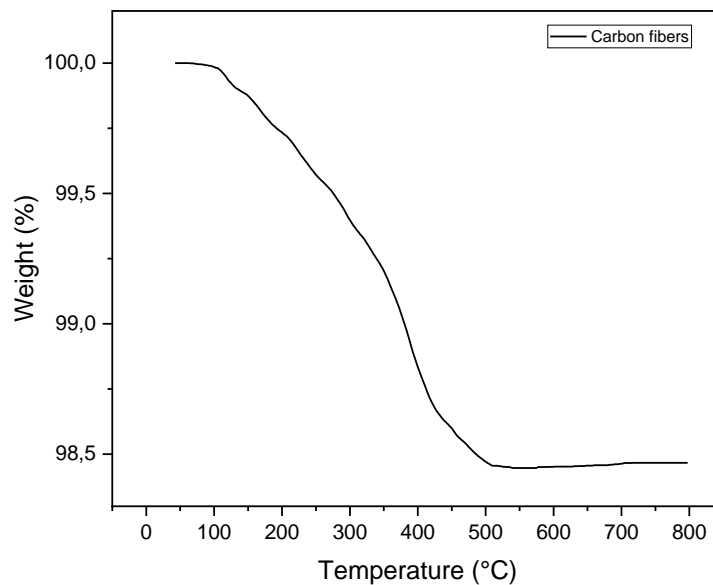


Figure 85: TGA curve of carbon fibers. ( $10^{\circ}\text{C}\cdot\text{min}^{-1}/\text{N}_2$ )

Regarding the previous study presented in Chapter III (p.78), the following experimental parameters was chosen for the production of carbon fabric reinforced composites (CFRC): a co-monomers over catalyst molar ratio of 2000, a polymerization temperatures of 185°C, 170°C and 160 °C for the PLLA/CF, 20 PLCL/GF and 30 PLCL/GF respectively, and a polymerization time of 2 h for the PLLA/CF and 5 h for the 20 and 30 PLCL/GF (Table 26). The choice of the polymerization temperatures was based on the previous results obtained in Chapter III. A compromise between high conversions of both monomers and high molecular weights was the key for the choice of these polymerization temperatures.

Table 26: TP-RTM parameters used to produce carbon fabric reinforced composites.

Sample	Matrix composition (L-LA:ε-CL)	[L-LA + ε-CL] / [Sn]	Polymerization temperature (°C)	Polymerization time (h)
PLLA/CF	100:0		185	2
20 PLCL/CF	80:20	2000	170	5
30 PLCL/CF	70:30		160	

Three composite plates of each composition were made, with ten layers of carbon fabric in each plate (FMR 29%). The glass fabric reinforced composite (GFRC) containing 10% of ε-CL exhibited similar mechanical behavior to the pure PLLA composite (cf. Chapter III, p.95), thus this formulation was not studied in carbon fabric reinforced composites (CFRC).

The obtained PLLA/CF, 20 PLCL/GF and 30 PLCL/GF composite plates display the same black nature (Figure 86). However, due to the black hue of the carbon fabric, it was not possible to identify the color of the matrix. Notably, the surface defects were more apparent in these composites compared to the glass fabric reinforced ones. These surface imperfections primarily arose from the flaws on the mold surface, attributed to wear and tear.

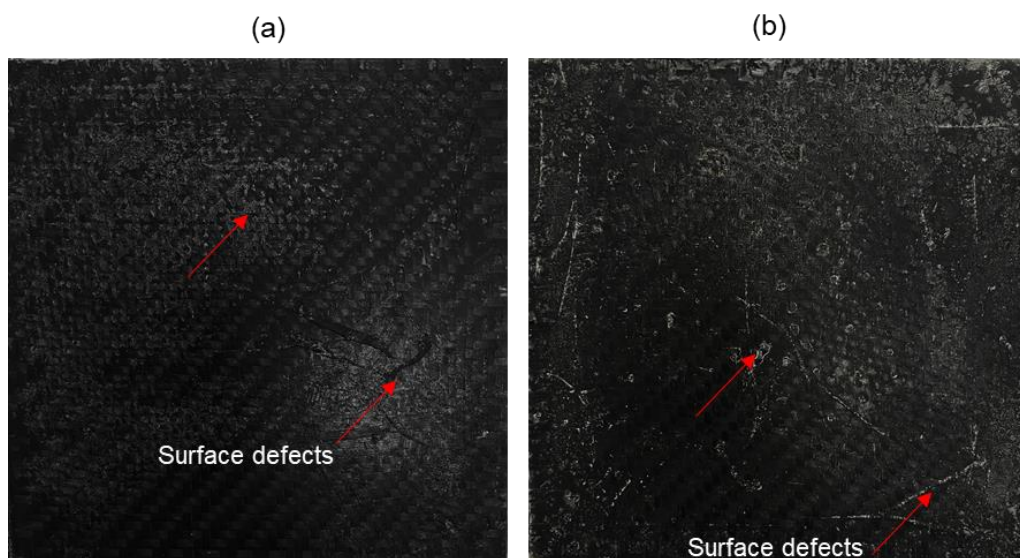


Figure 86: (a) PLLA / CF and (b) 20 PLCL/GF composite plates.

### 4.1.1 Conversions of monomers and molecular weights of matrices

The conversions of the co-monomers in the matrix were determined by  $^1\text{H}$  NMR and the molecular weights by SEC (Table 27). The  $^1\text{H}$  NMR spectra of all samples are presented in (Appendix 6.9, p.222). For the composite PLLA/CF, conversions of L-LA higher than 95 % and  $M_w$  ranging from 142,500  $\text{g}\cdot\text{mol}^{-1}$  to 158,700  $\text{g}\cdot\text{mol}^{-1}$  were obtained. In the case of the copolymer-matrix composites 20 PLCL/GF conversions exceeding 93% were measured for both monomers along with  $M_w$  ranging between 117,500  $\text{g}\cdot\text{mol}^{-1}$  and 130,700  $\text{g}\cdot\text{mol}^{-1}$ . Finally, the 30 PLCL/GF composites have conversions higher than 95 and 93 % for L-LA and  $\epsilon$ -CL respectively, with  $M_w$  between 119,000 and 132,700  $\text{g}\cdot\text{mol}^{-1}$ . All matrices showed medium width distribution with dispersity values between 1.75 and 2.17.

Table 27: Conversion of monomers and molecular weights of the matrices at different copolymer compositions.

Sample	Feed molar ratio		Conversion <sup>a</sup>		Molecular weight <sup>b</sup>	
	L-LA: $\epsilon$ -CL (mol %)	L-LA (%)	$\epsilon$ -CL (%)	$M_n$ ( $\text{g}\cdot\text{mol}^{-1}$ )	$M_w$ ( $\text{g}\cdot\text{mol}^{-1}$ )	$\bar{D}$
1-AA	100:0	96	-	90,700	142,500	1.57
2-AA		95	-	91,600	149,100	1.62
3-AA		96	-	114,000	158,700	1.39
1-BB	80:20	98	96	63,000	130,700	2.03
2-BB		96	93	53,900	117,500	2.17
3-BB		96	93	64,000	125,900	1.96
1-CC	70:30	95	93	56,500	119,000	2.10
2-CC		97	93	75,670	132,700	1.75
3-CC		95	95	65,900	130,900	1.98

Experimental conditions: Polymerization temperature: 185 °C (pure PLLA), 170 °C (L-LA: $\epsilon$ -CL=80:20), 160 °C (L-LA: $\epsilon$ -CL=70:30).  
<sup>a</sup> Determined by  $^1\text{H}$  NMR in  $\text{CDCl}_3$  <sup>b</sup> Determined by SEC in  $\text{CDCl}_3$  at 30°C, triple detection.

### 4.1.2 Copolymer matrices composition of PLCL/CF composites

The determination of the microstructure of the copolymer matrices was performed in the same manner as in Chapter III (see Section 3.3.2, p.86). The compositions closely matched the feed molar ratio for all PLCL/CF composites (Table 28). In the case of the three samples of 20 PLCL/CF, the  $I_{LA}$  values ranged from 7.44 to 7.54, and the  $I_{CL}$  values ranged between 1.56 and 1.59. These samples exhibited a randomness character (R) of approximately 0.7, indicating a moderate blocky arrangement.

For the three samples of 30 PLCL/CF, the  $I_{LA}$  values were found to be between 5.66 and 6.19, while the  $I_{CL}$  values ranged from 2.10 to 2.22. The randomness character for these samples was around 0.6, also suggesting a moderate blocky pattern. The randomness character (R) of the matrices with compositions of 20 and 30 % of  $\epsilon$ -CL was similar to the compositions made with glass fabric, already discussed in Section 3.3.2 (p. 86).

Table 28:  $^1H$  NMR characterization of PLCL copolymers.

Sample	Feed molar ratio	Copolymer composition		Average dyad relative molar fractions			Microstructural magnitudes of the copolymers				
	L-LA: $\epsilon$ -CL	L-LA (%)	$\epsilon$ -CL (%)	(LA-LA)	(LA-CL)	(CL-CL)	$I_{LA}$	$I_{CL}$	$(I_{LA})_{Random}$	$(I_{LA})_{Random}$	R
1-BB		82.6	17.4	0.7160	0.2191	0.0648	7.54	1.59	5.73	1.21	0.76
2-BB	80 : 20	82.5	17.5	0.7144	0.2203	0.0653	7.49	1.59	5.70	1.21	0.76
3-BB		82.7	17.3	0.7154	0.2222	0.0624	7.44	1.56	5.76	1.21	0.77
1-CC		73.0	27.0	0.6037	0.2528	0.1436	5.78	2.14	3.70	1.37	0.64
2-CC	70 : 30	73.6	26.4	0.6171	0.2377	0.1452	6.19	2.22	3.79	1.36	0.61
3-CC		73.0	27.0	0.6009	0.2576	0.1415	5.66	2.10	3.70	1.37	0.65

### 4.1.3 Thermal properties of the matrices

The thermal properties of the matrices were assessed through TGA analysis and one sample of each composition was analyzed. Pure PLLA matrix exhibited a decomposition onset temperature of 226 °C, reaching a maximum decomposition temperature of 294 °C (Figure 87 – a, Table 29). Regarding the copolymer matrices, the weight loss of 20 PLCL starts at 232 °C with a maximum at 305 °C. The composition 30 PLCL showed a degradation starting at 247 °C with a maximum at 330 °C. No residues were observed at 800 °C for any of the compositions (Table 29).

Table 29: TGA data of PLLA and PLCL matrices ( $N_2$ ,  $10\text{ }^\circ\text{C min}^{-1}$ )

<b>Sample</b>	<b>Matrix</b>	<b><math>T_{5\%}</math> (<math>^\circ\text{C}</math>)</b>	<b><math>T_{95\%}</math> (<math>^\circ\text{C}</math>)</b>	<b>Max DTG (<math>^\circ\text{C}</math>)</b>	<b>Slope (% weight <math>^\circ\text{C.min}^{-1}</math>)</b>	<b>Residual weight (%)</b>
1-AA	PLLA	226	314	294	-1.76	0
3-BB	20 PLCL	232 (+6)	357 (+43)	305 (+11)	-1.26	0
3-CC	30 PLCL	247 (+15)	392 (+78)	330 (+36)	-0.79	0
Commercial PCL	PCL	377	425	408	-2.44	0

The decomposition rates of both copolymers are lower than pure PLLA. Sample 1-AA (PLLA) showed a weight loss rate of  $1.76\text{ \% weight. }^\circ\text{C.min}^{-1}$  while the samples 3-BB (20 PLCL) and 3-CC (30 PLCL) have degradation rate of  $1.26$  and  $0.79\text{ \% weight. }^\circ\text{C.min}^{-1}$ . For the sake of comparison, pure PCL (commercial PCL) exhibit a degradation rate of  $2.44\text{ \% weight. }^\circ\text{C.min}^{-1}$ .

Figure 87 – b depicts the normalized first derivative of the weight loss in TGA curves for PLLA, PLCL copolymers and pure PCL. The peaks observed in PLLA differ slightly from those of PLCL. PLLA exhibits a single narrow peak, while PLCL displays a broader one. The degradation of lactide-rich sequences, which are less stable, initiates around  $250\text{ }^\circ\text{C}$ , while the  $\epsilon$ -caprolactone-rich sequences, which are less sensitive to heat, degrade at  $350\text{ }^\circ\text{C}$ . This trend is consistent with the observations made for the PLLA/GF and PLCL/GF composites.



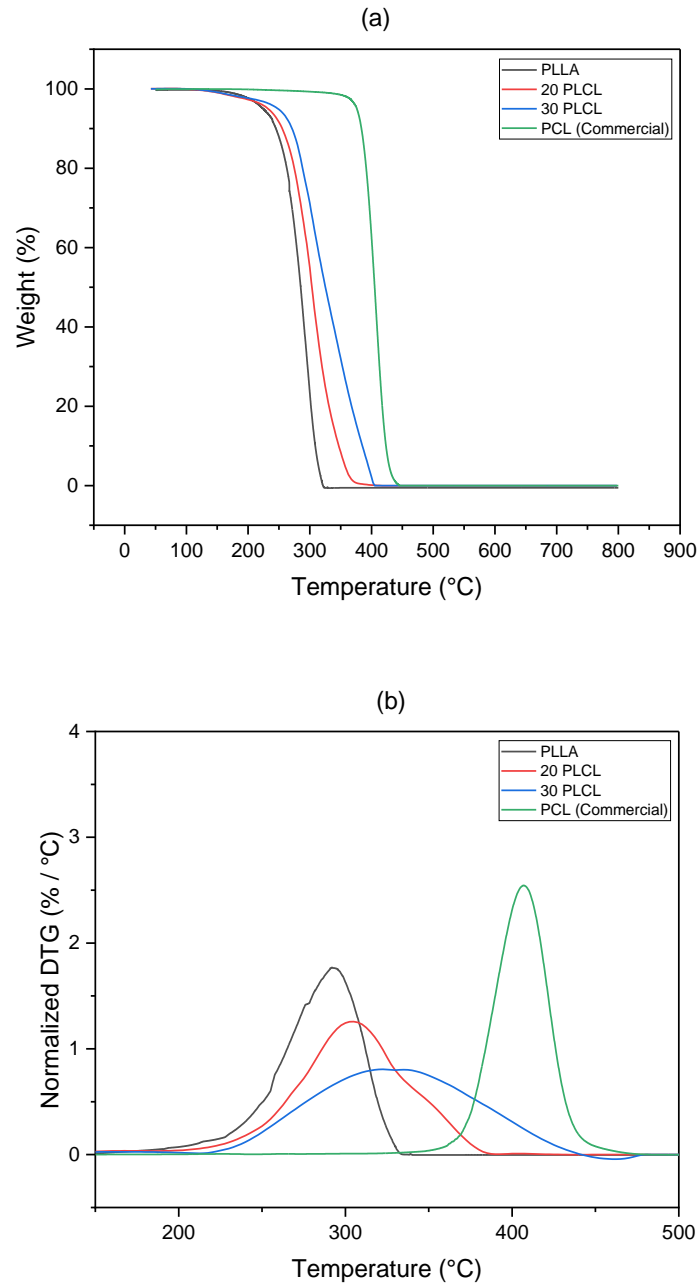


Figure 87: (a) TG curves of PLLA, PLCL matrices thermal degradation at heating rate of  $10^{\circ}\text{C min}^{-1}$ ; (b) Normalized DTG curves of PLLA and PLCL matrices thermal degradation at heating rate of  $10^{\circ}\text{C.min}^{-1}$ .

Regarding the DSC analysis, the PLLA/CF matrices showed  $T_g$  of  $54^{\circ}\text{C}$ ,  $T_m$  of  $171^{\circ}\text{C}$  and crystallinity between 45 and 48 %, with a marked melting peak (Figure 88, Table 30). The matrices of 20 PLCL/CF composites, display  $T_g$  around  $32^{\circ}\text{C}$ ,  $T_m$  of  $133^{\circ}\text{C}$  and very low crystallinity, around 1% (Figure 88 , Table 30). Finally, the matrices of 30 PLCL/CF showed  $T_g$  around  $17^{\circ}\text{C}$ .

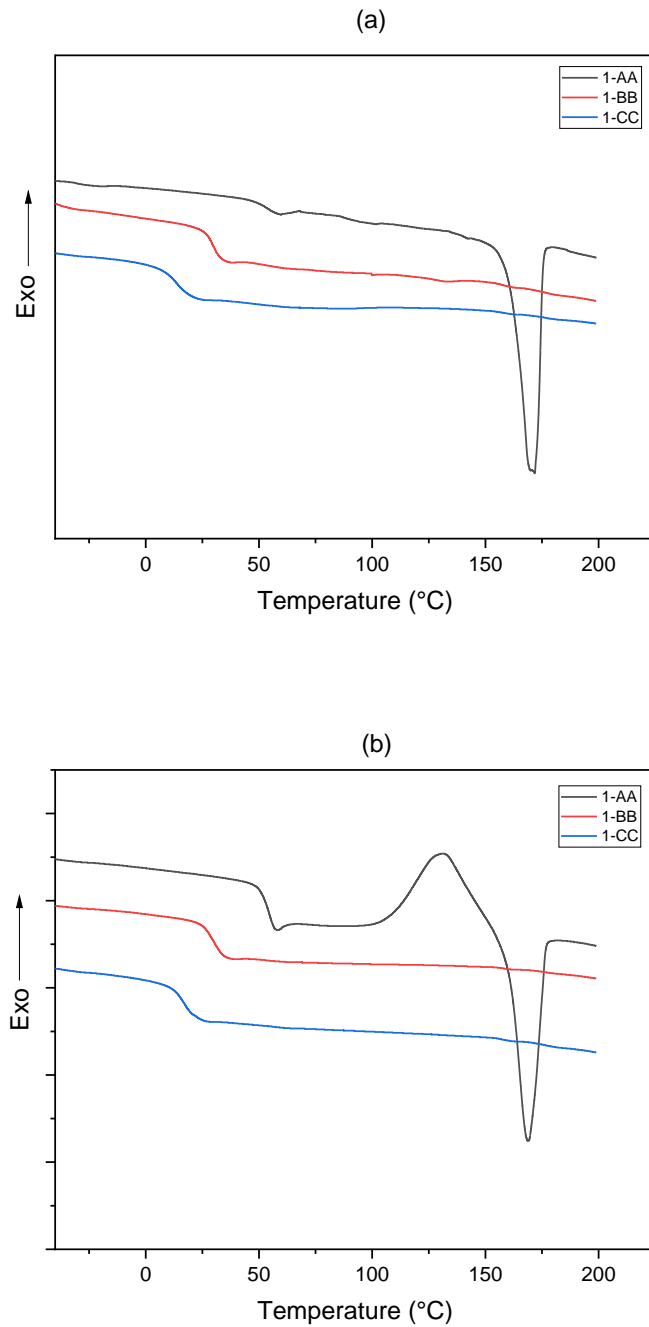


Figure 88: DSC curves at (a) first and (b) second scan of the matrices of CFRC. ( $10\text{ }^{\circ}\text{C}\cdot\text{min}^{-1}$ , under  $\text{N}_2$ )

Compared to the PLLA/GF, the matrices of PLLA/CF have similar thermal comportment. The matrix of PLLA/GF showed  $T_g$  around  $52\text{ }^{\circ}\text{C}$ ,  $T_m$  of  $169\text{ }^{\circ}\text{C}$  and crystallinity varying between 48 and 57 %. The 20 PLCL/CF matrices also have similar thermal properties than the matrices of 20 PLCL/GF composites, which disposes  $T_g$  of  $29\text{ }^{\circ}\text{C}$ ,  $T_m$  of  $133\text{ }^{\circ}\text{C}$  and crystallinity of 3%. The matrix of 30 PLCL/CF showed the same value of  $T_g$  obtained for the matrix of 30 PLCL/GF composite, with no melting.

Table 30: Thermal properties of carbon fabric reinforced composites.

<b>Sample</b>	<b>Matrix</b>	<b><math>T_g</math> (°C)</b>	<b><math>T_m</math> (°C)</b>	<b><math>\Delta H_f</math> (J.g<sup>-1</sup>)</b>	<b><math>X</math> (%)</b>
1-AA	PLLA	54	173	43.0	46.2
2-AA		53	171	39.0	45.0
3-AA		53	171	44.9	48.3
1-BB	20 PLCL	33	131	0.4	0.6
2-BB		29	133	0.1	0.1
3-BB		32	135	0.8	1.1
1-CC	30 PLCL	16	-	-	-
2-CC		17	-	-	-
3-CC		16	-	-	-

## 4.2 Characterization of voids on carbon fabric reinforced composites

To evaluate the impregnation of the fabrics by the matrix and the presence of voids, the composite plates were analyzed by digital microscopy. Both carbon fabric (CF) and glass fabric (GF) reinforced composites were produced using ten plies. This choice was made to facilitate a direct comparison between the impregnation quality and mechanical properties of the composites. The CF has a thickness of 0.25 mm, whereas the GF has a thickness of 0.30 mm. Consequently, a larger number of plies of CF would have been required to adequately fill the mold cavity. Nevertheless, all the carbon fabric reinforced composites were manufactured using ten plies for the sake of comparison with glass fabric composites. All carbon fabric reinforced composites present a 800  $\mu\text{m}$  thick layer of matrix (Figure 89), corresponding to the space which could be filled with more layers of carbon fabric.

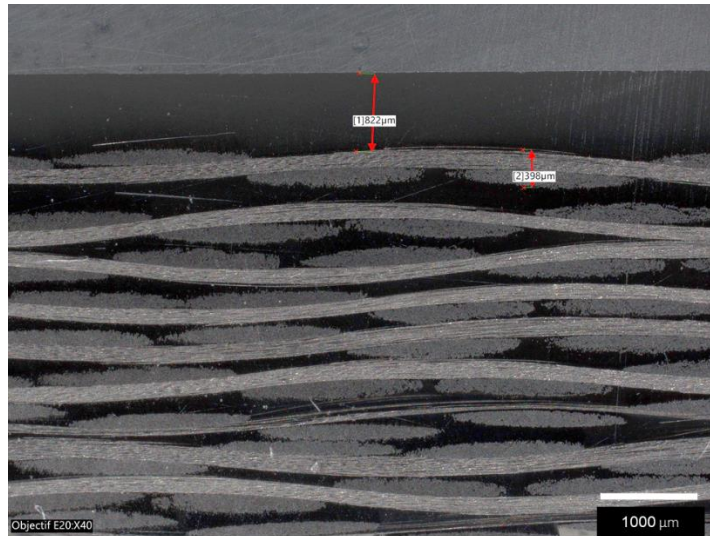


Figure 89: Digital micrograph of 20 PLLA/CF composite plate showing the layer of matrix on the reinforcement.

All the composites dispose of fiber mass ratio of 29% and fiber volume ratio of 22%. The fiber mass ratio (FMR) is directly associated with the lightweight nature of the composite. While glass fabric reinforced composites typically exhibit an FMR of around 46%, carbon fabric reinforced composites (CFRC) demonstrate an FMR of 29%, resulting in a significant weight reduction (Figure 90). In terms of the fiber volume ratio (FVR), GFRC registers values of approximately 29% while CFRC records 22%.

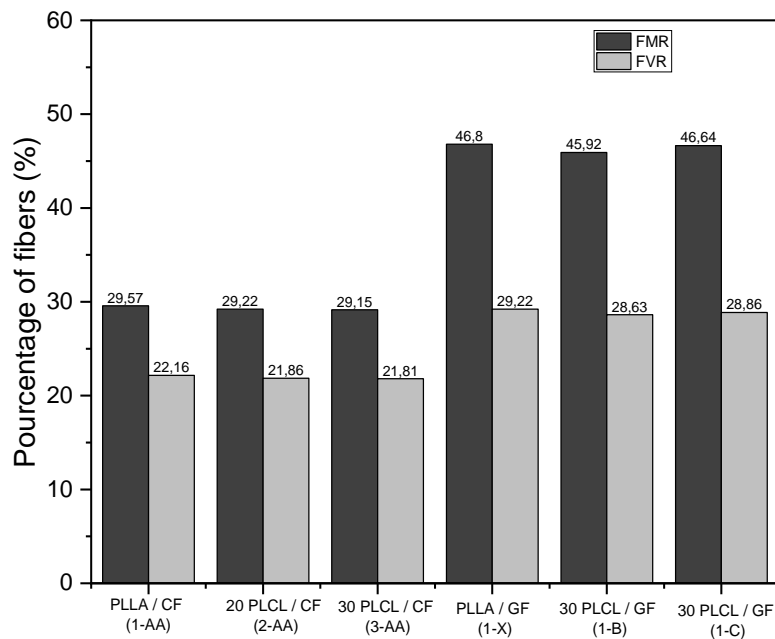


Figure 90: Comparison of fiber mass ratio and fiber volume ratio of GFRC and CFRC.

Due to the carbon fabric black nature, the identification of voids in carbon reinforced composites using digital microscope is more challenging than in glass-reinforced composites. Nevertheless, no voids were discernible at any scale on the digital micrographs, what can be attributed to the architecture of the fabric. Actually, compared to glass fabric, carbon fabric exhibits a more uniform structure with narrower gaps between the bundles (Figure 91). Furthermore, carbon fabric has greater rigidity than glass fabric, enabling easier manual restoration of bundle distortions during the molding process. As a result, the resin flow could experience fewer variations in velocity, which likely facilitated the impregnation of the carbon fabric by the matrix.

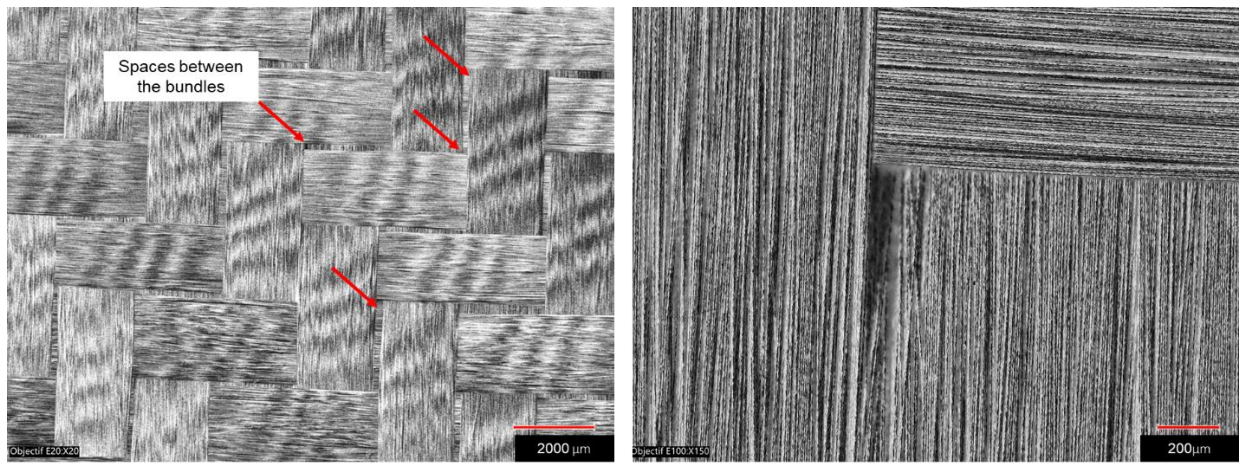


Figure 91: Digital micrograph of carbon fabric showing the spaces between the fiber tows.

The good impregnation of both longitudinal and transverse carbon fibers by the PLCL matrix, characterized by the complete absence of voids among the layers, fiber tows, and bundles is observed (Figure 5).

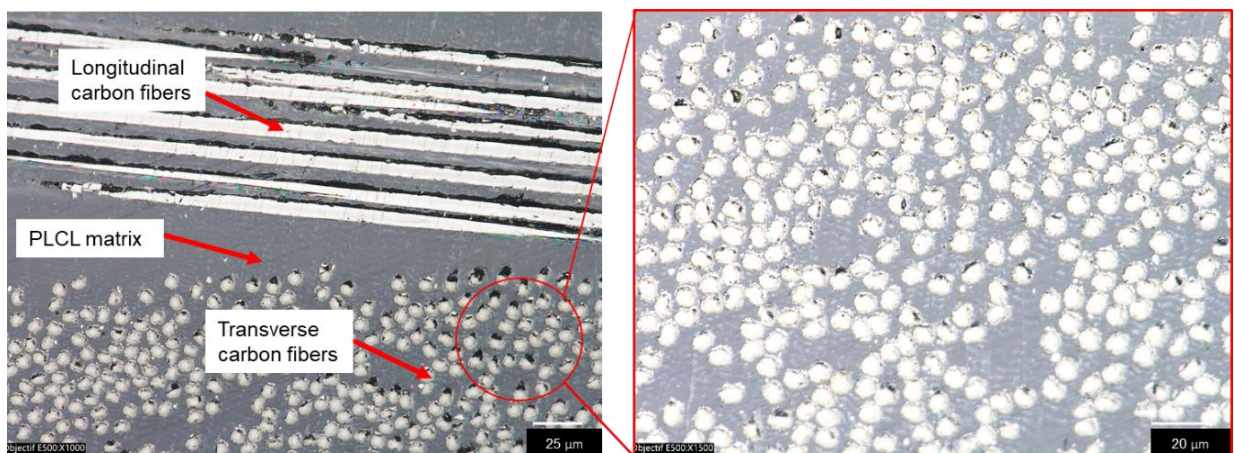


Figure 92: Digital micrographs showing the impregnation of the fibers on 20 PLCL/GF composite.

### 4.3 Three-point bending test of CFRC

Three-point bending test was chosen to evaluate the mechanical properties of CFRC. One plate of each composition (PLLA, 20 PLCL and 30 PLCL) was selected and five specimens of each composition were tested in three-point bending test.

The values of bending modulus ( $E_B$ ), bending strength ( $\sigma_B$ ), and bending strain represent the average results obtained from five specimens of each composite plate (Table 31). The mechanical behavior of the composites is dependent on the matrix nature. The PLLA/CF composite shows a brittle nature with low strain capability. In contrast, the 20 PLCL/CF composite begins to exhibit a ductile behavior, albeit with limited strain. Interestingly, the 30 PLCL/CF composite displays pronounced ductile behavior with a higher strain capacity (Figure 93).

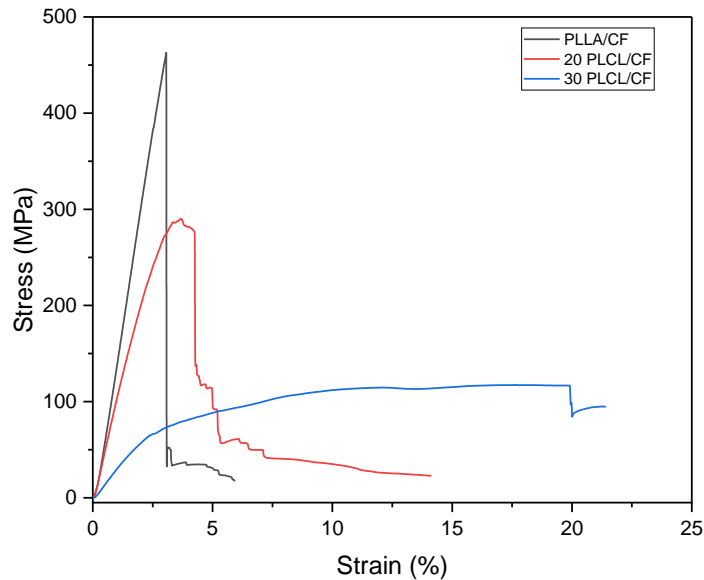


Figure 93: Strain x stress curve in three-point bending test of carbon fabric reinforced composites.

The PLLA/CF composite showed a bending modulus of 14.7 GPa, bending strength of 430 MPa and bending strain of 3.36 %. In a recent study published in 2023, researchers reported a bending modulus of 31.3 GPa and a bending strength of 502.1 MPa for carbon fabric reinforced PLLA composites produced by VARTM.<sup>215</sup> Although direct comparison with the PLLA/CF composite in this thesis is not possible due to the different fiber mass ratios (48.1% in the publication and 29.6% in the present work), there are some similarities in their bending properties that can be asserted. The higher values of bending properties measured in the study compared to those found in this thesis is linked to the higher fiber mass ratio in their

composites. Regarding the other composites, the 20 PLCL/CF displays  $E_B$  of 10.1 GPa,  $\sigma_B$  of 267 MPa and the 30 PLCL/CF one showed a  $E_B$  of 3.1 GPa,  $\sigma_B$  of 109 MPa.

Compared to the glass fabric reinforced PLLA composite (PLLA/GF), an increase of 42 % and 57 % in  $E_B$  and  $\sigma_B$  respectively was observed in the PLLA/CF composite (Figure 94). This increase was expected since the carbon fabric display a Young modulus 225 % higher than the glass one.<sup>57,49</sup> The values of bending strain measured for the PLLA/CF were also expected, since the carbon fabric display elongation at break 55 % lower than the glass fabric.<sup>57</sup> In terms of the fiber mass ratio, it is evident that the PLLA/CF composites are lighter than their glass fabric reinforced counterparts. The former exhibits a fiber mass ratio of 29%, while the latter has a ratio of 45%.

Table 31: Bending properties of carbon fabric reinforced composites.

Sample	Composite	Bending modulus (GPa)	Bending strength (MPa)	Bending strain (%)	FMR (%)	FVR (%)	$T_g$ (°C)	$\chi$ (%)
1-AA	PLLA/CF	14.7 ± 0.74	430 ± 24	3.36 ± 0.19	29.6	22.1	54	46.2
2-BB	20 PLCL/CF	10.1 ± 0.53	267 ± 14	3.56 ± 0.15	29.2	21.9	32	1.0
3-CC	30 PLCL/CF	3.1 ± 0.08	109 ± 3	19.9 ± 0.77	29.1	21.8	16	0.0

For the 20 PLCL/CF composite an increase of 198 % in  $E_B$  and 140 % in  $\sigma_B$  were measured, compared to the glass fabric reinforced PLCL composite (20 PLCL/GF) (Figure 94). The bending strain of 20 PLCL/CF decreases of about 84 % compared to the 20 PLCL/GF. Again, this result was expected since the elongation at break of carbon fabric are lower than the glass ones.

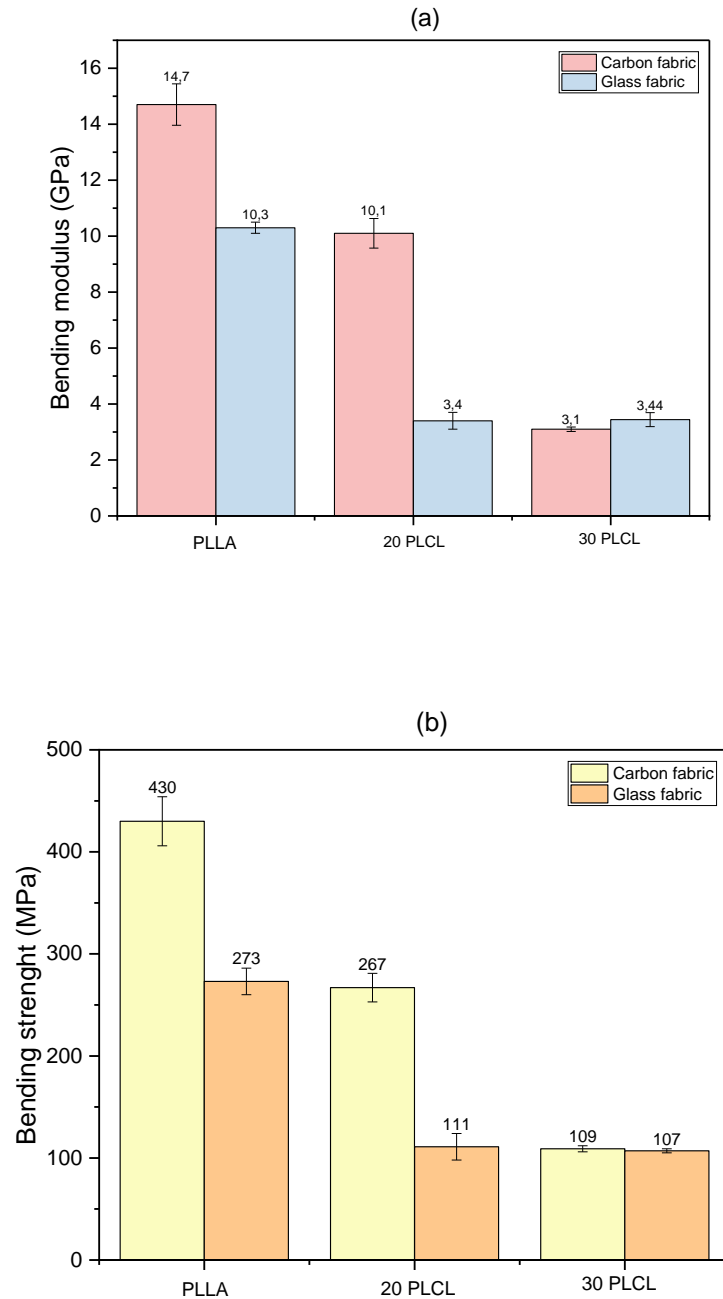


Figure 94: Comparison of (a) bending modulus and (b) bending strength of carbon and glass fabric reinforced composites.

The 30 PLCL/CF composites showed similar bending properties to the 30 PLCL/GF (Figure 94). In this case, the similarity in bending properties can be attributed to the glass transition temperature. Both composites dispose similar  $T_g$  of 17 °C. Once the composites display  $T_g$  below the room temperature, they have a rubbery behavior during the bending test.



The similarity on bending properties of carbon and glass fabric reinforced PLCL composites can be explained by the load transfer. The load applied to the composite during mechanical tests are first absorbed by the matrix and then is transferred to the reinforcement.

In the case of 30 PLCL/CF and 30 PLCL/GF during bending test, the fact that the matrix shows a rubbery behavior allows a high deformation of the specimen and the load are not or barely transferred to the reinforcements. One evidence of this phenomena is the bending strain, as both samples (30 PLCL/CF and 30 PLCL/GF) showed a value around 20%.

Some differences between the two composites could be established. In Figure 95, the strain – stress curve for the 30 PLCL/CF and 30 PLCL/GF composites have a similar shape, with an elastic domain until 2% of deformation and a plastic domain until the break. In the first composite, an elongation at break of 20% was observed, leading to specimen failure. On the other hand, the second composite showed an elongation at break of 17% but did not experience specimen failure. The bending test for the second composite was halted due to the deflection of the specimen, as it was no longer supported by the base.

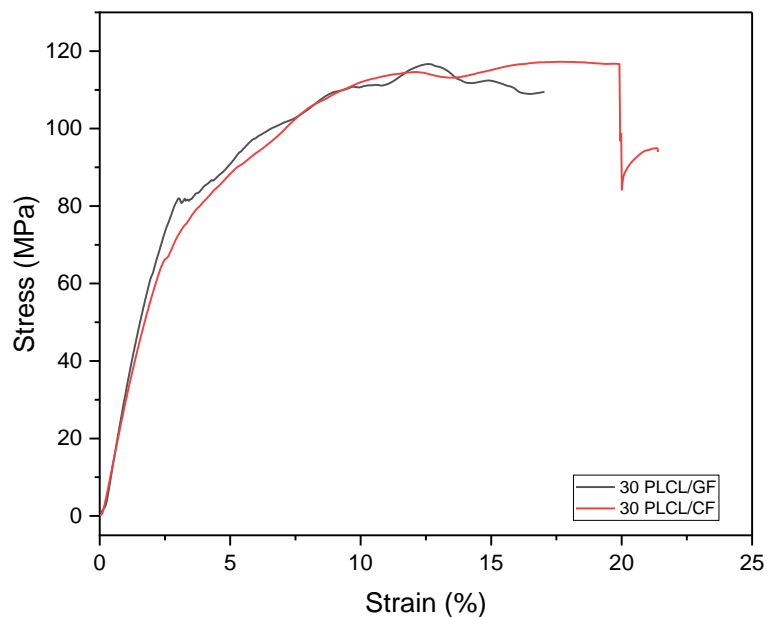


Figure 95: Strain x stress curve in three-point bending test for 30 PLCL/GF and 30 PLCL/CF composites.

After bending test, the specimens were analyzed by digital microscopy to identify the type of failure and also the morphology of the fracture. All specimens of carbon reinforced composites showed a V-shape after the test.

Regarding the composite PLLA/CF, a tensile fracture was identified in the specimen, with interlaminar matrix cracks and translaminar cracks (Figure 96). The micrograph of the bottom of the specimen reveals a distinct tensile fracture within the outermost layer, spanning the entire width of the specimen.

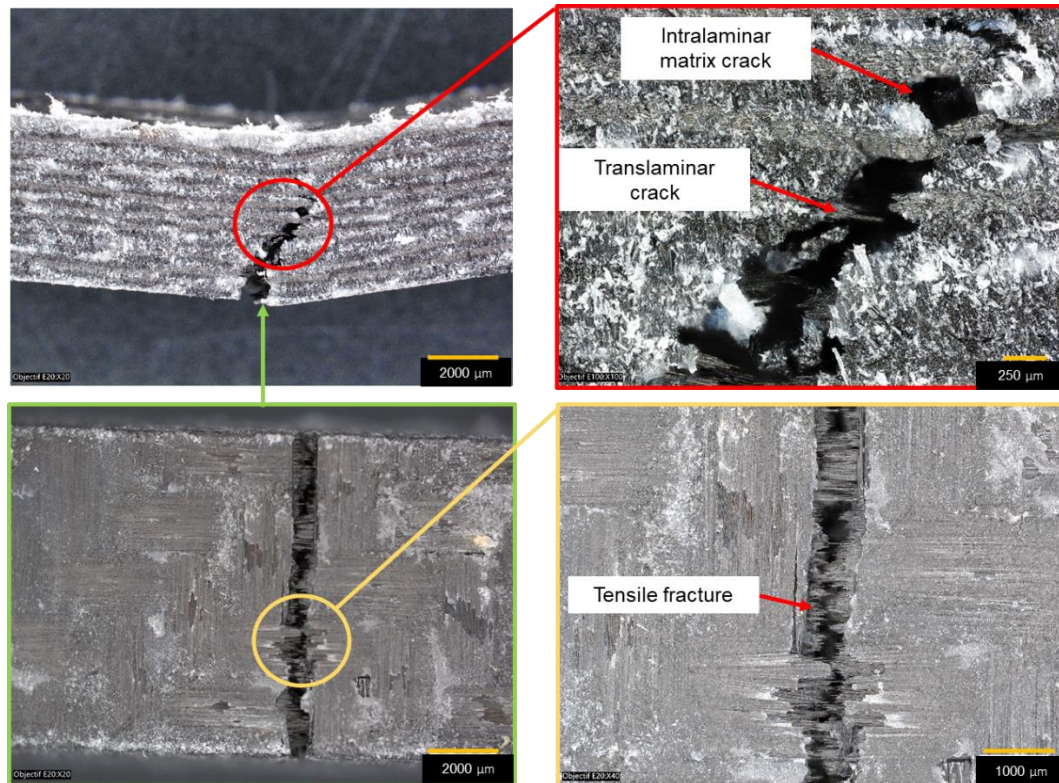


Figure 96: Digital micrographs showing the different types of failure observed in the PLLA/CF specimen.

The composite 20 PLCL/CF, also showed a failure by tensile fracture, with intralaminar matrix crack and translaminar crack (Figure 97). However, the extent of failure observed in this composite was smaller in magnitude compared to the failure observed in the PLLA/CF composite.

In the case of the PLLA/CF composite, the failure propagated diagonally from the bottom to the seventh outermost layer, while in the 20 PLCL/CF composite, the failure ceased in the middle of the specimen.

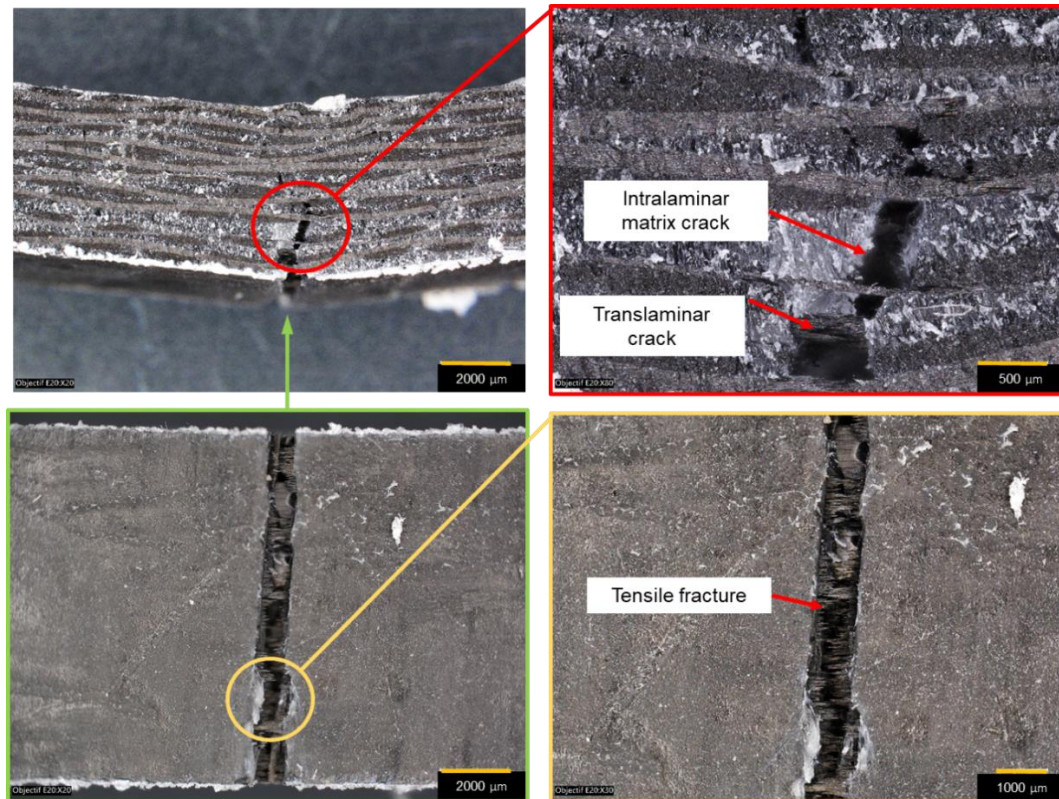


Figure 97: Digital micrographs showing the different types of failure observed in the 20 PLCL/CF specimen.

The same tendency of failure is observed for the 30 PLCL/CF composite. This sample also shows a tensile fracture with the same cracks mentioned previously (Figure 98). However, the magnitude of the tensile fracture is the smallest of the three composites, stopping at the third layer of carbon fabric.

The disparity in the magnitudes of failure can be attributed to the mechanical behavior of the matrix. As previously observed, PLLA demonstrates a brittle fracture, whereas PLCL exhibits a ductile fracture. Consequently, the 30 PLCL/CF composite, which contains the highest amount of  $\epsilon$ -CL, also demonstrates the highest bending strain. This implies that the specimen undergoes more deformation compared to the others, resulting in a smaller extent of failure. The magnitude of the tensile fracture in 30 PLCL/CF specimen is clearly smaller than in the other composites (Figure 98).

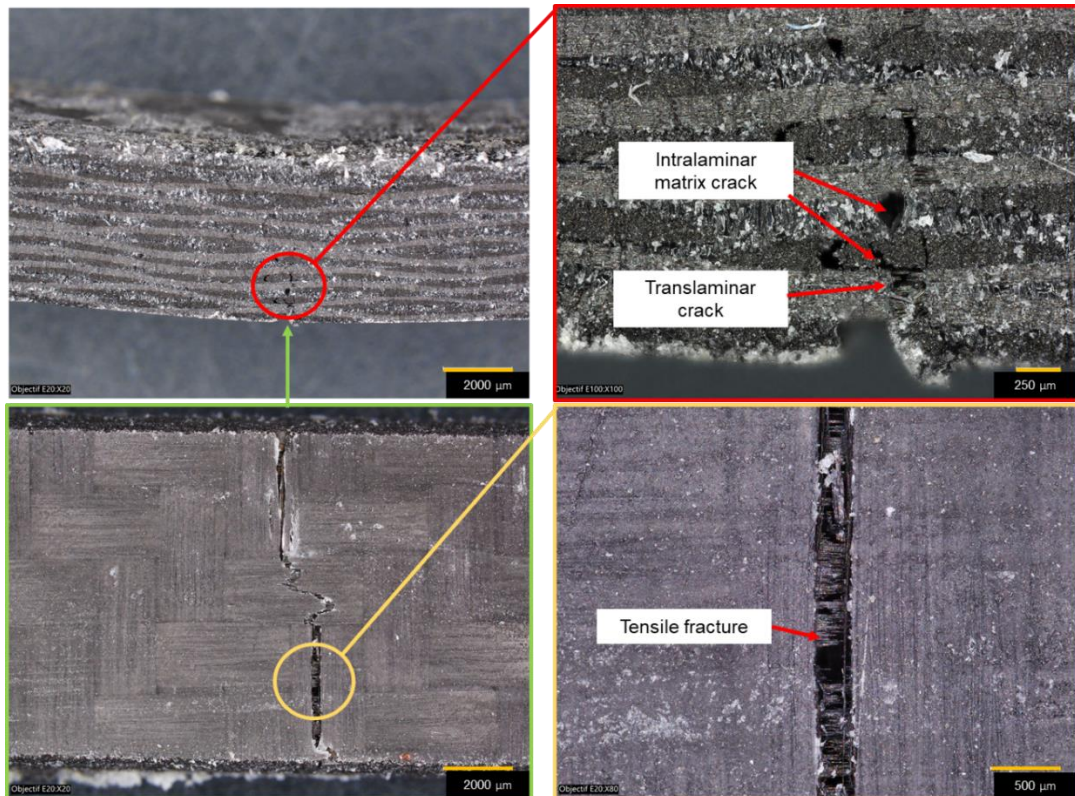


Figure 98: Digital micrographs showing the different types of failure observed in the 20 PLCL/GF specimen.

The carbon fabric reinforced composites showed different types of failures than the glass reinforced ones. For example, the PLLA/GF showed a multiple failure with tensile fracture, compressive fracture, translaminar crack and fiber pullout, while PLLA/CF showed a tensile fracture with intralaminar matrix crack and translaminar crack. The 20 and 30 PLCL/CF showed only a compressive damage while 20 and 30 PLCL/GF showed the same types of failure of PLLA/GF, in slower magnitudes. The different types of failure are attributed to the different natures of the fabric. The carbon fabric has a strain at break lower than the glass fabric, 1.8 and 4.0 % respectively.

Typically, the fiber and matrix in a composite material exhibit varying levels of strain at fracture. When the component with the lower strain at break fails, the load previously supported by that component is transferred to the other one. If the component with a higher strain at fracture can handle the extra load, the composite will undergo multiple fractures of the brittle component.

## 4.4 Conclusion

This chapter presents the production and characterization of carbon fabric reinforced PLLA and PLCL composites produced by TP-RTM. In addition to PLLA carbon fabric composites, carbon fabric reinforced poly(L-lactide-co- $\epsilon$ -caprolactone) composites with conversions exceeding 95 and 93 % for L-LA and  $\epsilon$ -CL respectively were obtained. Matrices with molecular weights of 142,500 - 158,700 g.mol<sup>-1</sup> for PLLA and 117,500 - 132,700 g.mol<sup>-1</sup> for PLCL were produced,  $M_w$  being identified as a critical parameter regarding the resulting mechanical properties of the composites. High molecular weights generally result in improved mechanical properties, such as increased strength and stiffness.

The presence of voids within the composites was investigated and characterized, as voids can significantly impact the mechanical properties and overall performance. Through visual observation and by digital microscopy, no voids could be identified. The evaluation of mechanical properties through the three-point bending test provides valuable insights into the flexural behavior, strength, load-bearing capacity, deformation characteristics, and failure modes of these composites. Comparisons between carbon fabric reinforced composites and the glass reinforced ones further enhance understanding of the unique properties and characteristics of the former. PLLA/CF and 20 PLCL/CF showed higher values of bending modulus and bending strength than its homonymous glass reinforced composites. However, the 30 PLCL/CF composite demonstrated similar behavior in the bending test as the 30 PLCL/GF composite, attributed to the glass transition temperature of the matrix being below room temperature (16°C).

In summary, the successful production of carbon fabric reinforced composites using TP-RTM marks a significant milestone, particularly as it represents the first-ever utilization of the manufacturing process for creating PLCL/CF composites. The utilization of various customized matrices allowed for the creation of composites with distinct thermal and mechanical properties, thereby opening up possibilities for diverse applications in the future.

## **CHAPTER V: Biocomposites and accelerated ageing**

This chapter is divided in two parts. The first one provides an overview of the production and characterization of biocomposites, specifically PLLA/flax composites, and their characterization in terms of molecular weight, thermal, and mechanical properties. The thermal stability of flax fibers was also studied in order to evaluate their applicability in TP-RTM conditions. In the second part, the impact of accelerated ageing on the composites developed in this study i.e. glass fabric reinforced composites (GFRC), carbon fabric reinforced composites (CFRC), and flax fabric reinforced composites (FFRC) was investigated. The study focused on the effects of temperature and UV-A irradiation on their thermal properties and molecular weight. Furthermore, the aged composites underwent three-point bending tests, and a correlation between the measured mechanical properties and the evolution of their crystallinity during ageing was established. The fractured specimens were also studied by digital microscopy analysis to determine the type of failure that occurred.



## 5.1 Flax fabric reinforced PLLA composites

In order to produce fully biodegradable composites, PLLA reinforced with flax fabric were produced by TP-RTM. The choice of flax as natural fiber was based on the literature, as it is until now the most used natural fiber to reinforce PLLA.<sup>61,118,216</sup> The availability of flax fibers was a major consideration in its selection, especially given that Europe is the leading global producer of these fibers. France, in particular, contributed significantly to the global production, reaching around 125,000 tonnes in 2022, with the main production hubs situated in Normandy, Hauts-de-France, and Ile-de-France regions.<sup>217</sup>

Many manufacturing processes were used to produce PLLA/flax composites such as injection molding, compression molding and extrusion, but until today, no PLLA/flax composite produced by TP-RTM are reported in literature.

Unlike the synthetic fabrics involved in Chapter III and IV, *i.e.* glass and carbon fabrics, flax fibers exhibit poor adhesion to the matrix and is hydrophilic.<sup>61</sup> Throughout history, various chemical treatments (*i.e.* acid treatment or coating) and physical treatments (*i.e.* plasma) have been employed to enhance the interfacial adhesion between flax fibers and the matrix.<sup>218,219</sup> However, in the current study, untreated flax fabric were used. This decision was made to initially explore the behavior of L-LA polymerization with untreated fibers and gain a preliminary understanding of PLLA/flax composites.

### 5.1.1 Production of flax fabric reinforced composites

The flax fibers used in this study were previously dried during 24h at 80 °C, to eliminate its moisture, which could negatively affect the mechanical properties.<sup>220</sup> The TP-RTM parameters used for the production of FFRC were fixed at a monomer over catalyst molar ratio of 2000, a polymerization temperature of 185 °C and a polymerization time of 2h, based on previous study done with PLLA/glass fabric.<sup>200</sup> Regarding the reinforcements, ten layers of unidirectional flax fabric (UD) were used, while only 5 layers of twill 2/2 flax fabric (TW) were necessary to fill completely the mold cavity. The resulting composite plates display a brown color, characteristic from flax reinforced composites (Figure 99).

In this chapter, the flax fabric reinforced composites (FFRC) will be abbreviated in PLLA/UD for the composite reinforced with unidirectional flax fabric and PLLA/TW for the composite reinforced with woven twill 2/2 flax fabric.



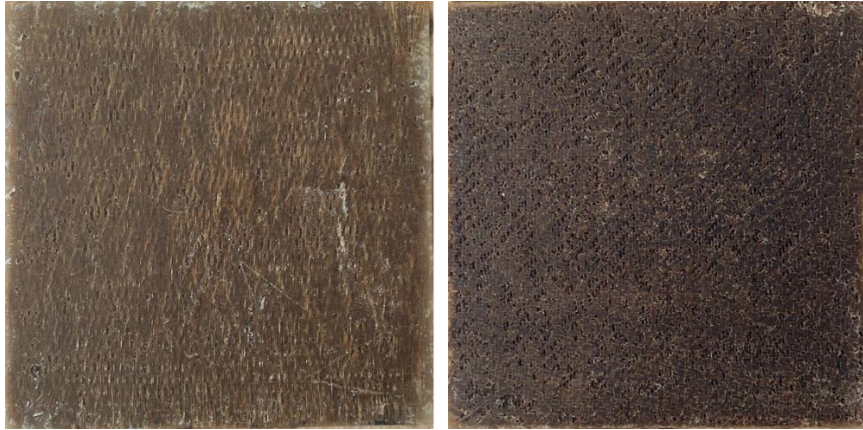


Figure 99: PLLA/UD (left) and PLLA/TW (right) composite plates.

### 5.1.2 Thermal stability of flax fabric

Prior to their use, the thermal stability of flax fibers was analyzed by TGA. The comprehension of the thermal degradation of flax fibers was crucial to develop composites by TP-RTM. The flax fabric should not degrade at the polymerization temperature of 185 °C.

Regarding the thermograms the first weight loss is observed at 100 °C for both flax fabrics, corresponding to the release of water (Figure 100). The second weight loss starts around 200°C for TW and UD flax. As evident from literature, this second weight loss is attributed to hemicellulose degradation.<sup>221,222</sup> The maximum DTG is observed at 357 °C for both flax fibers, which corresponds to cellulose degradation.<sup>223</sup> At 800 °C, a residual mass of 18% for TW flax and 10 % for UD flax. These residual mass is corroborating with the findings on literature, which can correspond to the residue left from hemicellulose and lignin.<sup>218,223</sup>

In general, hemicellulose exhibits decomposition at a lower temperature range, typically between 220 to 315 °C, whereas cellulose decomposes at a slightly higher range, around 300 to 400 °C. On the other hand, lignin undergoes decomposition over a much wider temperature span, ranging from 150 to 900 °C.<sup>224,225</sup> The degradation of the components of flax fibers initiates above the selected polymerization temperature, thereby ensuring the thermal stability of the fabrics throughout the polymerization process.

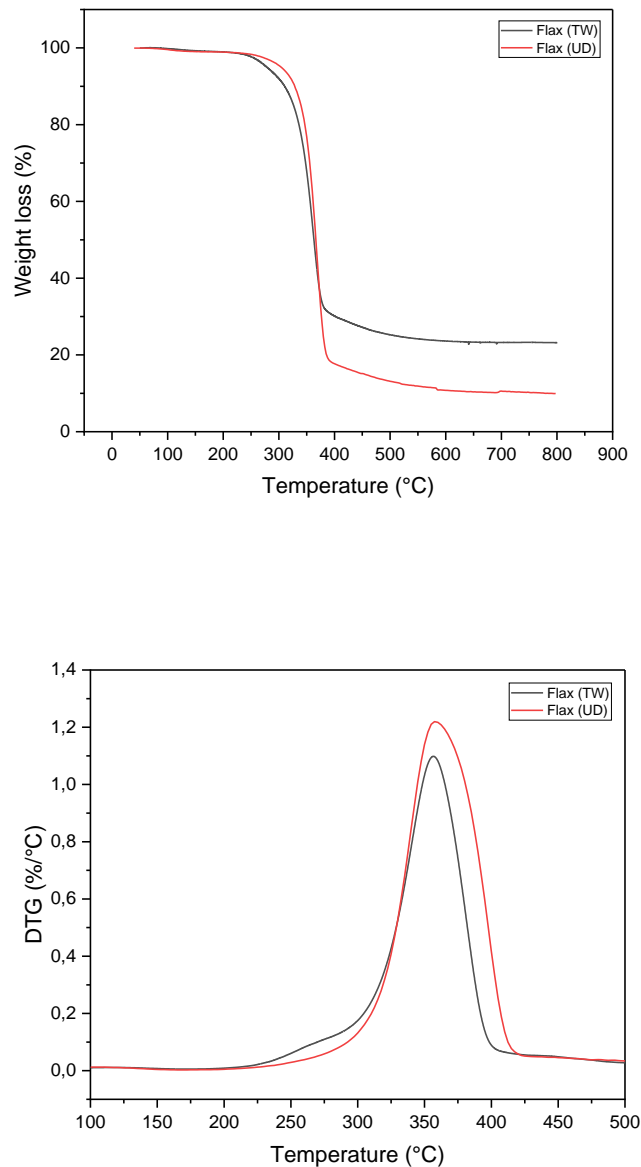


Figure 100: TG and DTG curves of flax fabrics.

### 5.1.3 Conversion and molecular weight

The conversion of L-LA is the main challenge to undertake regarding the polymerization of L-LA in the presence of flax fabrics. Indeed, the hydroxyl groups ( $-\text{OH}$ ) present in cellulose and hemicellulose could react with the catalyst preventing the polymerization, or react with the growing chain and conduct side transfer reactions which lower the  $M_n$  of the resulting PLLA matrix. However, conversions of L-LA higher than 94 % were obtained for all FFRC (Table 1). The  $^1\text{H}$  NMR spectra is presented in Appendix 6.10 (p. 224). These values are consistent with previous works conducted with glass and carbon fibers (p.86 and 127).

The L-LA conversions achieved with flax fibers in TP-RTM suggest that flax fibers do not adversely affect the polymerization of L-LA, as the conversions are comparable to those observed with inert fibers such as glass and carbon.

Table 32: Conversion of L-LA and molecular weight of PLLA matrices.

Sample	Reinforcement	L-LA <sup>a</sup> (%)	$M_n^b$ (g.mol <sup>-1</sup> )	$M_w^b$ (g.mol <sup>-1</sup> )	$\bar{D}$
1-UD	Unidirectional flax fabric (UD)	94	88,100	143,300	1.62
2-UD		94	87,200	143,300	1.62
1-TW	Twill 2/2 flax fabric (TW)	96	63,300	115,300	1.82
2-TW		96	61,600	115,500	1.87
3-TW		96	73,900	128,800	1.74
4-TW		96	81,300	131,900	1.62

Experimental conditions: monomer over catalyst ratio: 2000; polymerization temperature: 185 °C; polymerization time: 2h. <sup>a</sup> Determined by <sup>1</sup>H NMR in CDCl<sub>3</sub>. <sup>b</sup> Determined by SEC in CHCl<sub>3</sub>. The correction factor of 0.68 was applied to  $M_n$  and  $M_w$ .<sup>226</sup>

The  $M_w$  of PLLA matrices ranging from 115,300 to 143,300 g.mol<sup>-1</sup> were measured by SEC analysis and are consistent with previous  $M_w$  values measured for the PLLA matrices of PLLA/GF and PLLA / CF composites. Additionally, the measured values of  $M_w$  for the PLLA used as the matrix in flax-reinforced composites are close to that of commercially available PLLA (4032D- NatureWorks) of 137,300 g.mol<sup>-1</sup> (Section 2.3.2 p. 67).

Both analyses, <sup>1</sup>H NMR and SEC, let it to conclude that the presence of flax fibers does not prevent the ring opening polymerization of L-LA in TP-RTM experimental conditions. These results represent a step forward in the production of PLLA/flax composites.

#### 5.1.4 Thermal properties of PLLA matrices

The thermal behavior of PLLA matrices was determined by TGA. The PLLA matrices employed in both flax fabrics demonstrated comparable thermal degradation behavior, with  $T_{5\%}$  values of 235 °C and 236 °C for PLLA/UD and PLLA/TW, respectively. As for  $T_{95\%}$ , the PLLA matrices exhibited values of 317 °C and 319 °C for PLLA/UD and PLLA/TW, respectively (Figure 101– a). Finally, the maximum DTG for both matrices is around 294 °C (Figure 101– b).

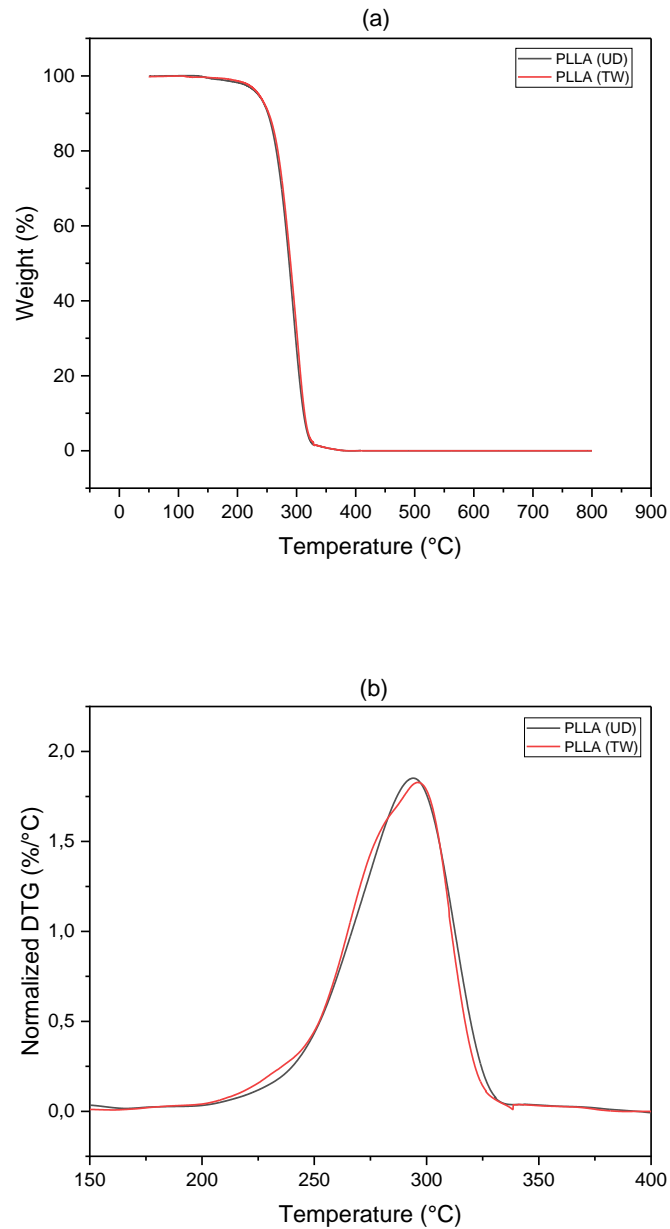


Figure 101: (a) TGA and (b) DTG of PLLA matrices.

Regarding the DSC analysis, the PLLA matrices showed melting temperatures ranging from 169 to 173 °C, glass transition temperatures around 53-54°C and crystallinity from 49 to 55 % (Table 33). All these values are consistent with the data obtained for PLLA/GF and PLLA/CF composites.

Table 33: Thermal properties of flax reinforced PLLA composites.

Sample	Reinforcement	$T_g$ (°C)	$T_m$ (°C)	$\Delta H$ (J.g <sup>-1</sup> )	X (%)
1-UD	Unidirectional flax fabric (UD)	54	169	45.5	49
2-UD		54	173	46.4	50
1-TW	Twill 2/2 flax fabric (TW)	53	173	45.8	49
2-TW		53	172	50.9	55
3-TW		53	173	49.0	53
4-TW		53	170	50.7	54

### 5.1.5 Characterization of voids on flax reinforced PLLA composites

In contrast to synthetic fibers such as glass and carbon, flax fibers possess an irregular and non-uniform structure, which can result in irregularities and voids within the composite material. The inherent irregularities in flax fibers can cause disruptions in the resin flow during the injection process, leading to the formation of voids and unfilled areas. The presence of voids and the impregnation of the PLLA matrix through the flax fibers were analyzed by digital microscopy.

In digital micrographs of cross sections PLLA/UD composites, the presence of meso-voids is present between the longitudinal flax fibers. These meso-voids are mainly present between the flax yarns with sizes between 500-2000  $\mu\text{m}$  (Figure 102).

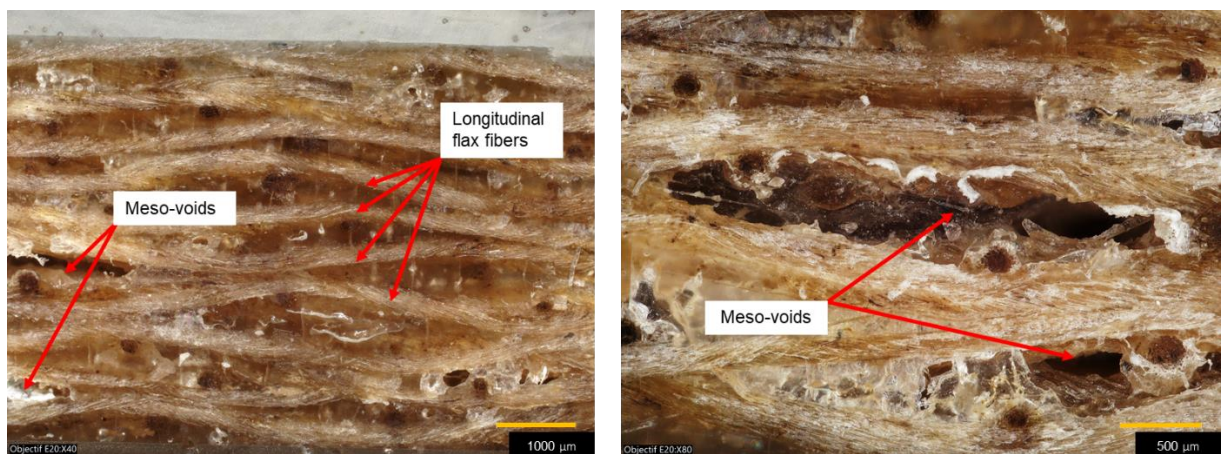


Figure 102: Digital micrographs of cross section of PLLA/UD composites.

Longitudinal cut was done in PLLA/UD plates to evaluate the impregnation of the PLLA matrix between the elementary flax fibers. In these micrographs, the morphology of the elementary fiber (lumen) is clearly distinct in flax bundles (Figure 103 – c – d). These individual fibers exhibit an irregular structure, and when they come together, they form bundles that also possess irregular shapes and arrangements. Even if these elementary fibers present an irregular structure, which could probably cause an irregular resin flow during injection, no voids were identified in this region.

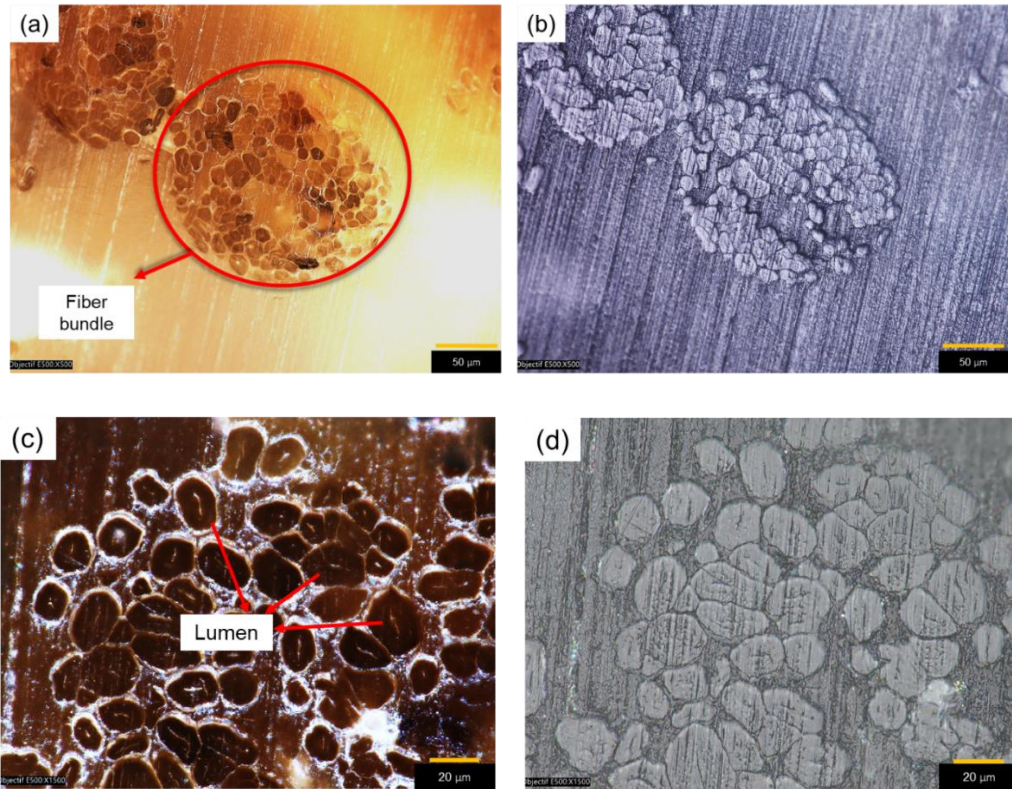


Figure 103: Digital micrographs in a longitudinal cut of PLLA/UD plate.

The meso-voids identified in cross section of PLLA/UD plates are also present in longitudinal cut, present between the fiber bundles (Figure 104).



Figure 104: Meso-voids present between flax fiber bundles in a longitudinal cut of PLLA/UD plates.

In PLLA/TW composites, meso-voids between the flax fiber bundles were also identified. Even if the meso-voids could not be quantified by digital microscopy, visually the number of voids was higher than in PLLA/UD composites.

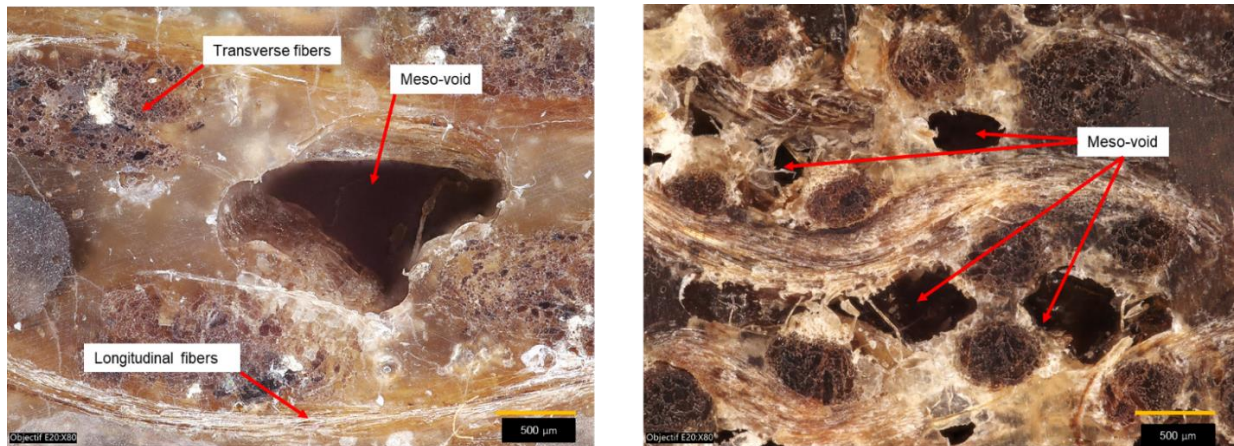


Figure 105: Digital micrographs of a cross section of PLLA/TW composites.

### 5.1.6 Mechanical properties of flax fabric reinforced composites

The mechanical properties of PLLA/flax composites were evaluated by three-point bending test. Five specimens were tested to failure, and the values presented correspond to the average of the five specimens (Table 34, Appendix 6.17).

As mentioned earlier, ten layers of unidirectional flax fabric were used and five layers of twill 2/2 flax fabric were used, given composites with different fiber mass and volume ratios. The PLLA/UD composites dispose fiber mass ratio (FMR) of 26 % and fiber volume ratio (FVR) of 25 %, while PLLA/TW show FMR of 31 % and FVR of 30 %. These disparities in FMR and FVR are due to the different numbers of layers used but also due to differences regarding the impregnation of the matrix. As observed previously, the impregnation of the matrix in PLLA/UD composites was more effective compared to PLLA/TW ones, primarily due to the difference in fiber architecture. Consequently, a larger amount of PLLA matrix was injected, resulting in a decrease in both the FMR and FVR.

To the PLLA/UD showed bending modulus ( $E_B$ ) of 9.30 GPa, bending strength ( $\sigma_B$ ) of 177 MPa and a strain at break of 2.86 % (Table 34). As up to date no PLLA/flax composites produced by TP-RTM were reported, the values obtained in bending test will be compared to values reported in the literature for PLLA/flax composites produced with other manufacturing process.

Table 34: Bending properties, glass transition temperature and crystallinity of FFRC.

Sample	Composite	Bending modulus (GPa)	Bending strength (MPa)	Bending strain (%)	FMR (%)	FVR (%)	T <sub>g</sub> (°C)	X (%)
1-UD	PLLA/UD	9.30 ± 0.26	177 ± 4	2.86 ± 0.05	26	25	54	49
1-TW	PLLA/TW	3.66 ± 0.18	50 ± 4	2.90 ± 0.71	31	30	53	49

PLA/unidirectional flax composites were made by compression molding using a flax preform and PLA fibers. The authors reported a  $E_B$  of 18 GPa and  $\sigma_B$  of 215 MPa, for composites with 49.5 % of fiber mass ratio.<sup>227</sup> In another study, in which PLA/unidirectional flax composites with 22 % of fiber mass ratio manufactured by film stacking, values of  $E_B$  of 13.8 GPa and  $\sigma_B$  of 160 MPa were reported.<sup>219</sup> In both studies, the authors acknowledged the presence of voids and the detrimental effects they had on the bending properties. Considering the differences in the manufacturing processes and fiber volume ratios, the bending modulus and bending strength values obtained for PLLA/unidirectional flax composites in this thesis are of a similar magnitude to those reported in the literature.

Regarding the failure of PLLA/UD composite tested on three-point bending test, all specimens showed a tensile fracture with interlaminar shear (Figure 106 – a – c). Translaminar cracks and intralaminar matrix cracks are observed closer to the tensile fracture (Figure 106 – b).



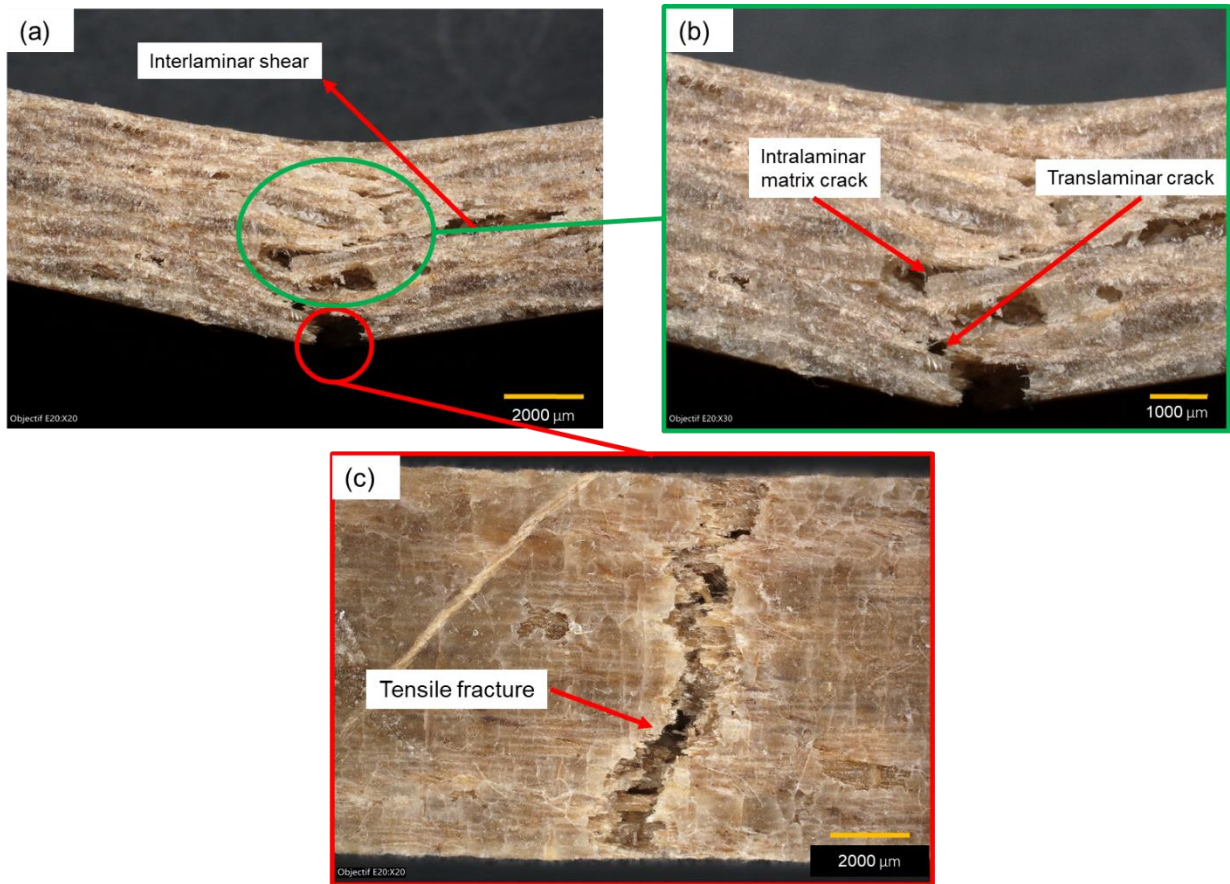


Figure 106: Digital micrographs of failure observed in the PLLA/UD specimen.

The PLLA/TW composite showed bending modulus ( $E_B$ ) of 3.66 GPa, bending strength ( $\sigma_B$ ) of 50 MPa and a strain at break of 2.9 % (Table 34). Compared to the PLLA/UD the bending properties of PLLA/TW composite are quite lower. A decrease of almost 40 and 30 % was observed in bending modulus and bending strength respectively. Assuming that the matrices in both PLLA/UD and PLLA/TW composites display identical thermal properties (same  $T_m$  and  $T_g$ ) and crystallinity of 49 %, which can influence their bending properties, any discrepancies in the values of  $E_B$  and  $\sigma_B$  are directly attributed to differences in fiber architecture and matrix impregnation.

A few studies about PLA reinforced with woven flax fabric are reported. Non-woven fabrics, especially unidirectional flax are more often associated with PLA. PLA reinforced with woven flax fibers (FMR of 33 %) were produced by film stacking process and a bending modulus of 3.9 GPa and a bending strength of 90 MPa was reported.<sup>228</sup> Another study reported values of 14 GPa and 135 MPa for bending modulus and bending strength respectively, for PLA / woven flax composites (FMR of 50 wt %) produced by compression of commingled fibers.<sup>229</sup>

As discussed previously, the impregnation of woven twill 2/2 flax fabric was less effective than in PLLA/UD composites. The presence of numerous voids in PLLA/TW composites justifies the lowest values of  $E_B$  and  $\sigma_B$  measured. The major failure identified in PLLA/TW composites after three-point bending test was the delamination (Figure 107). This failure could be induced by the presence of numerous voids localized between the flax fabrics, but also by the roughness of flax fibers present in the twill 2/2 fabric. Compared to the UD flax fibers, the TW flax fibers disposes a higher roughness, inducing the formation of voids since the wettability was less effective.

Another problem observed in PLLA/TW composites was the impregnation at the surface of the plate. The high level of roughness of these fibers provoke a less effective impregnation by the matrix since the resin flow is not homogeneous. In that way, some unfilled areas appeared and the external layer of matrix supposed to protect the flax fabric are not uniform (Figure 107 – c).

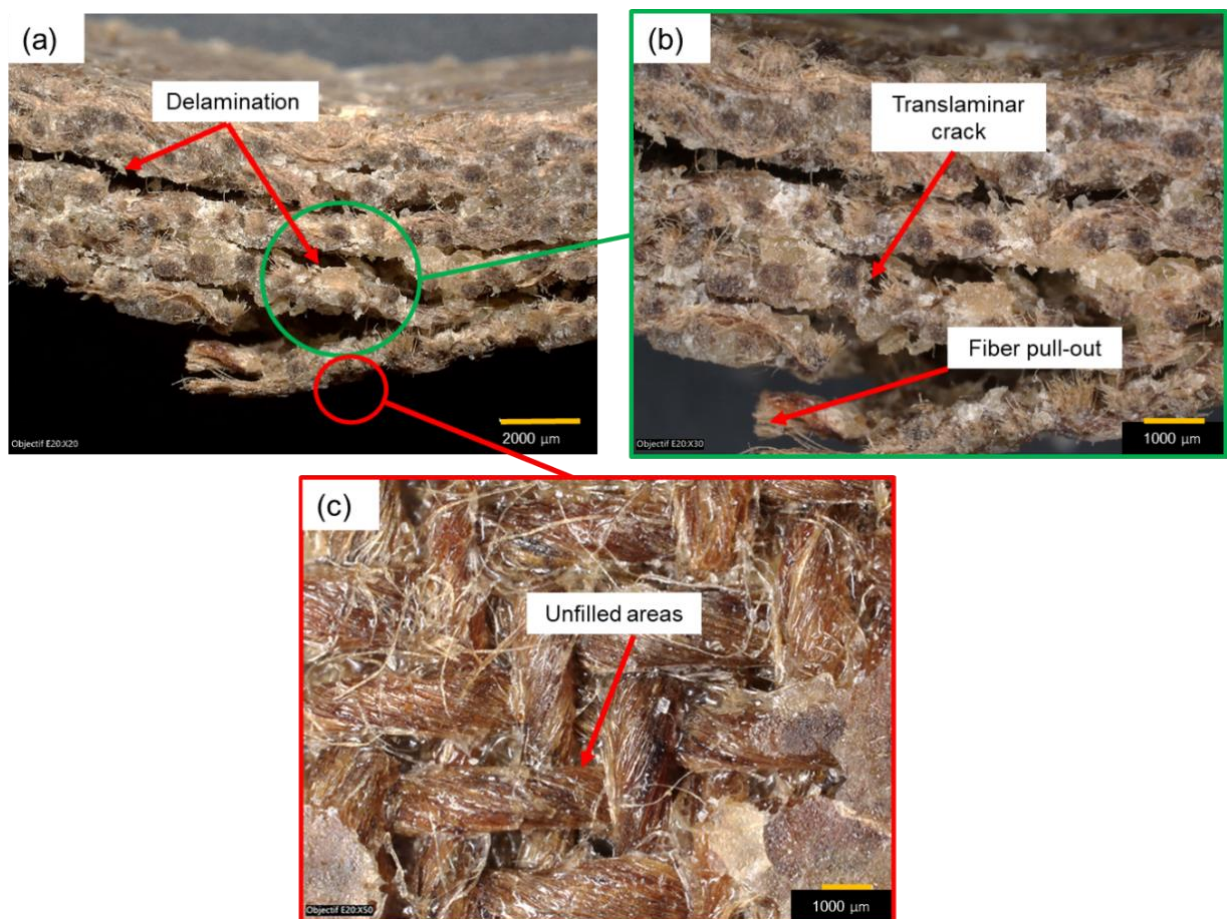


Figure 107: Digital micrographs of failure observed in the PLLA/UD specimen.

### 5.1.7 Conclusion

The production of PLLA/flax composites by TP-RTM was successfully achieved. The thermal stability of flax fibers was first investigated, and it can be concluded that these fibers can withstand temperatures up to 185 °C, which is the experimental temperature set up of TP-RTM.

Furthermore, the presence of flax fabric did not impact the polymerization reaction as so as the L-LA conversion, reaching up to 94%, is comparable to those obtained for GFRC and CFRC. Moreover, a relatively high  $M_w$  exceeding 115,000 g·mol<sup>-1</sup> was obtained, which is closer to the commercial PLLA standard (4032D – NatureWorks) with a value of 137,300 g·mol<sup>-1</sup>. In that frame, the PLLA matrix display similar  $T_g$  and  $T_m$  values as those observed in GFRC and CFRC, where the fibers are known to be inert.

However, when it comes to matrix impregnation, PLLA/TW composites exhibited less effective impregnation compared to PLLA/UD composites. This has a negative impact on the bending properties of the former, with a bending strength value 254% lower than that of PLLA/UD composite. The values of bending modulus and strength obtained for PLLA/UD composites produced by TP-RTM are higher than those produced by other manufacturing techniques, *i.e* compression molding and film stacking.

## 5.2 Ageing of composites

The durability of the composite material is a major factor to be considered during its design and before its manufacturing. In actual context, increasing the lifespan of composites is almost mandatory, in order to reduce the waste of materials and so promoting a greener and more sustainable future. To evaluate the long-term performance, durability, and compliance with standards, the accelerated ageing method was employed to assess the ageing of composites. It is important to note that the accelerated ageing tests conducted in this study represent a preliminary study on the aging of these materials, as the composites were aged for a relatively short period of one month.

The accelerated ageing of composites was done in an accelerated weathering tester chamber (QUV Q-Lab) according to the ISO 4892-3 standard. The composites were aged during 30 days at 50 °C exposed to UVA radiation (UVA-351 lamp-340 nm). Glass fabric reinforced composites (GFRC), carbon fabric reinforced composites (CFRC) and flax fabric reinforced composites (FFRC) were submitted to accelerated ageing and their thermal properties were evaluated by DSC after 15 and 30 days. The molecular weight and bending properties were evaluated after 30 days of ageing (Table 35). The specimens submitted to bending test were also analyzed by optical microscopy to assess the type of failure involved.

Table 35: Characterization of composite plates made after accelerated ageing test.

<b>Composite type</b>	<b>Composite composition</b>	<b>Sample</b>	<b>Polymerization temperature (°C)</b>	<b>Thermal properties</b>	<b>Molecular weight</b>	<b>Bending properties</b>
<i>Glass fabric reinforced composites (GFRC)</i>	PLLA/GF	G-1	185	Analyzed by DSC after 15 and 30 days of ageing	Analyzed by SEC after 30 days of ageing	Analyzed by three-point bending test after 30 days of ageing
	20 PLCL/GF	G-2	170			
	30 PLCL/GF	G-3	160			
<i>Carbon fabric reinforced composites (CFRC)</i>	PLLA / CF	C-1	185			
	20 PLCL/GF	C-2	170			
	30 PLCL/GF	C-3	160			
<i>Flax fabric reinforced composites (FFRC)</i>	PLLA/UD	F-1	185			
	PLLA/TW	F-2				

The effect of UV irradiation on the degradation of poly(L-lactide) and poly( $\epsilon$ -caprolactone) have been studied over the years.<sup>230,231,232,233,234</sup> Depending on the wavelength of UV irradiation, two photo-degradation mechanisms of PLLA are proposed in the literature: Norrish II mechanism for an UV light irradiation under 300 nm (UV-B), and radical mechanism for an irradiation under UV light between 300-400 nm (UV-A). The degradation of PCL under UV-B is always referred to occur by Norrish II mechanism.<sup>232</sup> To date, no studies about the mechanism of photodegradation of poly( $\epsilon$ -caprolactone) and poly(L-lactide-co- $\epsilon$ -caprolactone) irradiated by UV-A light were reported. In this study, the accelerated ageing was done with a UV light settled at 340 nm (UVA-A) and so the radical mechanism of photodegradation of PLLA seems to be the most probable.<sup>234</sup>

The photodegradation of PLLA by radical mechanism involves a classical hydrogen abstraction from the tertiary carbon in the  $\alpha$ -position of the ester function along the polymeric backbone, leading to the formation of macro radicals (Figure 108).<sup>235</sup> It is postulated that the initiation of the photochemical reaction is triggered by the presence of chromophoric defects in the polymer, occurring at very low concentrations. These macro radicals then react with oxygen, forming peroxy radicals, which, in turn, yield hydroperoxide by abstracting a labile hydrogen atom, thus propagating the chain reaction oxidation.

Once the hydroperoxide is formed, it can undergo decomposition, resulting in the generation of alkoxy and hydroxyl radicals. Among these radicals, the macro radical alkoxy assumes a critical role as the central intermediate in the reaction and can decompose through  $\beta$ -scission. This  $\beta$ -scission process can manifest in three distinct pathways, contingent upon the structure of the alkoxy radical. Of the three  $\beta$ -scissions, two result in chain scissions (1 and 3), which have been observed through SEC analysis. However, only reaction (1) generates anhydrides. As a result, this particular reaction is considered as the major mechanism involved during the photooxidation of PLA when exposed to wavelengths above 300 nm.<sup>230,235</sup>

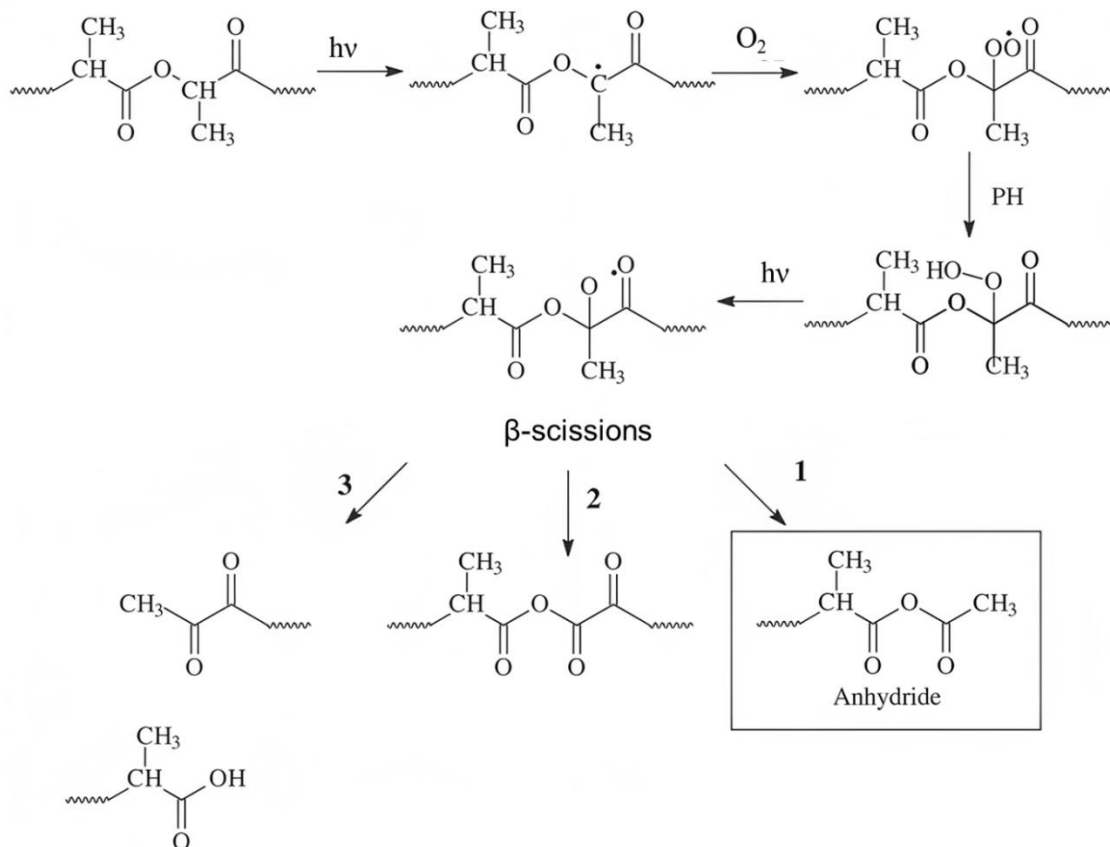


Figure 108: Main route of PLLA photooxidation.<sup>235</sup>

Independent of the photodegradation mechanism of PLLA or PLCL, the UV irradiation will promote the chain scissions in the polymer and consequently the molecular weight will drop and the dispersity increase. A quick and effective way to identify the chain scissions consists in evaluating the molecular weight by SEC analysis, which was performed in the matrices of all composites before and after ageing. This drop in the molecular weights will affect the thermal and mechanical properties of composites and it will be discussed next.

## 5.2.1 Investigating the impact of accelerated ageing test on thermal properties, molecular weight, and mechanical performance of composites

### 5.2.1.1 Glass fabric reinforced composites (GFRC)

The effects of UV irradiation and temperature on GFRC were initially assessed visually. Numerical photos depicting the GFRC specimens before and after ageing revealed that the yellow color of the unaged samples vanishes after 30 days of ageing, with the specimens adopting a whitish appearance (Figure 109). The bleaching of PLLA submitted to similar ageing conditions was reported in a previous study and it is attributed to UV irradiation.<sup>234</sup> However, the color changes of PLCL submitted to UV-A irradiation was not reported yet.



Figure 109: Unaged and aged (30 days, 50°C, UV-A 340 nm) GFRC specimens.

DSC analysis were performed on the matrices of GFRC and the thermograms are presented in Appendix 6.13 (p.232). The thermal properties of the GFRC matrix exhibit variations depending on its composition. In the case of PLLA/GF composites (sample G-1), the glass transition temperature ( $T_g$ ) increases with ageing time, reaching 59 °C after 30 days. The melting temperature ( $T_m$ ) remains nearly constant, showing a mere 1 °C increase compared to the unaged sample (Table 36).

Table 36: Thermal properties of GFRC after ageing.

Sample	Composite composition	Ageing time (days)	T <sub>g</sub> (°C)	T <sub>m</sub> (°C)
G-1	PLLA/GF	0	54	171
		15	58	172
		30	59	172
G-2	20 PLCL/GF	0	31	137
		15	33	141
		30	33	144
G-3	30 PLCL/GF	0	19	132
		15	24	140
		30	22	143

The T<sub>g</sub> and T<sub>m</sub> increases with the ageing time for the matrices of 20 PLCL/GF (sample G-2) and 30 PLCL/GF (sample G-3) composites (Table 36). An increase of 2 °C and 4 °C were reported for the T<sub>g</sub> of samples G-2 and G-3 respectively. Furthermore, the T<sub>m</sub> of sample G-2 increased by 7 °C, while sample G-3 exhibited a significant increase of 11 °C in T<sub>m</sub>.

After 30 days of ageing, the molecular weight of all composite matrices decreased drastically, and dispersity increased as expected (Table 37). This can be attributed to chain scissions of PLLA and PLCL caused by photooxidation, in which low molecular weight oligomers are formed.

Table 37: Evolution of molecular weight and dispersity of GFRC matrices after ageing.

Sample	Composite composition	Ageing time (days)	M <sub>n</sub> (g.mol <sup>-1</sup> )	M <sub>w</sub> (g.mol <sup>-1</sup> )	Đ
G-1 <sup>1</sup>	PLLA/GF	0	55,700	102,400	1.83
		30	18,400 (-67 %)	40,400 (-40 %)	2.19
G-2 <sup>2</sup>	20 PLCL/GF	0	79,900	124,900	1.56
		30	31,200 (-61 %)	68,900 (-55 %)	2.21
G-3 <sup>2</sup>	30 PLCL/GF	0	89,500	169,500	1.89
		30	18,000 (-80%)	43,400 (-26%)	2.40

<sup>1</sup> Determined by SEC in CHCl<sub>3</sub> RI detector M<sub>n</sub> and M<sub>w</sub> corrected by 0.68. <sup>2</sup> Determined by SEC in THF with RI detector; M<sub>n</sub> and M<sub>w</sub> corrected by 0.58 X [L-LA] + 0.56 x [ε-CL]

Regarding the thermal properties, the PLLA/GF sample (G-1) exhibited a 27% decrease in crystallinity after 30 days of ageing (Figure 110). Works found in the literature reported an increase of crystallinity of PLA submitted at similar conditions of ageing.<sup>234,236</sup> However, these studies were conducted on commercially available amorphous PLA without fibers. Currently, there are no reported studies on the accelerated aging of PLLA/GF composites, making it impossible to directly compare our findings with the existing literature. Nevertheless, considering that the crystallinity of PLLA was expected to increase after ageing but did not, it can be inferred that the glass fibers may have contributed to the decrease in crystallinity. It is worth noting that a slight increase in crystallinity of approximately 9% is observed after 30 days, compared to the 15-day period. It is possible that this crystallinity could further increase if the sample were subjected to an ageing time exceeding 30 days.

An increase of crystallinity about 334 % was found for the matrices of 20 PLCL/GF (G-2) and 30 PLCL/GF (G-3) (Figure 110). The crystalline region of 20 PLCL/GF and 30 PLCL/GF is attributed to L-LA-unit sequences as the  $\epsilon$ -CL-unit sequences are not able to crystallize. The ageing temperature of 50 °C is higher than the  $T_g$  of the composites matrices of 31 °C and 18 °C for G-2 and G-3 samples respectively. In that way, at 50 °C the mobility of crystallizable chains in the amorphous phase is enhanced.<sup>27,202</sup> This favorable mobility would favor the arrangement of L-LA-units into distinct crystalline regions, potentially forming novel crystalline structures and so increasing the crystallinity.<sup>27</sup>

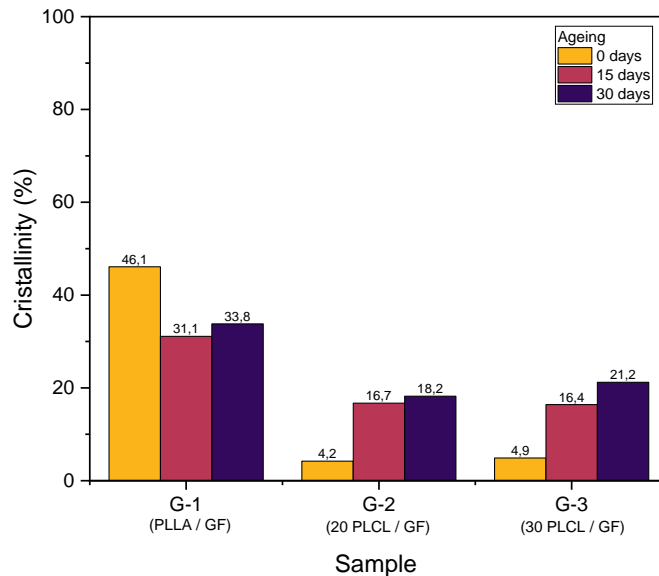


Figure 110: Evolution of crystallinity of GFRC matrices during ageing.



The bending properties of aged samples (G-1, G-2, G-3) were compared to the bending properties of unaged ones (2-X, 1-D, 2-E), already presented in Chapter III. All samples dispose of fiber mass ratio of 45 % and fiber volume ratio of 28 %. The strain x stress curves on bending test for aged GFRC are presented in Appendix 6.18 (p.249).

Minimal changes on bending modulus and bending strength were observed for unaged (sample 1-X) and aged (sample G-1) PLLA/GF composites. The  $E_B$  and  $\sigma_B$  of aged PLLA/GF composites decreased of 10 %, with a bending strain around 3 % (Table 38). The decrease of crystallinity justifies the decrease of bending properties in these composites.

Regarding composite 20 PLCL/GF, the aged sample (sample G-2) showed an increase of 100 % on  $E_B$  and an increase of 28 % on  $\sigma_B$  compared to the unaged one (sample 1-D), caused by the increase of crystallinity. Nonetheless, the bending strain dropped of 86 % (Table 38). This decrease on bending strain is quite predictable since the increase of crystallinity enhance the stiffness.

An increase of 32 % of  $E_B$  was reported for the aged 30 PLCL/GF composite (sample G-3) compared to the unaged one (sample 2-E) and the  $\sigma_B$  did not change if the standard deviation is considered.

This increase on bending modulus leads to an increase on stiffness and so the bending strain drops from 9 % to 3 % (Table 38). Again, this increase on bending modulus is attributed to the increase of crystallinity.

As shown previously (Table 37), the  $M_n$  and  $M_w$  values of all matrices decreased after 30 days of ageing. However, this decrease appears to have a minimal effect on the mechanical properties. In this specific scenario, the mechanical properties are notably influenced by the crystallinity. In the case of PLLA/GF composite, both the molecular weight and crystallinity decreased, impacting the bending properties. On the other hand, in the 20 PLCL/GF and 30 PLCL/GF composites, the molecular weight has decreased, but the crystallinity has increased, inducing an increase of the bending properties.

Table 38: Mechanical properties of unaged and aged GFRC.

Sample	Composite composition	State	FMR (%)	FVR (%)	$E_B$ (GPa)	$\sigma_B$ (MPa)	Strain (%)
1-X	PLLA/GF	Unaged	45.8	28.8	10.34 ± 0.20	273 ± 13	3.45 ± 0.10
G-1		Aged 30 days	44.4	27.6	9.29 ± 0.59 (-10 %)	246 ± 16 (-10 %)	3.25 ± 0.13 (-6 %)
1-D	20 PLCL/GF	Unaged	45.3	28.0	3.39 ± 0.30	111 ± 13	21.00 ± 1.00
G-2		Aged 30 days	45.6	28.3	6.81 ± 0.28 (+101 %)	142 ± 5 (+ 28 %)	2.88 ± 0.11 (-86 %)
2-E	30 PLCL/GF	Unaged	45.7	28,3	3.44 ± 0.25	107 ± 5	9.00 ± 1.00
G-3		Aged 30 days	45.4	28.5	4.53 ± 0.18 (+32 %)	95 ± 5 (-11 %)	3.28 ± 0.06 (-63 %)

The specimens were analyzed by optical microscopy after the bending test to identify the type of fracture. In the case of PLLA/GF composite (sample G-1), a tensile fracture with delamination and fiber pullout was observed (Figure 111 – a). For sample 20 PLCL/GF, failure occurred due to compression, and delamination was the major fracture observed (Figure 111 – b). Concerning the 30 PLCL/GF one, only compressive damage was observed (Figure 111 – c).

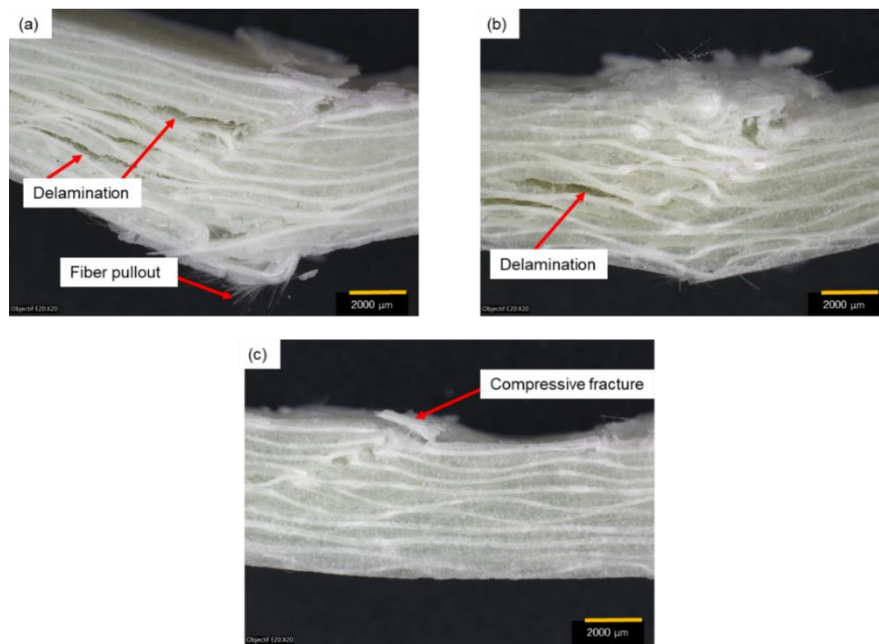


Figure 111: Optical micrographs of aged GFRC after bending test.

### 5.2.1.2 Carbon fabric reinforced composites

The same ageing protocol was applied to study the ageing of carbon-reinforced composites, *i.e.* 15 and 30 days, 50°C under UV-A at 340 nm. The initial effects of UV irradiation and temperature on CFRC were observed through visual inspection. Numerical photos revealed minor differences between the unaged and aged composites. Both PLLA and PLCL matrix composites retained their original black appearance after 30 days of ageing, with some whitish regions appearing on the surface of the specimens (Figure 114).

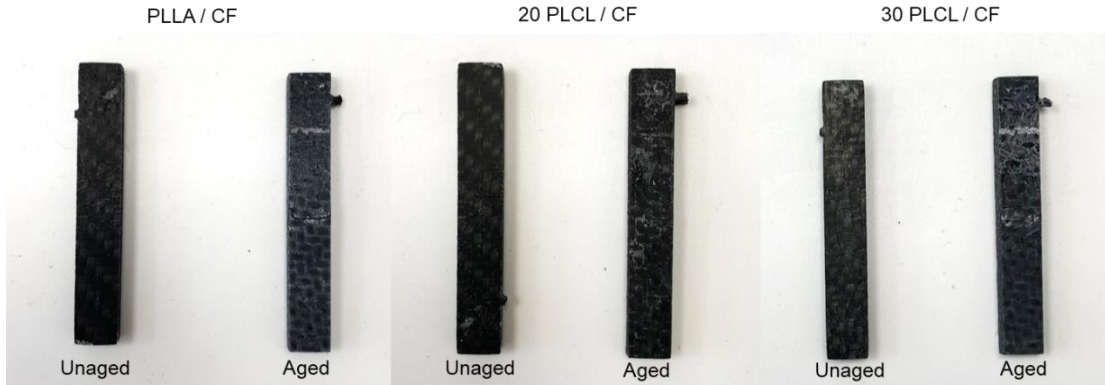


Figure 112: Unaged and aged CFRC (30 days, 50°C, UV-A at 340 nm).

In the case of carbon fabric reinforced composites, the evolution of thermal properties of the matrices are similar for all composites. The DSC thermograms are presented in Appendix 6.13 (p.232). The  $T_g$  of PLLA / CF matrix (sample C-1) increase slightly after 30 days of ageing, reaching 57 °C, an increase of 3 °C compared to the unaged sample, and a small increase in  $T_m$  of 1 °C is observed (Table 39). For the matrices of 20 PLCL/GF (sample C-2) and 30 PLCL/GF (sample C-3), an increase of 2 °C and 4 °C was reported for the  $T_g$  and the  $T_m$  of its composites increases 7 °C and 11 °C respectively (Table 39).

Table 39: Thermal properties of CFRC after ageing.

Sample	Composite composition	Ageing time (days)	$T_g$ (°C)	$T_m$ (°C)
C-1	PLLA / CF	0	54	171
		15	59	172
		30	57	172
C-2	20 PLCL/CF	0	31	137
		15	33	141
		30	33	144
C-3	30 PLCL/CF	0	19	132
		15	21	140
		30	23	143

The evolution of molecular weight of the CFRC matrices after ageing followed the same tendency as the GFRC matrices. A decrease of  $M_n$  and  $M_w$  and an increase of dispersity was observed for all CFRC matrices confirming the chain scissions during ageing (Table 39).

Table 40: Evolution of molecular weight and dispersity of CFRC matrices after ageing.

Sample	Composite composition	Ageing days	$M_n$ ( $g.mol^{-1}$ )	$M_w$ ( $g.mol^{-1}$ )	$\bar{D}$
G-1 <sup>1</sup>	PLLA/GF	0	114,000	158,800	1.39
		30	43,700 (-62 %)	95,300 (-40 %)	2.18
G-2 <sup>2</sup>	20 PLCL/GF	0	31,300	89,000	2.84
		30	25,600 (-18 %)	77,500 (-13 %)	3.02
G-3 <sup>2</sup>	30 PLCL/GF	0	24,400	67,700	2.76
		30	12,500 (-49 %)	43,000 (-36 %)	3.44

<sup>1</sup> Determined by SEC in  $CHCl_3$   $M_n$  and  $M_w$  corrected by 0.68. <sup>2</sup> Determined by SEC in THF;  $M_n$  and  $M_w$  corrected by  $0.58 \times [L-LA] + 0.56 \times [\epsilon-CL]$ .

Regarding the crystallinity, increases of 78 %, 27 % and 26 % were measured for PLLA / CF, 20 PLCL/GF and 30 PLCL/GF samples respectively (Figure 113). The increase of crystallinity of PLCL/CF matrix could be justified by the same arguments presented previously for the PLCL/GF one, with the formation of novel rich L-LA crystalline structures. However, an increase of crystallinity of PLLA/CF was reported, which not occurred in PLLA/GF composites. This could be explained by the colors of the composites. GFRC displays a whitish pale nature, while CRFC is entirely black. Glass fabric is naturally white, while carbon fabric appears black. White objects do not absorb UV light, as they primarily reflect most of the visible light that strikes them, rather than absorbing specific colors. UV light falls outside the range of visible light, so white objects reflect UV light along with the other colors in the visible spectrum. On the other hand, black objects, which represent the absence of visible light, can absorb most of the light that reaches them across the entire visible spectrum, including UV light. As a result, black objects convert the absorbed UV light into heat energy, leading to an increase in temperature.

In this way, it can be inferred that when CFRC plates are heated at a higher temperature than GFRC, even if both are kept at 50°C, the higher temperature in CFRC could facilitate the mobility of L-LA units through the amorphous phase. This, in turn, would explain the increase in crystallinity of the PLLA/CF compared to PLLA/GF.

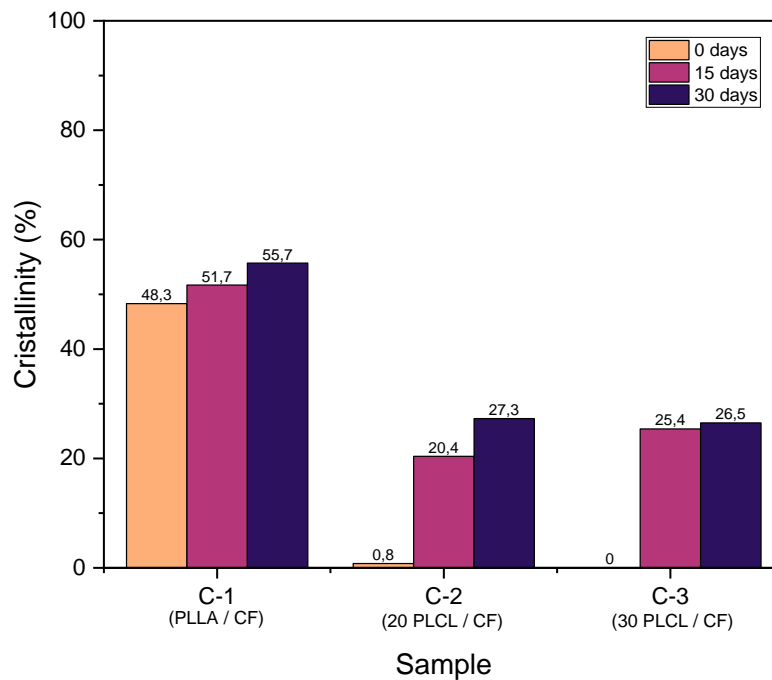


Figure 113: Evolution of crystallinity of CFRC matrices during ageing.

The bending properties of aged samples (C-1, C-2, C-3) were compared to the unaged ones (1-AA, 1-BB, 1-CC) already presented in Chapter IV. No remarkable changes in  $E_B$  and  $\sigma_B$  were observed for the aged PLLA / CF (C-1) (Table 41). The crystallinity of the latter increased slightly during ageing, from 48% to 56 % (Figure 113). This change in crystallinity was not enough to impact the bending properties.

In opposition, the aged 20 PLCL/GF (sample C-2) and aged 30 PLCL/GF (sample C-3) composites had their bending properties increased. Both samples showed an increase of crystallinity after ageing, reaching a value around 27 % for both samples. An increase of 40 % in  $E_B$  and 44 % in  $\sigma_B$  were reported for the sample C-2, with a decrease about 6 % in strain. Regarding the sample C-3, it  $E_B$  increased 77 % and the  $\sigma_B$  increased 38 %. This substantial increase in bending modulus resulted in a reduction in bending strain, decreasing from 20 % to 7 %.

Globally, the decrease of molecular weight in all samples (C-1, C-2, C-3) does not seem to negatively influence the mechanical properties of aged samples. Apparently, the decrease of molecular weight seems to be compensated by the increase of crystallinity and by the presence of carbon fabric.

Table 41: Mechanical properties of unaged and aged CFRC.

Sample	Composite composition	State	FMR (%)	FVR (%)	$E_B$ (GPa)	$\sigma_B$ (MPa)	Strain (%)
1-AA	PLLA/GF	Unaged	29.5	22.1	14.7 ± 0.74	430 ± 24	3.46 ± 0.19
C-1		Aged 30 days	29.1	21.6	13.5 ± 0.54 (-8 %)	416 ± 18 (- 3%)	3.54 ± 0.18 (+2 %)
1-BB	20 PLCL/GF	Unaged	29.2	21.8	10.1 ± 0.53	267 ± 14	3.56 ± 0.15
C-2		Aged 30 days	29.5	22.1	14.1 ± 0.36 (+ 40%)	384 ± 10 (+44 %)	3.34 ± 0.15 (-6 %)
1-CC	30 PLCL/GF	Unaged	29.1	21.8	3.1 ± 0.08	109 ± 3	19.9 ± 0.77
C-3		Aged 30 days	29.1	21.6	5.5 ± 0.33 (+77 %)	150 ± 10 (+38 %)	6.50 ± 0.40 (-67%)

All the aged CFRC specimens exhibited tensile fractures with varying magnitudes after the bending test. Specifically, PLLA / CF displayed a tensile fracture accompanied by intralaminar matrix cracks, translaminar cracks, and delamination (Figure 114 – a). In the case of 20 PLCL/GF sample, a tensile fracture was also observed, although no delamination was detected (Figure 114 – b). Lastly, 30 PLCL/GF sample exhibited a tensile fracture, with a small amount of intralaminar matrix crack, and a translaminar crack was observed at the bottom of the specimen (Figure 114 – c).

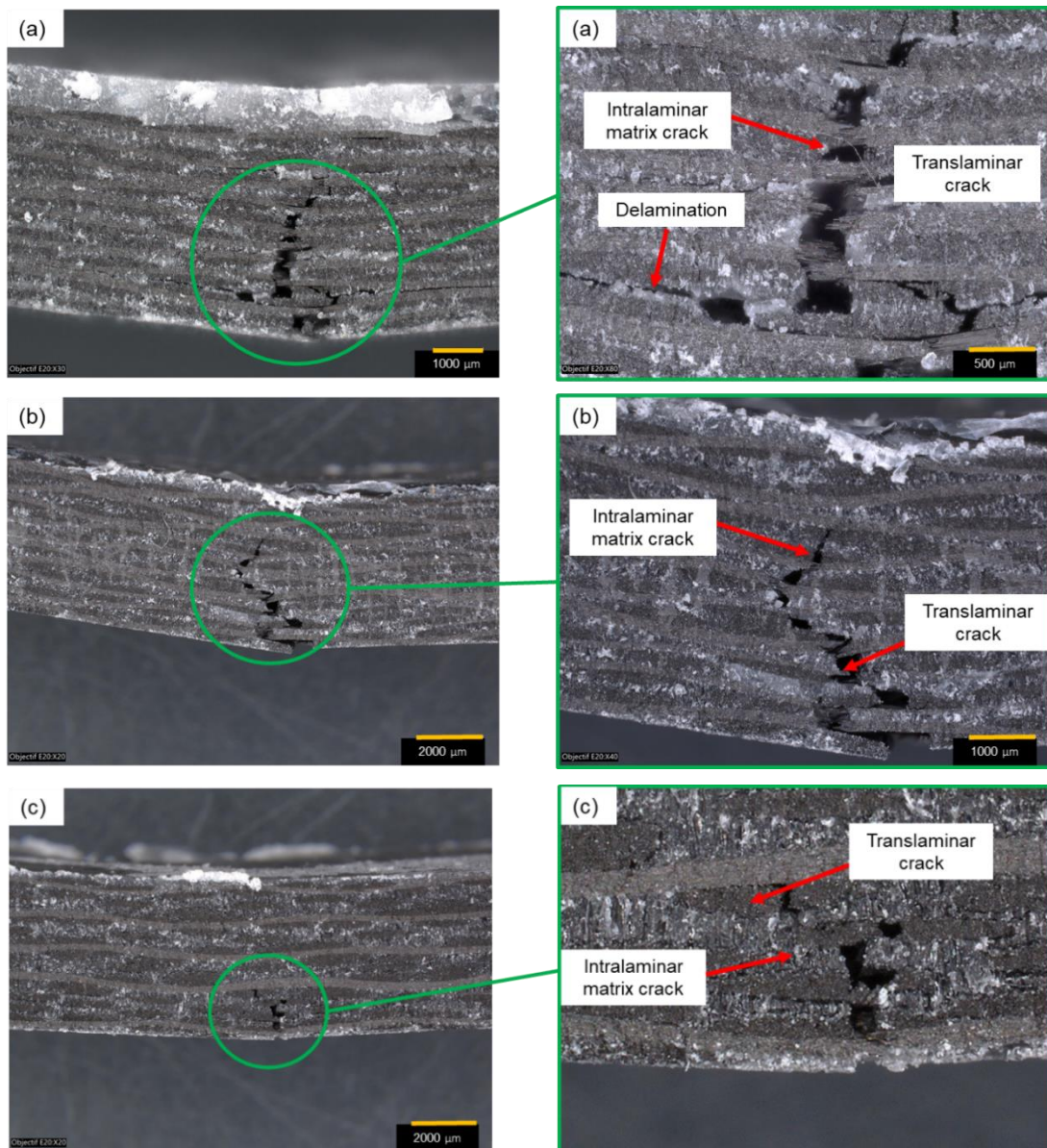


Figure 114: Optical micrographs of aged CFRC after bending test.

### 5.2.1.3 Flax fabric reinforced composites

Finally, the ageing of PLLA/flax composites was also studied, still in the same experimental conditions (15 or 30 days, 50°C and UV-A at 340 nm). After 30 days of ageing, numerical photos displayed a significant color change in the FFRC specimens. The initial characteristic brown color of FFRC turned to white (Figure 115). In the PLLA/TW specimen, the bleached surface evidenced the unfilled areas, that did not occurred in PLLA/UD composite.



Figure 115: Unaged and aged FFRC specimens.

The thermograms of aged PLLA/flax composites are presented in Appendix 6.13(p.232). The  $T_g$  of the PLLA/TW (sample F-1) matrix do not change drastically after 30 days, with a small decrease of 1 °C. However, the  $T_m$  is affected with a decrease from 170 °C to 160 °C (Table 42). Regarding the PLLA/UD matrix, its  $T_g$  increased from 3 °C and the  $T_m$  decreased from 173 °C to 168 °C (Table 42). The decrease of  $T_g$  and  $T_m$  of PLLA under UV irradiation are reported in the literature.<sup>233,234</sup>

These disparities in thermal properties between PLLA/UD and PLLA/TW matrix composites should not occur since the samples have the same matrix, PLLA, and the same reinforcement, flax fabric. The only difference in these composite plates is the fiber architecture, which could play different roles during the ageing.

Table 42: Evolution of thermal properties of FFRC during ageing.

Sample	Composite composition	Ageing time (days)	$T_g$ (°C)	$T_m$ (°C)
F-1	PLLA/TW	0	53	170
		15	51	163
		30	52	160
F-2	PLLA/UD	0	54	173
		15	56	167
		30	57	168



Due to the less effective impregnation of fibers in the PLLA/TW composite compared to the PLLA/UD composite, the presence of numerous voids increased the exposed area of the plate to UV irradiation. As a result, it can be inferred that the UV irradiation may cause more degradation to the matrix in PLLA/TW than in PLLA/UD. The extent of this degradation is supported by SEC analysis. After 30 days of ageing, the  $M_n$  of PLLA/TW decreased by 91%, while the  $M_n$  of PLLA/UD decreased by 78% (Table 43) and in both composites an increase on dispersity is observed.

Table 43: Evolution of molecular weight and dispersity of FFRC matrices before and after ageing.

Sample	Composite composition	Ageing days	$M_n$ ( $g.mol^{-1}$ )	$M_w$ ( $g.mol^{-1}$ )	$\bar{D}$
F-1	PLLA/TW	0	81,300	131,900	1.62
		30	7,600 (-91%)	22,200 (-83%)	2.91
F-2	PLLA/UD	0	87,200	143,300	1.64
		30	18,800 (-78%)	58,600 (-59%)	3.12

<sup>1</sup> Determined by SEC in  $CHCl_3$ .  $M_n$  and  $M_w$  corrected by 0.68. <sup>2</sup> Determined by SEC in THF;  $M_n$  and  $M_w$  corrected by  $0.58 \times [L-LA] + 0.56 \times [\epsilon-CL]$ .

The crystallinity of FFRC decreased during ageing. Previous studies suggest that the crystallinity of PLLA tends to increase when exposed to UV irradiation.<sup>234,237</sup> However, these studies take into account the ageing of pure PLLA and to date no studies about the ageing of PLLA/flax composites exposed to UV irradiation was conducted. After 30 days of ageing, the crystallinity of PLLA/TW matrix decreased from 57% to 25 % and those of PLLA/UD decreased from 50 % to 37% (Figure 116).

If comparing the crystallinity after 15 and 30 days of ageing, both composites showed a small increase in crystallinity, 12 % for PLLA/TW and 6 % for PLLA/UD. A possible increase in crystallinity could be observed in ageing times superior to 30 days.

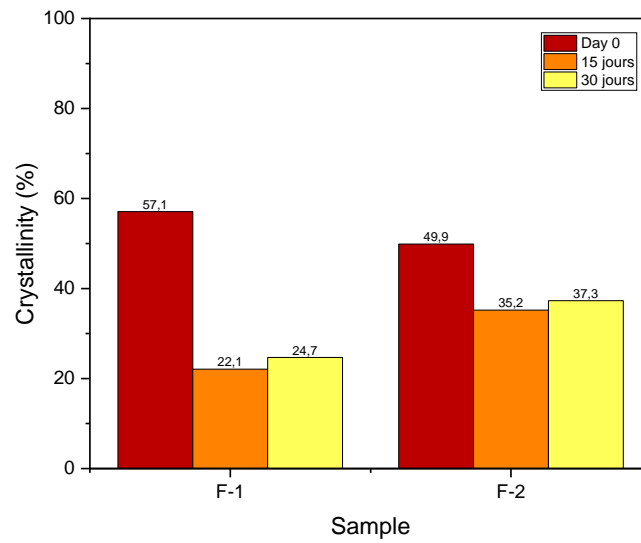


Figure 116: Evolution of crystallinity of FFRC matrices during ageing.

After ageing, the  $E_B$  of PLLA/TW decreased from 3.66 GPa to 2.40 GPa and the  $\sigma_B$  decreased from 50 MPa to 35 MPa. The strain only decreased of 3% (Table 44). These reductions in bending properties can be attributed to the decrease in crystallinity, which has dropped by 57% for the aged sample (sample F-1) compared to the unaged one (sample 1-TW).

Regarding PLLA/UD, the  $E_B$  remained constant after aging, maintaining a value of 9.3 GPa, while the  $\sigma_B$  decreased from 177 MPa to 150 MPa. The bending strain also decreased by 21% (Table 44). The changes in bending properties were less pronounced than in PLLA/TW because for this sample, a decrease in crystallinity of 25% was measured after aging.

Table 44: Mechanical properties of unaged and aged FFRC.

Sample	Composite	State	FMR (%)	FVR (%)	$E_B$ (GPa)	$\sigma_B$ (MPa)	Strain (%)
1-TW	PLLA/TW	Unaged	26.0	24.9	3.66 ± 0.18	50 ± 4	2.90 ± 0.71
F-1		Aged 30 days	26.0	24.9	2.40 ± 0.21 (-34 %)	35 ± 6 (-30 %)	2.80 ± 0.36 (-3 %)
1-UD	PLLA/UD	Unaged	31.3	30.4	9.30 ± 0.26	177 ± 4	2.86 ± 0.05
F-2		Aged 30 days	30.8	29.9	9.30 ± 0.92 (0 %)	150 ± 13 (-15%)	2.28 ± 0.22 (-21%)

The aged PLLA/TW showed an interlaminar shear fracture with an important delamination after bending test (Figure 117 - a). All five layers of composite plate were delaminated, indicating that the capacity of the matrix to keep cohesive the layers was impacted after ageing.

On the other hand, the aged PLLA/UD composite showed a tensile fracture with intralaminar matrix cracks, translaminar cracks, and some delamination at the top of the specimen (Figure 117 - b). These fractures were the same as those observed in the unaged samples.

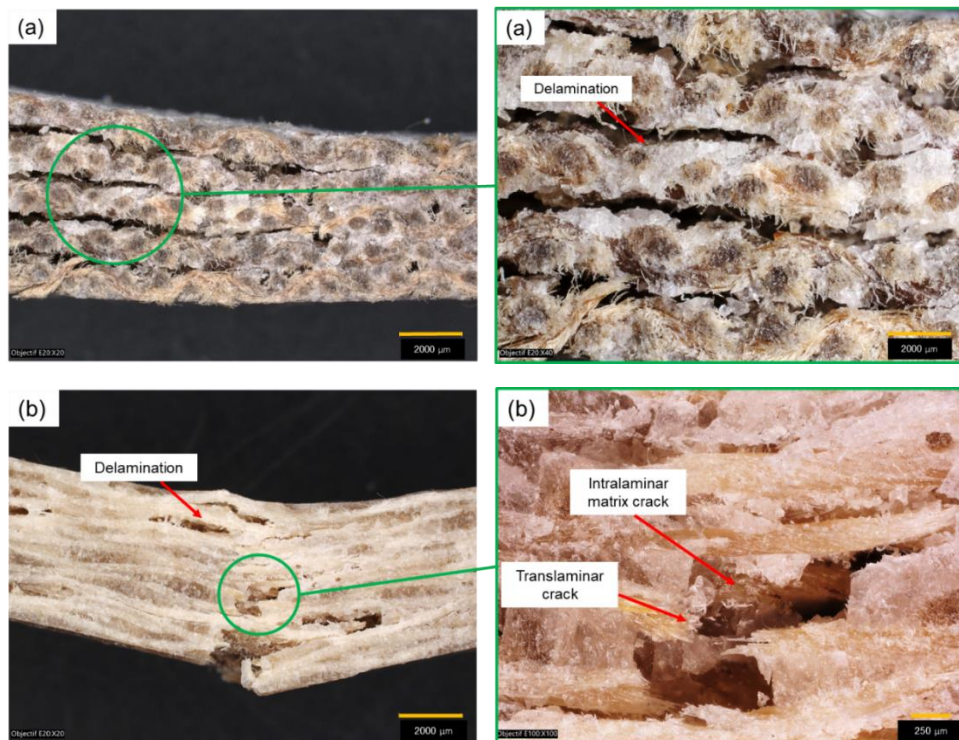


Figure 117: Optical micrographs of aged FFRC after bending test. (a) PLLA/TW and (b) PLLA/UD.

## 5.2.2 Conclusion

Preliminary studies about the accelerated ageing of GFRC, GFRC and FFRC were achieved. The composites were aged in an ageing chamber which simulates the irradiation of sun behind a glass. The external conditions applied on the material have a direct influence on its physicochemical and mechanical properties.

Globally, the PLLA matrix composites showed a small decrease of the bending properties, due to the decrease in their crystallinities. The PLCL matrix composites showed an increase in bending properties, governed by the increase in their crystallinities. In all PLLA and PLCL matrix composites, the molecular weights decreased along with the increase of the dispersity, indicating that chain scissions occurred during ageing.

Regarding the mechanical properties, the crystallinity plays a more important role than the molecular weight for all composites. Despite the decrease in molecular weight observed in all composites, the bending properties of PLCL matrix composites showed an increase.

This improvement can be attributed to the increase of crystallinity in the PLCL matrix during the ageing process.

### **5.3 General conclusion**

This chapter presents significant findings regarding the production and characterization of PLLA/flax composites using TP-RTM. The investigation reveal that flax fibers can withstand temperatures up to 185 °C, making them suitable for TP-RTM conditions to produce PLLA matrix composites. The presence of flax fabrics did not prevent the polymerization of L-LA. High conversion of L-LA was measured and the molecular weights are closer to the commercial PLA (4032D – NatureWorks).

However, there are variations in matrix impregnation, with PLLA/TW composites showing less effective impregnation and lower bending properties compared to PLLA/UD composites. Nonetheless, the latter exhibit bending modulus and strength of 9.30 GPa and 177 MPa respectively, higher than the values found in the literature for the same composite produced by other manufacturing techniques.

Additionally, the study of accelerated ageing of GFRC, CFRC, and FFRC reveals that external conditions directly influence their physicochemical and mechanical properties. During ageing, PLLA/GF and PLLA / FF composites experience a slight decrease in bending properties due to reduced crystallinity. A decrease of 10 and 34 % in bending modulus were reported to the aged PLLA/GF and PLLA/TW composites respectively.

The PLCL matrices of all composites (GFRC, CFRC, FFRC) showed increased bending properties attributed to higher crystallinity levels. Aged 20 PLCL/GF and 20 PLCL/GF composites showed an increase of 101 and 40 % in bending modulus. Aged 30 PLCL/GF and 30 PLCL/GF compositeS showed an increase of 77 and 32 % in bending modulus. Chain scissions occurred during ageing in all PLLA and PLCL matrix composites, leading to a decrease in molecular weight and increase of the dispersity.

Overall, the results highlight the importance of crystallinity in determining the mechanical properties of all composites, outweighing the influence of molecular weight changes. This chapter provides valuable insights into the production, characterization, and ageing behavior of biocomposites, contributing to the understanding and potential applications of these materials in various fields. Further research in this area may lead to enhanced manufacturing processes and improved properties for biocomposite materials.



### General conclusion

In a sustainable approach of composites production, bio-based and biodegradable matrix composites were produced by TP-RTM. Throughout this work, PLLA was selected as the main component of the composites matrix, but due to its brittleness, L-LA was copolymerized with  $\epsilon$ -CL in TP-RTM, in order to improve its mechanical properties. A comprehensive exploration of the production of PLLA and PLCL matrix composites by TP-RTM has been undertaken. PLCL/glass fabric, PLLA and PLCL/carbon fabric, and PLLA/flax fabric composites were developed. A significant advancement on the use of bio-based and biodegradable thermoplastics in TP-RTM was done. This strategic shift aims to promote sustainable composite production by embracing bio-based and biodegradable polymers, reducing reliance on petroleum-based resins.

The production of PLCL/glass fabric composites by TP-RTM was successfully conducted, with fiber mass ratio of 45-48 %. Three compositions of PLCL matrix were tested with 10 (10 PLCL), 20 (20 PLCL) and 30 (30 PLCL) mol% of  $\epsilon$ -CL. These composites produced at 185 °C showed conversions higher than 95 % for both L-LA and  $\epsilon$ -CL and high  $M_w$  up to 90,600 g.mol<sup>-1</sup> %. Regarding the thermal properties, it was proved that the melting and glass transition temperatures decreased when increasing the  $\epsilon$ -CL content. The microstructure of these copolymers produced at 185 °C displays a random distribution, supported by the Bernoullian model, in which the degree of randomness measured was higher than 0.8, proven its random character, and thus in line with the DSC results.

In PLLA and PLCL/GF composites, meso-voids were identified between the bundles of the fabric, but no voids were identified between the fibers. The tensile properties of 10 and 20 PLCL/GF composites disposed of similar values of Young modulus and tensile strength, around 6.5 GPa and 250 MPa. The values of tensile properties for 30 PLCL/GF was divided by two, compared to the precedent compositions. Regarding the bending properties, it was reported that the bending modulus as well the bending strength decreases with increasing the  $\epsilon$ -CL content. Values of bending modulus for 10, 20 and 30 PLCL/GF composites around 9, 3 and 0.3 GPa were measured, while the bending strength decreases from 256 MPa (10 PLCL/GF) to 21 MPa (30 PLCL/GF). Regarding the bending test, a shape recovery compartment was observed for the composites containing 20 and 30 mol% of  $\epsilon$ -CL in its composition, as the specimens returned to their initial shape, without delamination. With the impact test, it was proved that the increase of impact strength was related to the increase of  $\epsilon$ -CL in copolymer chain.

## General conclusion

---

The highest value of impact strength was measured for the composite 30 PLCL/GF, with a value of 262 kJ.m<sup>2</sup>, corresponding to an increase of 90 % compared to the impact strength of PLLA/GF composite. This increase on impact strength proves that the main objective of this thesis, which was to reduce the brittleness of PLLA, was reached.

The influence of polymerization temperature of PLCL/GF composites on monomers conversions, molecular weights, thermal and mechanical properties was studied. Temperatures of 150, 160 and 170 °C were tested and the conversion of monomers as well as the molecular weights of the resulting matrices were examined to establish the polymerization temperature leading to the most relevant specimens. For composites 20 PLCL/GF, it was found that the optimal polymerization temperature was 170 °C, while it was 160°C for the 30 PLCL/GF one. Globally, the decrease of polymerization temperature permitted the increase of molecular weight and consequently an improvement of the mechanical properties. In the optimal polymerization temperature,  $M_w$  higher than 119,000 g.mol<sup>-1</sup> was reached. Also, the decrease of polymerization temperatures changed the microstructure of the copolymers, from a random character ( $R \approx 0.8$ ) to a rather moderate blocky character ( $R \approx 0.5$ ).

To produce composites with lightweight structure, carbon fabric was used to produce CFRC. The optimal polymerization temperatures tested in GFRC were used to produce CFRC. PLLA/CF, 20 PLCL/CF and 30 PLCL/CF composites were produced with fiber mass ratio of 29 % Once the 10 PLCL/GF sample showed similar behavior to the PLLA/GF composite in tensile and bending tests, this formulation was not tested with carbon fabric. The thermal behavior of these composites followed the same tendency as the GFRC, with glass transition temperature and melting temperature decreasing with the increase of  $\epsilon$ -CL content. In these matrices composites the copolymers showed a moderate blocky character with R value around 0.6. Compared to GFRC, the CFRC showed an important increase in bending properties.

Fully biodegradable composites produced with PLLA as matrix and flax fabric as reinforcement were also produced in this study by TP-RTM. Very promising results regarding the use of PLLA matrix reinforced by natural fibers within TP-RTM technique were obtained. The study demonstrated that flax fibers can be effectively incorporated without compromising the polymerization reaction, showcasing potential applications in creating sustainable composites with desirable thermal and mechanical properties. In addition, the bending properties of flax fabric reinforced composites produced by TP-RTM are slightly higher than the same composites produced by other manufacturing techniques.

## General conclusion

---

Accelerated ageing tests were performed on all composites. These materials were subjected to aging within a simulated chamber that replicated sun exposure behind glass. Across the board, PLLA matrix composites exhibited a marginal decline in bending properties due to reduced crystallinity. Conversely, PLCL matrix composites displayed increased bending properties linked to the increase on its crystallinity. In both PLLA and PLCL matrix composites, molecular weights declined along with increased dispersity, indicating the occurrence of chain scissions during aging. Regarding mechanical properties, crystallinity emerged as a more critical factor than molecular weight for all composites.

This Ph.D. thesis contributes to the development of unprecedented PLCL matrix composites reinforced with glass and carbon fabric by TP-RTM. The journey undertaken here not only opens doors to promote the use of thermoplastics in RTM process but also underscores the promising role of composite materials produced with bio-based and biodegradable matrices. Future research endeavors hold the potential to refine and broaden the applications of biocomposites, fueling innovation in this dynamic field.



## Outlook

Several aspects can be deliberated upon, offering a foundational platform for future research, building upon the findings presented within this research. Several topics derived from this Ph.D. thesis could be subject to further research studies, the first one is the shape recovery properties.

### 6.1 Shape recovery properties

During three-point bending tests, a shape recovery compartment of 30 PLCL matrix composites reinforced with glass fabrics was observed. This compartment was expected since poly(L-lactide-co- $\epsilon$ -caprolactone) is known for its shape memory property.<sup>112,113</sup> However, the high deformation of these composites could provoke damage of the reinforcement, which was not observed on 30 PLCL/GF composite. To evaluate the shape recovery properties of this composite, cyclic three-point bending tests were conducted (Section 2.4.4, p.67)

Regarding 30 PLCL/GF sample produced at 185 °C, a shape recovery of 73 % was measured at the first cycle (Table 45). This values increases at 86 and 84 % for 30 PLCL/GF composites produced at 160 and 170 °C respectively. The most promising results were obtained with 30 PLCL/GF composites produced at 160 and 170 °C displaying a  $R_r$  value of 77 % after five cycles (Table 45, Figure 118). The literature reports that the shape recovery increases with the increase of the  $\epsilon$ -CL and so the preliminary studies presented here are in line with the precedent works.<sup>112</sup>

Table 45: Shape recovery value for 30 PLCL/GF composites submitted to cyclic three-point bending test.

Sample	Cycle	$\Delta L_d$ (mm)	$\Delta U_d$ (mm)	Recovery (%)
30 PLCL/GF 160 °C	1	5.32	4.59	86.3
	2	5.32	4.39	82.5
	3	5.32	4.29	80.6
	4	5.32	4.18	78.6
	5	5.32	4.07	76.5
30 PLCL/GF 170 °C	1	5.33	4.46	83.7
	2	5.33	4.32	81.1
	3	5.33	4.24	79.5
	4	5.33	4.16	78.0
	5	5.33	4.10	76.9
30 PLCL/GF 185 °C	1	5.32	3.88	72.9
	2	5.32	3.64	68.4
	3	5.32	3.48	65.4
	4	5.32	3.38	63.5
	5	5.32	3.27	61.5

## Outlook

---

The ability of PLCL copolymers to regain their shape is influenced by their semi-crystalline character. The crystalline regions, created by L-LA, act as anchors that hold the material together, while the less structured part made of  $\epsilon$ -CL allow the material to stretch and return to its original shape. According to DSC analysis (Table 24, p.112), the crystallinity of PLCL copolymers decreases with increasing the  $\epsilon$ -CL content. The matrix of 30 PLCL/GF composites produced at 185 °C are completely amorphous and so the shape recovery was less effective than in the 30 PLCL/GF produced at 160 and 170 °C, since these matrices are semi-crystalline ( $\chi = 13\%$ ). In future researches, the cyclic three-point bending test could be associated to other mechanical tests to study in detail the shape memory effect. In that frame, cyclic mechanical tests under temperature could be conducted, in which the composites can be submitted to different temperatures, under and above its  $T_g$ .

Considering the preliminary studies, a focus should be done on composites with 30 mol% of  $\epsilon$ -CL, but compositions with 20 mol% of  $\epsilon$ -CL should be studied as well. In depth studies should be carried out to understand the role of the copolymers microstructure on shape memory properties. Also, the mechanical tests to investigate the shape memory properties should be applied to the carbon fabric reinforced composites.

The other topics that could be explored are the measurement of void content, the improvement of wettability of flax fabric, the production of PLCL/flax fabric composites, accelerated ageing and fire resistance are shortly described hereafter.

## Outlook

---

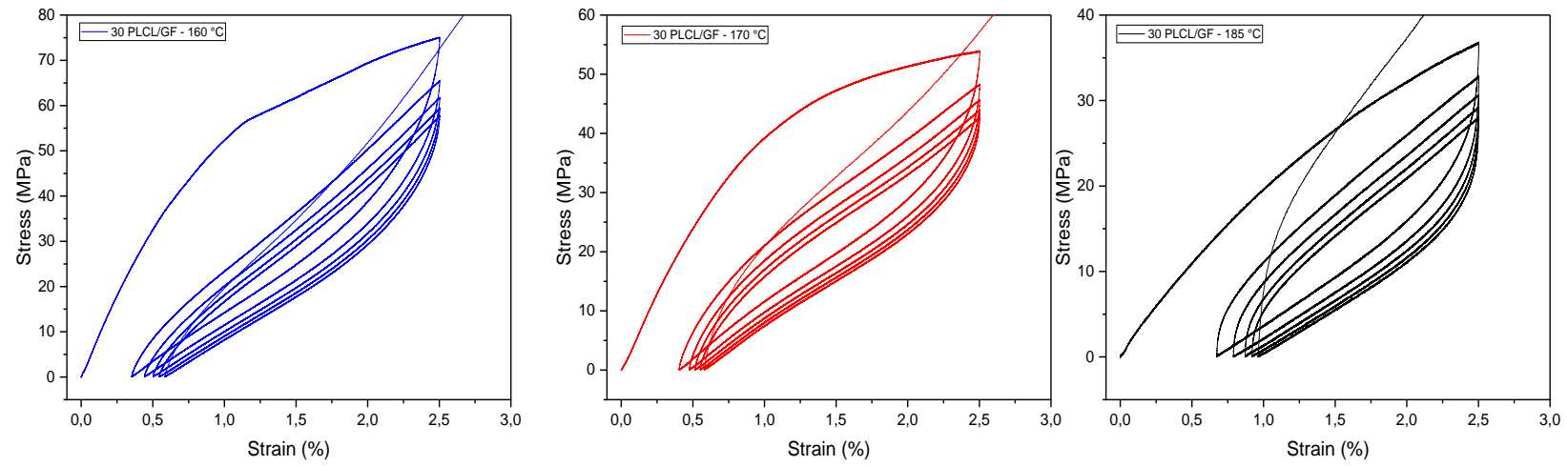


Figure 118: Strain x stress curves on cyclic three-point bending test of 30 PLCLC/GF composites produced at various temperature.

### 6.2 Measurement of void content

Another topic to explore in future researches is the exploration of voids in the composites. During this work, the voids were observed but were not quantified. The composites could be analyzed by X-ray tomography (non-destructive) or by burn-off method (destructive) to quantify exactly the voids content.

### 6.3 Improvement of wettability of flax fabric

A subject ripe for investigation in forthcoming research is the improvement of the wettability of flax fabric by surface modification (physical and chemical modification). As discussed before, even though PLLA/flax composites were produced by TP-RTM for the first time, the wettability of flax fabric need to be improved in order to enhance the cohesion between the matrix and the reinforcement. In that way, the presence of voids in PLLA/flax composites could be reduced and increase its mechanical properties.

### 6.4 Production of PLCL/flax fabric composites

During this thesis, PLLA/flax fabric composites were produced by TP-RTM. However, the different PLCL matrices tested with glass and carbon fabrics were not tested with flax fabrics. Experiments should be done with the PLCL matrix with different  $\epsilon$ -CL ratios. Until now, the potential impact of the presence of flax fabric on the ring-opening polymerization of  $\epsilon$ -CL in TP-RTM is unknown. Also, the use of other natural fibers (*i.e* hemp, kenaf...) should be tested with PLLA and PLCL matrices.

### 6.5 Accelerated ageing tests

The preliminary accelerated ageing tests conducted on GFRC, CFRC and FFRC were carried out to assess the long-term durability and performances of these composites. In future works, ageing tests in different conditions *i.e* humidity, UV, temperature should be conducted. These tests are crucial to understand the behavior of these composites under certain conditions to approve its applicability.

### 6.6 Fire resistance

In order to be applicable across various industry sectors such as automotive and aerospace, the materials must undergo specific qualifications and certifications. One of the most important ones is the fire resistance. In the future, flame retardants could be possibly incorporated to the PLLA and PLCL matrices using the TP-RTM process. Studies about the potential impact of flame retardants on the ring-opening polymerization of L-LA and  $\epsilon$ -CL should be studied. Also, the flame retardancy of reinforcements should be explored.

Recent studies reported the polymerization of  $\epsilon$ -caprolactam in TP-RTM in the presence of flame retardants.<sup>239</sup> According to the authors, the flame retardants used, *i.e.* red phosphorous, magnesium oxide and dechlorane, did not affect the polymerization reaction. This study shows that the use of flame retardants in TP-RTM process is thus possible.

### 6.7 Applications of composites

The composites developed here exhibit distinct mechanical properties which are adapted to several applications (Figure 119). Up to date, the number of studies on PLLA glass fabric composites is not that high and so the number of applications of this composite are minor.<sup>37</sup> RTP company is the first industrial producers of PLA/GF composites for appliance, automotive, consumer goods, electrical & electronics, and construction markets.<sup>240</sup>

Regarding PLCL/GF composites, since these ones have never been produced before by any process, no applications exist yet. PLCL/GF composites produced in this work can possibly find applications in different sectors.

Since they display impact properties 90 % higher than the PLLA/GF composite, applications requiring high impact strength *i.e.* luggage, sporting equipment and electronic device casing could be considered. Both PLLA and PLCL/GF composites could also find applications in automotive components such as dashboards, door panels, trim, spare tire covers and floor mats. In aerospace, these composites could be used in non-structural interior components of aircraft if the latter respond to the fire resistance requirements.

Regarding the PLLA and PLCL/CF composites, they can find similar applications to the glass reinforced homologues. An attention should be done to its applicability on aerospace sector, once these composites display mechanical properties higher than the glass reinforced ones. Also, the PLLA and SPLCL/CF composites are lighter than the glass reinforced ones, displaying 20 % less of weight.

Bio-based polymers reinforced with natural fibers have been used since the 2000s in automotive industry. In 2003, Toyota used PLA/kenaf composites to make interior parts *i.e.* door trims.<sup>241</sup> PLLA/flax fabric composites seem to be adapted to the automotive industry, once kenaf display similar mechanical properties than flax.<sup>70</sup> Some authors also reported that PLLA/flax composites find applicability in non-load-bearing applications in construction, *i.e.* architectural panels and interior elements.<sup>37</sup>

## Outlook

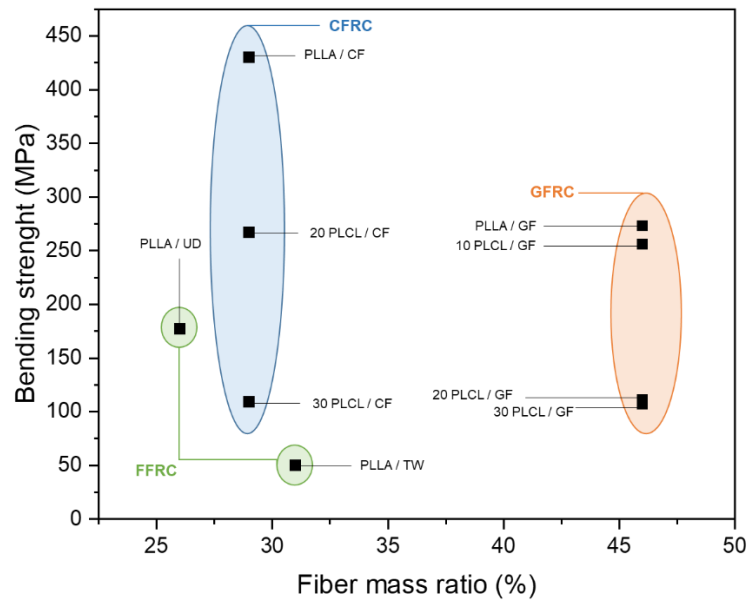


Figure 119: Bending strength of glass fabric reinforced composites (GFRC), carbon fabric reinforced composites (CFRC) and flax fabric reinforced composites (FFRC).

To summarize, this research highlights the remarkable versatility and potential of custom-designed composite materials in diverse sectors. As the field continues to evolve, it holds promise for the realization of innovative applications that leverage the unique properties of these engineered materials.

## Outlook

---

## List of figures

---

### List of figures

Figure 1: Scheme of composite material with unidirectional fibers. ....	7
Figure 2: Classification of textile fibers. <sup>50</sup> .....	10
Figure 3: Different forms of fibers. <sup>1</sup> .....	11
Figure 4: Different forms of patterns of woven fabrics. <sup>53</sup> .....	11
Figure 5: Continuous glass filament forming. ....	13
Figure 6: Tensile strength of epoxy/glass composites. <sup>1</sup> .....	14
Figure 7: Tensile strength versus tensile modulus of PAN/pitch carbon fibers. <sup>57</sup> .....	15
Figure 8: Microstructure of flax fiber cell.....	16
Figure 9: Different forms of flax fibers: (a) mat, (b) roving, (c) fabric, (d) short fibers, (e) yarn. <sup>62</sup> .....	17
Figure 10: Classification of biodegradable polymers. <sup>66</sup> .....	18
Figure 11: Bio-based polymers – Evolution of worldwide production capacities 2021 to 2027. <sup>67</sup> .....	19
Figure 12: Biodegradability of some polymers in various environments. <sup>67</sup> .....	20
Figure 13: Structures of L-, D- and D,L-lactic acids. <sup>74</sup> .....	22
Figure 14: Structure of lactides. <sup>81</sup> .....	22
Figure 15: Different routes for synthesis of poly (lactid acid). <sup>77</sup> .....	23
Figure 16: Reactions involved in polymerization of lactides initiated with Sn(Oct) <sub>2</sub> /ROH system. <sup>84</sup> .....	25
Figure 17: Number of publications per year between 2000-2022 for PLLA matrix composites, PLLA/PLCL blends and poly(L-lactide-co-ε-caprolactone). <sup>88</sup> .....	27
Figure 18: Charpy notched impact strength of PLA/PCL blends. <sup>92</sup> .....	28
Figure 19: Tensile stress of PLA/Flax composite compared to PP/Flax (30 and 40 wt% of flax fibers). <sup>118</sup> .....	32
Figure 20: Mechanical properties of the PLA/GF composites: (a) strength, (b) modulus, and (c) impact strength. <sup>20</sup> .....	32
Figure 21: Classification of the principal manufacturing techniques of composites production. ....	34
Figure 22: (a) Schematic representation of filament winding (b) Schematic of pressure vessel produced by filament winding. <sup>2</sup> .....	34
Figure 23: Schematic representation of pultrusion process. <sup>70</sup> .....	35
Figure 24: Scheme of the compression molding process. <sup>55</sup> .....	36
Figure 25: Schematic representation of single-screw injection molding machine. ....	36



## List of figures

---

Figure 26: Scheme of the vacuum infusion process. <sup>131</sup> .....	37
Figure 27: Schematic representation of RTM machine.....	39
Figure 28: Mixing head used in thermoplastic resin transfer molding (TP-RTM) multi- component machine for highly reactive thermoplastic systems. ....	39
Figure 29: Injection strategies for a square plate in single port with dimensions L x L. (a) radial injection (b) edge injection (c) peripheral injection. The flow front starts in the darkest zones in all schemes. The letter "d" corresponds to the diameter of the inlet and outlet. <sup>137,151</sup> .....	42
Figure 30: Configuration of TP-RTM square plate mold for peripheral injection strategy. (2) upper mold (3) lower mold. ....	42
Figure 31: Flow front position in a 0.1 m x 0.2 m x 0.01 m resin transfer molding (RTM) mold for (a) isotropic and (b) anisotropic permeability distributions. <sup>153</sup> .....	44
Figure 32: Formation of voids during longitudinal and transverse flow in liquid composite molding. <sup>141</sup> .....	45
Figure 33: Micrographs of cross-sections of laminates manufactured by a variant of VARTM (i.e., a vacuum-assisted process – (VAP)) under experiment conditions for (a) woven reinforcements and (b) non-crimp reinforcements. (Based on reference <sup>155</sup> ) .....	45
Figure 34: Viscosity of cyclic butylene terephthalate oligomer (CBT) reactive system as function of time in different polymerization conditions. (a) different catalyst contents at 190 °C (b) different polymerization temperatures with 0.5 wt% of catalyst. <sup>174</sup> .....	51
Figure 35: Physical aspect of reinforcements.....	59
Figure 36: (a) General view of TP-RTM machine; (b) Right and (c) left side of unit control. .	60
Figure 37: Aluminum beaker placed in the middle of the TP-RTM tank. ....	60
Figure 38: Aluminum mold used to produce composite plates. ....	61
Figure 39: Mold cavity with pre-disposed glass fabric. ....	62
Figure 40: Composite plate before demold, showing the polymer in mold channels.....	64
Figure 41: Schematic representation of the temperature process versus time during the production of composite plates in TP-RTM. ....	65
Figure 42: <sup>1</sup> H NMR spectra of 20 PLCL ([L-LA]:[ε-CL] = 80:20) in CDCl <sub>3</sub> . ....	66
Figure 43: Cycles of heating and cooling used in DSC analysis.....	68
Figure 44: Type 1B specimen. ....	69
Figure 45: Instantaneous moment of performing the three-point bending test.....	70
Figure 46: Scheme of designation describing the direction of blow. ....	71
Figure 47: Scheme of hydrostatic weighing technique used to calculate the values of volumetric masses of polymer matrices. ....	73
Figure 48: Example of mounted sample of PLLA matrix composite.....	74

## List of figures

---

Figure 49: (a) QUV tester chamber (b) bending specimens placed in holders.....	75
Figure 50: Viscosity of molten L-lactide at different temperatures. <sup>80</sup> .....	80
Figure 51: Evolution of monomers conversion and the melting time.....	81
Figure 52: Evolution of the average sequence lengths of different copolymer compositions.	88
Figure 53: TGA curves of PLLA and PLCL matrices (10°C.min <sup>-1</sup> under N <sub>2</sub> ).....	89
Figure 54: Normalized DTG curves of PLLA and PLCL matrices thermal degradation at heating rate of 10 °C.min <sup>-1</sup> .....	89
Figure 55: Digital micrograph (a) in reflection and (b) in transmission of glass fabric showing the spaces between the fiber tows. ....	93
Figure 56: Digital micrographs showing macro-voids in (a) 10 PLCL/GF and (b) 30 PLCL/GF composites. ....	93
Figure 57: Digital micrograph of 20 PLCL/GF composite plate showing the meso-voids between the bundles.....	94
Figure 58: Digital micrograph of 20 PLCL/GF composite plate showing the interface between the matrix and the meso-void.....	94
Figure 59: Digital micrograph of 20 PLCL/GF composite with absence of micro-voids intra-bundles. ....	95
Figure 60: Strain x stress curve in tensile test of PLLA/GF, 10 PLCL/GF, 20 PLCL/GF and 30 PLCL/GF composites.....	97
Figure 61: Specimens after tensile test (a) PLLA/GF (b) 10 PLCL/GF (c) 20 PLCL/GF (d) 30 PLCL/GF.....	97
Figure 62: Micrographs of the surface of the fracture after tensile test (a) PLLA/GF (b) 10 PLCL/GF (c) 20 PLCL/GF (d) 30 PLCL/GF specimens. ....	98
Figure 63: Detailed micrographs of (a) PLLA/GF and (b) 10 PLCL/GF specimens showing different types of fracture. ....	99
Figure 64: Detailed micrograph of 20 PLLA/GF specimen showing different types of fracture. ....	99
<i>Figure 65: Detailed micrographs of 30 PLCL/GF specimen showing (a) different types of fracture and (b) intralaminar matrix crack.....</i>	<i>100</i>
Figure 66: Strain – stress curve in three point bending test of PLLA/GF, 10 PLCL/GF, 20 PLCL/GF, and 30 PLCL/GF composites. ....	102
Figure 67: Specimens after three point bending test (a) PLLA/GF (b) 10 PLCL/GF (c) 20 PLCL/GF (d) 30 PLCL/GF.....	102
Figure 68: Digital micrographs showing the different types of failure observed in the PLLA/GF specimen.....	103
Figure 69: Digital micrograph showing the failure observed in the 10 PLLA/GF specimen. ....	103

## List of figures

---

Figure 70: Representative stress-strain graphs for PLLA/GF and 10 PLCL/GF.....	104
Figure 71: Digital micrographs of the 20 PLCL/GF and 30 PLCL/GF specimens.....	105
Figure 72: Impact strength of GFRC. ....	106
Figure 73: Digital micrograph showing the failure observed in the impacted surface of PLLA/GF (a-I), 10 PLCL/GF (b-I) and opposed impact surfaces of PLLA/GF (a-II) and 10 PLCL/GF (b-II) specimen. ....	106
Figure 74: Digital micrograph showing the failure observed in the impacted surface of 20 PLCL/GF (a-I), 30 PLCL/GF (b-I) and opposed impact surfaces of 20 PLCL/GF (a-II) and 30 PLCL/GF (b-II) specimen. ....	107
Figure 75: Variation of color of the composite plates.....	108
Figure 76: Randomness character vs. polymerization temperature for 20 PLCL/GF and 30 PLCL/GF composites.....	111
Figure 77: Bending modulus vs $M_w$ of 20 PLCL/GF composites produced at various temperatures .....	114
Figure 78: Bending modulus vs $M_w$ of 30 PLCL/GF composites produced at various temperatures. ....	115
Figure 79: (a) Strain x stress curve in three point bending test for 20 PLCL/GF composites produced at various temperatures, (b) comparison of bending properties of 20 PLCL/GF composites produced at various temperatures.....	117
Figure 80: Specimens of 20 PLCL/GF composites after three point bending test. View from (a) central loading member and (b) opposite to loading member.....	118
Figure 81: Digital micrograph showing the failure observed in the 20 PLLA/GF specimens produced at various temperatures: (a-b) 170 °C, (b-c) 160 °C, (e-f) 150 °C. ....	119
Figure 82: (a) Strain x stress curve in three point bending test for 30 PLCL/GF composites produced at various temperatures, (b) comparison of bending properties of 30 PLCL/GF composites produced at various temperatures.....	120
Figure 83: Specimens of 30 PLCL/GF composites after three point bending test. View from (a) central loading member and (b) opposite to loading member.....	121
Figure 84: Digital micrographs showing the damage observed in the 20 PLLA/GF specimens produced at various temperatures: (a) sample 1-E, (b) 2-E, (e) 3-E. ....	121
Figure 85: TGA curve of carbon fibers.(10°C.min <sup>-1</sup> / N <sub>2</sub> ).....	125
Figure 86: (a) PLLA / CF and (b) 20 PLCL/GF composite plates.....	126
Figure 87: (a) TG curves of PLLA, PLCL matrices thermal degradation at heating rate of 10° C min <sup>-1</sup> ; (b) Normalized DTG curves of PLLA and PLCL matrices thermal degradation at heating rate of 10 °C.min <sup>-1</sup> .....	130

## List of figures

---

Figure 88: DSC curves at (a) first and (b) second scan of the matrices of CFRC. ( $10\text{ }^{\circ}\text{C}\cdot\text{min}^{-1}$ , under $\text{N}_2$ ) .....	131
Figure 89: Digital micrograph of 20 PLLA/CF composite plate showing the layer of matrix on the reinforcement.....	133
Figure 90: Comparison of fiber mass ratio and fiber volume ratio of GFRC and CFRC. ....	133
Figure 91: Digital micrograph of carbon fabric showing the spaces between the fiber tows. ....	134
Figure 92: Digital micrographs showing the impregnation of the fibers on 20 PLCL/GF composite. ....	134
Figure 93: Strain x stress curve in three-point bending test of carbon fabric reinforced composites. ....	135
Figure 94: Comparison of (a) bending modulus and (b) bending strength of carbon and glass fabric reinforced composites. ....	137
Figure 95: Strain x stress curve in three-point bending test for 30 PLCL/GF and 30 PLCL/CF composites. ....	138
Figure 96: Digital micrographs showing the different types of failure observed in the PLLA/CF specimen. ....	139
Figure 97: Digital micrographs showing the different types of failure observed in the 20 PLCL/CF specimen.....	140
Figure 98: Digital micrographs showing the different types of failure observed in the 20 PLCL/GF specimen.....	141
Figure 99: PLLA/UD (left) and PLLA/TW (right) composite plates. ....	146
Figure 100: TG and DTG curves of flax fabrics. ....	147
Figure 101: (a) TGA and (b) DTG of PLLA matrices.....	149
Figure 102: Digital micrographs of cross section of PLLA/UD composites. ....	150
Figure 103: Digital micrographs in a longitudinal cut of PLLA/UD plate.....	151
Figure 104: Meso-voids present between flax fiber bundles in a longitudinal cut of PLLA/UD plates.....	151
Figure 105: Digital micrographs of a cross section of PLLA/TW composites. ....	152
Figure 106: Digital micrographs of failure observed in the PLLA/UD specimen.....	154
Figure 107: Digital micrographs of failure observed in the PLLA/UD specimen.....	155
Figure 108: Main route of PLLA photooxidation. <sup>235</sup> .....	158
Figure 109: Unaged and aged (30 days, $50^{\circ}\text{C}$ , UV-A 340 nm) GFRC specimens. ....	159
Figure 110: Evolution of crystallinity of GFRC matrices during ageing. ....	161
Figure 111: Optical micrographs of aged GFRC after bending test. ....	163
Figure 112: Unaged and aged CFRC (30 days, $50^{\circ}\text{C}$ , UV-A at 340 nm). ....	164

## List of figures

---

Figure 113: Evolution of crystallinity of CFRC matrices during ageing. ....	166
Figure 114: Optical micrographs of aged CFRC after bending test. ....	168
Figure 115: Unaged and aged FFRC specimens. ....	169
Figure 116: Evolution of crystallinity of FFRC matrices during ageing. ....	171
Figure 117: Optical micrographs of aged FFRC after bending test. (a) PLLA/TW and (b) PLLA/UD. ....	172
Figure 118: Strain x stress curves on cyclic three-point bending test of 30 PLCLC/GF composites produced at various temperature. ....	180
Figure 119: Bending strength of glass fabric reinforced composites (GFRC), carbon fabric reinforced composites (CFRC) and flax fabric reinforced composites (FFRC). ....	183
Figure 120: $^1\text{H}$ NMR spectra of the reactive system at different melting temperatures ( $\text{CDCl}_3$ , 300 MHz). ....	219
Figure 121: $^1\text{H}$ NMR spectra of pure PLLA and 20 PLCL synthesized at different polymerization temperatures ( $\text{CDCl}_3$ , 300 MHz). ....	219
Figure 124: $^1\text{H}$ NMR spectra of PLLA matrices showing the peaks corresponding to L-LA and PLLA ( $\text{CDCl}_3$ , 300 MHz). ....	220
Figure 125: $^1\text{H}$ NMR spectra of 10 PLCL matrices showing the peaks corresponding to $\epsilon$ -CL. PLCL. L-LA and PLLA ( $\text{CDCl}_3$ , 300 MHz). ....	220
Figure 126: $^1\text{H}$ NMR spectra of 20 PLCL matrices showing the peaks corresponding to $\epsilon$ -CL. PLCL. L-LA and PLLA ( $\text{CDCl}_3$ , 300 MHz). ....	220
Figure 127: $^1\text{H}$ NMR spectra of 30 PLCL matrices showing the peaks corresponding to $\epsilon$ -CL. PLCL. L-LA and PLLA ( $\text{CDCl}_3$ , 300 MHz). ....	221
Figure 128: $^1\text{H}$ NMR spectra of 20 PLCL matrices at different polymerization temperatures showing the peaks corresponding to $\epsilon$ -CL. PLCL. L-LA and PLLA ( $\text{CDCl}_3$ , 300 MHz). ....	221
Figure 129: $^1\text{H}$ NMR spectra of 30 PLCL matrices at different polymerization temperatures showing the peaks corresponding to $\epsilon$ -CL. PLCL. L-LA and PLLA ( $\text{CDCl}_3$ , 300 MHz). ....	222
Figure 130: $^1\text{H}$ NMR spectra of PLLA matrices showing the peaks corresponding to L-LA and PLLA ( $\text{CDCl}_3$ , 300 MHz). ....	222
Figure 131: $^1\text{H}$ NMR spectra of 80/20 PLCL matrices showing the peaks corresponding to $\epsilon$ -CL, PLCL, L-LA and PLLA ( $\text{CDCl}_3$ , 300 MHz). ....	223
Figure 132: $^1\text{H}$ NMR spectra of 70/30 PLCL matrices showing the peaks corresponding to $\epsilon$ -CL, PLCL, L-LA and PLLA ( $\text{CDCl}_3$ , 300 MHz). ....	223
Figure 133: $^1\text{H}$ NMR spectra of PLLA matrices of flax fabric reinforced composites ( $\text{CDCl}_3$ , 300 MHz). ....	224
Figure 134: DSC curves at first scan of PLLA matrices. ....	225
Figure 135: DSC curves at second scan of PLLA matrices. ....	225

## List of figures

---

Figure 136: DSC curves at first scan of 10 PLCL matrices.....	226
Figure 137: DSC curves at second scan of 10 PLCL matrices.....	226
Figure 138: DSC curves at first scan of 20 PLCL matrices.....	227
Figure 139: DSC curves at second scan of 20 PLCL matrices.....	227
Figure 140: : DSC curves at first scan of 30 PLCL matrices.....	228
Figure 141: DSC curves at second scan of 30 PLCL matrices.....	228
Figure 142: DSC curves at first scan of PLLA matrices (10°C.min <sup>-1</sup> , under N <sub>2</sub> ). ....	229
Figure 143: DSC curves at second scan of PLLA matrices (10°C.min <sup>-1</sup> , under N <sub>2</sub> ).....	229
Figure 144: DSC curves at first scan of 20 PLCL matrices (10°C.min <sup>-1</sup> , under N <sub>2</sub> ). ....	230
Figure 145: DSC curves at second scan of 20 PLCL matrices (10°C.min <sup>-1</sup> , under N <sub>2</sub> ). ....	230
Figure 146: DSC curves at first scan of 30 PLCL matrices (10°C.min <sup>-1</sup> , under N <sub>2</sub> ). ....	231
Figure 147: DSC curves at second scan of 30 PLCL matrices (10°C.min <sup>-1</sup> , under N <sub>2</sub> ). ....	231
Figure 148: DSC curves of the matrix of PLLA/GF composite (sample G-1) at 1 <sup>st</sup> scan. ...	232
Figure 149: DSC curves of the matrix of PLLA/GF composite (sample G-1) at 2 <sup>nd</sup> scan. ...	232
Figure 150: DSC curves of the matrix of 20 PLCL/GF composite (sample G-2) at 1 <sup>st</sup> scan. .....	233
Figure 151: DSC curves of the matrix of 20 PLCL/GF composite (sample G-2) at 2 <sup>nd</sup> scan. .....	233
Figure 152: DSC curves of the matrix of 30 PLCL/GF composite (sample G-3) at 1 <sup>st</sup> scan. .....	234
Figure 153: DSC curves of the matrix of 30 PLCL/GF composite (sample G-3) at 2 <sup>nd</sup> scan. .....	234
Figure 154: DSC curves of the matrix of PLLA / CF composite (sample C-1) at 1 <sup>st</sup> scan...	235
Figure 155: DSC curves of the matrix of PLLA / CF composite (sample C-1) at 2 <sup>nd</sup> scan...	235
Figure 156: DSC curves of the matrix of 20 PLCL/GF composite (sample C-2) at 1 <sup>st</sup> scan. .....	236
Figure 157: DSC curves of the matrix of 20 PLCL/GF composite (sample C-2) at 2 <sup>nd</sup> scan. .....	236
Figure 158: DSC curves of the matrix of 30 PLCL/GF composite (sample C-3) at 1 <sup>st</sup> scan. .....	237
Figure 159: DSC curves of the matrix of 30 PLCL/GF composite (sample C-3) at 2 <sup>st</sup> scan. .....	237
Figure 160: DSC curves of the matrix of PLLA/TW composite (sample F-1)at 1 <sup>st</sup> scan. ....	238
Figure 161: DSC curves of the matrix of PLLA/TW composite (sample F-1) at 2 <sup>nd</sup> scan. ...	238
Figure 162: DSC curves of the matrix of PLLA/UD composite (sample F-2) at 1 <sup>st</sup> scan.....	239
Figure 163: DSC curves of the matrix of PLLA/UD (sample F-2) at 2 <sup>nd</sup> scan.....	239

## List of figures

---

Figure 164: Strain x stress curve in tensile test of PLLA/GF (sample 1-X) composite. ....	240
Figure 165: Strain x stress curve in tensile test of 10 PLCL/GF (sample 1-A) composite. .	240
Figure 166: Strain x stress curve in tensile test of 20 PLCL/GF (sample 1-B) composite. ..	241
Figure 167: Strain x stress curve in tensile test of 30 PLCL/GF (sample 1-C) composite. ...	241
Figure 168: Strain x stress curve in three-point bending test of PLLA/GF (sample 2-X) composite. ....	242
Figure 169: Strain x stress curve in three-point bending test of 10 PLCL/GF (sample 2-A) composite. ....	242
Figure 170: Strain x stress curve in three-point bending test of 20 PLCL/GF (sample 2-B) composite. ....	243
Figure 171: Strain x stress curve in three-point bending test of 30 PLCL/GF (sample 2-C) composite. ....	243
Figure 172: Strain x stress curve in three-point bending test of 20 PLCL/GF composite (Sample 1-D) produced at 170 °C. ....	244
Figure 173: Strain x stress curve in three-point bending test of 20 PLCL/GF composite (Sample 2-D) produced at 160 °C. ....	244
Figure 174: Strain x stress curve in three-point bending test of 20 PLCL/GF composite (Sample 3-D) produced at 150 °C. ....	245
Figure 173: Strain x stress curve in three-point bending test of 30 PLCL/GF composite (Sample 1-E) produced at 170 °C. ....	245
Figure 174: Strain x stress curve in three-point bending test of 30 PLCL/GF composite (Sample 2-E) produced at 160 °C. ....	246
Figure 175: Strain x stress curve in three-point bending test of 30 PLCL/GF composite (Sample 3-E) produced at 150 °C. ....	246
Figure 176: Strain x stress curve in three-point bending test of PLLA/CF composite (Sample 1-AA). ....	247
Figure 177: Strain x stress curve in three-point bending test of 20 PLCL/GF composite (Sample 1-BB). ....	247
Figure 178: Strain x stress curve in three-point bending test of 30 PLCL/GF composite (Sample 1-CC). ....	248
Figure 179: Strain - stress curves on three-point bending test of PLLA/UD composite. ....	249
Figure 180: Strain - stress curves on three-point bending test of PLLA/TW composite. ....	249
Figure 181: Strain x stress curve on three-point bending of PLLA/TW composite. ....	250
Figure 182: Strain x stress curve on three-point bending of PLLA/UD composite. ....	250
Figure 183: Strain x stress curve on three-point bending of PLLA/GF composite (sample G-1). ....	251

## List of figures

---

Figure 184: Strain x stress curve on three-point bending of 20 PLCL/GF composite (sample G-2). .....	251
Figure 185: Strain x stress curve on three-point bending of 30 PLCL/GF composite (sample G-3). .....	252
Figure 186: Strain x stress curve on three-point bending of PLLA/CF composite (sample C-1). .....	252
Figure 187: Strain x stress curve on three-point bending of 20 PLCL/GF composite (sample C-2). .....	253
Figure 188: Strain x stress curve on three-point bending of 30 PLCL/GF composite (sample C-3). .....	253
Figure 189: Strain x stress curve on three-point bending of PLLA/TW composite (sample F-1). .....	254
Figure 190: Strain x stress curve on three-point bending of PLLA/UD composite (sample F-2). .....	254



## References

- (1) Gay, D.; Hoa, S. V.; Tsai, S. W. *Composite Materials: Design and Applications*; CRC Press LLC, **2003**. <https://doi.org/https://doi.org/10.1201/b17106>.
- (2) Chawla, K. K. *Composite Materials*; Springer New York: New York, NY, **2012**; Vol. 48. <https://doi.org/10.1007/978-0-387-74365-3>.
- (3) Tcherdyntsev, V. V. Reinforced Polymer Composites. *Polymers (Basel)*. **2021**, *13* (4), 564. <https://doi.org/10.3390/polym13040564>.
- (4) Sathishkumar, T. P.; Satheeshkumar, S.; Naveen, J. Glass Fiber-Reinforced Polymer Composites - A Review. *J. Reinf. Plast. Compos.* **2014**, *33* (13), 1258–1275. <https://doi.org/10.1177/0731684414530790>.
- (5) Fiber Reinforced Polymer Market - FRP Composites - Industry Trends & Growth <https://www.mordorintelligence.com/industry-reports/fiber-reinforced-polymer-frp-composites-market> (accessed 2023 -06 -23).
- (6) La Mantia, F. P.; Morreale, M. Green Composites: A Brief Review. *Compos. Part A Appl. Sci. Manuf.* **2011**, *42* (6), 579–588. <https://doi.org/10.1016/j.compositesa.2011.01.017>.
- (7) Chang, B. P.; Mohanty, A. K.; Misra, M. Studies on Durability of Sustainable Biobased Composites: A Review. *RSC Adv.* **2020**, *10* (31), 17955–17999. <https://doi.org/10.1039/C9RA09554C>.
- (8) Kim, J. R.; Sharma, S. The Development and Comparison of Bio-Thermoset Plastics from Epoxidized Plant Oils. *Ind. Crops Prod.* **2012**, *36* (1), 485–499. <https://doi.org/10.1016/j.indcrop.2011.10.036>.
- (9) Gurunathan, T.; Mohanty, S.; Nayak, S. K. A Review of the Recent Developments in Biocomposites Based on Natural Fibres and Their Application Perspectives. *Compos. Part A Appl. Sci. Manuf.* **2015**, *77*, 1–25. <https://doi.org/10.1016/j.compositesa.2015.06.007>.
- (10) Tucker, N. Clean Production. In *Green Composites*; Elsevier, 2017; pp 95–121. <https://doi.org/10.1016/B978-0-08-100783-9.00005-8>.
- (11) Thorpe, B. B. *Citizen 's Guide to Clean Production*; University of Massachusetts, 1999.
- (12) Cousins, D. S.; Suzuki, Y.; Murray, R. E.; Samaniuk, J. R.; Stebner, A. P. Recycling Glass Fiber Thermoplastic Composites from Wind Turbine Blades. *J. Clean. Prod.* **2019**, *209*, 1252–1263. <https://doi.org/10.1016/j.jclepro.2018.10.286>.

- (13) Pegoretti, A. Towards Sustainable Structural Composites: A Review on the Recycling of Continuous-Fiber-Reinforced Thermoplastics. *Adv. Ind. Eng. Polym. Res.* **2021**, *4* (2), 105–115. <https://doi.org/10.1016/j.aiepr.2021.03.001>.
- (14) Tapper, R. J.; Longana, M. L.; Norton, A.; Potter, K. D.; Hamerton, I. An Evaluation of Life Cycle Assessment and Its Application to the Closed-Loop Recycling of Carbon Fibre Reinforced Polymers. *Compos. Part B Eng.* **2020**, *184* (November 2019), 107665. <https://doi.org/10.1016/j.compositesb.2019.107665>.
- (15) Muzzy, J. D.; Kays, A. O. Thermoplastic vs. Thermosetting Structural Composites. *Polym. Compos.* **1984**, *5* (3), 169–172. <https://doi.org/10.1002/pc.750050302>.
- (16) Chung, D. D. L. Polymer-Matrix Composites: Structure and Processing. In *Carbon Composites*; Elsevier, **2017**; pp 161–217. <https://doi.org/10.1016/B978-0-12-804459-9.00003-8>.
- (17) Liu, J.; Zhang, L.; Shun, W.; Dai, J.; Peng, Y.; Liu, X. Recent Development on Bio-Based Thermosetting Resins. *J. Polym. Sci.* **2021**, *59* (14), 1474–1490. <https://doi.org/10.1002/pol.20210328>.
- (18) Ning, H.; Lu, N.; Hassen, A. A.; Chawla, K.; Selim, M.; Pillay, S. A Review of Long Fibre Thermoplastic (LFT) Composites. *Int. Mater. Rev.* **2020**, *65* (3), 164–188. <https://doi.org/10.1080/09506608.2019.1585004>.
- (19) Venkatraman, P.; Gohn, A. M.; Rhoades, A. M.; Foster, E. J. Developing High Performance PA 11/Cellulose Nanocomposites for Industrial-Scale Melt Processing. *Compos. Part B Eng.* **2019**, *174* (May), 106988. <https://doi.org/10.1016/j.compositesb.2019.106988>.
- (20) Wang, G.; Zhang, D.; Wan, G.; Li, B.; Zhao, G. Glass Fiber Reinforced PLA Composite with Enhanced Mechanical Properties, Thermal Behavior, and Foaming Ability. *Polymer (Guildf)*. **2019**, *181* (September). <https://doi.org/10.1016/j.polymer.2019.121803>.
- (21) Sritham, E.; Phunsombat, P.; Chaishome, J. Tensile Properties of PLA/PBAT Blends and PLA Fibre-Reinforced PBAT Composite. *MATEC Web Conf.* **2018**, *192*, 03014. <https://doi.org/10.1051/matecconf/201819203014>.
- (22) Miranda Campos, B.; Bourbigot, S.; Fontaine, G.; Bonnet, F. Thermoplastic Matrix-based Composites Produced by Resin Transfer Molding: A Review. *Polym. Compos.* **2022**, *43* (5), 2485–2506. <https://doi.org/10.1002/pc.26575>.
- (23) Louisy, E.; Samyn, F.; Bourbigot, S.; Fontaine, G.; Bonnet, F. Preparation of Glass

- Fabric/Poly(L-Lactide) Composites by Thermoplastic Resin Transfer Molding. *Polymers (Basel)*. **2019**, *11* (2). <https://doi.org/10.3390/polym11020339>.
- (24) Castro-Aguirre, E.; Iñiguez-Franco, F.; Samsudin, H.; Fang, X.; Auras, R. Poly(Lactic Acid)—Mass Production, Processing, Industrial Applications, and End of Life. *Adv. Drug Deliv. Rev.* **2016**, *107*, 333–366. <https://doi.org/10.1016/j.addr.2016.03.010>.
- (25) Staffa, L. H.; Bettini, S. H. P.; Chinelatto, M. A. Mechanical Properties of PLA/PCL Blends Compatibilized with PEG-b-PCL Multiblock Copolymer. *Macromol. Symp.* **2022**, *406* (1), 1–7. <https://doi.org/10.1002/masy.202200039>.
- (26) Fortelny, I.; Ujcic, A.; Fambri, L.; Slouf, M. Phase Structure, Compatibility, and Toughness of PLA/PCL Blends: A Review. *Front. Mater.* **2019**, *6* (August), 1–13. <https://doi.org/10.3389/fmats.2019.00206>.
- (27) Fernández, J.; Etxeberria, A.; Sarasua, J. R. Synthesis, Structure and Properties of Poly(L-Lactide-Co- $\epsilon$ -Caprolactone) Statistical Copolymers. *J. Mech. Behav. Biomed. Mater.* **2012**, *9*, 100–112. <https://doi.org/10.1016/j.jmbbm.2012.01.003>.
- (28) Zhang, M.; Chang, Z.; Wang, X.; Li, Q. Synthesis of Poly(L-Lactide-Co- $\epsilon$ -Caprolactone) Copolymer: Structure, Toughness, and Elasticity. *Polymers (Basel)*. **2021**, *13* (8). <https://doi.org/10.3390/polym13081270>.
- (29) Karbhari, V. M. Fabrication, Quality and Service-Life Issues for Composites in Civil Engineering. In *Durability of Composites for Civil Structural Applications*; Elsevier, 2007; pp 13–30. <https://doi.org/10.1533/9781845693565.1.13>.
- (30) Friedrich, K.; Fakirov, S.; Zhang, Z. *Polymer Composites: From Nano-to Macro-Scale*; Springer, 2005.
- (31) Radlmaier, V.; Heckel, C.; Winnacker, M.; Erber, A.; Koerber, H. Effects of Thermal Cycling on Polyamides during Processing. *Thermochim. Acta* **2017**, *648*, 44–51. <https://doi.org/10.1016/j.tca.2016.12.011>.
- (32) Liang, J. Z.; Du, Q.; Tsui, G. C. P.; Tang, C. Y. Tensile Properties of Graphene Nano-Platelets Reinforced Polypropylene Composites. *Compos. Part B Eng.* **2016**, *95*, 166–171. <https://doi.org/10.1016/j.compositesb.2016.04.011>.
- (33) Kuboki, T.; Lee, Y. H.; Park, C. B.; Sain, M. Mechanical Properties and Foaming Behavior of Cellulose Fiber Reinforced High-Density Polyethylene Composites. *Polym. Eng. Sci.* **2009**, *49* (11), 2179–2188. <https://doi.org/10.1002/pen.21464>.
- (34) Yan, W.; Han, K. Q.; Qin, L. L.; Yu, M. H. Study on Long Fiber-Reinforced Thermoplastic

- Composites Prepared by in Situ Solid-State Polycondensation. *J. Appl. Polym. Sci.* **2004**, *91* (6), 3959–3965. <https://doi.org/10.1002/app.13627>.
- (35) Studer, J.; Dransfeld, C.; Jauregui Cano, J.; Keller, A.; Wink, M.; Masania, K.; Fiedler, B. Effect of Fabric Architecture, Compaction and Permeability on through Thickness Thermoplastic Melt Impregnation. *Compos. Part A Appl. Sci. Manuf.* **2019**, *122* (November 2018), 45–53. <https://doi.org/10.1016/j.compositesa.2019.04.008>.
- (36) Gong, Y.; Yang, G. All-Polyamide Composites Prepared by Resin Transfer Molding. *J. Mater. Sci.* **2010**, *45* (19), 5237–5243. <https://doi.org/10.1007/s10853-010-4565-6>.
- (37) Murariu, M.; Dubois, P. PLA Composites: From Production to Properties. *Adv. Drug Deliv. Rev.* **2016**, *107*, 17–46. <https://doi.org/10.1016/j.addr.2016.04.003>.
- (38) Yang, Y.; Wang, T.; Wang, S.; Cong, X.; Zhang, S.; Zhang, M.; Luan, J.; Wang, G. Strong Interface Construction of Carbon Fiber–Reinforced PEEK Composites: An Efficient Method for Modifying Carbon Fiber with Crystalline PEEK. *Macromol. Rapid Commun.* **2020**, *41* (24), 1–7. <https://doi.org/10.1002/marc.202000001>.
- (39) Bodaghi, M.; Park, C. H.; Krawczak, P. Reactive Processing of Acrylic-Based Thermoplastic Composites: A Mini-Review. *Front. Mater.* **2022**, *9* (June), 1–8. <https://doi.org/10.3389/fmats.2022.931338>.
- (40) Bartus, S. D.; Vaidya, U. K.; Ulven, C. A. Design and Development of a Long Fiber Thermoplastic Bus Seat. *J. Thermoplast. Compos. Mater.* **2006**, *19* (2), 131–154. <https://doi.org/10.1177/0892705706062184>.
- (41) Andrews, B.; Pillay, S.; Ning, H. Long Fiber Thermoplastic Thin-Walled Baseplates for Missile Applications and Methods of Manufacture. Patent No: US 8,846,189 B1, **2014**.
- (42) Fellingine, F.; Conte, P.; Rametta, R.; Migali, A.; Manni, O.; Barone, L.; Maffezzoli, A. Long Fiber PP-Glass Composites for the Design and Manufacturing of a Recyclable Sail Boat. *WIT Trans. Built Environ.* **2003**, *68*, 49–58.
- (43) Murray, R. E.; Roadman, J.; Beach, R. Fusion Joining of Thermoplastic Composite Wind Turbine Blades: Lap-Shear Bond Characterization. *Renew. Energy* **2019**, *140*, 501–512. <https://doi.org/10.1016/j.renene.2019.03.085>.
- (44) Markarian, J. Long Fibre Reinforced Thermoplastics Continue Growth in Automotive. *Plast. Addit. Compd.* **2007**, *9* (2), 20–23. [https://doi.org/10.1016/S1464-391X\(07\)70025-9](https://doi.org/10.1016/S1464-391X(07)70025-9).
- (45) Gomez, C.; Salvatori, D.; Caglar, B.; Trigueira, R.; Orange, G.; Michaud, V. Resin

- Transfer Molding of High-Fluidity Polyamide-6 with Modified Glass-Fabric Preforms. *Compos. Part A Appl. Sci. Manuf.* **2021**, *147*. <https://doi.org/10.1016/j.compositesa.2021.106448>.
- (46) Ageyeva, T.; Sibikin, I.; Karger-Kocsis, J. Polymers and Related Composites via Anionic Ring-Opening Polymerization of Lactams: Recent Developments and Future Trends. *Polymers (Basel)*. **2018**, *10* (4). <https://doi.org/10.3390/polym10040357>.
- (47) Ilyas, R. A.; Zuhri, M. Y. M.; Aisyah, H. A.; Asyraf, M. R. M.; Hassan, S. A. Natural Fiber-Reinforced Polylactic Acid , Polylactic Acid. **2022**.
- (48) Samir, A.; Ashour, F. H.; Hakim, A. A. A.; Bassyouni, M. Recent Advances in Biodegradable Polymers for Sustainable Applications. *npj Mater. Degrad.* **2022**, *6* (1). <https://doi.org/10.1038/s41529-022-00277-7>.
- (49) Cevahir, A. Glass Fibers. In *Fiber Technology for Fiber-Reinforced Composites*; Elsevier, **2017**; pp 99–121. <https://doi.org/10.1016/B978-0-08-101871-2.00005-9>.
- (50) Asim, M.; Jawaid, M.; Saba, N.; Nasir, M.; Thariq, M.; Sultan, H. *1. Processing of Hybrid Polymer Composites—a Review*, Elsevier Ltd, **2017**. <https://doi.org/10.1016/B978-0-08-100789-1.00001-0>.
- (51) Salvatori, D.; Caglar, B.; Michaud, V. 3D Spacers Enhance Flow Kinetics in Resin Transfer Molding with Woven Fabrics. *Compos. Part A Appl. Sci. Manuf.* **2019**, *119* (October 2018), 206–216. <https://doi.org/10.1016/j.compositesa.2019.01.023>.
- (52) Ahmad, J. *Machining of Polymer Composites*; Springer US: Boston, MA, **2009**. <https://doi.org/10.1007/978-0-387-68619-6>.
- (53) HexForce. HexForce® Reinforcements: Technical Fabrics Handbook, **2017**.
- (54) Durai Prabhakaran, R. T. Are Reactive Thermoplastic Polymers Suitable for Future Wind Turbine Composite Materials Blades? *Mech. Adv. Mater. Struct.* **2014**, *21* (3), 213–221. <https://doi.org/10.1080/15376494.2013.834090>.
- (55) Park, C. H.; Lee, W. I. *Compression Molding in Polymer Matrix Composites*; Woodhead Publishing Limited, **2012**. <https://doi.org/10.1533/9780857096258.1.47>.
- (56) Sims, G. D.; Broughton, W. R. Glass Fiber Reinforced Plastics-Properties. In *Comprehensive Composite Materials*; Elsevier Ltd, **2018**; pp 151–197.
- (57) Newcomb, B. A.; Chae, H. G. The Properties of Carbon Fibers. In *Handbook of Properties of Textile and Technical Fibres*; Elsevier, **2018**; pp 841–871. <https://doi.org/10.1016/B978-0-08-101272-7.00021-3>.

- (58) Fitzer, E. Pan-Based Carbon Fibers—Present State and Trend of the Technology from the Viewpoint of Possibilities and Limits to Influence and to Control the Fiber Properties by the Process Parameters. *Carbon N. Y.* **1989**, 27 (5), 621–645. [https://doi.org/10.1016/0008-6223\(89\)90197-8](https://doi.org/10.1016/0008-6223(89)90197-8).
- (59) Baker, D. A.; Rials, T. G. Recent Advances in Low-Cost Carbon Fiber Manufacture from Lignin. *J. Appl. Polym. Sci.* **2013**, 130 (2), 713–728. <https://doi.org/10.1002/app.39273>.
- (60) Ogale, A. A.; Zhang, M.; Jin, J. Recent Advances in Carbon Fibers Derived from Biobased Precursors. *J. Appl. Polym. Sci.* **2016**, 133 (45), 1–13. <https://doi.org/10.1002/app.43794>.
- (61) More, A. P. Flax Fiber–Based Polymer Composites: A Review. *Adv. Compos. Hybrid Mater.* **2022**, 5 (1), 1–20. <https://doi.org/10.1007/s42114-021-00246-9>.
- (62) Yan, L.; Chouw, N.; Jayaraman, K. Flax Fibre and Its Composites - A Review. *Compos. Part B Eng.* **2014**, 56, 296–317. <https://doi.org/10.1016/j.compositesb.2013.08.014>.
- (63) Kong, C.; Park, H.; Lee, J. Study on Structural Design and Analysis of Flax Natural Fiber Composite Tank Manufactured by Vacuum Assisted Resin Transfer Molding. *Mater. Lett.* **2014**, 130, 21–25. <https://doi.org/10.1016/j.matlet.2014.05.042>.
- (64) Dong, X.; Liu, X.; Hou, Q.; Wang, Z. From Natural Environment to Animal Tissues: A Review of Microplastics(Nanoplastics) Translocation and Hazards Studies. *Sci. Total Environ.* **2023**, 855 (June 2022), 158686. <https://doi.org/10.1016/j.scitotenv.2022.158686>.
- (65) Smith, A. M.; Moxon, S.; Morris, G. A. *Biopolymers as Wound Healing Materials*; Elsevier Ltd, **2016**; Vol. 2. <https://doi.org/10.1016/B978-1-78242-456-7.00013-1>.
- (66) Avérous, L. Synthesis, Properties, Environmental and Biomedical Applications of Polylactic Acid. *Handb. Biopolym. Biodegrad. Plast. Prop. Process. Appl.* **2013**, No. 2008, 171–188. <https://doi.org/10.1016/B978-1-4557-2834-3.00009-4>.
- (67) Skoczinski, P.; Carus, M.; Tweddle, G.; Ruiz, P.; de Guzman, D.; Ravenstijn, J.; Káb, H.; Hark, N.; Dammer, L. *Bio-Based Building Blocks and Polymers – Global Capacities, Production and Trends 2022-2027*; **2023**. <https://doi.org/10.52548/CMZD8323>.
- (68) Rudnik, E. *Biodegradability Testing of Compostable Polymer Materials*; Elsevier, **2013**. <https://doi.org/10.1016/B978-1-4557-2834-3.00011-2>.
- (69) Rudin, A.; Choi, P. Biopolymers. In *The Elements of Polymer Science & Engineering*; Elsevier, **2013**; pp 521–535. <https://doi.org/10.1016/B978-0-12-382178-2.00013-4>.

- (70) Riedel, U. Biocomposites. In *Polymer Science: A Comprehensive Reference*; Elsevier, **2012**; Vol. 1–10, pp 295–315. <https://doi.org/10.1016/B978-0-444-53349-4.00268-5>.
- (71) KUENY, R. Biocomposites : Composites de Hautes Technologies En Renfort de Fibres Naturelles et Matrice de Résines Naturelles, Université de Lorraine, **2013**.
- (72) Inamuddin; Altalhi, T. Handbook of Bioplastics and Biocomposites Engineering Applications. *Handb. Bioplastics Biocomposites Eng. Appl.* **2021**, 1–656. <https://doi.org/10.1002/9781119160182>.
- (73) Jamshidian, M.; Tehrany, E. A.; Imran, M.; Jacquot, M.; Desobry, S. Poly-Lactic Acid: Production, Applications, Nanocomposites, and Release Studies. *Compr. Rev. Food Sci. Food Saf.* **2010**, 9 (5), 552–571. <https://doi.org/10.1111/j.1541-4337.2010.00126.x>.
- (74) Masutani, K.; Kimura, Y. *PLA Synthesis and Polymerization*; **2014**.
- (75) Pang, X.; Zhuang, X.; Tang, Z.; Chen, X. Polylactic Acid (PLA): Research, Development and Industrialization. *Biotechnol. J.* **2010**, 5 (11), 1125–1136. <https://doi.org/10.1002/biot.201000135>.
- (76) Carothers, W. H.; Dorough, G. L.; Natta, F. J. van. Studies of Polymerization and Ring Formation: The Reversible Polymerization of Six-Membered Cyclic Esters. *J. Am. Chem. Soc.* **1932**, 54 (2), 761–772. <https://doi.org/10.1021/ja01341a046>.
- (77) Sin, L. T.; Tveen, B. S. *Polylactic Acid A Practical Guide for the Processing, Manufacturing, and Applications of PLA*; **2019**; Vol. 53.
- (78) Ajioka, M.; Enomoto, K.; Suzuki, K.; Yamaguchi, A. Basic Properties of Polylactic Acid Produced by The. *Bull. Chem. Soc. Jpn.* **1995**, pp 2125–2131.
- (79) Maharana, T.; Mohanty, B.; Negi, Y. S. Melt-Solid Polycondensation of Lactic Acid and Its Biodegradability. *Prog. Polym. Sci.* **2009**, 34 (1), 99–124. <https://doi.org/10.1016/j.progpolymsci.2008.10.001>.
- (80) Cunha, B. L. C.; Bahú, J. O.; Xavier, L. F.; Crivellin, S.; de Souza, S. D. A.; Lodi, L.; Jardini, A. L.; Maciel Filho, R.; Schiavon, M. I. R. B.; Cárdenas Concha, V. O.; Severino, P.; Souto, E. B. Lactide: Production Routes, Properties, and Applications. *Bioengineering* **2022**, 9 (4). <https://doi.org/10.3390/bioengineering9040164>.
- (81) Masutani, K.; Kimura, Y. Chapter 1. PLA Synthesis. From the Monomer to the Polymer. In *Poly(lactic acid) Science and Technology : Processing, Properties, Additives and Applications*; **2014**; pp 1–36. <https://doi.org/10.1039/9781782624806-00001>.
- (82) Ristić, I. S.; Tanasić, L.; Nikolić, L. B.; Cakić, S. M.; Ilić, O. Z.; Radičević, R. Ž.; Budinski-

- Simendić, J. K. The Properties of Poly(l-Lactide) Prepared by Different Synthesis Procedure. *J. Polym. Environ.* **2011**, *19* (2), 419–430. <https://doi.org/10.1007/s10924-011-0297-1>.
- (83) Cheng, Y.; Deng, S.; Chen, P.; Ruan, R. Polylactic Acid (PLA) Synthesis and Modifications: A Review. *Front. Chem. China* **2009**, *4* (3), 259–264. <https://doi.org/10.1007/s11458-009-0092-x>.
- (84) Slomkowski, S.; Penczek, S.; Duda, A. Polylactides-an Overview. *Polym. Adv. Technol.* **2014**, *25* (5), 436–447. <https://doi.org/10.1002/pat.3281>.
- (85) Szuman, K.; Krucińska, I.; Boguń, M.; Draczyński, Z. PLA/PHA-Biodegradable Blends for Pneumothermic Fabrication of Nonwovens. *Autex Res. J.* **2016**, *16* (3), 119–127. <https://doi.org/10.1515/aut-2015-0047>.
- (86) Miranda Campos, B.; Fontaine, G.; Bourbigot, S.; Stoclet, G.; Bonnet, F. Poly(l-Lactide-Co-ε-Caprolactone) Matrix Composites Produced in One Step by In Situ Polymerization in TP-RTM. *ACS Appl. Polym. Mater.* **2022**, *4* (10), 6797–6802. <https://doi.org/10.1021/acsapm.2c01056>.
- (87) Wang, G.; Zhang, D.; Li, B.; Wan, G.; Zhao, G.; Zhang, A. Strong and Thermal-Resistance Glass Fiber-Reinforced Polylactic Acid (PLA) Composites Enabled by Heat Treatment. *Int. J. Biol. Macromol.* **2019**, *129*, 448–459. <https://doi.org/10.1016/j.ijbiomac.2019.02.020>.
- (88) Timeline - Overview for poly(l-lactide-... in Publications - Dimensions [https://app.dimensions.ai/analytics/publication/overview/timeline?search\\_mode=content&year\\_from=2000&year\\_to=2023&search\\_text=poly\(l-lactide-co-e-caprolactone\)&search\\_type=kws&search\\_field=full\\_search](https://app.dimensions.ai/analytics/publication/overview/timeline?search_mode=content&year_from=2000&year_to=2023&search_text=poly(l-lactide-co-e-caprolactone)&search_type=kws&search_field=full_search) (accessed **2023 -01 -09**).
- (89) Wang, L.; Ma, W.; Gross, R. A.; McCarthy, S. P. Reactive Compatibilization of Biodegradable Blends of Poly(Lactic Acid) and Poly(ε-Caprolactone). *Polym. Degrad. Stab.* **1998**, *59* (1–3), 161–168. [https://doi.org/10.1016/S0141-3910\(97\)00196-1](https://doi.org/10.1016/S0141-3910(97)00196-1).
- (90) Iqbal, M. Z.; Abdala, A. A.; Liberatore, M. W. Synthesis and Characterization of Polyethylene/Oxidized Polyethylene Miscible Blends and Role of OPE as a Viscosity Control. *J. Appl. Polym. Sci.* **2016**, *133* (28), 1–11. <https://doi.org/10.1002/app.43521>.
- (91) Ferri, J. M.; Fenollar, O.; Jorda-Vilaplana, A.; García-Sanoguera, D.; Balart, R. Effect of Miscibility on Mechanical and Thermal Properties of Poly(Lactic Acid)/ Polycaprolactone Blends. *Polym. Int.* **2016**, *65* (4), 453–463. <https://doi.org/10.1002/pi.5079>.
- (92) Ostafinska, A.; Fortelny, I.; Nevoralova, M.; Hodan, J.; Kredatusova, J.; Slouf, M.



- Synergistic Effects in Mechanical Properties of PLA/PCL Blends with Optimized Composition, Processing, and Morphology. *RSC Adv.* **2015**, 5 (120), 98971–98982. <https://doi.org/10.1039/c5ra21178f>.
- (93) Botlhoko, O. J.; Ramontja, J.; Ray, S. S. Morphological Development and Enhancement of Thermal, Mechanical, and Electronic Properties of Thermally Exfoliated Graphene Oxide-Filled Biodegradable Polylactide/Poly( $\epsilon$ -Caprolactone) Blend Composites. *Polymer (Guildf)*. **2018**, 139, 188–200. <https://doi.org/10.1016/j.polymer.2018.02.005>.
- (94) Rao, R. U.; Venkatanarayana, B.; Suman, K. N. S. Enhancement of Mechanical Properties of PLA/PCL (80/20) Blend by Reinforcing with MMT Nanoclay. *Mater. Today Proc.* **2019**, 18, 85–97. <https://doi.org/10.1016/j.matpr.2019.06.280>.
- (95) Urquijo, J.; Dagr  ou, S.; Guerrica-Echevarr  a, G.; Eguiaz  bal, J. I. Structure and Properties of Poly(Lactic Acid)/Poly( $\epsilon$ -Caprolactone) Nanocomposites with Kinetically Induced Nanoclay Location. *J. Appl. Polym. Sci.* **2016**, 133 (33), 1–11. <https://doi.org/10.1002/app.43815>.
- (96) Stirling, E.; Champouret, Y.; Visseaux, M. Catalytic Metal-Based Systems for Controlled Statistical Copolymerisation of Lactide with a Lactone. *Polym. Chem.* **2018**, 9 (19), 2517–2531. <https://doi.org/10.1039/c8py00310f>.
- (97) Howarth, J.; Mareddy, S. S. R.; Mativenga, P. T. Energy Intensity and Environmental Analysis of Mechanical Recycling of Carbon Fibre Composite. *J. Clean. Prod.* **2014**, 81, 46–50. <https://doi.org/10.1016/j.jclepro.2014.06.023>.
- (98) Lasprilla, A. J. R.; Martinez, G. A. R.; Lunelli, B. H.; Jardini, A. L.; Filho, R. M. Poly-Lactic Acid Synthesis for Application in Biomedical Devices - A Review. *Biotechnol. Adv.* **2012**, 30 (1), 321–328. <https://doi.org/10.1016/j.biotechadv.2011.06.019>.
- (99) Kramschuster, A.; Turng, L.-S. Fabrication of Tissue Engineering Scaffolds. In *Handbook of Biopolymers and Biodegradable Plastics*; Elsevier, **2013**; pp 427–446. <https://doi.org/10.1016/B978-1-4557-2834-3.00017-3>.
- (100) Schwach, G.; Coudane, J.; Engel, R.; Vert, M. Ring Opening Polymerization of D,L-Lactide in the Presence of Zinc Metal and Zinc Lactate. *Polym. Int.* **1998**, 46 (3), 177–182. [https://doi.org/10.1002/\(SICI\)1097-0126\(199807\)46:3<177::AID-PI937>3.0.CO;2-S](https://doi.org/10.1002/(SICI)1097-0126(199807)46:3<177::AID-PI937>3.0.CO;2-S).
- (101) Darensbourg, D. J.; Karroonnirun, O. Ring-Opening Polymerization of L -Lactide and  $\epsilon$ -Caprolactone Utilizing Biocompatible Zinc Catalysts. Random Copolymerization of  $\epsilon$ -Lactide and  $\epsilon$ -Caprolactone. *Macromolecules* **2010**, 43 (21), 8880–8886.

<https://doi.org/10.1021/ma101784y>.

- (102) Jeong, S. I.; Kim, B.-S.; Lee, Y. M.; Ihn, K. J.; Kim, S. H.; Kim, Y. H. Morphology of Elastic Poly(L-Lactide-Co- $\epsilon$ -Caprolactone) Copolymers and in Vitro and in Vivo Degradation Behavior of Their Scaffolds. *Biomacromolecules* **2004**, *5* (4), 1303–1309. <https://doi.org/10.1021/bm049921i>.
- (103) Fernández, J.; Meaurio, E.; Chaos, A.; Etxeberria, A.; Alonso-Varona, A.; Sarasua, J. R. Synthesis and Characterization of Poly(L-Lactide/ $\epsilon$ -Caprolactone) Statistical Copolymers with Well Resolved Chain Microstructures. *Polymer (Guildf)*. **2013**, *54* (11), 2621–2631. <https://doi.org/10.1016/j.polymer.2013.03.009>.
- (104) De Castro, M. L.; Wang, S. H. Statistical Copolymers of L,L-Lactide and  $\epsilon$ -Caprolactone. *Polym. Bull.* **2003**, *51* (2), 151–158. <https://doi.org/10.1007/s00289-003-0200-x>.
- (105) Liu, X.; Okada, M.; Maeda, H.; Fujii, S.; Furuzono, T. Hydroxyapatite/Biodegradable Poly(L-Lactide–Co- $\epsilon$ -Caprolactone) Composite Microparticles as Injectable Scaffolds by a Pickering Emulsion Route. *Acta Biomater.* **2011**, *7* (2), 821–828. <https://doi.org/10.1016/j.actbio.2010.08.023>.
- (106) Yang, Z.; Peng, H.; Wang, W.; Liu, T. Crystallization Behavior of Poly( $\epsilon$ -Caprolactone)/Layered Double Hydroxide Nanocomposites. *J. Appl. Polym. Sci.* **2010**, *116* (5), 2658–2667. <https://doi.org/10.1002/app>.
- (107) Tainio, J.; Paakinaho, K.; Ahola, N.; Hannula, M.; Hyttinen, J.; Kellomäki, M.; Massera, J. In Vitro Degradation of Borosilicate Bioactive Glass and Poly(L-Lactide-CO- $\epsilon$ -Caprolactone) Composite Scaffolds. *Materials (Basel)*. **2017**, *10* (11), 1–13. <https://doi.org/10.3390/ma10111274>.
- (108) Zhao, T.; Zhang, H.; Li, P.; Liang, J. Effect of Tourmaline Nanoparticles on the Anticoagulation and Cytotoxicity of Poly(L-Lactide- $\epsilon$ -Caprolactone) Electrospun Fibrous Membranes. *RSC Adv.* **2019**, *9* (2), 704–710. <https://doi.org/10.1039/C8RA07700B>.
- (109) Ando, H.; Kawasaki, N.; Yamano, N.; Uegaki, K.; Nakayama, A. Biodegradation of a Poly( $\epsilon$ -Caprolactone-Co-L-Lactide)–Visible-Light-Sensitive TiO<sub>2</sub> Composite with an on/off Biodegradation Function. *Polym. Degrad. Stab.* **2015**, *114*, 65–71. <https://doi.org/10.1016/j.polymdegradstab.2015.02.003>.
- (110) Li, K.; Huang, J.; Gao, H.; Zhong, Y.; Cao, X.; Chen, Y.; Zhang, L.; Cai, J. Reinforced Mechanical Properties and Tunable Biodegradability in Nanoporous Cellulose Gels: Poly(L-Lactide-Co-Caprolactone) Nanocomposites Kai. *Biomacromolecules* **2016**, *17* (4), 1506–1515. <https://doi.org/10.1021/acs.biomac.6b00109>.

- (111) Amirian, M.; Sui, J.; Chakoli, A. N.; Cai, W. Properties and Degradation Behavior of Surface Functionalized MWCNT/Poly(L-Lactide-Co-ε-Caprolactone) Biodegradable Nanocomposites. *J. Appl. Polym. Sci.* **2010**, *122* (5), 3133–3144. <https://doi.org/DOI.10.1002/app.34317>.
- (112) Lu, X. L.; Cai, W.; Gao, Z. Y.; Zhao, L. C. Shape Memory Property of Poly(L-Lactide-Co-ε-Caprolactone) Copolymers. *Mater. Sci. Eng. A* **2006**, *438–440* (SPEC. ISS.), 857–861. <https://doi.org/10.1016/j.msea.2006.04.120>.
- (113) Lu, X. L.; Cai, W.; Gao, Z. Y. Shape-Memory Behaviors of Biodegradable Poly(L-Lactide-Co-ε-Caprolactone) Copolymers. *J. Appl. Polym. Sci.* **2008**, *108* (2), 1109–1115. <https://doi.org/10.1002/app.27703>.
- (114) Amirian, M.; Chakoli, A. N.; Sui, J.; Cai, W. Enhanced Shape Memory Effect of Poly(L-Lactide-Co-ε-Caprolactone) Biodegradable Copolymer Reinforced with Functionalized MWCNTs. *J. Polym. Res.* **2012**, *19* (2), 1–10. <https://doi.org/10.1007/s10965-011-9777-1>.
- (115) Zhang, X.-J.; Yang, Q.-S.; Shang, J.-J.; Liu, X.; Leng, J. The Shape Memory Properties of Multi-Layer Graphene Reinforced Poly(L-Lactide-Co-ε-Caprolactone) by an Atomistic Investigation. *Smart Mater. Struct.* **2021**, *30* (5), 055005. <https://doi.org/10.1088/1361-665X/abeef9>.
- (116) NatureWorks. *Technology Focus Report : Polylactic Acid Containing Fillers and Fibers*; **2007**.
- (117) Pickering, K. L.; Efendy, M. G. A.; Le, T. M. A Review of Recent Developments in Natural Fibre Composites and Their Mechanical Performance. *Compos. Part A Appl. Sci. Manuf.* **2016**, *83*, 98–112. <https://doi.org/10.1016/j.compositesa.2015.08.038>.
- (118) Oksman, K.; Skrifvars, M.; Selin, J.-F. Natural Fibres as Reinforcement in Polylactic Acid (PLA) Composites. *Compos. Sci. Technol.* **2003**, *63* (9), 1317–1324. [https://doi.org/10.1016/S0266-3538\(03\)00103-9](https://doi.org/10.1016/S0266-3538(03)00103-9).
- (119) Bodros, E.; Pillin, I.; Montrelay, N.; Baley, C. Could Biopolymers Reinforced by Randomly Scattered Flax Fibre Be Used in Structural Applications? *Compos. Sci. Technol.* **2007**, *67* (3–4), 462–470. <https://doi.org/10.1016/j.compscitech.2006.08.024>.
- (120) Jaszkievicz, A., Bledzki, A. K., & Franciszczak, P. Improving the Mechanical Performance of PLA Composites with Natural, Man-Made Cellulose and Glass Fibers — a Comparison to PP Counterparts. *Polymer* **2013**, *58* (6), 435–442.
- (121) Ferreira, R. T. L.; Amatte, I. C.; Dutra, T. A.; Bürger, D. Experimental Characterization

- and Micrography of 3D Printed PLA and PLA Reinforced with Short Carbon Fibers. *Compos. Part B Eng.* **2017**, *124*, 88–100. <https://doi.org/10.1016/j.compositesb.2017.05.013>.
- (122) Bochnia, J.; Blasiak, M.; Koziar, T. A Comparative Study of the Mechanical Properties of FDM 3D Prints Made of PLA and Carbon Fiber-Reinforced PLA for Thin-Walled Applications. *Materials (Basel)*. **2021**, *14* (7062), 1–24. <https://doi.org/10.3390/ma14227062>.
- (123) Rudd, C. D.; Long, A. C.; Kendall, K. N.; Mangin, C. G. E. Introduction to Liquid Composite Moulding. *Liq. Mould. Technol.* **1997**, 1–37. <https://doi.org/10.1533/9781845695446.1>.
- (124) Bickerton, S.; Govignon, Q.; Kelly, P. Resin Infusion/Liquid Composite Moulding (LCM) of Advanced Fibre-Reinforced Polymer (FRP). In *Advanced Fibre-Reinforced Polymer (FRP) Composites for Structural Applications*; Elsevier, **2013**; pp 155–186. <https://doi.org/10.1533/9780857098641.2.155>.
- (125) Kenny, J. M.; Nicolais, L. Science and Technology of Polymer Composites Mechanical Properties of Polymeric Matrices. In *Comprehensive Polymer Science and Supplements*; Pergamon Press plc., **1996**; pp 471–525. <https://doi.org/10.1016/B978-0-08-096701-1.00236-6>.
- (126) Chang, I. Y.; Lees, J. K. Recent Development in Thermoplastic Composites: A Review of Matrix Systems and Processing Methods. *J. Thermoplast. Compos. Mater.* **1988**, *1* (3), 277–296. <https://doi.org/10.1177/089270578800100305>.
- (127) Minchenkov, K.; Vedernikov, A.; Safonov, A. Thermoplastic Pultrusion : A Review. **2021**. <https://doi.org/https://doi.org/10.3390/polym13020180>.
- (128) Joshi, S. C. *The Pultrusion Process for Polymer Matrix Composites*; Woodhead Publishing Limited, **2012**. <https://doi.org/10.1533/9780857096258.3.381>.
- (129) Fu, H.; Xu, H.; Liu, Y.; Yang, Z.; Kormakov, S.; Wu, D.; Sun, J. Overview of Injection Molding Technology for Processing Polymers and Their Composites. *ES Mater. Manuf.* **2020**, *8*, 3–23. <https://doi.org/10.30919/esmm5f713>.
- (130) Nunes, J. P.; Silva, J. F. Sandwiched Composites in Aerospace Engineering. In *Advanced Composite Materials for Aerospace Engineering*; Elsevier, **2016**; pp 129–174. <https://doi.org/10.1016/B978-0-08-100037-3.00005-5>.
- (131) Abdurrohman, K.; Siahaan, M. Effect of Mesh-Peel Ply Variation on Mechanical Properties of E-Glas Composite by Infusion Vacuum Method. *J. Phys. Conf. Ser.* **2018**,

1005 (1), 012009. <https://doi.org/10.1088/1742-6596/1005/1/012009>.

- (132) Rudd, C. D.; Long, A. C.; Kendall, K. N.; Mangin, C. G. E. Introduction to Liquid Composite Moulding. In *Liquid Moulding Technologies*; **1997**; pp 1–37. <https://doi.org/10.1533/9781845695446.1>.
- (133) Choi, C. W.; Jin, J. W.; Lee, H.; Huh, M.; Kang, K. W. Optimal Polymerization Conditions in Thermoplastic-Resin Transfer Molding Process for Mechanical Properties of Carbon Fiber-Reinforced PA6 Composites Using the Response Surface Method. *Fibers Polym.* **2019**, *20* (5), 1021–1028. <https://doi.org/10.1007/s12221-019-8901-4>.
- (134) Ageyeva, T.; Sibikin, I.; Kovács, J. G. Review of Thermoplastic Resin Transfer Molding: Process Modeling and Simulation. *Polymers (Basel)*. **2019**, *11* (10). <https://doi.org/10.3390/polym11101555>.
- (135) Boros, R.; Sibikin, I.; Ageyeva, T.; Kovács, J. G. Development and Validation of a Test Mold for Thermoplastic Resin Transfer Molding of Reactive PA-6. *Polymers (Basel)*. **2020**, *12* (4), 1–13. <https://doi.org/10.3390/POLYM12040976>.
- (136) Murray, J. J.; Robert, C.; Gleich, K.; McCarthy, E. D.; Ó Brádaigh, C. M. Manufacturing of Unidirectional Stitched Glass Fabric Reinforced Polyamide 6 by Thermoplastic Resin Transfer Moulding. *Mater. Des.* **2020**, *189*, 108512. <https://doi.org/10.1016/j.matdes.2020.108512>.
- (137) Shojaei, A.; Ghaffarian, S. R.; Karimian, S. M. H. Modeling and Simulation Approaches in the Resin Transfer Molding Process: A Review. *Polym. Compos.* **2003**, *24* (4), 525–544. <https://doi.org/10.1002/pc.10050>.
- (138) Schmidhuber, S.; Fries, E.; Zimmermann, P. It Couldn't Be More Hybrid. *Kunststoffe Int.* **2017**, *107* (1–2), 36–38.
- (139) Friedrich, M.; Exner, W.; Wietgreffe, M. Sensitivity Analysis of Influencing Factors on Impregnation Process of Closed Mould RTM. *CEAS Aeronaut. J.* **2011**, *2* (1–4), 195–202. <https://doi.org/10.1007/s13272-011-0032-6>.
- (140) Matsuzaki, R.; Seto, D.; Todoroki, A.; Mizutani, Y. In Situ Void Content Measurements during Resin Transfer Molding. *Adv. Compos. Mater.* **2013**, *22* (4), 239–254. <https://doi.org/10.1080/09243046.2013.801822>.
- (141) Mehdikhani, M.; Gorbatikh, L.; Verpoest, I.; Lomov, S. V. Voids in Fiber-Reinforced Polymer Composites: A Review on Their Formation, Characteristics, and Effects on Mechanical Performance. *J. Compos. Mater.* **2019**, *53* (12), 1579–1669. <https://doi.org/10.1177/0021998318772152>.

- (142) Rijswijk, K. van; Teuwen, J. J. E.; Bersee, H. E. N.; Beukers, A. Textile Fiber-Reinforced Anionic Polyamide-6 Composites. Part I: The Vacuum Infusion Process. *Compos. Part A Appl. Sci. Manuf.* **2009**, *40* (1), 1–10. <https://doi.org/10.1016/j.compositesa.2008.03.018>.
- (143) Emel, V. N.; Verevkin, S. P.; Pimerzin, A. A. The Thermodynamic Properties of DL and L Lactides. *Russ. J. Phys. Chem. A* **2009**, *83* (December), 2013–2021. <https://doi.org/10.1134/S0036024409120024>.
- (144) Chen, D.; Arakawa, K.; Xu, C. Reduction of Void Content of Vacuum-Assisted Resin Transfer Molded Composites by Infusion Pressure Control. **2015**. <https://doi.org/10.1002/pc>.
- (145) Klunker, F.; Danzi, M.; Ermanni, P. Fiber Deformation as a Result of Fluid Injection: Modeling and Validation in the Case of Saturated Permeability Measurements in through Thickness Direction. *J. Compos. Mater.* **2015**, *49* (9), 1091–1105. <https://doi.org/10.1177/0021998314530766>.
- (146) Potter, K. *RTM Mould Tool Design*; **1997**. [https://doi.org/10.1007/978-94-009-0021-9\\_4](https://doi.org/10.1007/978-94-009-0021-9_4).
- (147) Yu, Y.; Storti, G.; Morbidelli, M. Kinetics of Ring-Opening Polymerization of L-Lactide. *Ind. Eng. Chem. Res.* **2011**, *50* (13), 7927–7940. <https://doi.org/10.1021/ie200117n>.
- (148) Sedush, N. G.; Chvalun, S. N. Kinetics and Thermodynamics of L-Lactide Polymerization Studied by Differential Scanning Calorimetry. *Eur. Polym. J.* **2015**, *62*, 198–203. <https://doi.org/10.1016/j.eurpolymj.2014.11.038>.
- (149) Merhi, D.; Michaud, V.; Kämpfer, L.; Vuilliomenet, P.; Månson, J. A. E. Transverse Permeability of Chopped Fibre Bundle Beds. *Compos. Part A Appl. Sci. Manuf.* **2007**, *38* (3), 739–746. <https://doi.org/10.1016/j.compositesa.2006.09.006>.
- (150) H.Darcy. Les Fontaines Publiques de La Ville de Dijon : Exposition et Application Des Principes à Suivre et Des Formules À [...]. **1865**, 343.
- (151) Koorevaar, A. Controlled vacuum infusion (CVI) technology <http://www.polyworx.com/asp/art090213/> (accessed 2021 -06 -07).
- (152) May, D.; Aktas, A.; Advani, S. G.; Berg, D. C.; Endruweit, A.; Fauster, E.; Lomov, S. V.; Long, A.; Mitschang, P.; Abaimov, S.; Abliz, D.; Akhatov, I.; Ali, M. A.; Allen, T. D.; Bickerton, S.; Bodaghi, M.; Caglar, B.; Caglar, H.; Chiminelli, A.; Correia, N.; Cosson, B.; Danzi, M.; Dittmann, J.; Ermanni, P.; Francucci, G.; George, A.; Grishaev, V.; Hancioglu, M.; Kabachi, M. A.; Kind, K.; Deléglise-Lagardère, M.; Laspalas, M.; Lebedev, O. V.; Lizaranzu, M.; Liotier, P. J.; Middendorf, P.; Morán, J.; Park, C. H.;

- Pipes, R. B.; Pucci, M. F.; Raynal, J.; Rodriguez, E. S.; Schledjewski, R.; Schubnel, R.; Sharp, N.; Sims, G.; Sozer, E. M.; Sousa, P.; Thomas, J.; Umer, R.; Wijaya, W.; Willenbacher, B.; Yong, A.; Zaremba, S.; Ziegmann, G. In-Plane Permeability Characterization of Engineering Textiles Based on Radial Flow Experiments: A Benchmark Exercise. *Compos. Part A Appl. Sci. Manuf.* **2019**, *121* (October 2018), 100–114. <https://doi.org/10.1016/j.compositesa.2019.03.006>.
- (153) Chen, Y. F.; Rodriguez, A.; Minaie, B. A Methodology to Determine Permeability Distribution of a Preform in Resin Transfer Molding Process. *J. Reinf. Plast. Compos.* **2011**, *30* (2), 169–178. <https://doi.org/10.1177/0731684410391511>.
- (154) Kang, M. K.; Lee, W. II; Hahn, H. T. Formation of Microvoids during Resin-Transfer Molding Process. *Compos. Sci. Technol.* **2000**, *60* (12–13), 2427–2434. [https://doi.org/10.1016/S0266-3538\(00\)00036-1](https://doi.org/10.1016/S0266-3538(00)00036-1).
- (155) Bodaghi, M.; Costa, R.; Gomes, R.; Silva, J.; Correia, N.; Silva, F. Experimental Comparative Study of the Variants of High-Temperature Vacuum-Assisted Resin Transfer Moulding. *Compos. Part A Appl. Sci. Manuf.* **2020**, *129* (July 2019). <https://doi.org/10.1016/j.compositesa.2019.105708>.
- (156) van Rijswijk, K.; Bersee, H. E. N. Reactive Processing of Textile Fiber-Reinforced Thermoplastic Composites - An Overview. *Compos. Part A Appl. Sci. Manuf.* **2007**, *38* (3), 666–681. <https://doi.org/10.1016/j.compositesa.2006.05.007>.
- (157) Nuyken, O.; Pask, S. D. Ring-Opening Polymerization-An Introductory Review. *Polymers (Basel)*. **2013**, *5* (2), 361–403. <https://doi.org/10.3390/polym5020361>.
- (158) Jérôme, C.; Lecomte, P. Recent Advances in the Synthesis of Aliphatic Polyesters by Ring-Opening Polymerization. *Adv. Drug Deliv. Rev.* **2008**, *60* (9), 1056–1076. <https://doi.org/10.1016/j.addr.2008.02.008>.
- (159) Semperger, O. V.; Suplicz, A. The Effect of the Parameters of T-RTM on the Properties of Polyamide 6 Prepared by in Situ Polymerization. *Materials (Basel)*. **2019**, *13* (1), 4. <https://doi.org/10.3390/ma13010004>.
- (160) Sibikin, I.; Karger-Kocsis, J. Toward Industrial Use of Anionically Activated Lactam Polymers: Past, Present and Future. *Adv. Ind. Eng. Polym. Res.* **2018**, *1* (1), 48–60. <https://doi.org/10.1016/j.aiepr.2018.06.003>.
- (161) Ó Máirtín, P.; McDonnell, P.; Connor, M. T.; Eder, R.; Ó Brádaigh, C. M. Process Investigation of a Liquid PA-12/Carbon Fibre Moulding System. *Compos. - Part A Appl. Sci. Manuf.* **2001**, *32* (7), 915–923. [https://doi.org/10.1016/S1359-835X\(01\)00005-7](https://doi.org/10.1016/S1359-835X(01)00005-7).

- (162) Ali, U.; Karim, K. J. B. A.; Buang, N. A. A Review of the Properties and Applications of Poly (Methyl Methacrylate) (PMMA). *Polym. Rev.* **2015**, *55* (4), 678–705. <https://doi.org/10.1080/15583724.2015.1031377>.
- (163) Suzuki, Y.; Cousins, D.; Wassgren, J.; Kappes, B. B.; Dorgan, J.; Stebner, A. P. Kinetics and Temperature Evolution during the Bulk Polymerization of Methyl Methacrylate for Vacuum-Assisted Resin Transfer Molding. *Compos. Part A Appl. Sci. Manuf.* **2018**, *104*, 60–67. <https://doi.org/10.1016/j.compositesa.2017.10.022>.
- (164) Pantelelis, N.; Bistekos, E.; Emmerich, R.; Gerard, P.; Zoller, A.; Gallardo, R. R. Compression RTM of Reactive Thermoplastic Composites Using Microwaves and Cure Monitoring. *Procedia CIRP* **2020**, *85*, 246–251. <https://doi.org/10.1016/j.procir.2019.10.005>.
- (165) Geyer, R.; Jambeck, J. R.; Law, K. L. Production, Use, and Fate of All Plastics Ever Made. *Sci. Adv.* **2017**, *3* (7), 25–29. <https://doi.org/10.1126/sciadv.1700782>.
- (166) Labet, M.; Thielemans, W. Synthesis of Polycaprolactone: A Review. *Chem. Soc. Rev.* **2009**, *38* (12), 3484–3504. <https://doi.org/10.1039/b820162p>.
- (167) Hedrick, J. L.; Magbitang, T.; Connor, E. F.; Glauser, T.; Volksen, W.; Hawker, C. J.; Lee, V. Y.; Miller, R. D. Application of Complex Macromolecular Architectures for Advanced Microelectronic Materials. *Chem. - A Eur. J.* **2002**, *8* (15), 3308–3319. [https://doi.org/10.1002/1521-3765\(20020802\)8:15<3308::AID-CHEM3308>3.0.CO;2-D](https://doi.org/10.1002/1521-3765(20020802)8:15<3308::AID-CHEM3308>3.0.CO;2-D).
- (168) Corden, T. J.; Jones, I. A.; Rudd, C. D.; Christian, P.; Downes, S. Initial Development into a Novel Technique for Manufacturing a Long Fibre Thermoplastic Bioabsorbable Composite: In-Situ Polymerisation of Poly- $\epsilon$ -Caprolactone. *Compos. Part A Appl. Sci. Manuf.* **1999**, *30* (6), 737–746. [https://doi.org/10.1016/S1359-835X\(98\)00189-4](https://doi.org/10.1016/S1359-835X(98)00189-4).
- (169) Christian, P.; Jones, I. A.; Rudd, C. D.; Campbell, R. I.; Corden, T. J. Monomer Transfer Moulding and Rapid Prototyping Methods for Fibre Reinforced Thermoplastics for Medical Applications. *Compos. - Part A Appl. Sci. Manuf.* **2001**, *32* (7), 969–976. [https://doi.org/10.1016/S1359-835X\(01\)00009-4](https://doi.org/10.1016/S1359-835X(01)00009-4).
- (170) Rasal, R. M.; Janorkar, A. V.; Hirt, D. E. Poly(Lactic Acid) Modifications. *Prog. Polym. Sci.* **2010**, *35* (3), 338–356. <https://doi.org/10.1016/j.progpolymsci.2009.12.003>.
- (171) Tripathy, A. R.; Chen, W.; Kukureka, S. N.; MacKnight, W. J. Novel Poly(Butylene Terephthalate)/Poly(Vinyl Butyral) Blends Prepared by in Situ Polymerization of Cyclic Poly(Butylene Terephthalate) Oligomers. *Polymer (Guildf)*. **2003**, *44* (6), 1835–1842.



[https://doi.org/10.1016/S0032-3861\(03\)00029-6](https://doi.org/10.1016/S0032-3861(03)00029-6).

- (172) Z.A Mohd, I.; K.G, G.; J.Karger-Kocsis. On the In-Situ Polymerization of Cyclic Butylene Terephthalate Oligomers: DSC and Rheological Studies. *Polym. Eng. Sci.* **2006**, 743–750. <https://doi.org/10.1002/pen>.
- (173) Parton, H.; Baets, J.; Lipnik, P.; Goderis, B.; Devaux, J.; Verpoest, I. Properties of Poly(Butylene Terephthalate) Polymerized from Cyclic Oligomers and Its Composites. *Polymer (Guildf)*. **2005**, 46 (23), 9871–9880. <https://doi.org/10.1016/j.polymer.2005.07.082>.
- (174) Yan, C.; Liu, L.; Zhu, Y.; Xu, H.; Liu, D. Properties of Polymerized Cyclic Butylene Terephthalate and Its Composites via Ring-Opening Polymerization. *J. Thermoplast. Compos. Mater.* **2018**, 31 (2), 181–201. <https://doi.org/10.1177/0892705717697774>.
- (175) Parton, H.; Verpoest, I. In Situ Polymerization of Thermoplastic Composites Based on Cyclic Oligomers. *Polym. Compos.* **2005**, 26 (1), 60–65. <https://doi.org/10.1002/pc.20074>.
- (176) Caprolactam price index - businessanalytiq  
<https://businessanalytiq.com/procurementanalytics/index/caprolactam-price-index/>  
(accessed 2023 -08 -09).
- (177) Ricco, L.; Russo, S.; Orefice, G.; Riva, F. Caprolactam-Laurolactam Copolymers: Fast Activated Anionic Synthesis, Thermal Properties and Structural Investigations. *Macromol. Chem. Phys.* **2001**, 202 (10), 2114–2121. [https://doi.org/10.1002/1521-3935\(20010601\)202:10<2114::AID-MACP2114>3.0.CO;2-F](https://doi.org/10.1002/1521-3935(20010601)202:10<2114::AID-MACP2114>3.0.CO;2-F).
- (178) Kim, I.; White, J. L. Reactive Copolymerization of Various Monomers Based on Lactams and Lactones in a Twin-Screw Extruder. *J. Appl. Polym. Sci.* **2005**, 96 (5), 1875–1887. <https://doi.org/10.1002/app.21494>.
- (179) Auclerc, M.; Sahyoun, J.; Tauleigne, A.; Da Cruz-Boisson, F.; Vanhille Bergeron, A.; Garois, N.; Cassagnau, P.; Bounor-Legaré, V. Development of Copolyamide-66/6 Cross-Linked Foams by a One-Step Reactive Extrusion Process. *Ind. Eng. Chem. Res.* **2019**, 58 (27), 11750–11762. <https://doi.org/10.1021/acs.iecr.9b00312>.
- (180) Puffr, R.; Stehliceck, J.; Kovarova, J. Block Copolymers of Hexano-6-Lactam with N - Methylated Aliphatic ( Co ) Polyamides. *Polymer (Guildf)*. **2000**, 41, 3111–3120.
- (181) Herzog, J.; Wendel, R.; Weidler, P. G.; Wilhelm, M.; Rosenberg, P.; Henning, F. Moisture Adsorption and Desorption Behavior of Raw Materials for the T-Rtm Process. *J. Compos. Sci.* **2021**, 5 (1), 1–9. <https://doi.org/10.3390/jcs5010012>.

- (182) Kouparitsas, C. E.; Kartalis, C. N.; Varelidis, P. C.; Tsenoglou, C. J.; Papaspyrides, C. D. Recycling of the Fibrous Fraction of Reinforced Thermoset Composites. *Polym. Compos.* **2002**, 23 (4), 682–689. <https://doi.org/10.1002/pc.10468>.
- (183) Li, X.; Bai, R.; McKechnie, J. Environmental and Financial Performance of Mechanical Recycling of Carbon Fibre Reinforced Polymers and Comparison with Conventional Disposal Routes. *J. Clean. Prod.* **2016**, 127 (2016), 451–460. <https://doi.org/10.1016/j.jclepro.2016.03.139>.
- (184) Li, M. X.; Lee, D.; Lee, G. H.; Kim, S. M.; Ben, G.; Lee, W. II; Choi, S. W. Effect of Temperature on the Mechanical Properties and Polymerization Kinetics of Polyamide-6 Composites. *Polymers (Basel)*. **2020**, 12 (5), 1–20. <https://doi.org/10.3390/POLYM12051133>.
- (185) Brüggemann Chemical. Ap-nylon® additives [https://www.brueggemann.com/\\_Resources/Persistent/e9946d7a55dde1180d6f744b90746cd2c91a2593/BRU\\_\\_\\_ApNylonAdditives\\_ENG\\_2016\\_Web\\_03.pdf](https://www.brueggemann.com/_Resources/Persistent/e9946d7a55dde1180d6f744b90746cd2c91a2593/BRU___ApNylonAdditives_ENG_2016_Web_03.pdf) (accessed 2021 -09 -07).
- (186) Bhudolia, S. K.; Joshi, S. C.; Bert, A.; Yi Di, B.; Makam, R.; Gohel, G. Flexural Characteristics of Novel Carbon Methylmethacrylate Composites. *Compos. Commun.* **2019**, 13 (December 2018), 129–133. <https://doi.org/10.1016/j.coco.2019.04.007>.
- (187) Arkema. Liquid thermoplastic resin for tougher composites <https://www.arkema-america.com/export/shared/.content/media/downloads/products-documentations/incubator/brochure-elium-2017.pdf> (accessed 2021 -09 -10).
- (188) Abt, T.; Sánchez-Soto, M. A Review of the Recent Advances in Cyclic Butylene Terephthalate Technology and Its Composites. *Crit. Rev. Solid State Mater. Sci.* **2017**, 42 (3), 173–217. <https://doi.org/10.1080/10408436.2016.1160820>.
- (189) Polymer, C.; Pbt, P. T. Cyclics CBT ® 100 Thermoplastic Resin Contact Songhan Plastic Technology Co., Ltd. [http://www.lookpolymers.com/polymer\\_Cyclics-CBT-100-Thermoplastic-Resin.php](http://www.lookpolymers.com/polymer_Cyclics-CBT-100-Thermoplastic-Resin.php) (accessed 2021 -09 -10).
- (190) Farah, S.; Anderson, D. G.; Langer, R. Physical and Mechanical Properties of PLA, and Their Functions in Widespread Applications — A Comprehensive Review. *Adv. Drug Deliv. Rev.* **2016**, 107, 367–392. <https://doi.org/10.1016/j.addr.2016.06.012>.
- (191) Herbert, I. R. *NMR Spectroscopy of Polymers*, 1st ed.; Ibbet, R. N., Ed.; Chapman & Hall, 1993. <https://doi.org/10.1007/978-94-011-2150-7>.
- (192) Kricheldorf, H. R.; Weidner, S. M. Polymerization of L-Lactide with SnCl<sub>2</sub>: A Low Toxic

- and Eco-Friendly Catalyst. *J. Polym. Environ.* **2021**, *29* (8), 2504–2516. <https://doi.org/10.1007/s10924-020-02042-w>.
- (193) Kricheldorf, H. R.; Weidner, S. M.; Scheliga, F. SnOct<sub>2</sub>-Catalyzed and Alcohol-Initiated ROPS of L-Lactide—Control of the Molecular Weight and the Role of Cyclization. *Macromol. Chem. Phys.* **2022**, *223* (6), 1–10. <https://doi.org/10.1002/macp.202100464>.
- (194) Kowalski, A.; Duda, A.; Penczek, S. Polymerization of L,L-Lactide Initiated by Aluminum Isopropoxide Trimer or Tetramer. *Macromolecules* **1998**, *31* (7), 2114–2122. <https://doi.org/10.1021/ma971737k>.
- (195) Save, M.; Soum, A. Controlled Ring-Opening Polymerization of Lactones and Lactide Initiated by Lanthanum Isopropoxide, 2. *Macromol. Chem. Phys.* **2002**, *203* (18), 2591–2603. <https://doi.org/10.1002/macp.200290043>.
- (196) Meimoun, J.; Sutapin, C.; Stoclet, G.; Favrelle, A.; Roussel, P.; Bria, M.; Chirachanchai, S.; Bonnet, F.; Zinck, P. Lactide Lactone Chain Shuttling Copolymerization Mediated by an Aminobisphenolate Supported Aluminum Complex and Al(O<sup>i</sup>Pr)<sub>3</sub>: Access to New Polylactide Based Block Copolymers. *J. Am. Chem. Soc.* **2021**, *143* (50), 21206–21210. <https://doi.org/10.1021/jacs.1c09744>.
- (197) E. W. Fischer, Hans J. Sterzel, and G. W. Investigation of the Structure of Solution Grown Crystals of Lactide Copolymers by Means of Chemical Reactions By. *Kolloid-Zeitschrift und Zeitschrift für Polym.* **1973**, *251*, 980–990.
- (198) Prirodno-, N. S.; Vrane, M. Fizičko - Hemijska Karakterizacija Binarnih Smeša Jonskih Tečnosti i Laktona i Njihova Primena Kao Elektrolita Za Litijum-Jonske Baterije, Univerzitet u Novom Sadu, **2018**.
- (199) Louisy, E.; Samyn, F.; Bourbigot, S.; Fontaine, G.; Bonnet, F. Preparation of Glass Fabric/Poly(L-Lactide) Composites by Thermoplastic Resin Transfer Molding. *Polymers (Basel)*. **2019**, *11* (2), 339. <https://doi.org/10.3390/polym11020339>.
- (200) Louisy, E.; Sp, D.; Bonnet, F.; Ga, P.; Pr, F.; Directrice, R. R.; Universit, F. B.; Cnrs, B. S.; Universit, L. S.; Ecole, L.; Sup, N.; Sup, E. N.; Sup, E. N.; Prof, C.; Samyn, F. Synthèse de Composites à Matrice Polylactide Par Procédé RTM (Resin Transfer Molding), Université de Lille, **2019**.
- (201) Kricheldorf, H. R.; Jonti, J. M.; Berl, M. Polylactones 3. Copolymerization of Glycolide with L, L-lactide and Other Lactones. *Die Makromol. Chemie* **1985**, *38* (12), 25–38.
- (202) Fernández, J.; Etxeberria, A.; Ugartemendia, J. M.; Petisco, S.; Sarasua, J. R. Effects

- of Chain Microstructures on Mechanical Behavior and Aging of a Poly(L-Lactide-Co- $\epsilon$ -Caprolactone) Biomedical Thermoplastic-Elastomer. *J. Mech. Behav. Biomed. Mater.* **2012**, *12*, 29–38. <https://doi.org/10.1016/j.jmbbm.2012.03.008>.
- (203) Kricheldorf, H. R.; Sumbé, M. V.; Kreiser-Saunders, I. Polylactones. 20. Polymerization of  $\epsilon$ -Caprolactone with Tributyltin Derivatives: A Mechanistic Study. *Macromolecules* **1991**, *24* (8), 1944–1949. <https://doi.org/10.1021/ma00008a035>.
- (204) Fernández, J.; Etxeberría, A.; Sarasua, J. R. Effects of Repeat Unit Sequence Distribution and Residual Catalyst on Thermal Degradation of Poly(l-Lactide/ $\epsilon$ -Caprolactone) Statistical Copolymers. *Polym. Degrad. Stab.* **2013**, *98* (7), 1293–1299. <https://doi.org/10.1016/j.polymdegradstab.2013.04.003>.
- (205) K. Nalampang; Molloy, R.; Punyodom, W. Synthesis and Characterization of Poly(L-Lactide-Co- $\epsilon$ -Caprolactone) Copolymers: Influence of Sequential Monomer Addition on Chain Microstructure. *Polym. Adv. Technol.* **2008**, No. November 2007, 229–236. <https://doi.org/10.1002/pat>.
- (206) Jamshidi, K.; Hyon, S.-H.; Ikada, Y. Thermal Characterization of Polylactides. *Polymer (Guildf)*. **1988**, *29* (12), 2229–2234. [https://doi.org/10.1016/0032-3861\(88\)90116-4](https://doi.org/10.1016/0032-3861(88)90116-4).
- (207) Sivalingam, G.; Madras, G. Thermal Degradation of Binary Physical Mixtures and Copolymers of Poly( $\epsilon$ -Caprolactone), Poly(d, l-Lactide), Poly(Glycolide). *Polym. Degrad. Stab.* **2004**, *84* (3), 393–398. <https://doi.org/10.1016/j.polymdegradstab.2003.12.008>.
- (208) Mark, J. E. *The Polymer Data Handbook*, **2009**; Vol. 131.
- (209) Zuza, E.; Meaurio, E.; Sarasua, J.-R. Biodegradable Polylactide-Based Composites. In *Composites from Renewable and Sustainable Materials*; InTech, **2016**. <https://doi.org/10.5772/65468>.
- (210) Nunes, R. W.; Martin, J. R.; Johnson, J. F. Influence of Molecular Weight and Molecular Weight Distribution on Mechanical Properties of Polymers. **1982**, *22* (4).
- (211) Kadiyala, A. K.; Devlin, K.; Lee, S.; Comer, A. Evaluation of the Flexural Properties and Failure Evolution of a Hybrid Composite Manufactured by Automated Dry Fibre Placement Followed by Liquid Resin Infusion. *Compos. Part A Appl. Sci. Manuf.* **2022**, *154*, 106764. <https://doi.org/10.1016/j.compositesa.2021.106764>.
- (212) Deokar, M. D.; Idage, S. B.; Idage, B. B.; Sivaram, S. Synthesis and Characterization of Well-Defined Random and Block Copolymers of  $\epsilon$ -Caprolactone with L-Lactide as an

- Additive for Toughening Polylactide: Influence of the Molecular Architecture. *J. Appl. Polym. Sci.* **2016**, 133 (14), n/a-n/a. <https://doi.org/10.1002/app.43267>.
- (213) Kenney, J. F. Properties of Block versus Random Copolymers. *Polym. Eng. Sci.* **1968**, 8 (3), 216–226. <https://doi.org/10.1002/pen.760080307>.
- (214) Sharma, M.; Gao, S.; Mäder, E.; Sharma, H.; Wei, L. Y.; Bijwe, J. Carbon Fiber Surfaces and Composite Interphases. *Compos. Sci. Technol.* **2014**, 102, 35–50. <https://doi.org/10.1016/j.compscitech.2014.07.005>.
- (215) Wu, F.; Yang, S.; Huang, L.; Hu, J.; Li, G.; Chen, H.; Fang, H. In Situ Preparation of Carbon Fiber Fabric Reinforced Poly(Lactic Acid) Composites by Vacuum-Assisted Resin Transfer Molding. *Polym. Compos.* **2023**, No. April, 1–8. <https://doi.org/10.1002/pc.27378>.
- (216) Sanivada, U. K.; Mármol, G.; Brito, F. P.; Figueiro, R. PLA Composites Reinforced with Flax and Jute Fibers—a Review of Recent Trends, Processing Parameters and Mechanical Properties. *Polymers (Basel)*. **2020**, 12 (10), 1–29. <https://doi.org/10.3390/polym12102373>.
- (217) In focus: an economic overview of flax in 2022 | ALLIANCE <https://allianceflaxlinenhemp.eu/en/flax-linen-economic-observatory> (accessed 2023 - 07 -26).
- (218) Ehsanimehr, S.; Sonnier, R.; Badawi, M.; Ducos, F.; Kadi, N.; Skrifvars, M.; Saeb, M. R.; Vahabi, H. Sustainable Flame-Retardant Flax Fabrics by Engineered Layer-by-Layer Surface Functionalization with Phytic Acid and Polyethylenimine. *Fire Technol.* **2023**. <https://doi.org/10.1007/s10694-023-01387-7>.
- (219) Georgiopoulos, P.; Kontou, E.; Georgousis, G. Effect of Silane Treatment Loading on the Flexural Properties of PLA/Flax Unidirectional Composites. *Compos. Commun.* **2018**, 10 (October 2017), 6–10. <https://doi.org/10.1016/j.coco.2018.05.002>.
- (220) Baley, C.; Le Duigou, A.; Bourmaud, A.; Davies, P. Influence of Drying on the Mechanical Behaviour of Flax Fibres and Their Unidirectional Composites. *Compos. Part A Appl. Sci. Manuf.* **2012**, 43 (8), 1226–1233. <https://doi.org/10.1016/j.compositesa.2012.03.005>.
- (221) Shenoy Heckadka, S.; Pai Ballambat, R.; Bhagavath, P.; Kini, M. V.; Sinha, R. K.; Sonali, M. ; Sen, D. Thermogravimetric Analysis of Flax, Jute, and UHMWPE Fibers and Their Composites with Melamine and Phenol Formaldehyde Resins. *Cogent Eng.* **2023**, 10 (1). <https://doi.org/10.1080/23311916.2023.2209990>.

- (222) Waters, C. L.; Janupala, R. R.; Mallinson, R. G.; Lobban, L. L. Staged Thermal Fractionation for Segregation of Lignin and Cellulose Pyrolysis Products: An Experimental Study of Residence Time and Temperature Effects. *J. Anal. Appl. Pyrolysis* **2017**, *126* (May), 380–389. <https://doi.org/10.1016/j.jaap.2017.05.008>.
- (223) Van De Velde, K.; Kiekens, P. Thermal Degradation of Flax: The Determination of Kinetic Parameters with Thermogravimetric Analysis. *J. Appl. Polym. Sci.* **2002**, *83* (12), 2634–2643. <https://doi.org/10.1002/app.10229>.
- (224) Pereira, P.; Ferreira, D. P.; Araújo, J. C.; Ferreira, A.; Figueiro, R. The Potential of Graphene Nanoplatelets in the Development of Smart and Multifunctional Ecocomposites. *Polymers (Basel)*. **2020**, *12* (10), 2189. <https://doi.org/10.3390/polym12102189>.
- (225) Yang, H.; Yan, R.; Chen, H.; Lee, D. H.; Zheng, C. Characteristics of Hemicellulose, Cellulose and Lignin Pyrolysis. *Fuel* **2007**, *86* (12–13), 1781–1788. <https://doi.org/10.1016/j.fuel.2006.12.013>.
- (226) Kowalski, A.; Libiszowski, J.; Duda, A.; Penczek, S. Polymerization of L, L-Dilactide Initiated by Tin(II) Butoxide. *Macromolecules* **2000**, *33* (6), 1964–1971. <https://doi.org/10.1021/ma991751s>.
- (227) Akonda, M.; Alimuzzaman, S.; Shah, D. U.; Rahman, A. N. M. M. Physico-Mechanical, Thermal and Biodegradation Performance of Random Flax/Poly(lactic Acid) and Unidirectional Flax/Poly(lactic Acid) Biocomposites. *Fibers* **2018**, *6* (4). <https://doi.org/10.3390/fib6040098>.
- (228) Kanakannavar, S.; Pitchaimani, J. Fabrication and Mechanical Properties of Braided Flax Fabric Poly(lactic Acid) Bio-Composites. *J. Text. Inst.* **2022**, *113* (5), 833–845. <https://doi.org/10.1080/00405000.2021.1907958>.
- (229) Pornwannachai, W.; Horrocks, A. R.; Kandola, B. K. Surface Modification of Commingled Flax/PP and Flax/PLA Fibres by Silane or Atmospheric Argon Plasma Exposure to Improve Fibre–Matrix Adhesion in Composites. *Fibers* **2021**, *10* (1), 2. <https://doi.org/10.3390/fib10010002>.
- (230) Gardette, M.; Thérias, S.; Gardette, J. L.; Murariu, M.; Dubois, P. Photooxidation of Poly(lactide)/Calcium Sulphate Composites. *Polym. Degrad. Stab.* **2011**, *96* (4), 616–623. <https://doi.org/10.1016/j.polymdegradstab.2010.12.023>.
- (231) Tsuji, H.; Echizen, Y.; Saha, S. K.; Nishimura, Y. Photodegradation of Poly(L-Lactic Acid): Effects of Photosensitizer. *Macromol. Mater. Eng.* **2005**, *290* (12), 1192–1203.

<https://doi.org/10.1002/mame.200500278>.

- (232) Tsuji, H.; Echizen, Y.; Nishimura, Y. Photodegradation of Biodegradable Polyesters: A Comprehensive Study on Poly(L-Lactide) and Poly( $\epsilon$ -Caprolactone). *Polym. Degrad. Stab.* **2006**, *91* (5), 1128–1137. <https://doi.org/10.1016/j.polymdegradstab.2005.07.007>.
- (233) Copinet, A.; Bertrand, C.; Govindin, S.; Coma, V.; Couturier, Y. Effects of Ultraviolet Light (315 Nm), Temperature and Relative Humidity on the Degradation of Polylactic Acid Plastic Films. *Chemosphere* **2004**, *55* (5), 763–773. <https://doi.org/10.1016/j.chemosphere.2003.11.038>.
- (234) Lesaffre, N.; Bellayer, S.; Vezin, H.; Fontaine, G.; Jimenez, M.; Bourbigot, S. Recent Advances on the Ageing of Flame Retarded PLA: Effect of UV-Light and/or Relative Humidity. *Polym. Degrad. Stab.* **2017**, *139*, 143–164. <https://doi.org/10.1016/j.polymdegradstab.2017.04.007>.
- (235) Larché, J.-F.; Bussière, P.-O.; Thérias, S.; Gardette, J.-L. Photooxidation of Polymers: Relating Material Properties to Chemical Changes. *Polym. Degrad. Stab.* **2012**, *97* (1), 25–34. <https://doi.org/10.1016/j.polymdegradstab.2011.10.020>.
- (236) Müller, P.; Imre, B.; Bere, J.; Móczó, J.; Pukánszky, B. Physical Ageing and Molecular Mobility in PLA Blends and Composites. *J. Therm. Anal. Calorim.* **2015**, *122* (3), 1423–1433. <https://doi.org/10.1007/s10973-015-4831-6>.
- (237) Zaidi, L.; Kaci, M.; Bruzard, S.; Bourmaud, A.; Grohens, Y. Effect of Natural Weather on the Structure and Properties of Polylactide/Cloisite 30B Nanocomposites. *Polym. Degrad. Stab.* **2010**, *95* (9), 1751–1758. <https://doi.org/10.1016/j.polymdegradstab.2010.05.014>.
- (238) Abdullah, S. A.; Jumahat, A.; Abdullah, N. R.; Frommann, L. Determination of Shape Fixity and Shape Recovery Rate of Carbon Nanotube-Filled Shape Memory Polymer Nanocomposites. *Procedia Eng.* **2012**, *41* (Iris), 1641–1646. <https://doi.org/10.1016/j.proeng.2012.07.362>.
- (239) Kovács, Z.; Pomázi, Á.; Toldy, A. The Flame Retardancy of Polyamide 6—Prepared by in Situ Polymerisation of  $\epsilon$ -Caprolactam—for T-RTM Applications. *Polym. Degrad. Stab.* **2021**, *195*, 109797. <https://doi.org/10.1016/j.polymdegradstab.2021.109797>.
- (240) RTP Company's Glass Fiber-Reinforced PLA Bioplastic Compounds Improve Strength and Thermal Performance - Renewable Carbon News <https://renewable-carbon.eu/news/rtp-companys-glass-fiber-reinforced-pla-bioplastic-compounds-improve-strength-and-thermal-performance/> (accessed 2023 -08 -21).

- (241) Akampumuza, O.; Wambua, P. M.; Ahmed, A.; Li, W.; Qin, X. H. Review of the Applications of Biocomposites in the Automotive Industry. *Polym. Compos.* **2017**, *38* (11), 2553–2569. <https://doi.org/10.1002/pc.23847>.



## Appendix

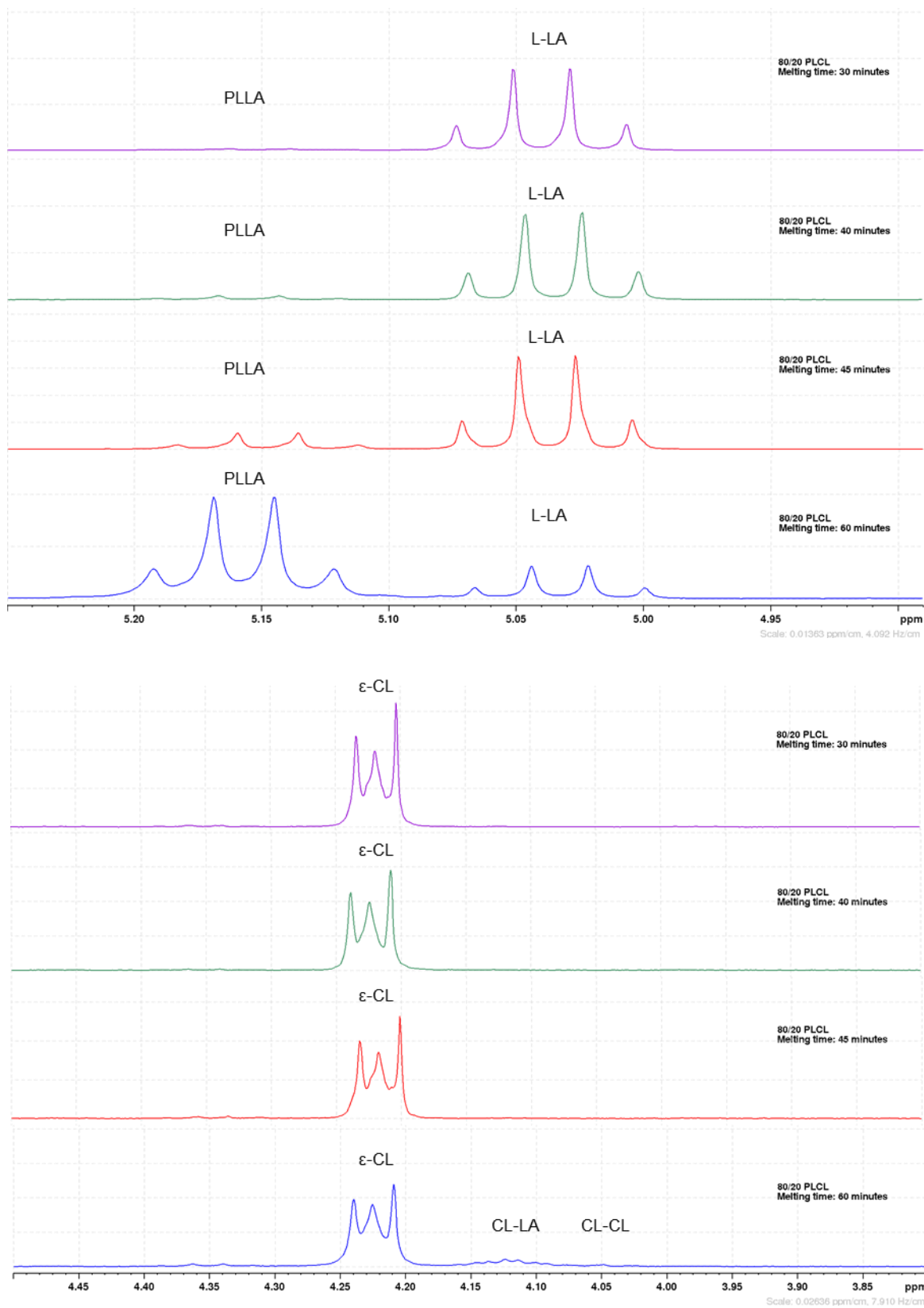
6.8 Glass fabric reinforced composites –<sup>1</sup>H NMR spectra of PLLA and PLCL matrices.

Figure 120:  $^1\text{H}$  NMR spectra of the reactive system at different melting temperatures ( $\text{CDCl}_3$ , 300 MHz).

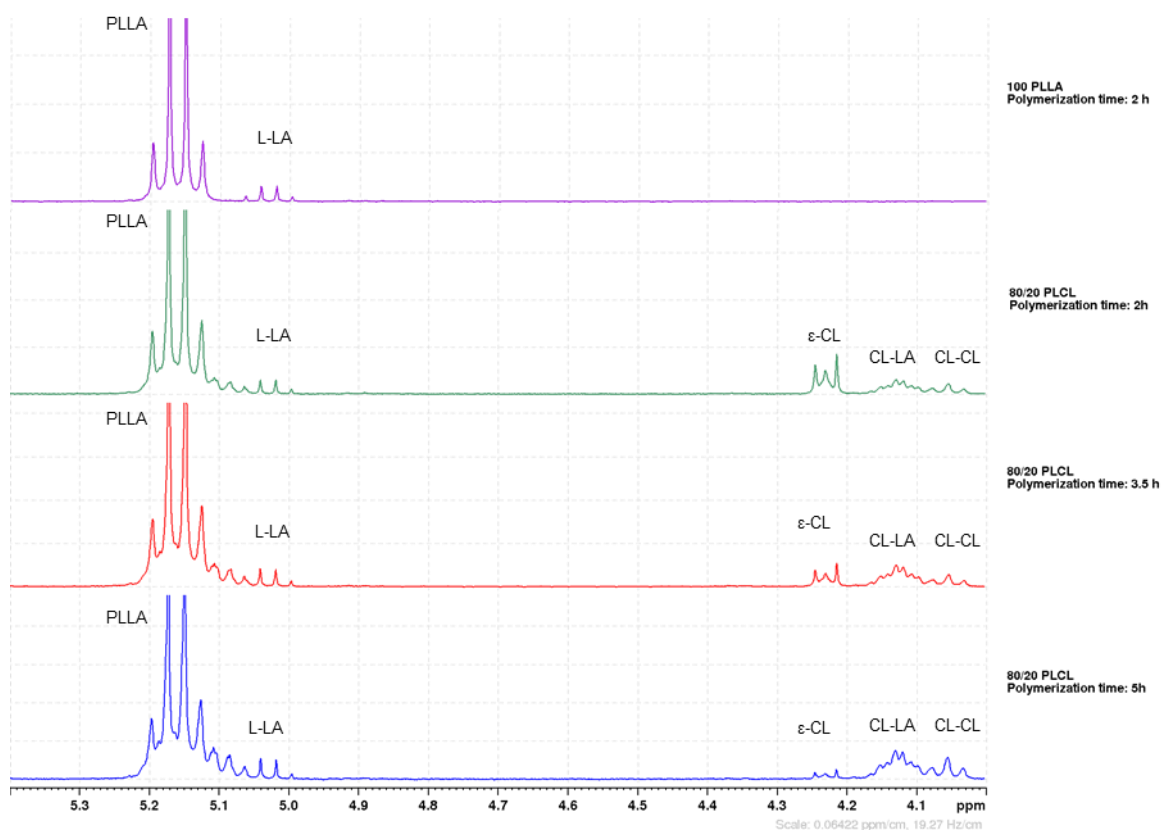


Figure 121:  $^1\text{H}$  NMR spectra of pure PLLA and 20 PLCL synthesized at different polymerization temperatures ( $\text{CDCl}_3$ , 300 MHz).

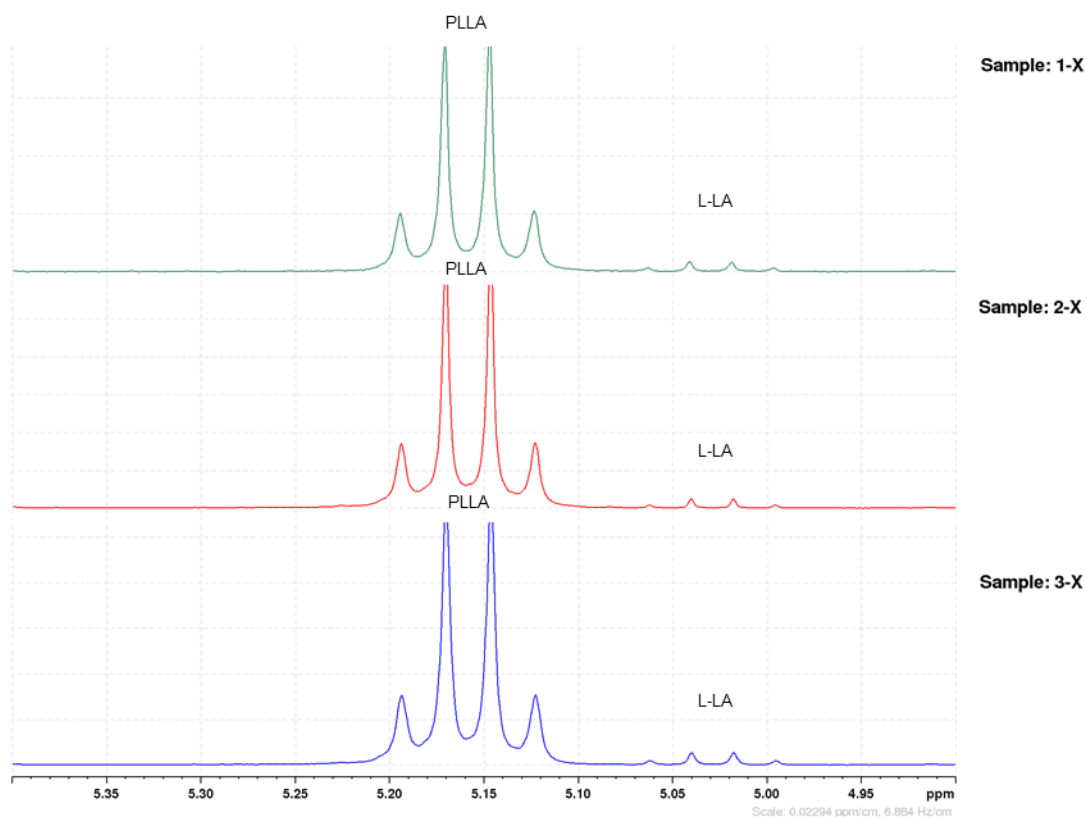


Figure 122:  $^1\text{H}$  NMR spectra of PLLA matrices showing the peaks corresponding to L-LA and PLLA ( $\text{CDCl}_3$ , 300 MHz).

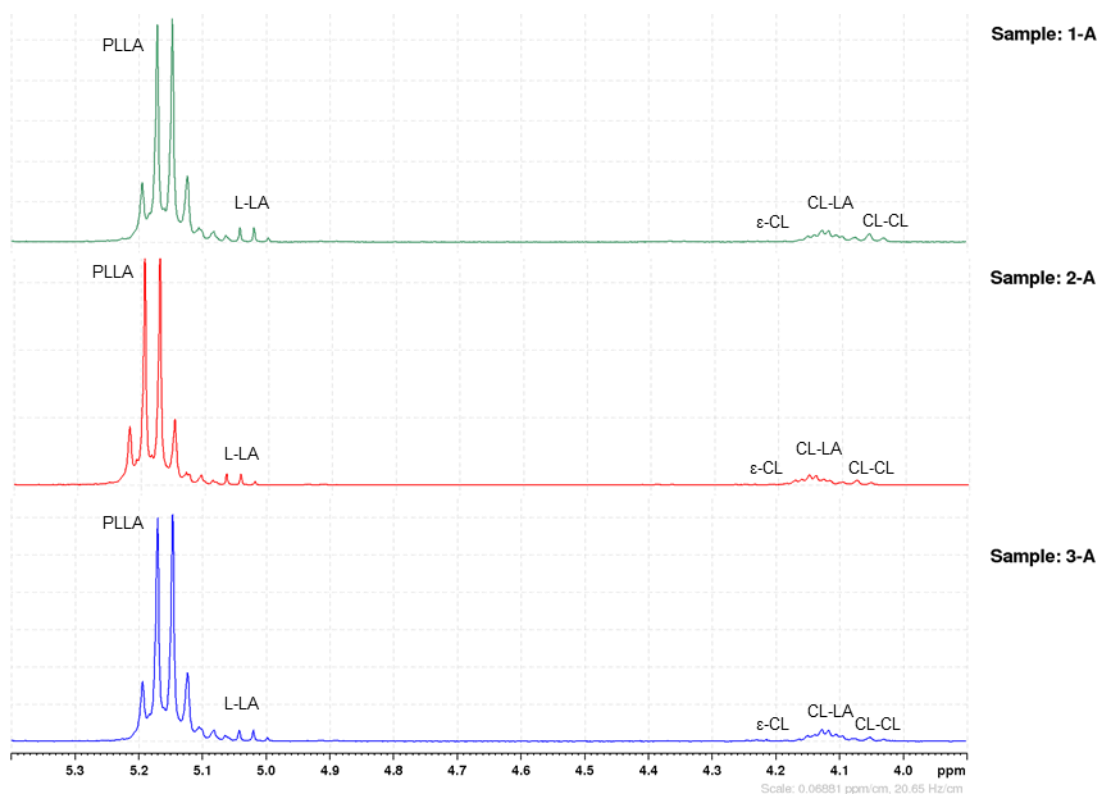


Figure 123:  $^1\text{H}$  NMR spectra of 10 PLCL matrices showing the peaks corresponding to  $\epsilon$ -CL, PLCL, L-LA and PLLA ( $\text{CDCl}_3$ , 300 MHz).

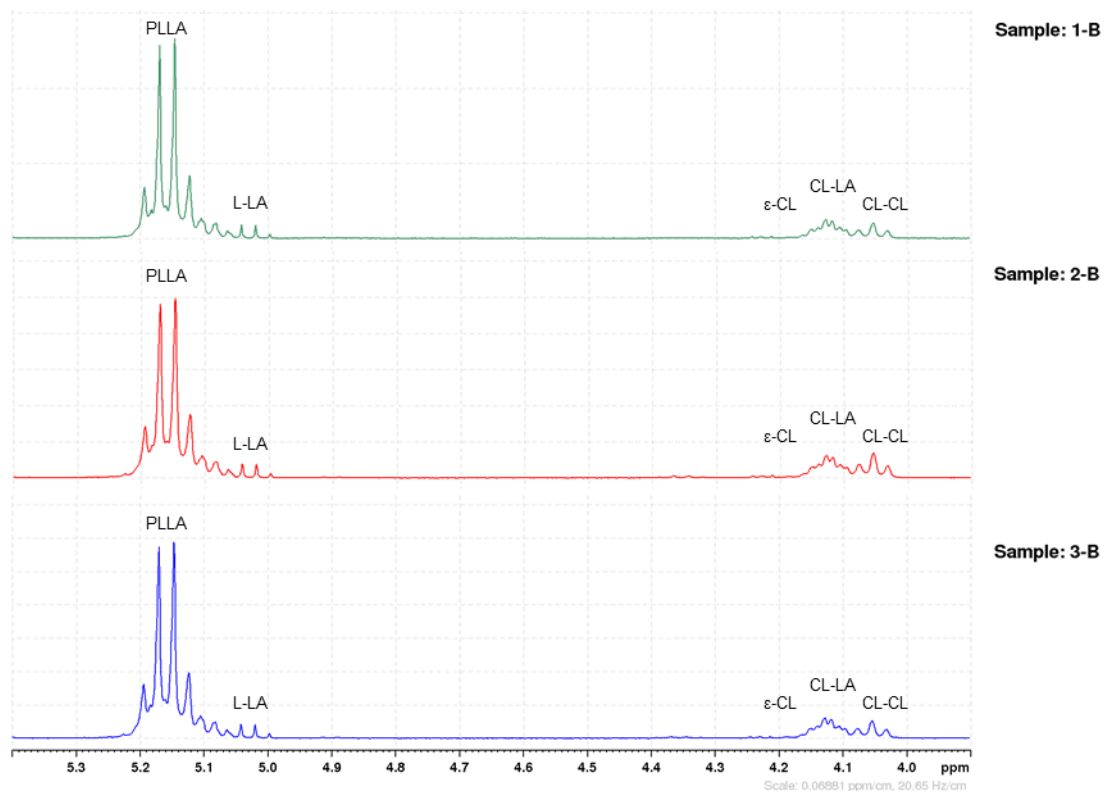


Figure 124:  $^1\text{H}$  NMR spectra of 20 PLCL matrices showing the peaks corresponding to  $\epsilon$ -CL, PLCL, L-LA and PLLA ( $\text{CDCl}_3$ , 300 MHz).

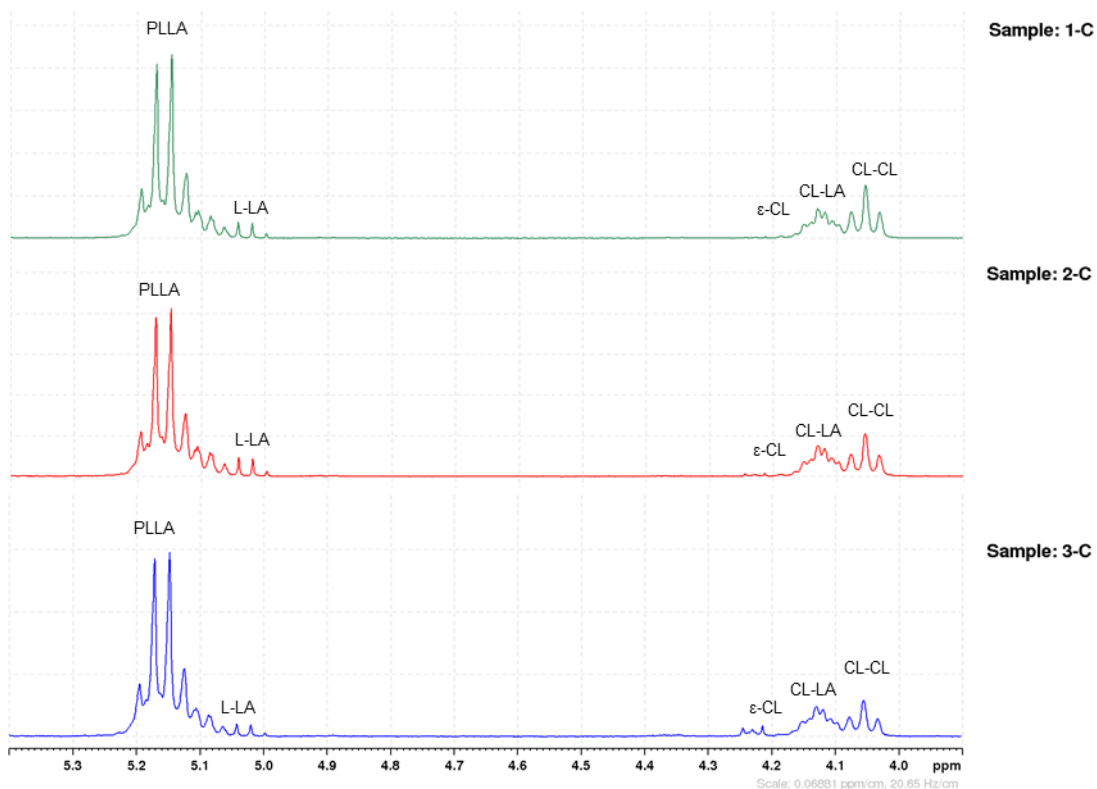


Figure 125:  $^1\text{H}$  NMR spectra of 30 PLCL matrices showing the peaks corresponding to  $\epsilon$ -CL, PLCL, L-LA and PLLA ( $\text{CDCl}_3$ , 300 MHz).

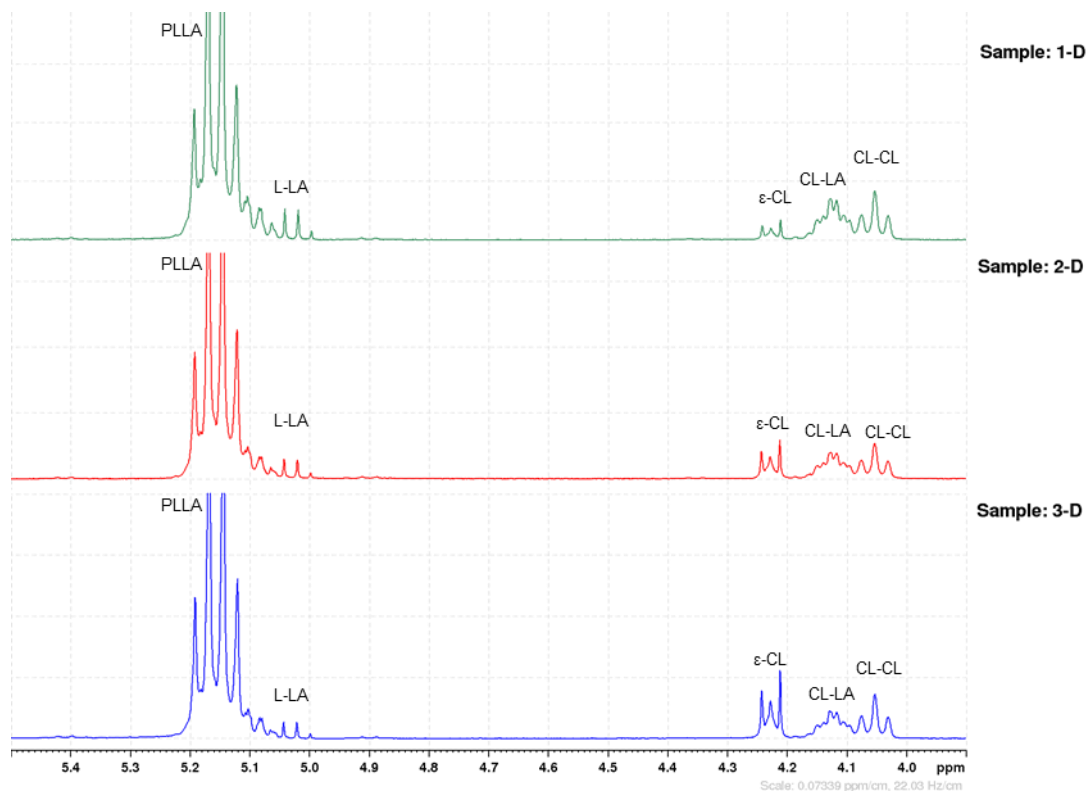


Figure 126:  $^1\text{H}$  NMR spectra of 20 PLCL matrices at different polymerization temperatures showing the peaks corresponding to  $\epsilon$ -CL, PLCL, L-LA and PLLA ( $\text{CDCl}_3$ , 300 MHz).

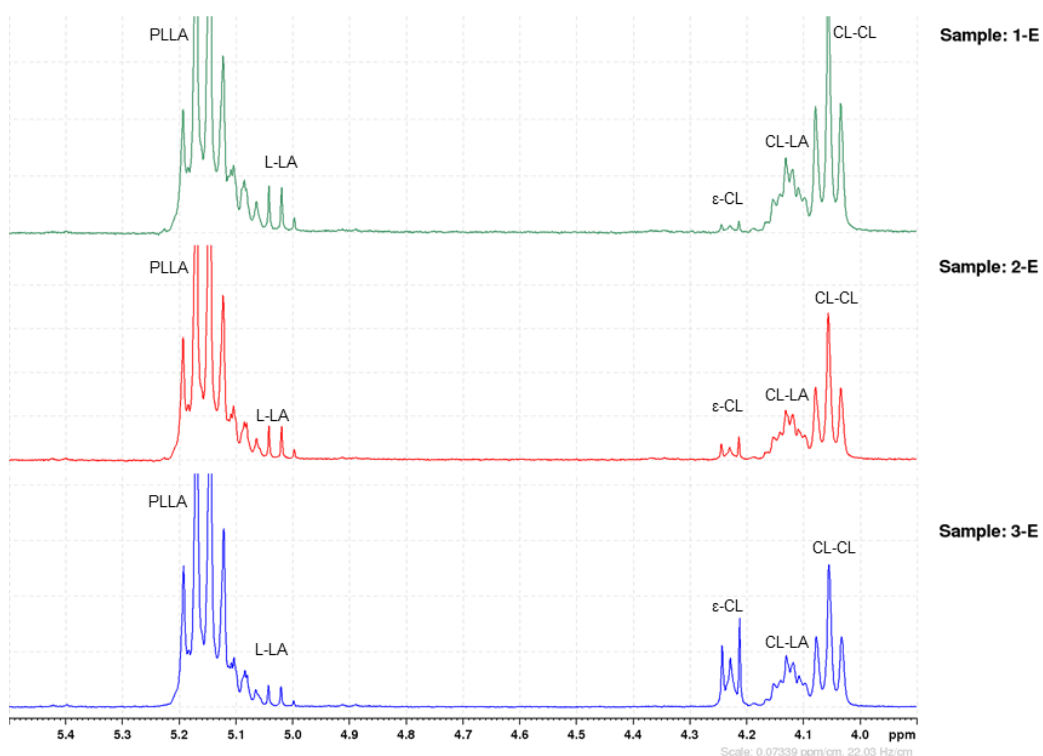


Figure 127:  $^1\text{H}$  NMR spectra of 30 PLCL matrices at different polymerization temperatures showing the peaks corresponding to  $\epsilon$ -CL, PLCL, L-LA and PLLA ( $\text{CDCl}_3$ , 300 MHz).

## 6.9 Carbon fabric reinforced composites – $^1\text{H}$ NMR spectra of PLLA and PLCL matrices

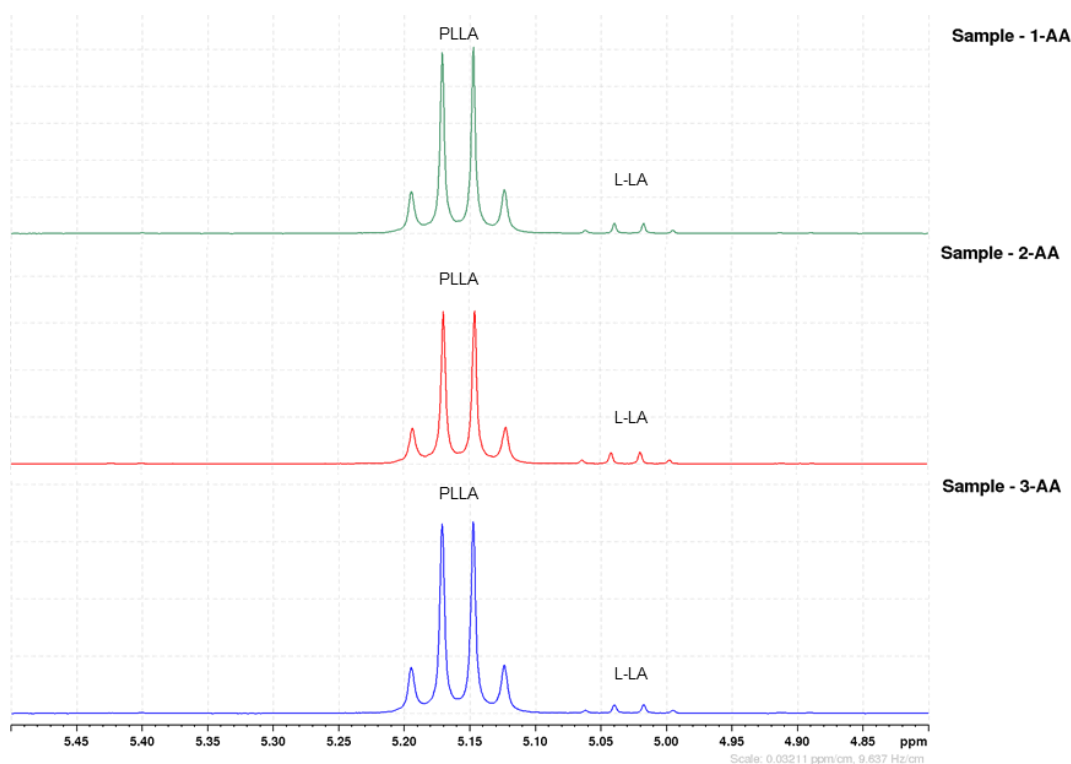


Figure 128:  $^1\text{H}$  NMR spectra of PLLA matrices showing the peaks corresponding to L-LA and PLLA ( $\text{CDCl}_3$ , 300 MHz).

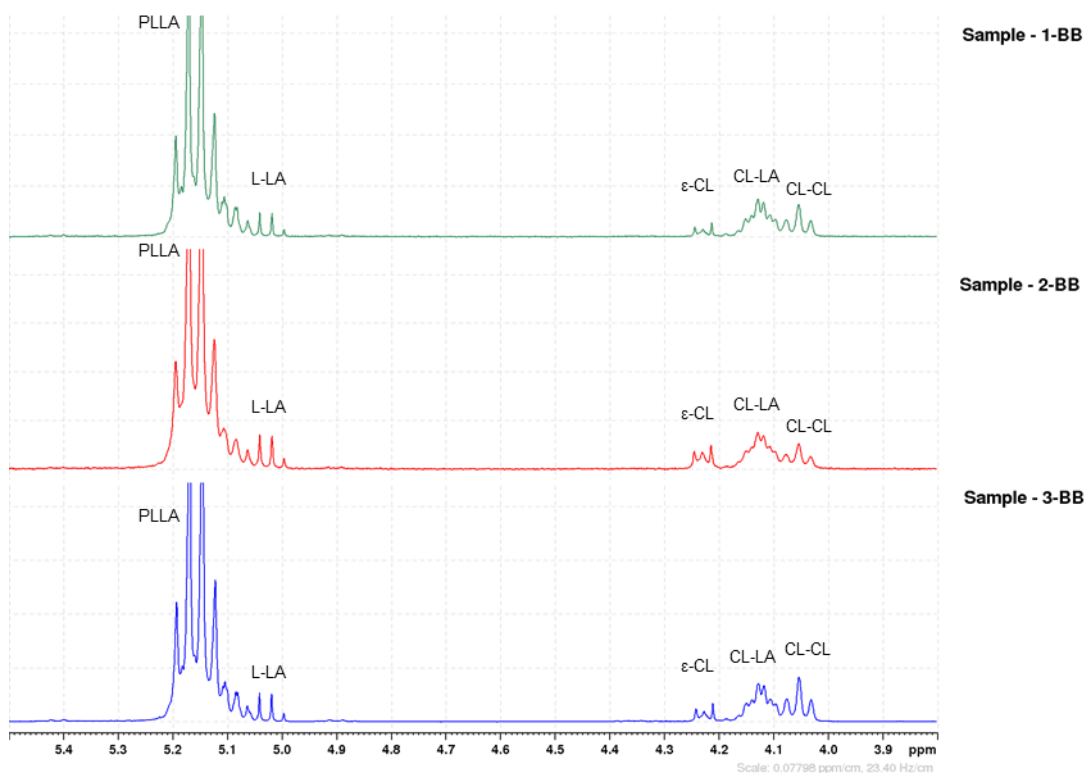


Figure 129:  $^1\text{H}$  NMR spectra of 80/20 PLCL matrices showing the peaks corresponding to  $\epsilon\text{-CL}$ , PLCL, L-LA and PLLA ( $\text{CDCl}_3$ , 300 MHz).

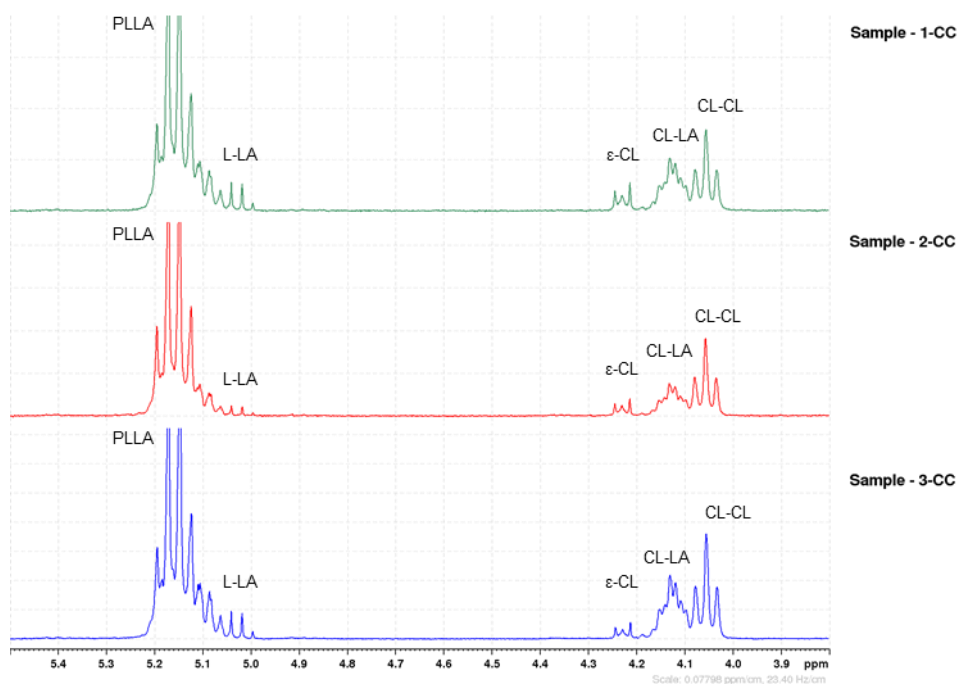


Figure 130:  $^1\text{H}$  NMR spectra of 70/30 PLCL matrices showing the peaks corresponding to  $\epsilon\text{-CL}$ , PLCL, L-LA and PLLA ( $\text{CDCl}_3$ , 300 MHz).

## 6.10 Flax fabric reinforced composites – $^1\text{H}$ NMR spectra of PLLA matrices

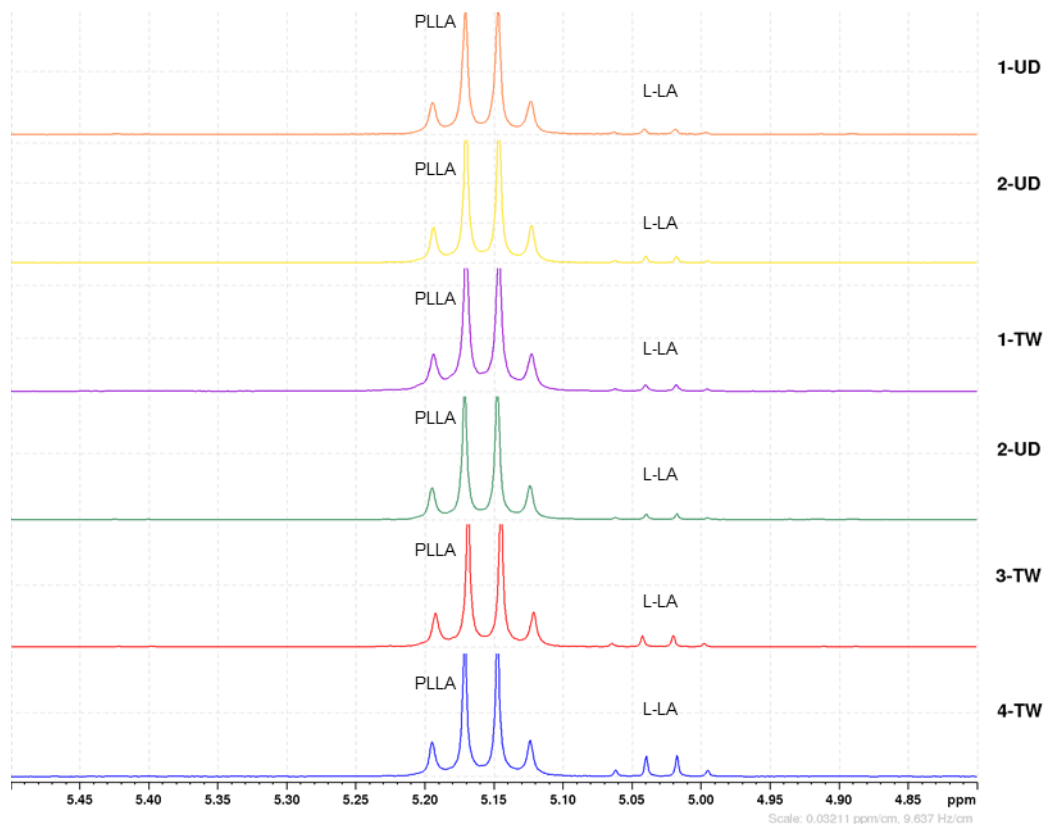


Figure 131:  $^1\text{H}$  NMR spectra of PLLA matrices of flax fabric reinforced composites ( $\text{CDCl}_3$ , 300 MHz).

## 6.11 Glass fabric reinforced composites – DSC curves of PLLA and PLCL matrices.

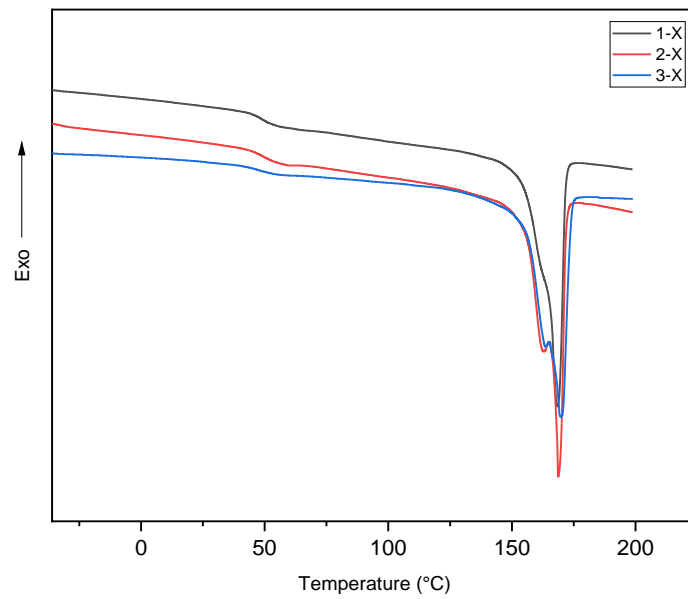


Figure 132: DSC curves at first scan of PLLA matrices.

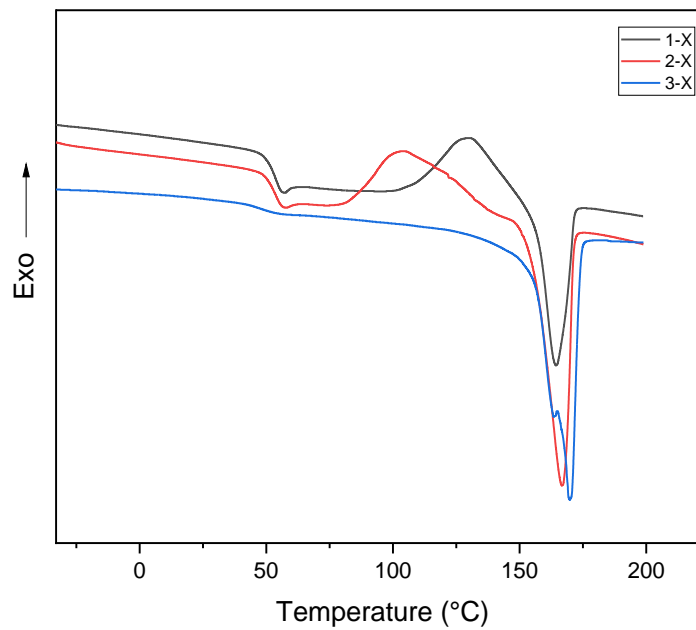


Figure 133: DSC curves at second scan of PLLA matrices.



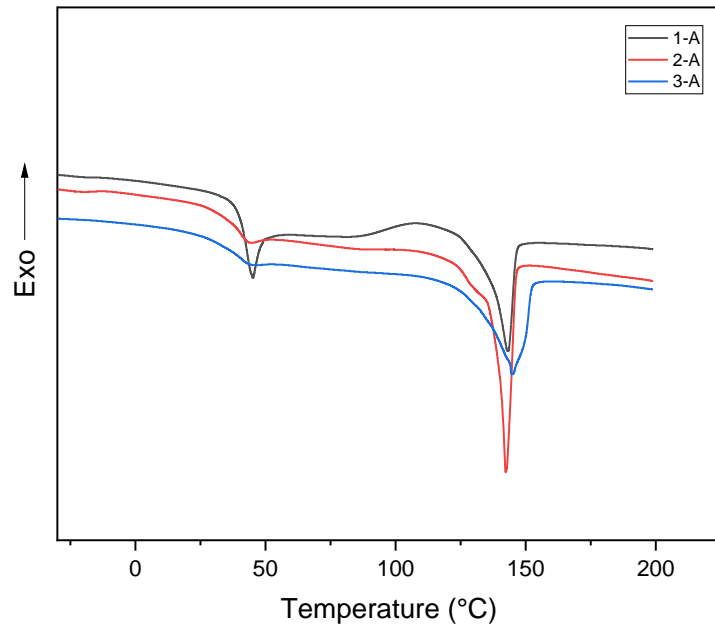


Figure 134: DSC curves at first scan of 10 PLCL matrices.

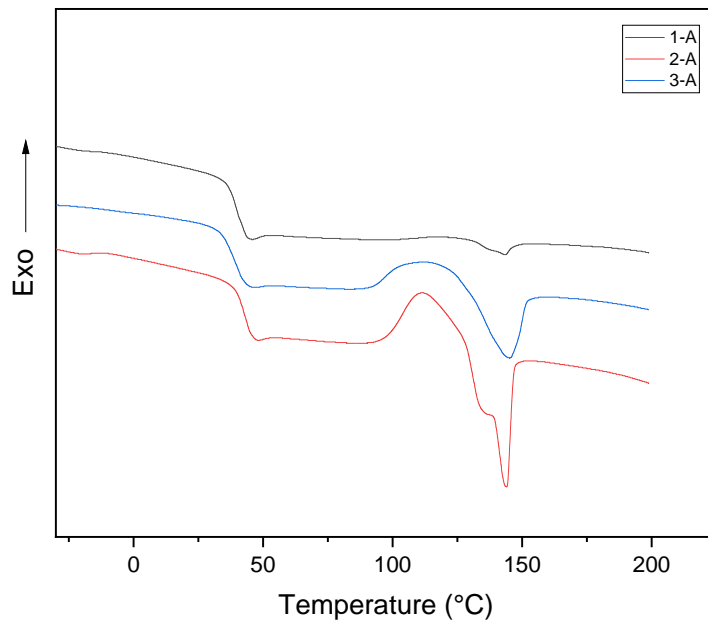


Figure 135: DSC curves at second scan of 10 PLCL matrices.

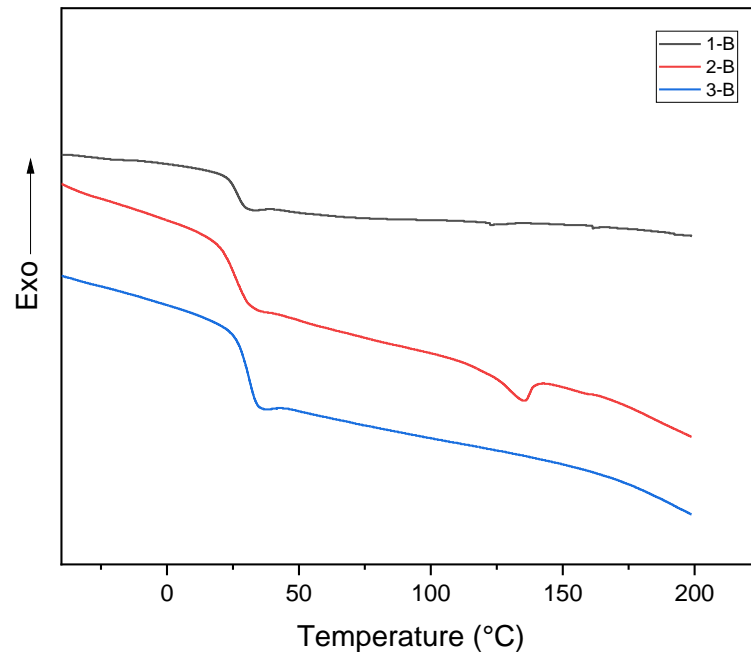


Figure 136: DSC curves at first scan of 20 PLCL matrices.

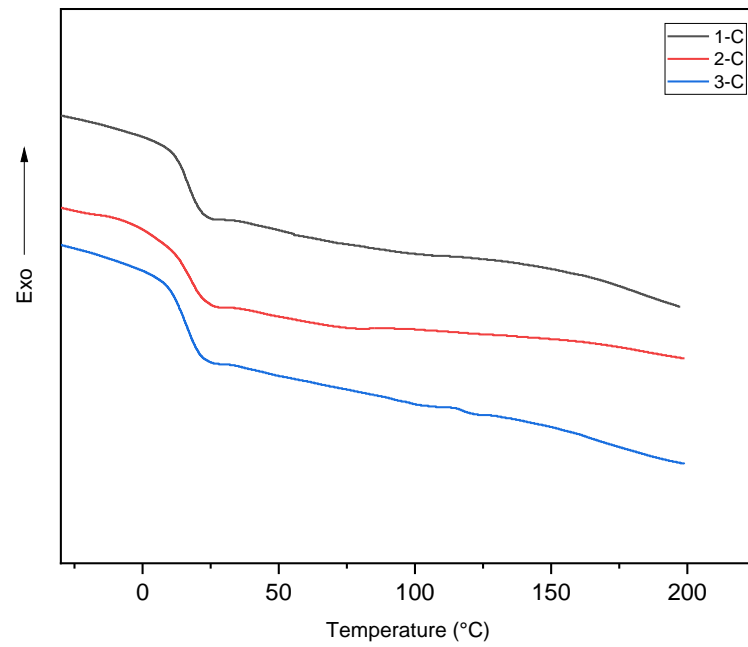


Figure 137: DSC curves at second scan of 20 PLCL matrices.

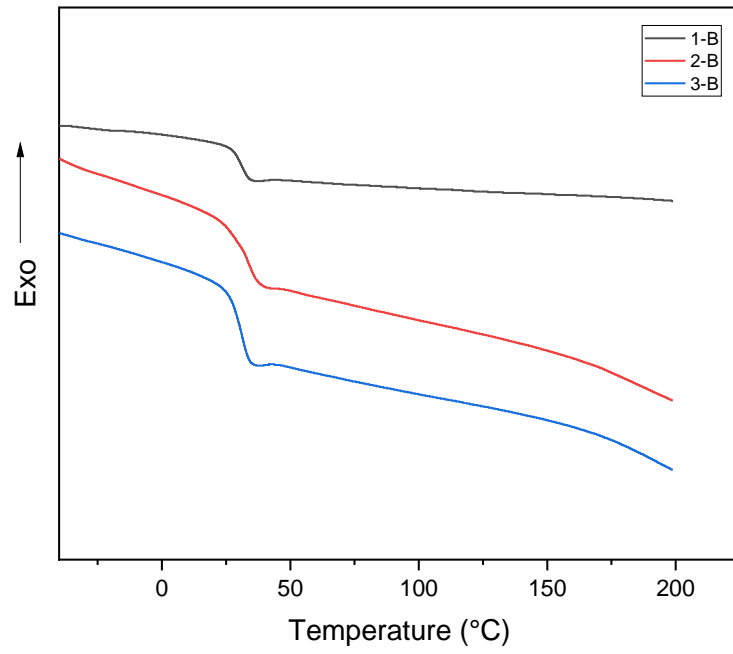


Figure 138: : DSC curves at first scan of 30 PLCL matrices.

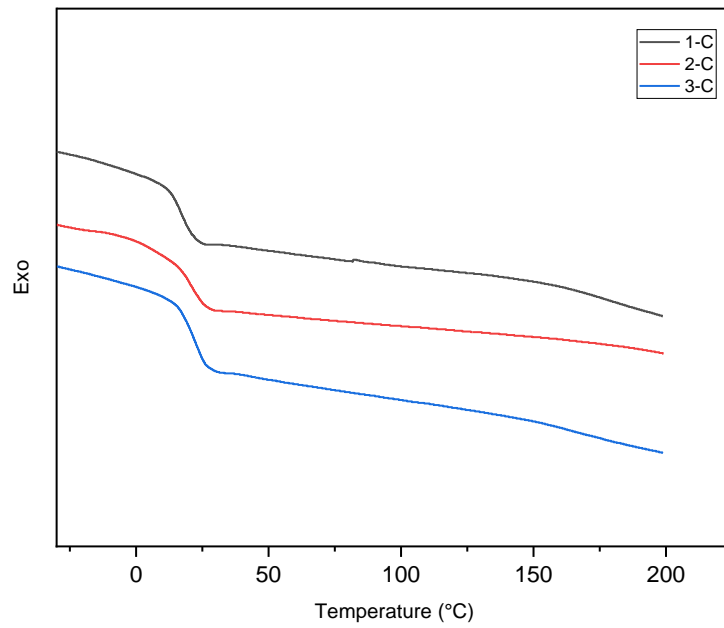


Figure 139: DSC curves at second scan of 30 PLCL matrices.

## 6.12 Carbon fabric reinforced composites – DSC curves of PLLA and PLCL matrices

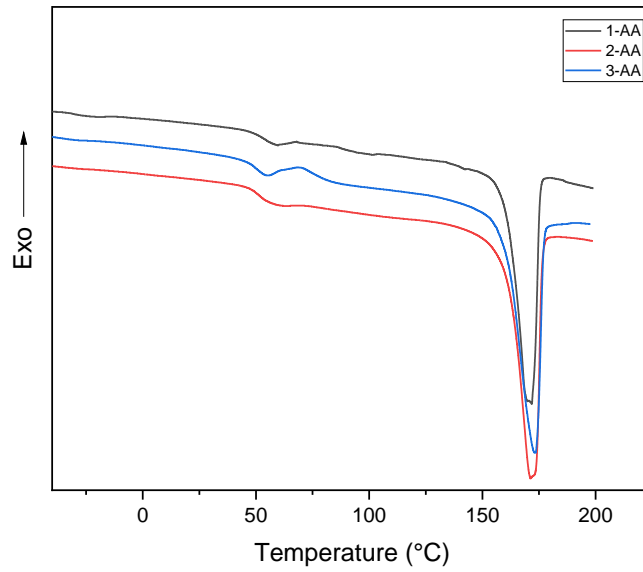


Figure 140: DSC curves at first scan of PLLA matrices ( $10^{\circ}\text{C}\cdot\text{min}^{-1}$ , under  $\text{N}_2$ ).

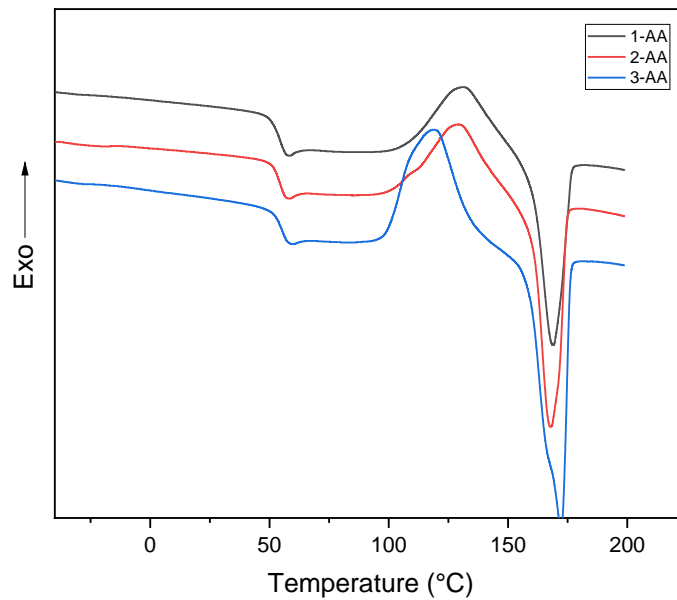


Figure 141: DSC curves at second scan of PLLA matrices ( $10^{\circ}\text{C}\cdot\text{min}^{-1}$ , under  $\text{N}_2$ ).

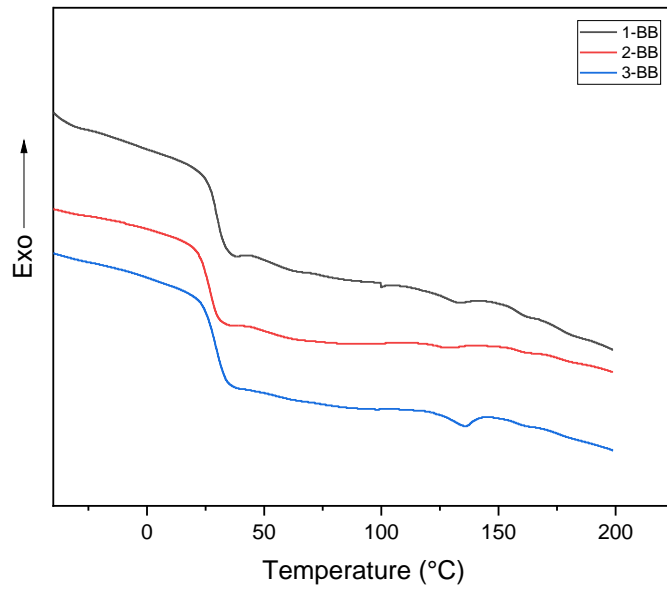


Figure 142: DSC curves at first scan of 20 PLCL matrices ( $10^{\circ}\text{C}\cdot\text{min}^{-1}$ , under  $\text{N}_2$ ).

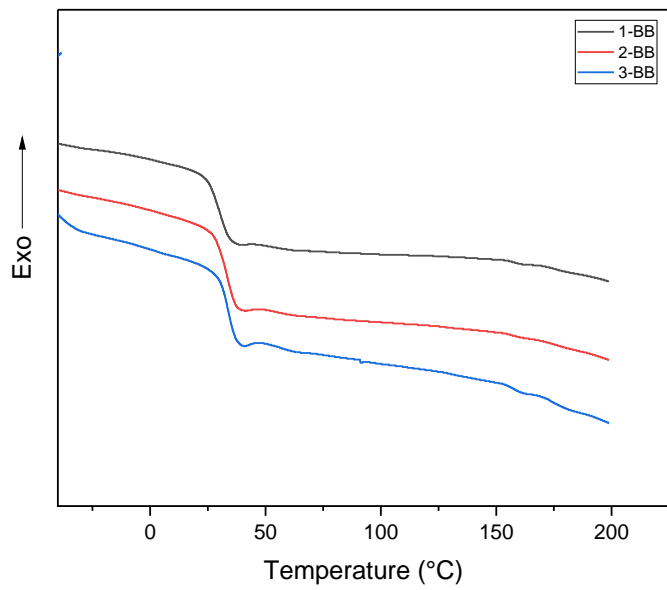


Figure 143: DSC curves at second scan of 20 PLCL matrices ( $10^{\circ}\text{C}\cdot\text{min}^{-1}$ , under  $\text{N}_2$ ).

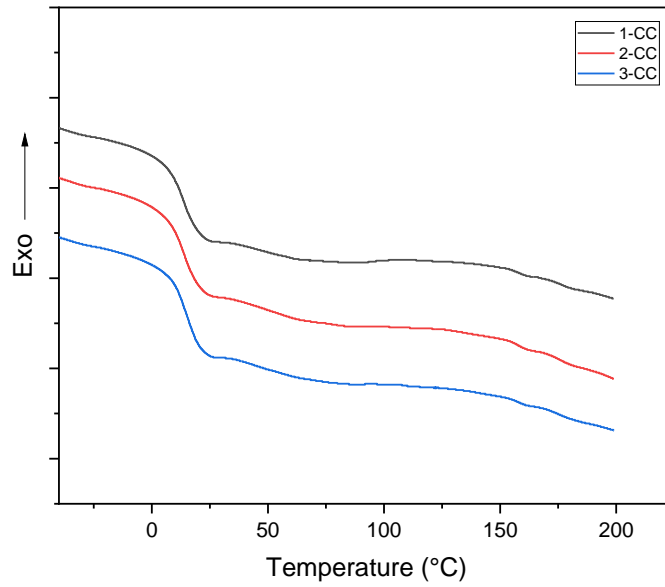


Figure 144: DSC curves at first scan of 30 PLCL matrices ( $10^{\circ}\text{C}\cdot\text{min}^{-1}$ , under  $\text{N}_2$ ).

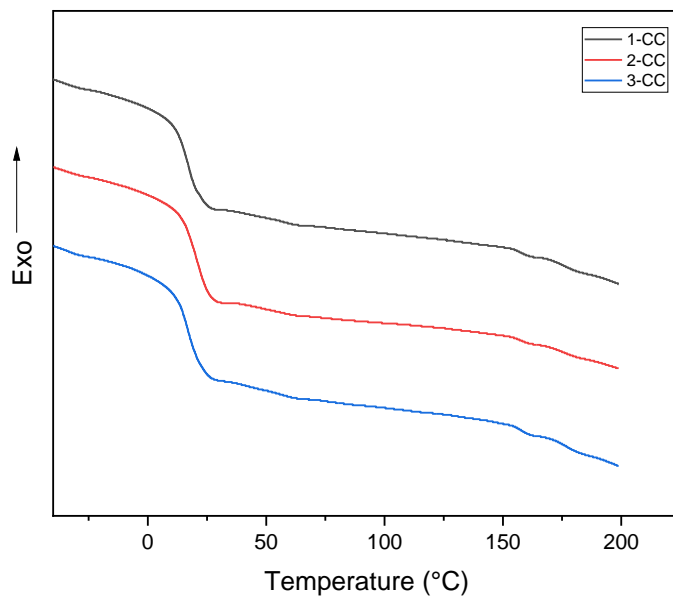


Figure 145: DSC curves at second scan of 30 PLCL matrices ( $10^{\circ}\text{C}\cdot\text{min}^{-1}$ , under  $\text{N}_2$ ).

### 6.13 Accelerated ageing – DSC curves of PLLA and PLCL matrices

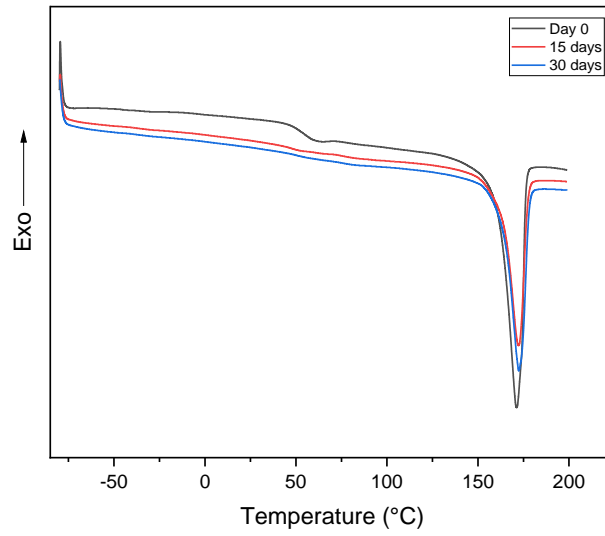


Figure 146: DSC curves of the matrix of PLLA/GF composite (sample G-1) at 1<sup>st</sup> scan.

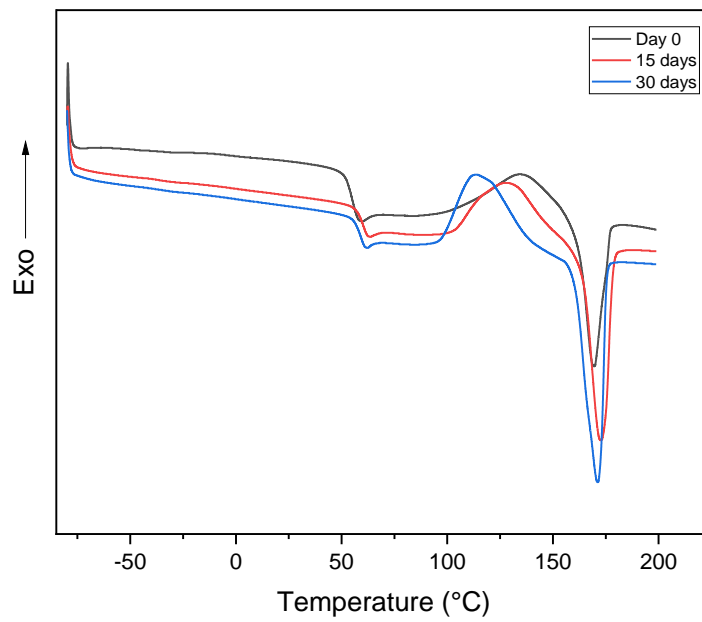


Figure 147: DSC curves of the matrix of PLLA/GF composite (sample G-1) at 2<sup>nd</sup> scan.

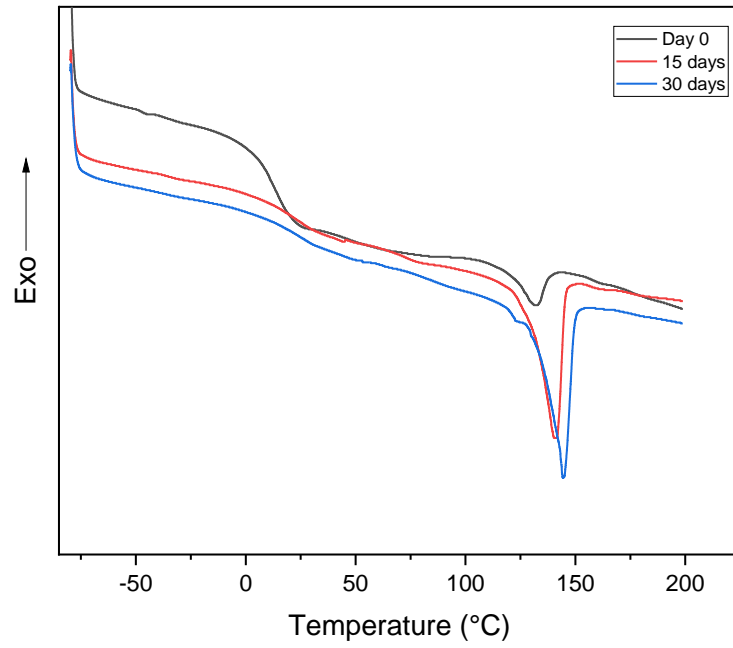


Figure 148: DSC curves of the matrix of 20 PLCL/GF composite (sample G-2) at 1<sup>st</sup> scan.

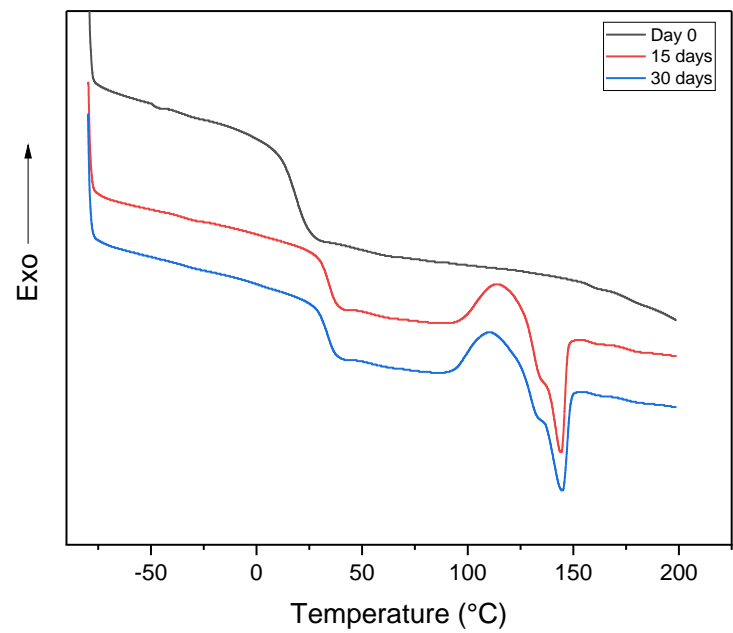


Figure 149: DSC curves of the matrix of 20 PLCL/GF composite (sample G-2) at 2<sup>nd</sup> scan.



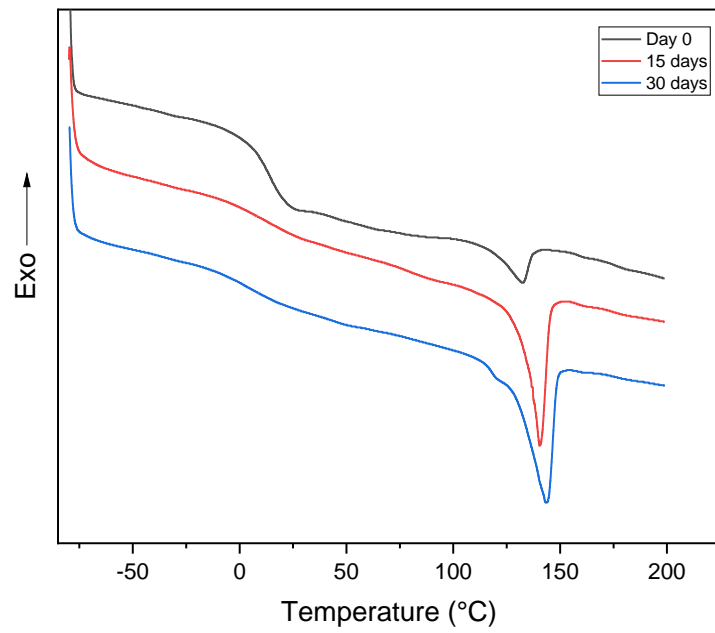


Figure 150: DSC curves of the matrix of 30 PLCL/GF composite (sample G-3) at 1<sup>st</sup> scan.

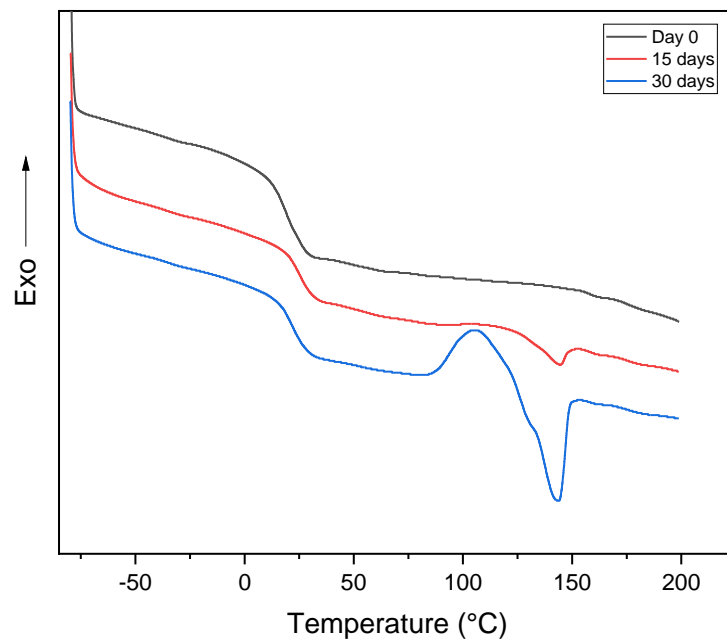


Figure 151: DSC curves of the matrix of 30 PLCL/GF composite (sample G-3) at 2<sup>nd</sup> scan.

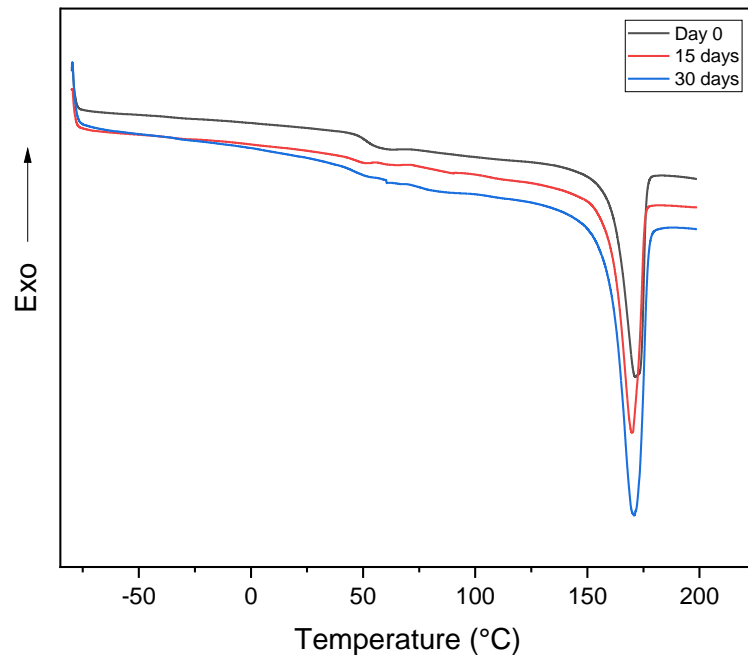


Figure 152: DSC curves of the matrix of PLLA / CF composite (sample C-1) at 1<sup>st</sup> scan.

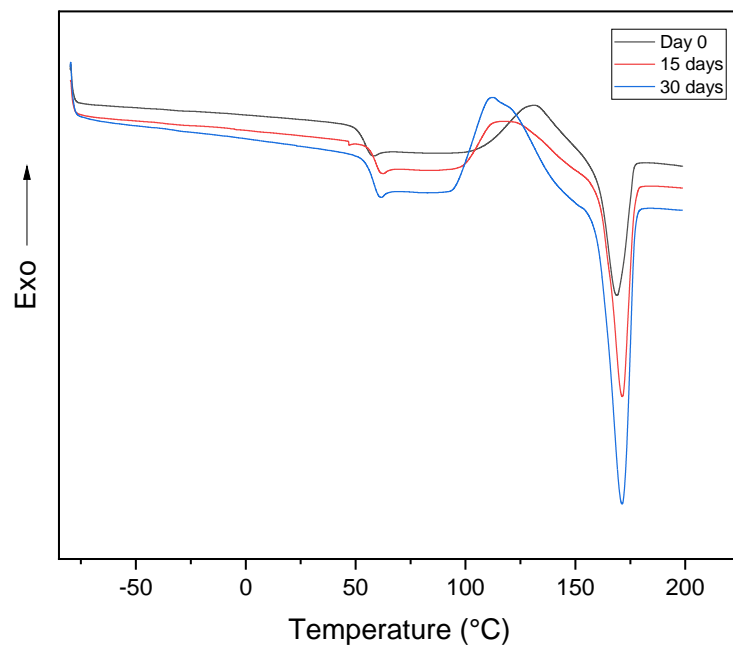


Figure 153: DSC curves of the matrix of PLLA / CF composite (sample C-1) at 2<sup>nd</sup> scan.

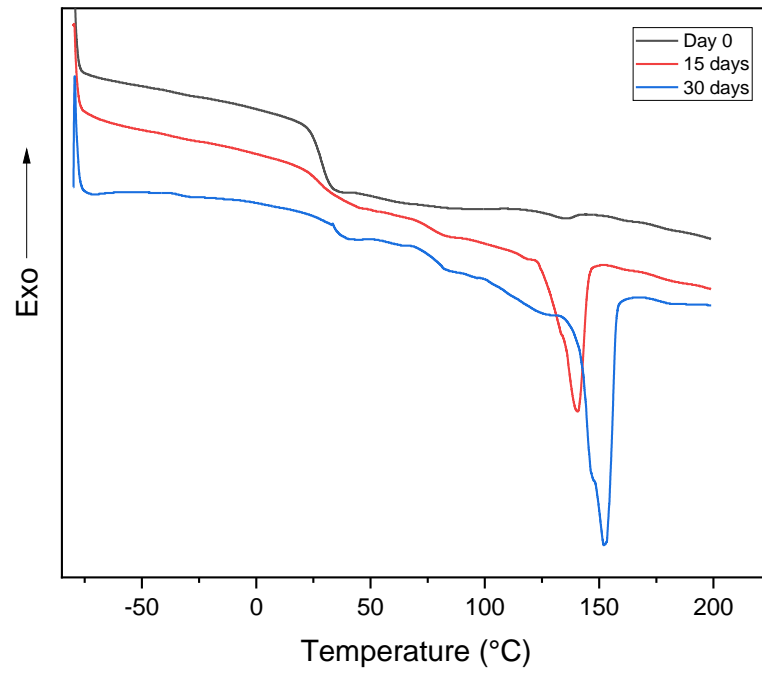


Figure 154: DSC curves of the matrix of 20 PLCL/GF composite (sample C-2) at 1<sup>st</sup> scan.

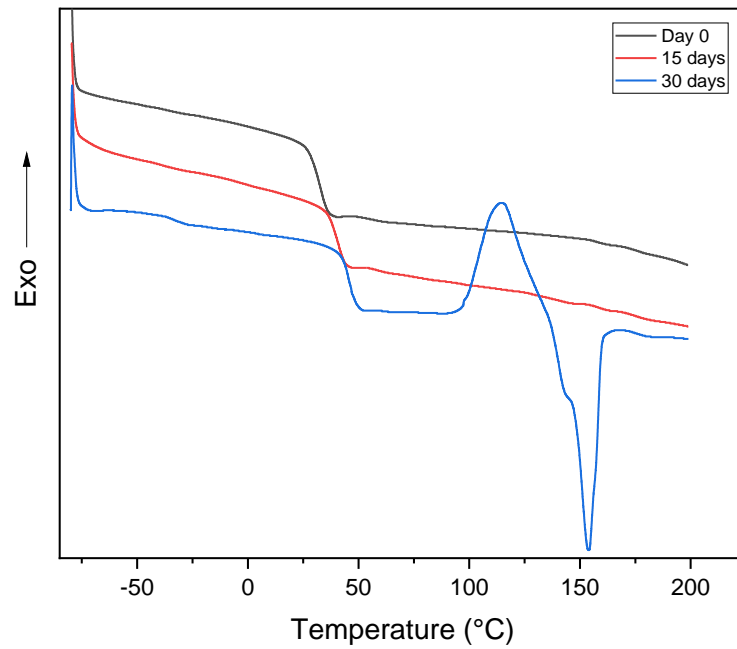


Figure 155: DSC curves of the matrix of 20 PLCL/GF composite (sample C-2) at 2<sup>nd</sup> scan.

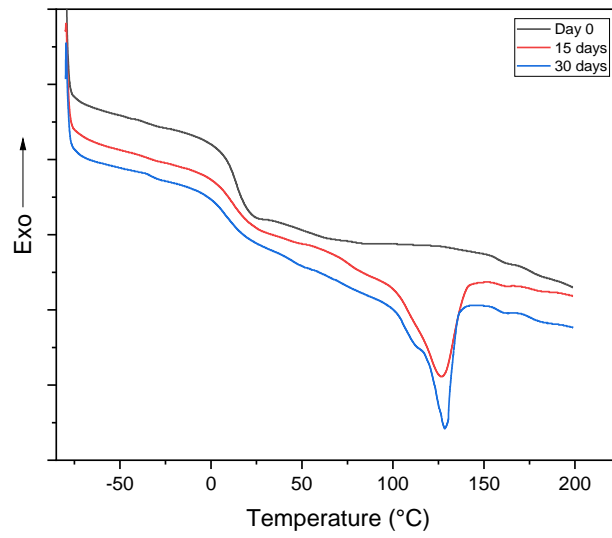


Figure 156: DSC curves of the matrix of 30 PLCL/GF composite (sample C-3) at 1<sup>st</sup> scan.

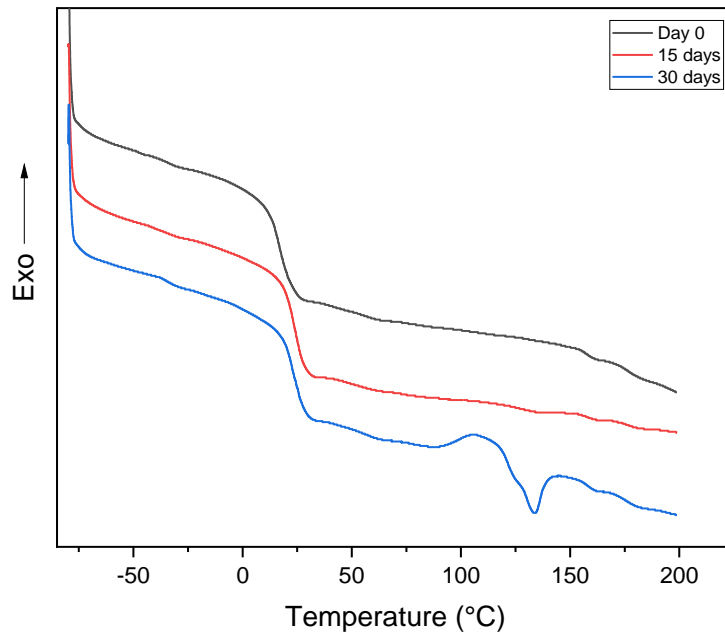


Figure 157: DSC curves of the matrix of 30 PLCL/GF composite (sample C-3) at 2<sup>nd</sup> scan.

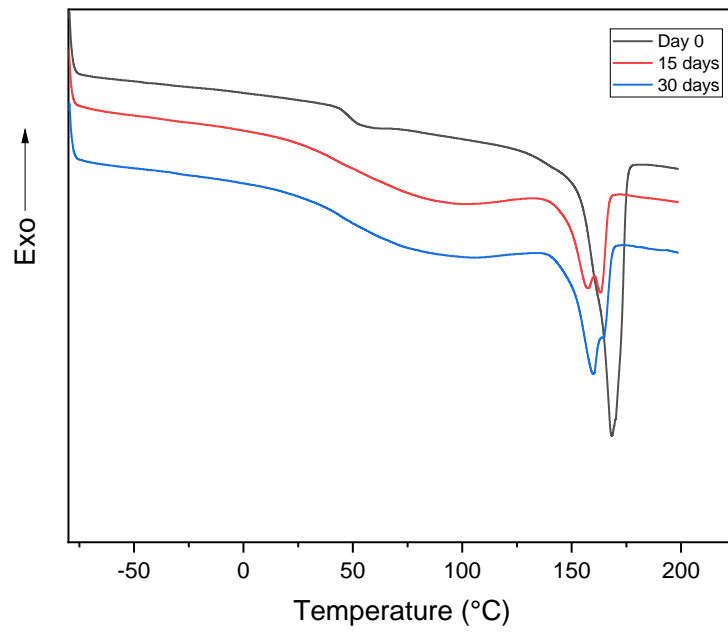


Figure 158: DSC curves of the matrix of PLLA/TW composite (sample F-1) at 1<sup>st</sup> scan.

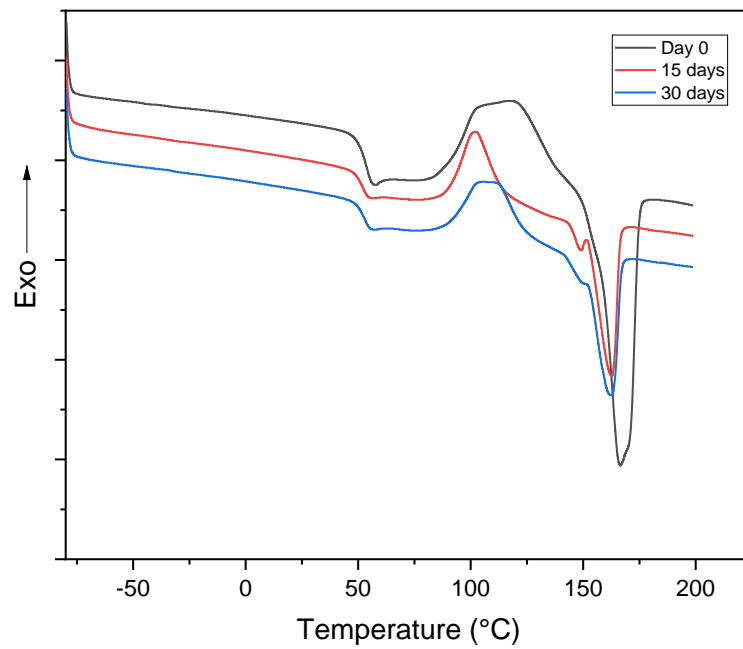


Figure 159: DSC curves of the matrix of PLLA/TW composite (sample F-1) at 2<sup>nd</sup> scan.

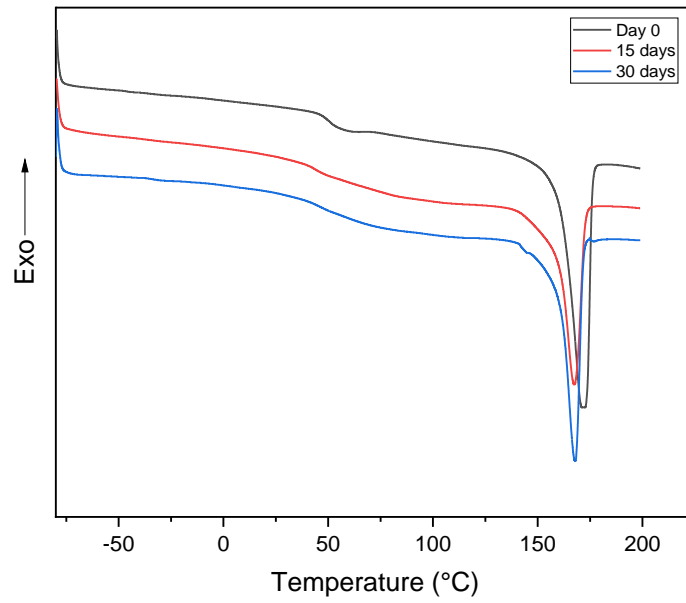


Figure 160: DSC curves of the matrix of PLLA/UD composite (sample F-2) at 1<sup>st</sup> scan.

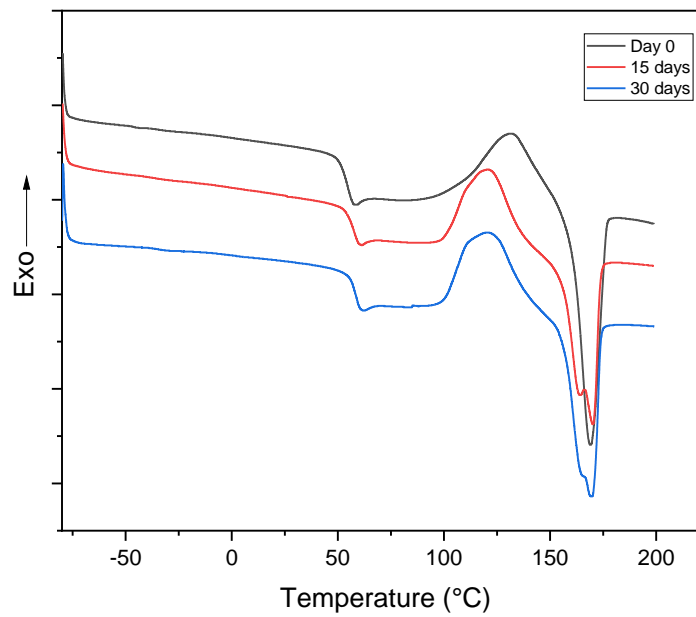


Figure 161: DSC curves of the matrix of PLLA/UD (sample F-2) at 2<sup>nd</sup> scan.

### 6.14 Glass fabric reinforced composites – Tensile test curves

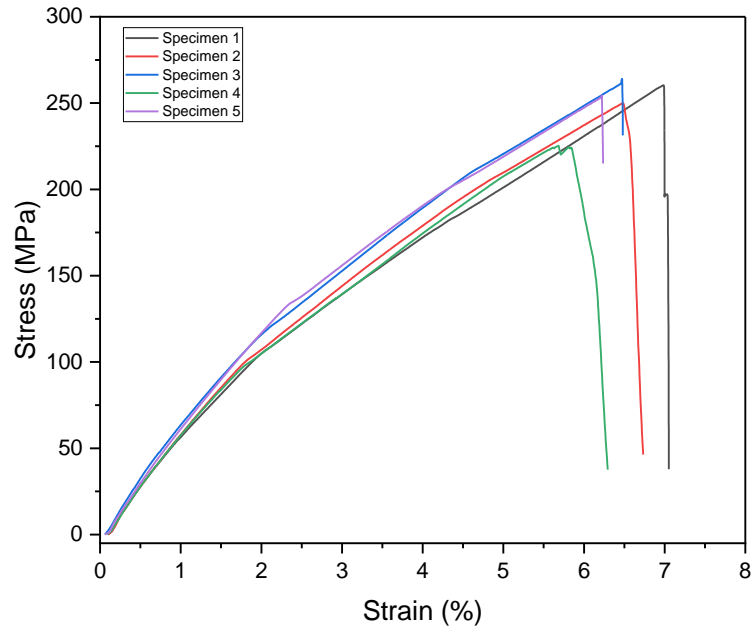


Figure 162: Strain x stress curve in tensile test of PLLA/GF (sample 1-X) composite.

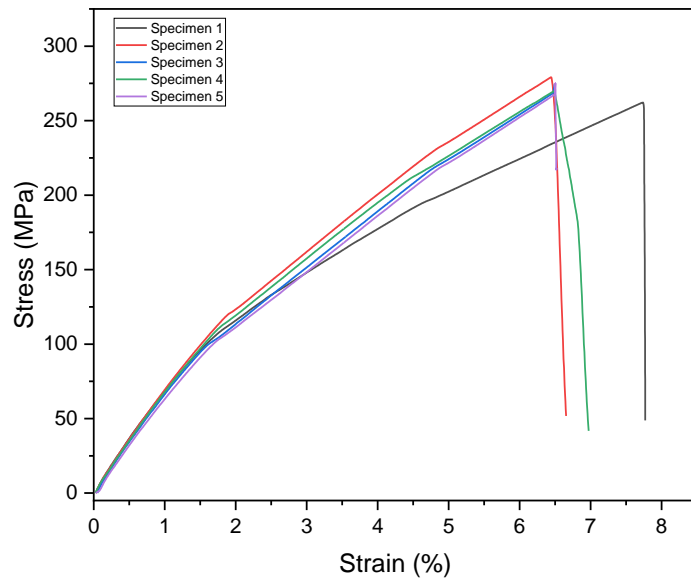


Figure 163: Strain x stress curve in tensile test of 10 PLCL/GF (sample 1-A) composite.

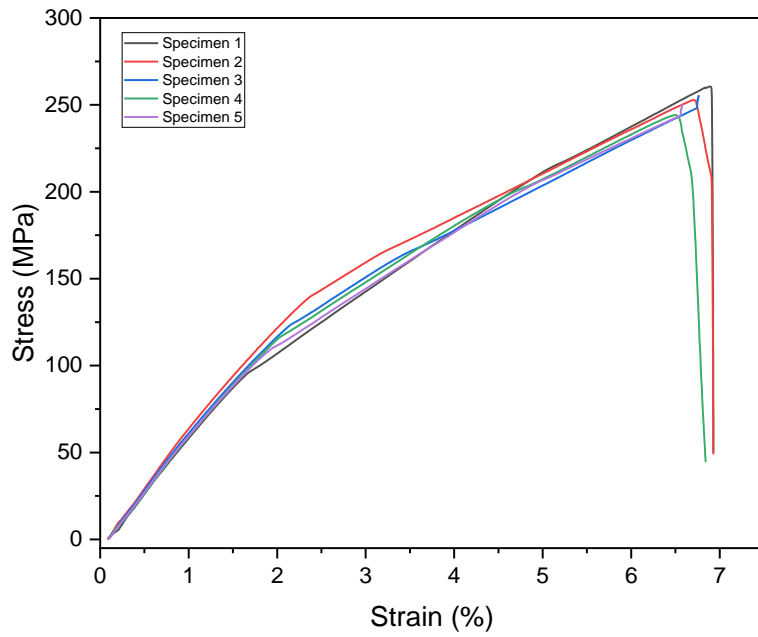


Figure 164: Strain x stress curve in tensile test of 20 PLCL/GF (sample 1-B) composite.

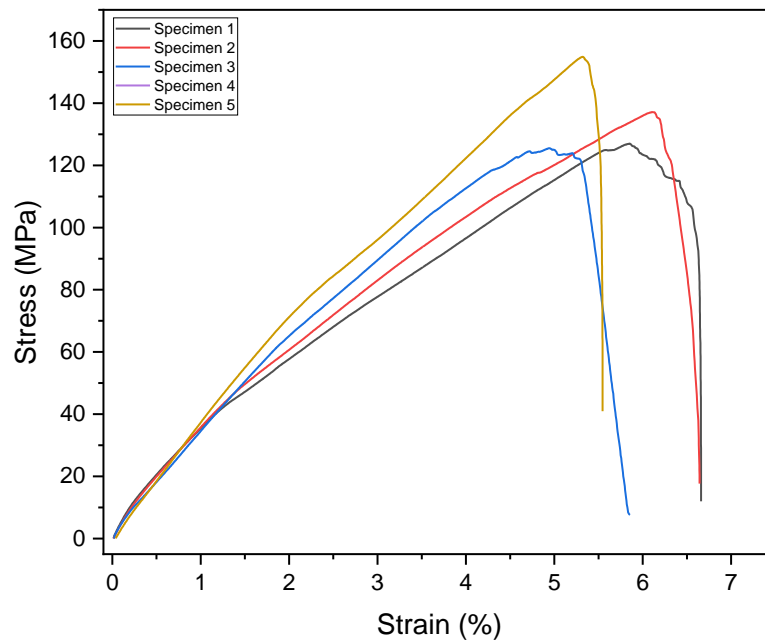


Figure 165: Strain x stress curve in tensile test of 30 PLCL/GF (sample 1-C) composite.



## 6.15 Glass fabric reinforced composites – Three-point bending test curves

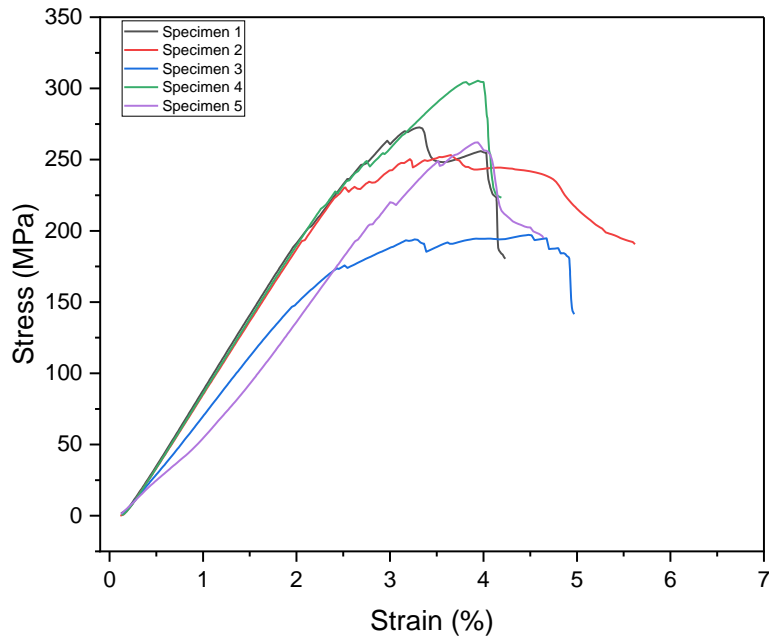


Figure 166: Strain x stress curve in three-point bending test of PLLA/GF (sample 2-X) composite.

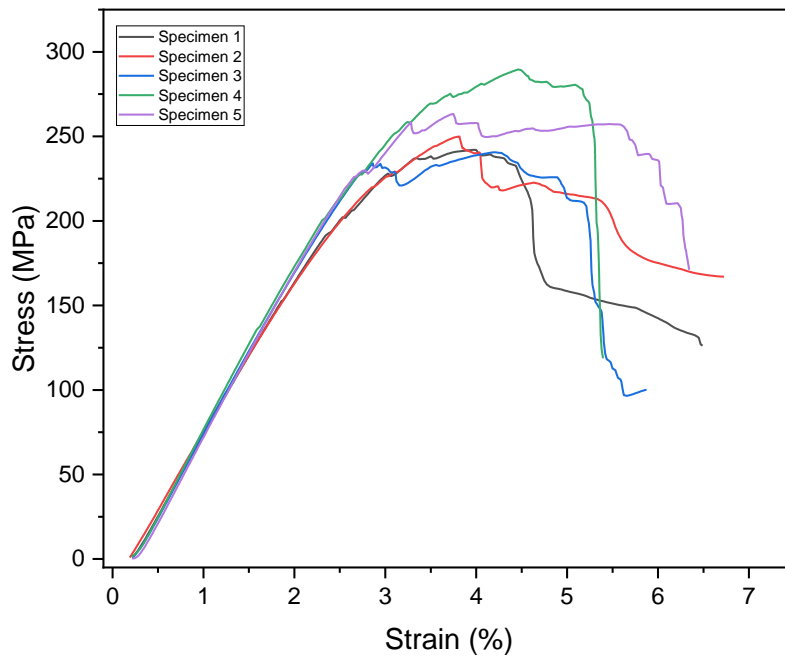


Figure 167: Strain x stress curve in three-point bending test of 10 PLCL/GF (sample 2-A) composite.

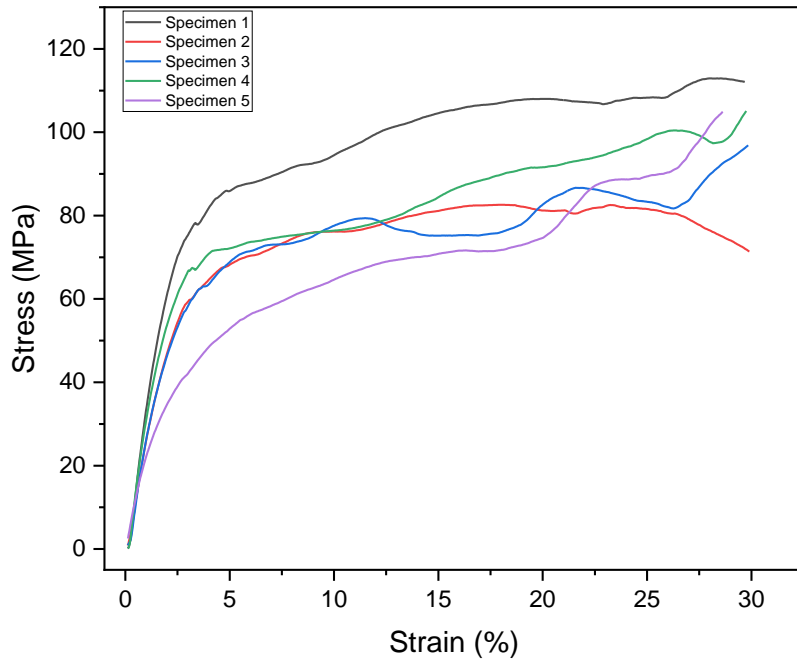


Figure 168: Strain x stress curve in three-point bending test of 20 PLCL/GF (sample 2-B) composite.

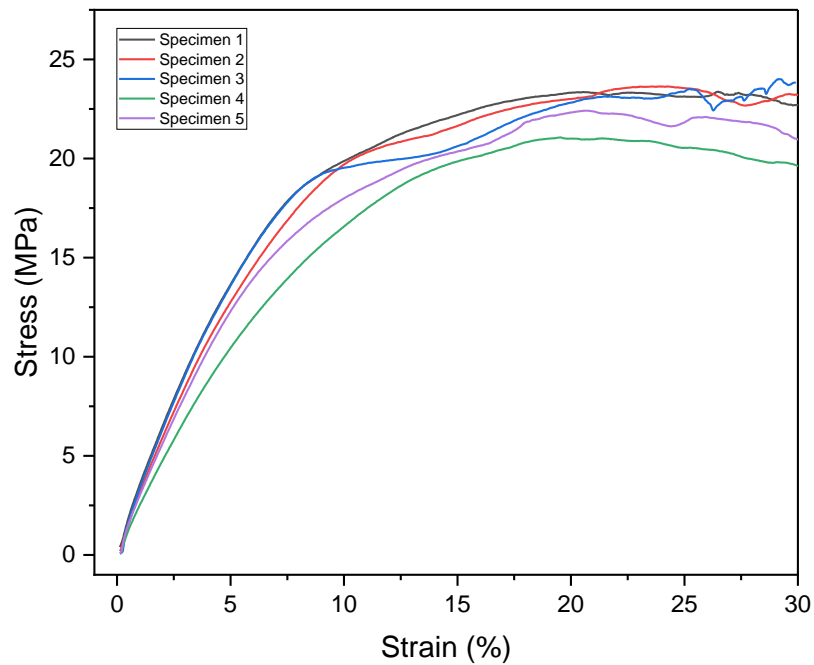


Figure 169: Strain x stress curve in three-point bending test of 30 PLCL/GF (sample 2-C) composite.

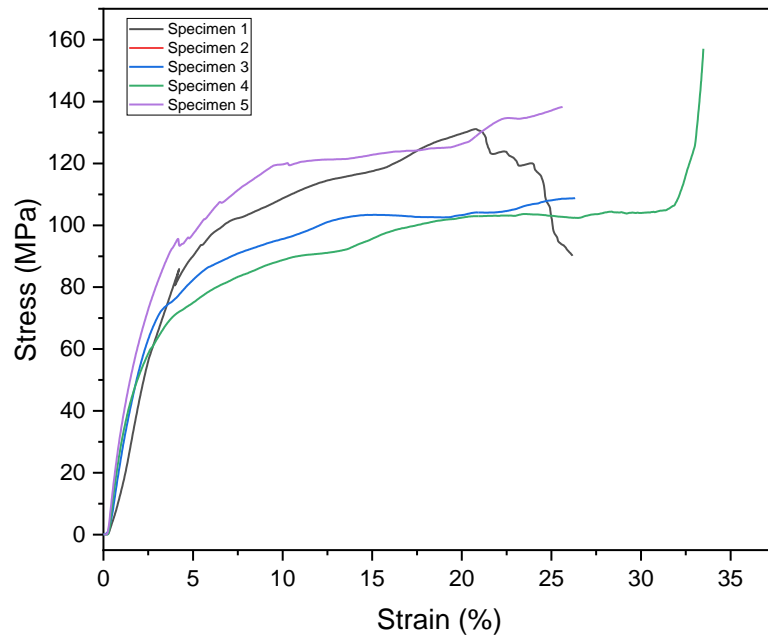


Figure 170: Strain x stress curve in three-point bending test of 20 PLCL/GF composite (Sample 1-D) produced at 170 °C.

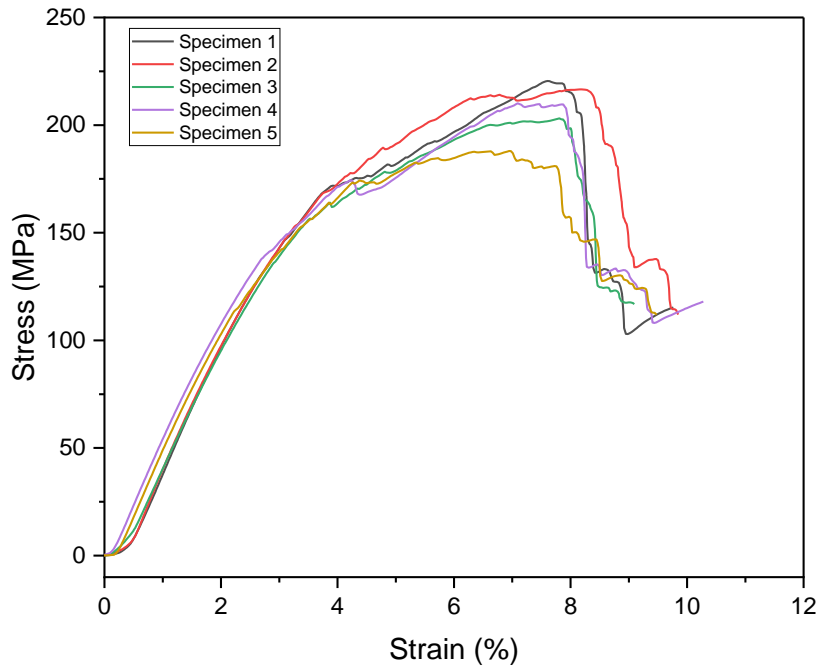


Figure 171: Strain x stress curve in three-point bending test of 20 PLCL/GF composite (Sample 2-D) produced at 160 °C.

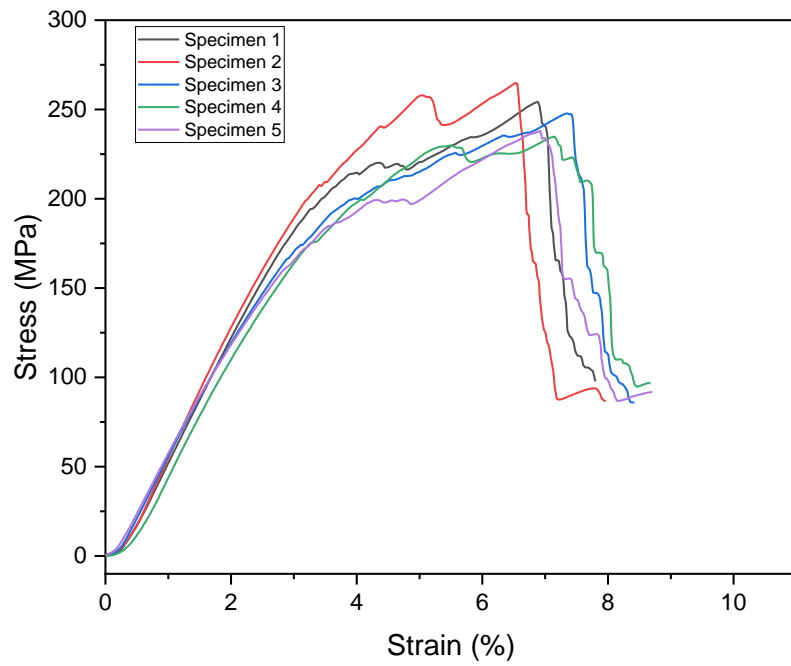


Figure 172: Strain x stress curve in three-point bending test of 20 PLCL/GF composite (Sample 3-D) produced at 150 °C.

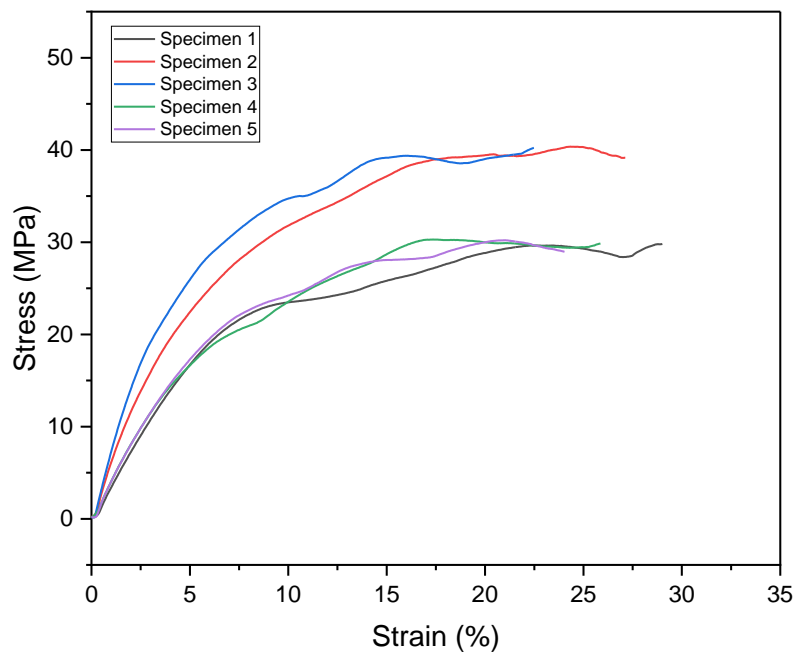


Figure 173: Strain x stress curve in three-point bending test of 30 PLCL/GF composite (Sample 1-E) produced at 170 °C.

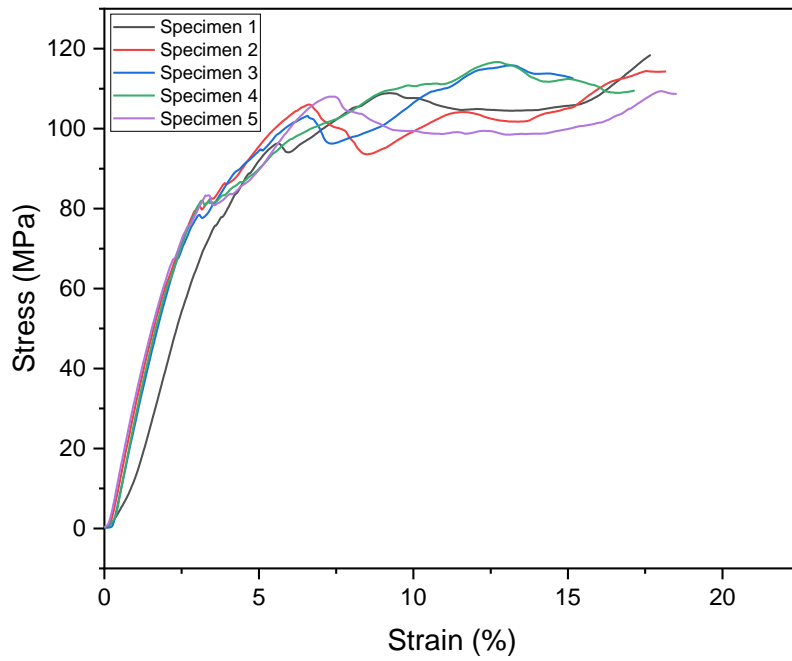


Figure 174: Strain x stress curve in three-point bending test of 30 PLCL/GF composite (Sample 2-E) produced at 160 °C.

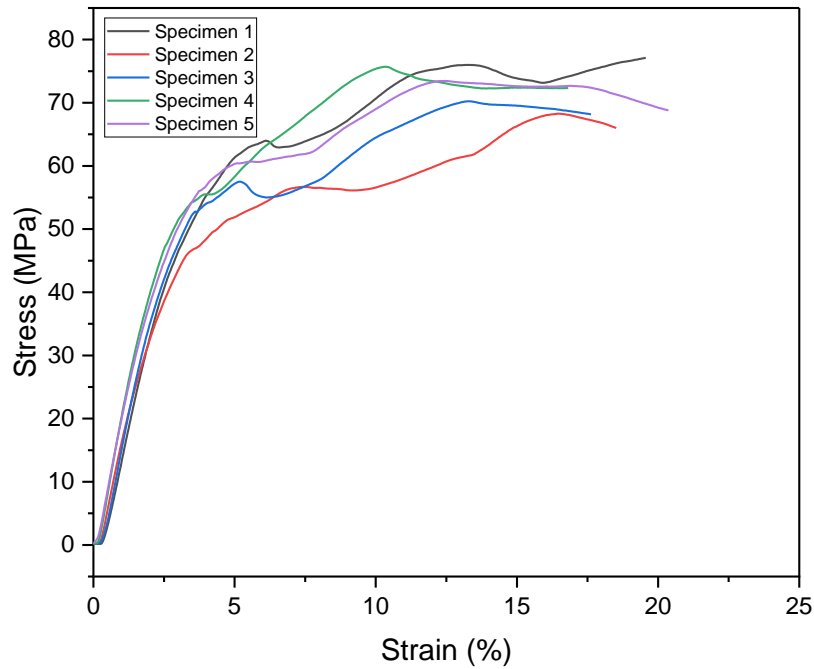


Figure 175: Strain x stress curve in three-point bending test of 30 PLCL/GF composite (Sample 3-E) produced at 150 °C.

## 6.16 Carbon fabric reinforced composites – Three-point bending test curves

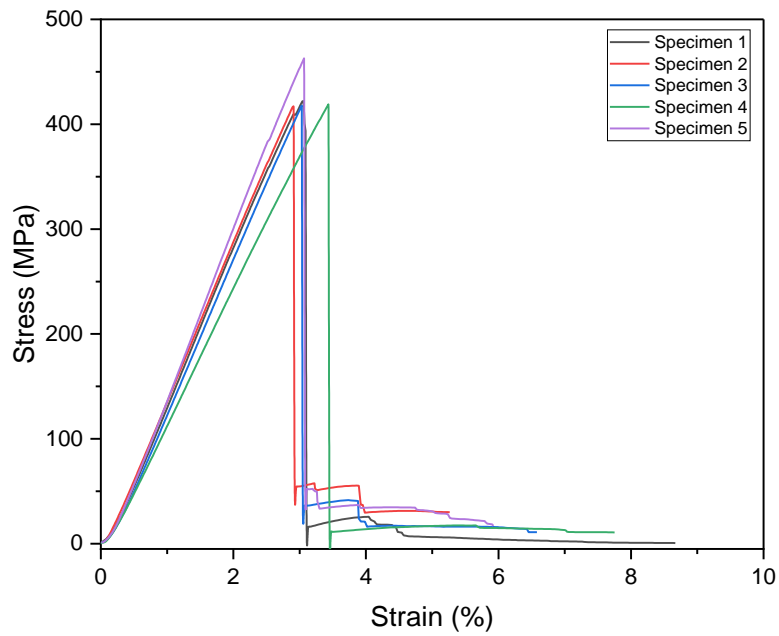


Figure 176: Strain x stress curve in three-point bending test of PLLA/CF composite (Sample 1-AA).

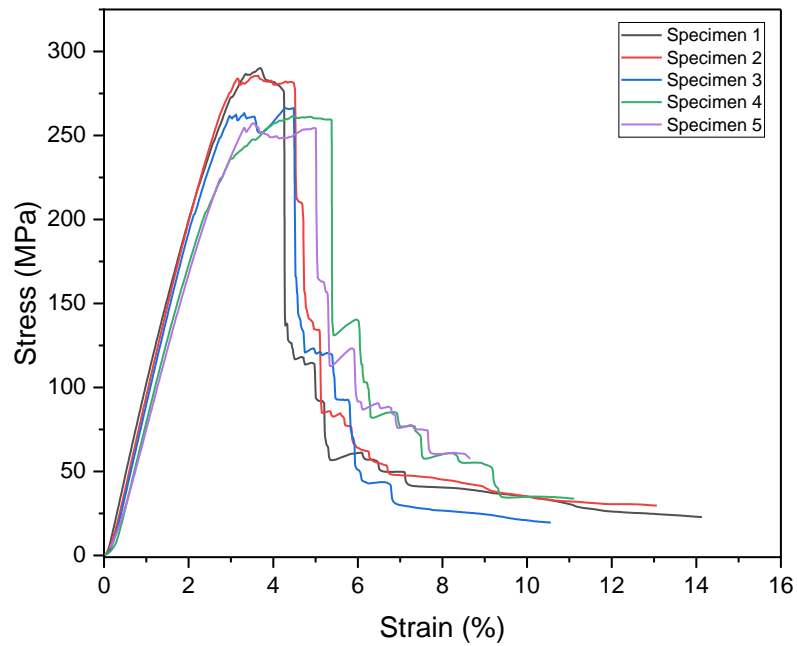


Figure 177: Strain x stress curve in three-point bending test of 20 PLCL/GF composite (Sample 1-BB).

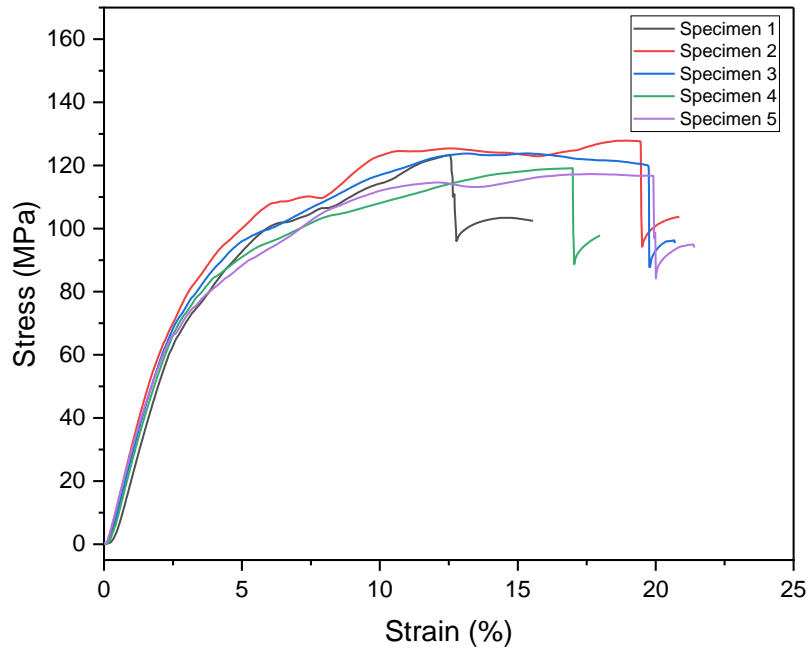


Figure 178: Strain x stress curve in three-point bending test of 30 PLCL/GF composite (Sample 1-CC).

### 6.17 Flax fabric reinforced composites – Three-point bending test curves

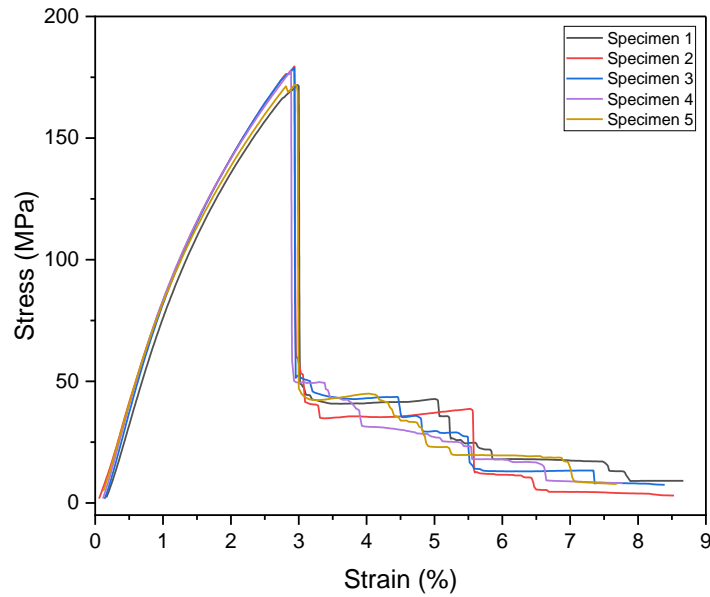


Figure 179: Strain - stress curves on three-point bending test of PLLA/UD composite.

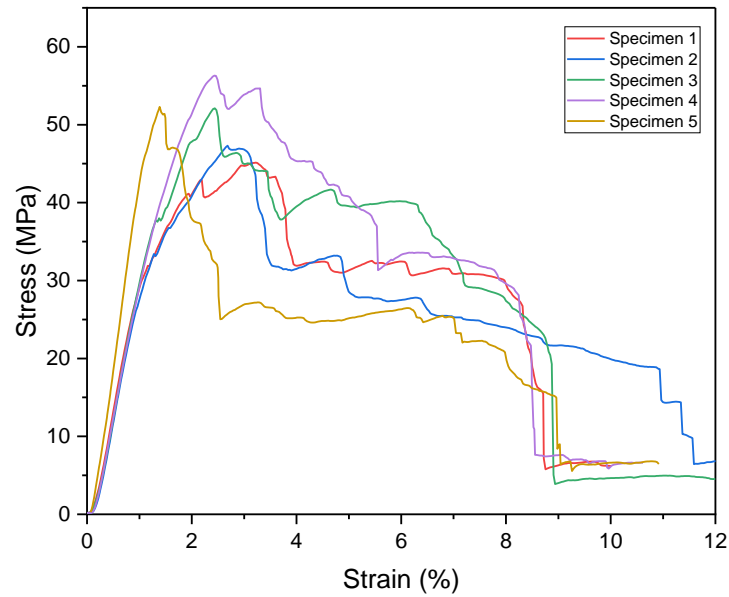


Figure 180: Strain - stress curves on three-point bending test of PLLA/TW composite.

### 6.18 Accelerated ageing – Three-point bending test



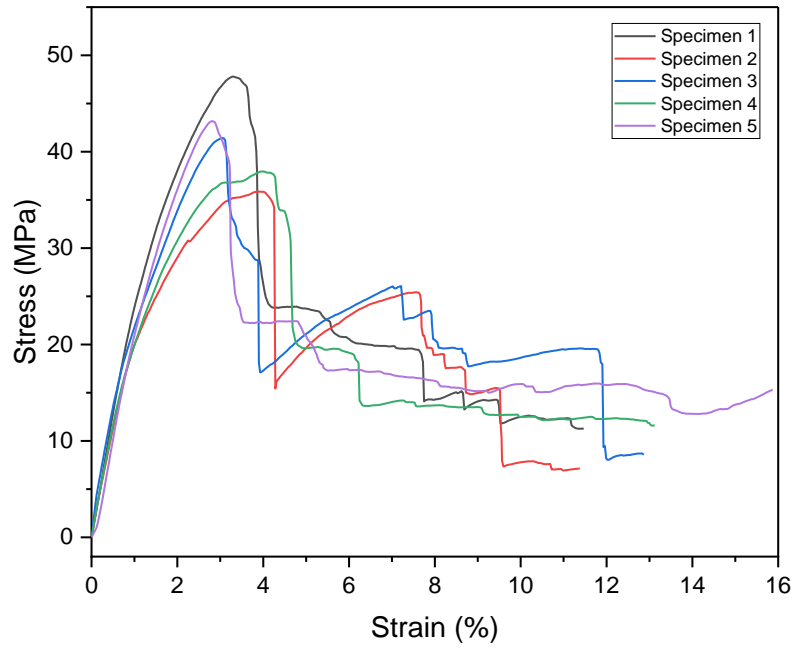


Figure 181: Strain x stress curve on three-point bending of PLLA/TW composite.

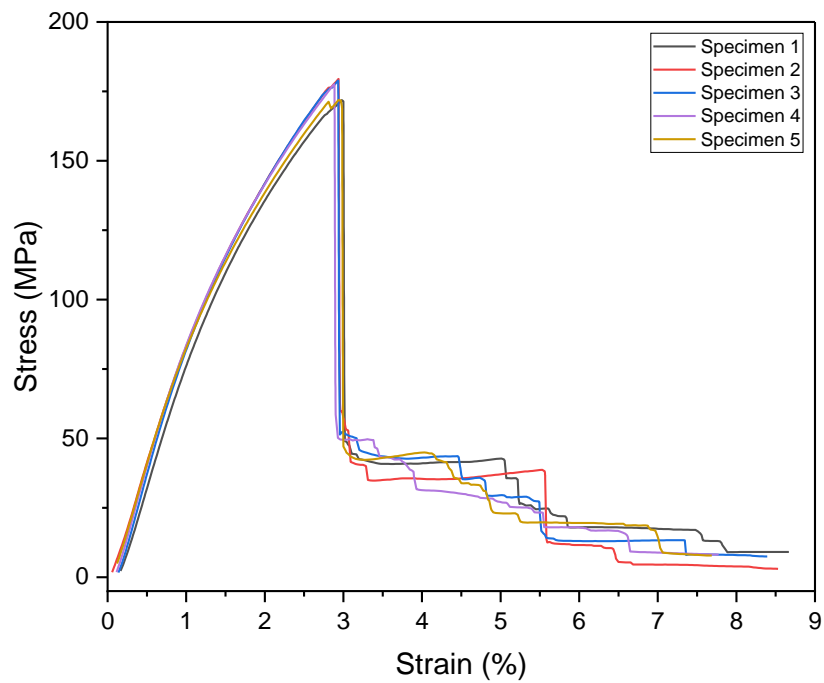


Figure 182: Strain x stress curve on three-point bending of PLLA/UD composite.

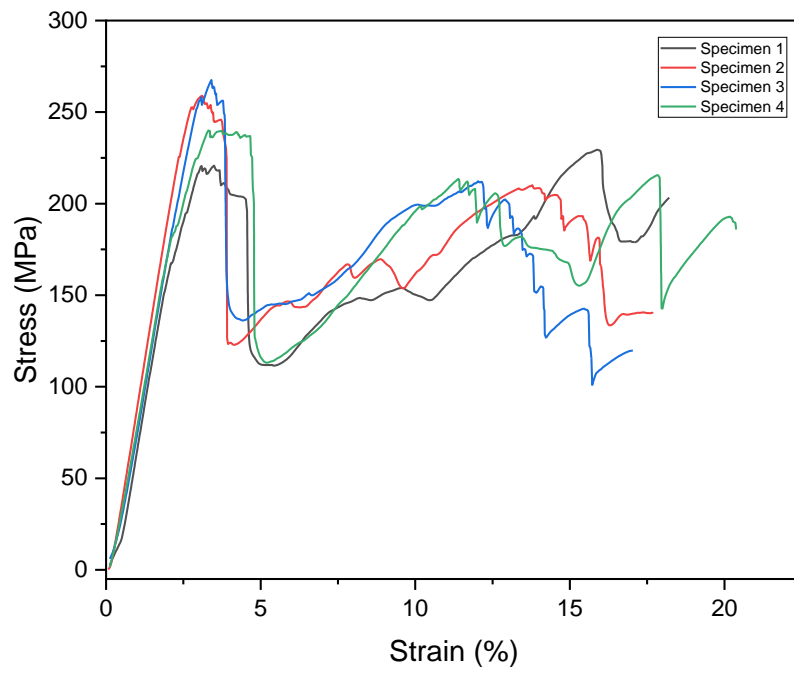


Figure 183: Strain x stress curve on three-point bending of PLLA/GF composite (sample G-1).

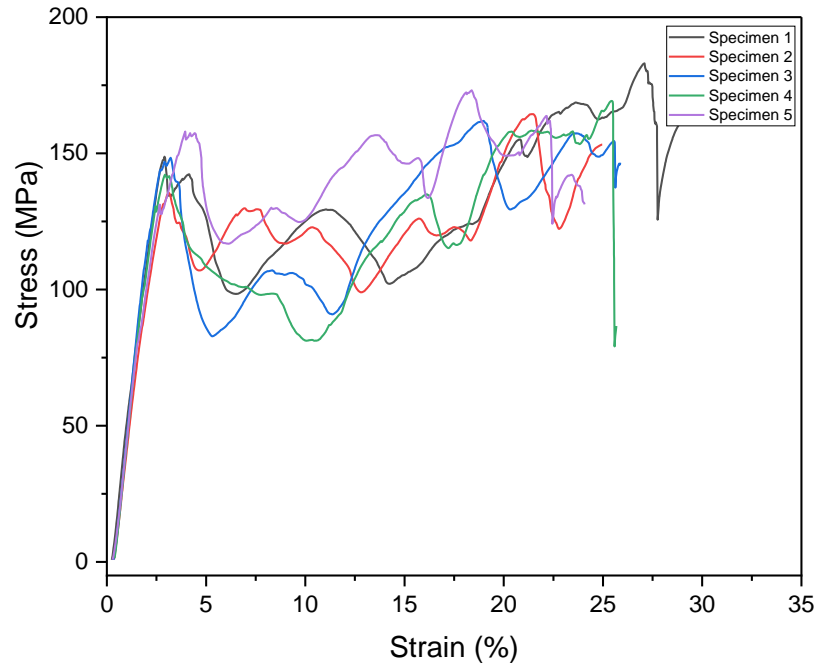


Figure 184: Strain x stress curve on three-point bending of 20 PLCL/GF composite (sample G-2).

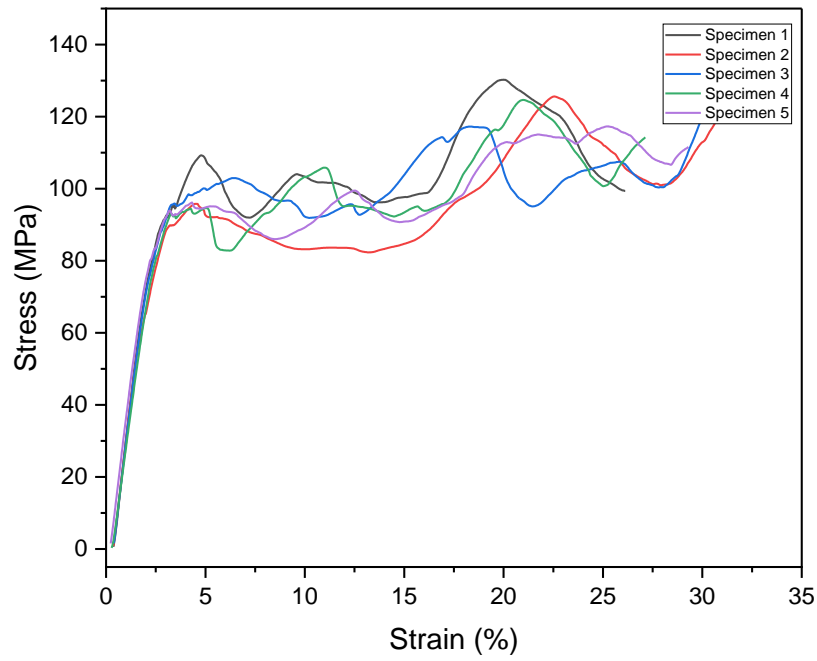


Figure 185: Strain x stress curve on three-point bending of 30 PLCL/GF composite (sample G-3).

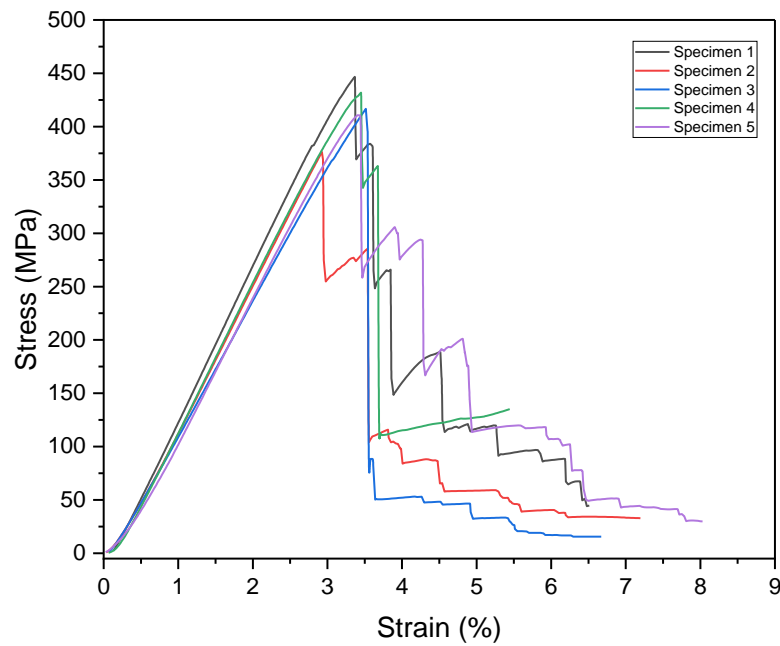


Figure 186: Strain x stress curve on three-point bending of PLLA/CF composite (sample C-1).

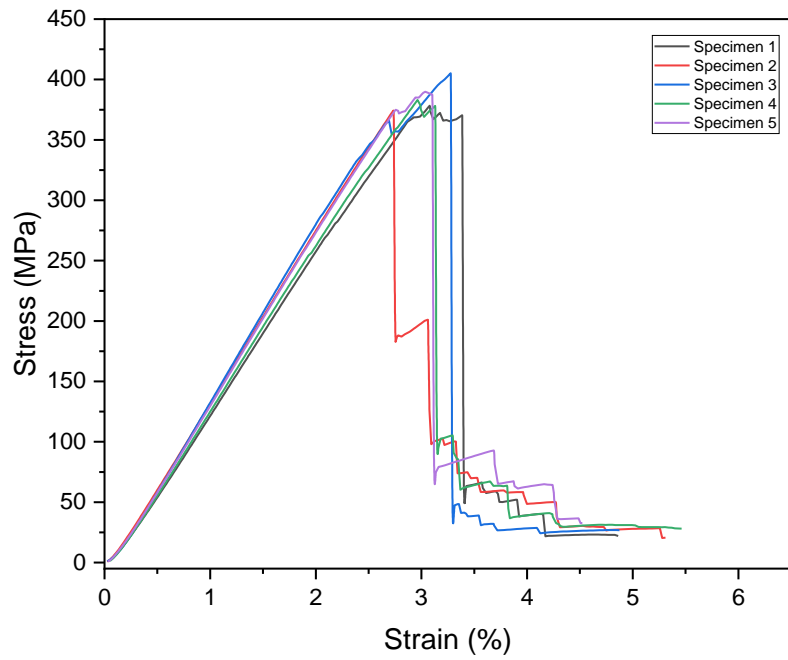


Figure 187: Strain x stress curve on three-point bending of 20 PLCL/GF composite (sample C-2).

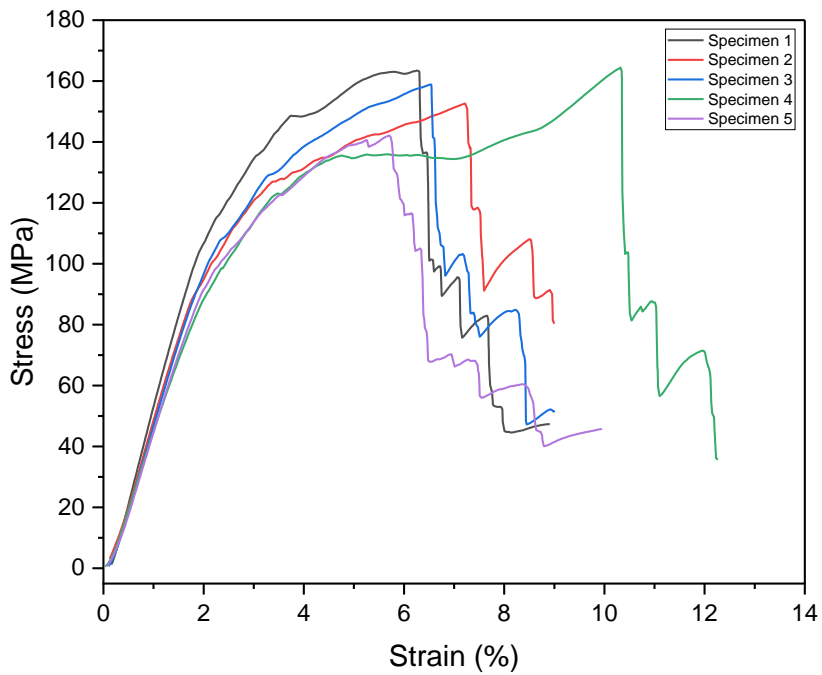


Figure 188: Strain x stress curve on three-point bending of 30 PLCL/GF composite (sample C-3).

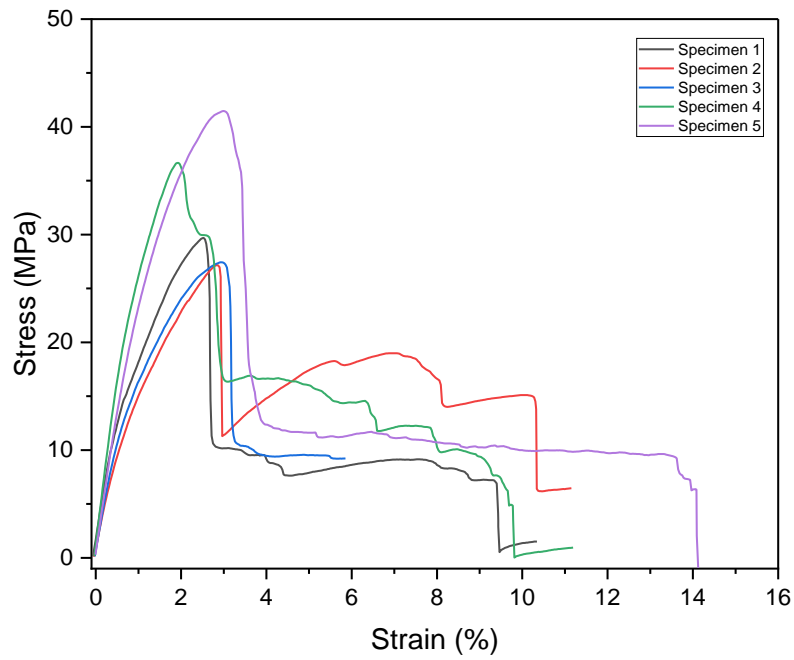


Figure 189: Strain x stress curve on three-point bending of PLLA/TW composite (sample F-1).

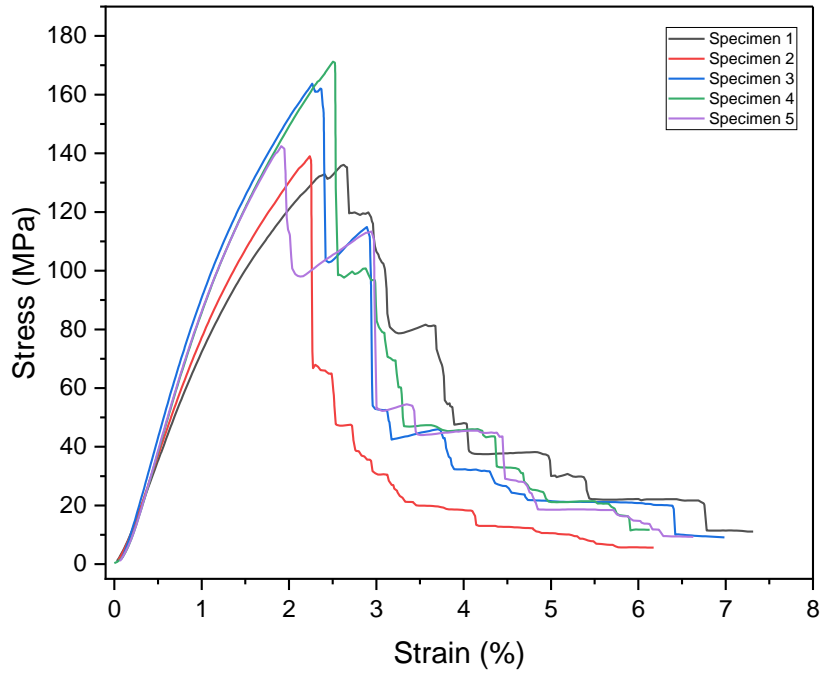


Figure 190: Strain x stress curve on three-point bending of PLLA/UD composite (sample F-2).



## Composites à matrice copolymère à base de PLLA produits par TP-RTM

Cette étude présente la production de composites à matrice copolymère à base de poly(L-lactide) par Moulage par Transfert de Résine Thermoplastique (TP-RTM). Dans ce procédé, la polymérisation in-situ par ouverture de cycle du L-lactide (L-LA) et de l' $\epsilon$ -caprolactone ( $\epsilon$ -CL) a été réalisée en une seule étape pour obtenir des composites à matrice copolymères poly(L-lactide-co- $\epsilon$ -caprolactone) (PLCL) biodégradable. L'incorporation de l' $\epsilon$ -CL dans la matrice avait pour objectif de réduire la fragilité du PLLA. La matrice PLCL résultante a été associée à des renforts de verre ou de carbone. Différents rapports molaires L-LA/ $\epsilon$ -CL ont été testés, ce qui a permis de développer des composites présentant des propriétés chimiques, thermiques et mécaniques variées. Les paramètres expérimentaux du procédé TP-RTM ont été optimisés pour créer des composites avec moins de vides possibles. Ensuite, ces composites ont été caractérisés pour évaluer la conversion du monomère, la masse molaire et les propriétés thermiques des matrices ainsi que les propriétés mécaniques des composites résultants. Il a été constaté que les composites PLCL/verre tissée présentent une résistance aux chocs plus élevée par rapport à leurs homologues à base de PLLA. D'autre part, les composites PLCL/renfort de carbone présentent des propriétés de légèreté remarquables avec une grande résistance à la flexion. Les fractures des composites après les essais mécaniques ont été étudiées pour identifier le type d'endommagement au cours de ces essais. Dans une approche plus durable, des composites entièrement biodégradables de PLLA/lin tissé ont été produits par TP-RTM, et leurs propriétés chimiques, thermiques et mécaniques ont également été étudiées. De plus, le vieillissement accéléré de l'ensemble de ces composites sous température et irradiation UV a été étudié. A l'issue du vieillissement, une relation entre la cristallinité, la masse molaire des matrices et les propriétés de flexion a pu être établie.

## Copolymer-based PLLA matrix composites produced by TP-RTM

The present study experimentally investigated the production of poly(L-lactide)-based matrix composites by Thermoplastic Resin Transfer Molding (TP-RTM). In this process, the in-situ ring opening polymerization of L-lactide (L-LA) and  $\epsilon$ -caprolactone ( $\epsilon$ -CL) was performed in a single step to achieve composites with a biodegradable poly(L-lactide-co- $\epsilon$ -caprolactone) (PLCL) matrix in one step synthesis. The incorporation of  $\epsilon$ -CL in the matrix was aimed at reducing the brittleness of PLLA. The resulting PLCL matrix was reinforced with glass or carbon fabrics. Different L-LA/ $\epsilon$ -CL molar ratios were tested, leading to the development of composites with various chemical, thermal, and mechanical properties. The TP-RTM parameters were optimized to produce composites with reduced voids. Subsequently, these composites were characterized to evaluate monomers conversions, molecular weights and thermal properties of the matrices, as long as the mechanical properties of the resulting composites. It was found that PLCL/glass fabric composites exhibit higher impact resistance compared to their PLLA-based counterparts. On the other hand, PLCL/carbon fabric composites display remarkable lightweight properties with high bending strength. The fractures of the composites after mechanical tests were studied to identify the failure type during these experiments. In a more sustainable approach, fully biodegradable PLLA/flax composites were produced using TP-RTM, and their chemical, thermal, and mechanical properties were also studied. Furthermore, the impact of accelerated aging, i.e under temperature and UV irradiation, was studied on all composites. After aging, a relationship between crystallinity, matrices molecular weights and bending properties was established.